CAUSES OF CONFINED SPACE HYPOXIA DURING UNDERGROUND CONSTRUCTION IN THE LAMBETH GROUP BENEATH LONDON

A thesis submitted to Imperial College, London, in partial fulfilment of the requirements for the degree of Doctor of Philosophy.

Timothy Guy de Carteret Newman

October 2013

Department of Civil and Environmental Engineering

Imperial College London SW7 2AZ

Abstract

Hypoxic ground gas is rarely reported in London despite its frequent occurrence in the Upnor Formation and the serious health and safety implications for underground working. The death of two engineers by asphyxiation and recent interception of pressurised hypoxic gas by two ground investigation boreholes highlight the urgent need for research into this hazard which until now has been extremely limited.

Glauconite is legally and widely assumed to cause the oxygen loss in confined spaces but this research proves it incapable of doing so. Visual inspection and laboratory analysis, using optical and infrared spectroscopy, scanning electron microscopy and X-ray diffraction techniques confirm fresh glauconite within highly oxidised soil samples throughout the lower Lambeth Group and Thanet Sand Formation. The low concentration of pyrite and organic materials eliminates these as alternative causes.

A poorly known but common bright blue-green mineral, green rust, is instead shown to be a very potent and plausible reducing agent. However, laboratory analysis under anoxic conditions has yet to prove its existence in the Upnor Formation, largely because of its extremely rapid oxidation, although the results are consistent with its presence in fresh samples. Significant preservation techniques were implemented to prevent oxidation of soil samples prior to laboratory analysis and improvements identified for future research. The presence of green rust during underground construction within the Upnor Formation will have serious implications for the health and safety of personnel.

Measurements of soil suction, using the filter paper technique, show that the air entry value of the Lower Mottled Beds is such that they will act as an impermeable barrier to upward migration of hypoxic gas, trapping it within the underlying Upnor Formation. Field tests indicate that the gas is formed during periods of dewatering and may be influenced by changes in barometric pressure.

Acknowledgements

This research has not been possible without the contribution of a large number of friends and colleagues.

First, I am indebted to Dr Richard Ghail, for his continued support and guidance; he was always available for discussion and to answer my many questions and I have been most fortunate to have him as my supervisor. I would also like to thank Dr Jamie Standing for helping me to overcome the complexities of partially saturated soil mechanics and for his advice during the filter paper tests.

Acknowledgement goes to John Greenwood for getting this mission started in the first place, to John Harris for ensuring its successful launch and Thames Water for providing the funds.

Special thanks go to Dr Jackie Skipper for inspiring me with her enthusiasm for the Lambeth Group deposits and to Dr Jenny Huggett for sharing her vast knowledge of glauconite and in particular for providing answers to my continual bombardment of questions. Also to Dr Richard Court and Prof. Mark Sephton for their help and comments on the FTIR and Dr Jens Najorka at the Natural History Museum, in dealing with the mountain of samples for XRD.

I am extremely grateful to Dr Sam Shaw (formerly Leeds now Manchester University) and Dr Christine Rogers for their generous offer of the SEM and for sharing thoughts and advice on how to capture green rust.

Thanks also go to my fellow PhD student, Khalid Al Haj, for helping me undertake the initial filter paper tests. Much time was spent in the laboratory and I am also grateful for all of the help given to me by Steve Ackerley, Graham Keefe and Alan Bolsher, not least for his 'Bolsher Box' and general entrepreneurial propositions.

This research has benefitted from the continual supply of soil samples from the Tideway Tunnel geotechnical team and thanks must go to Graeme Swinbourne and Lorraine O'Keeffe for their field marshalling skills; to Alistair Campbell, Chris McCormick, Gareth Cooper and Andy Thrower for organising the safe despatch of samples to the laboratory; to Dimitrios Kalianidis for his help with the Teviot Street pump out test and to Carol Green for being thrown in at the deep end (literally!) during construction of the Abbey Mills shaft.

A vast array of borehole monitoring data has contributed to this research and I am very appreciative of the foot-soldiering efforts of Greg Bowl and Andrew Swinbourne in capturing this, come rain or shine. Back in the office, I have been fortunate for so much help and useful discussion with Neill Hadlow, Birva Patel, Carol Mozuraitis, Tim Connolly and John Andrews.

In researching the past, I am grateful to Gaynor Haywood, Thames Water's librarian, for the provision of archive data and to Tom Power, Andy Miller and Eddie Woods for delving into their memories. I am also grateful to Mike Black and Ursula Lawrence at Crossrail and Ivan Hodgson, Chris Menkiti, Andrew Aplin and Darren Page for the valuable data that they provided.

Finally, thanks go to Nadia, Benjamin and Dominic, for their patience and in bearing with me during the long hours of study.

Declaration

The work presented in this dissertation was carried out in the Department of Civil and Environmental Engineering at Imperial College London. This thesis is the result of my own work and any quotation from, or description of, the work of others is acknowledged herein by reference to the sources, whether published or unpublished.

This dissertation is not the same as any that I have submitted for any degree, diploma or other qualification at any other university. No part of this thesis has been or is being currently submitted for any such degree, diploma or other qualification.

The copyright of this thesis rests with the author and is made available under a Creative Commons Attribution Non-Commercial No Derivatives licence. Researchers are free to copy, distribute or transmit the thesis on condition that they attribute it, that they do not use it for commercial purposes and that they do not alter, transform or build upon it. For any reuse or redistribution, researchers must make clear to others the licence terms of this work.

Signed

Dated

Contents

Abstract 2

Acknowledgements 3

Declaration 5

1 INTRODUCTION 16

1.1 Background 16

1.2 Objectives 16

1.3 Thesis structure 17

2 LITERATURE REVIEW 18

2.1 Composition of breathable air 18

2.2 Confined Space Hypoxia syndrome 19

2.3 Case histories of deoxygenated air 19

2.3.1 General 19

2.3.2 Underground excavations 20

2.3.3 Boreholes (and near-surface inspection chambers) 23

2.3.4 Other case histories higher in the Lambeth sequence 27

2.4 Causal mechanisms 29

2.4.1 The introduction of air into the ground 29

2.4.2 Fluctuations in the lower aquifer 32

2.4.3 Effects of barometric pressure 34

2.4.4 Chemical-oxygen demand 35

2.5 Containment of ground gas by an impermeable barrier 36

3 THE LOWER LAMBETH GROUP DEPOSITS 39

3.1 Introduction 39

3.2 The Lambeth Group 41

3.2.2 Environment of deposition 44

3.2.3 Thanet Sand Formation 46

3.2.4 Upnor Formation 49

3.2.5 Lower Mottled Beds 59
3.2.6 Pedogenic alteration of the Upnor Formation 64
3.3 Glauconite 67
3.3.1 Introduction 67
3.3.2 Environment of deposition 68
3.3.3 Formation and growth 68
3.3.4 Maturation 69
3.3.5 Characterisation by X-Ray diffraction 70
3.3.6 Weathering and alteration 71
3.3.7 Field evidence 72
3.3.8 Hand specimen – observational experiment 72
3.4 Pyrite 73
3.4.1 Formation 73
3.4.2 Shape and morphology 73
3.4.3 Oxidation and alteration 74
3.4.4 Cause of oxygen depletion: LUL Old Street 75
3.5 Green Rust 76
3.5.1 Introduction 76
3.5.2 Formation by reduction 78
3.5.3 Formation by oxidation 79
3.5.4 Environment of formation 79
3.5.5 Difficulties in sample analysis 80
3.6 Summary 80
4 EXPERIMENTAL METHODOLOGY 82
4.1 Laboratory testing 82
4.2 Field sample recovery 82
4.2.1 Rotary core samples 82
4.2.2 Hand-dug tub samples 85

4.2.3 Hand-driven U38 tube samples 86
4.3 Apparatus 92
4.3.1 Introduction 92
4.3.2 Identification of oxidised mineralogy 93
4.3.3 Identification of reduced to oxidised transformation 101
4.3.4 Soil suction filter paper test equipment 107
4.4 Field Tests 110
4.4.1 Borehole gas monitoring 110
4.4.2 Borehole gas sampling 111
4.4.3 Borehole pump-out test 112
5 EXPERIMENTAL RESULTS 115
5.1 Identification of oxidised mineralogy 115
5.1.1 X-Ray diffraction 115
5.1.2 Optical microscopy 118
5.1.3 Scanning Electron Microscopy (SEM) 122
5.2 Identification of reduced to oxidised mineral transition 125
5.2.1 Position Sensitive X-Ray diffraction 125
5.2.2 ATR FTIR spectroscopy 125
5.3 Soil suction filter paper test results 131
5.3.1 Introduction 131
5.3.2 Matrix suction 134
5.3.3 Soil Water Retention Curves (SWRCs) 136
5.4 Field tests 147
5.4.1 Borehole gas monitoring 147
5.4.2 Borehole gas sampling 151
5.4.3 Borehole pump-out test 151
5.4.4 Borehole permeability tests 153
5.4.5 VHT in Borehole SR1031 154

5.5 Further laboratory experimentation 154

6 CONCLUSIONS 156

6.1 Research summary 156

6.2 Conclusions 158

6.3 Recommendations for future research 160

APPENDIX A Method statement for borehole gas sampling.

APPENDIX B Borehole pump out test site location plan.

APPENDIX C Petrographic thin sections.

APPENDIX D Report on SEM by Dr S. Shaw and Dr C. Rogers.

APPENDIX E Report on XRD by Dr J. Najorka.

APPENDIX F FTIR data.

APPENDIX G Filter paper test data.

APPENDIX H Tideway Tunnel borehole gas-monitoring data.

Figures

Figure 2.1 Location of occurrences of oxygen depletion 20

Figure 2.2 Schematic geological section through the Effra Storm Relief Sewer Tunnel 21

Figure 2.3 Schematic geological long section: Coppermills to Stoke Newington 22

Figure 2.4 Schematic geological long section through the NLFRS tunnel 23

Figure 2.5 Gas monitoring data for Borehole 278D/2 24

Figure 2.6 Schematic geological long section for the TWRM Northern Extension 25

Figure 2.7 Gas quantities in Borehole SA1066D 26

Figure 2.8 Evidence of pressurised gas blow-out in Borehole SR2071 27

Figure 2.9 The 'Windows of London' 30

Figure 2.10 Location of Tideway Tunnel groundwater sampling boreholes 31

Figure 2.11 Changing groundwater table contours for the lower aquifer 33

Figure 2.12 Example of a soil water retention curve (SWRC) 37

Figure 3.1 The London Tideway Tunnels alignment 39

Figure 3.2 Tideway Tunnel boreholes intersecting the Lambeth Group 40

Figure 3.3 The geological succession for London 42

Figure 3.4 The thickness of the Lambeth Group deposits in London 43

Figure 3.5 The Thames Tideway Tunnel – geological model 43

Figure 3.6 The palaeogeographical setting during deposition of the Lambeth Group 44

Figure 3.7 Palaeofacies setting during deposition of the Lambeth Group 45

Figure 3.8 Diachronous boundaries between Lambeth Group strata 46

Figure 3.9 Thickness of the Thanet Sand Formation across London 47

Figure 3.10 Core sample of the Bullhead Bed 47

Figure 3.11 Core sample of the Thanet Sand (sample 5015/51) 48

Figure 3.12 Particle Size Distribution for the Thanet Sand 49

Figure 3.13 Thickness of the Upnor Formation across London 50

Figure 3.14 A selection of Upnor Formation lithologies 51

Figure 3.15 Bioturbation structures (sample 5015/44) 52

Figure 3.16 Matrix-supported flint gravel (sample 4208/5) 52

Figure 3.17 Glauconitic Sand (TWRM Honor Oak shaft) 53

Figure 3.18 Clay layer within the Glauconitic Sand (sample 5018/60) 54

Figure 3.19 Laminated Sediments (TWRM northern extension – tunnel face) 55

Figure 3.20 Pebble Bed material recovered in rotary core 56

Figure 3.21 Thickness of the upper Pebble Bed across London 57

Figure 3.22 PSD grading envelopes for the Upnor Formation 58

Figure 3.23 Soil classification of the Upnor Formation 59

Figure 3.24 Plasticity within the Upnor Formation 59

Figure 3.25 The Mid-Lambeth Hiatus 60

Figure 3.26 Thickness of the Lower Mottled Beds across London 61

Figure 3.27 Rotary core samples from the Lower Mottled Beds 62

Figure 3.28 Soil classification of the Lower Mottled Beds 62

Figure 3.29 Plasticity within the Lower Mottled Beds 63

Figure 3.30 PSD grading envelope for the Lower Mottled Beds 63

Figure 3.31 Examples of calcrete in Tideway Tunnel core 64

Figure 3.32 Pedogenic effects seen in the upper Pebble Bed 65

Figure 3.33 Depth of pedogenic alteration across London 65

Figure 3.34 Thickness of unaltered (fresh) Upnor Formation across London 66

Figure 3.35 Contrasting Lower Lambeth Group lithologies 66

Figure 3.36 Unweathered glauconite in pedogenically altered Upnor Formation 67

Figure 3.37 Schematic representation of the stages of growth of a glauconite grain 70

Figure 3.38 Partially weathered glauconite 71

Figure 3.39 Observation for colour change during oxidation of the Upnor Formation 73

Figure 3.40 Fine crystal of pyrite within crack in a glauconite grain 74

Figure 3.41 General view of an ordered representation of a green rust 2 lattice (not to scale) containing sulphate interlayer anions 76

Figure 3.42 Hexagonal green rust crystals 78

Figure 4.1 Borehole sample location plan 83
Figure 4.2 Core waxing and cling film preservation 84
Figure 4.3 Vacuum seal preservation of rotary core sample 85
Figure 4.4 U38 sampling at Abbey Mills 86
Figure 4.5 Geological log of the Abbey Mills shaft (sample locations in red) 88
Figure 4.6 The top of the Upnor Formation, showing effects of slight weathering 89
Figure 4.7 Contact between pedogenically altered and fresh Upnor Formation 89
Figure 4.8 Pedogenically altered and fresh Upnor Formation on muck pile 90
Figure 4.9 Glauconitic sand exposed during excavation 90
Figure 4.10 Clay-rich band towards the base of the Upnor Formation 91
Figure 4.11 Contact between Upnor and Thanet Sand formations 91
Figure 4.12 Probable nodule of green rust from Abbey Mills 92
Figure 4.13 Phillips 1820 automated X-ray diffractometer 94
Figure 4.14 Geometric conditions for X-ray diffraction according to Bragg's Law 95
Figure 4.15 Mounting of sample via pipette onto a silicon wafer 96
Figure 4.16 Olympus EX41 optical microscope 97
Figure 4.17 Preparation of petrographic thin section 98
Figure 4.18 Quanta FEG 650 Scanning Electron Microscope 99
Figure 4.19 Preparation of samples for SEM analysis 100
Figure 4.20 Anaerobic chamber (glove box) 101
Figure 4.21 Sample preparation for XRD-PSD analysis 104
Figure 4.22 Enraf Nonius Powder XRD-PSD machine 104
Figure 4.23 Sample preparation for FTIR analysis 106
Figure 4.24 Thermo-Nicolet 5700 Fourier Transform Infrared (FTIR) spectrometer 106
Figure 4.25 Production of an evanescent wave 107
Figure 4.26 Sample preparation for the filter paper test 109
Figure 4.27 Location of gas monitoring boreholes 111
Figure 4.28 Schematic cross section through pump out test boreholes 113

Figure 4.29 Borehole pump out test site 114
Figure 5.1 Identification of glauconite/illite by XRD 115
Figure 5.2 Identification of goethite by XRD 116
Figure 5.3 Identification of kaolinite by XRD 117
Figure 5.4 Identification of glauconite by optical microscopy 118
Figure 5.5 Partially weathered glauconite identified in the Lower Mottled Beds 119
Figure 5.6 Unweathered glauconite identified in pedogenically weathered sediment 120
Figure 5.7 Unweathered glauconite identified in pedogenically weathered sediment 120
Figure 5.8 Unweathered glauconite identified in fresh Upnor Formation 121
Figure 5.9 Thanet Sand in thin section 121
Figure 5.10 Evidence of clay enrichment in the basal Thanet Sand 122
Figure 5.11 Identification of iron oxide in pedogenically altered Upnor Formation 122
Figure 5.12 Identification of zinc in pedogenically altered Upnor Formation 123
Figure 5.13 Identification of glauconite in pedogenically altered Upnor Formation 123
Figure 5.14 Identification of pyrite within fresh Upnor Formation 124
Figure 5.15 Background mineral data for FTIR analysis 126
Figure 5.16 FTIR spectra for the Lower Mottled Beds (sample 5006/36) 127
Figure 5.17 FTIR spectra for the Upnor Formation (sample 4207/3) 128
Figure 5.18 Possible goethite in pedogenic Upnor Formation (sample 4009/2) 129
Figure 5.19 Survival of glauconite in baked, oxidised sediment (sample 5018/61) 130
Figure 5.20 FTIR spectra of shelly Upnor Formation (sample 4204/3) 130
Figure 5.21 FTIR spectra for the Thanet Sand Formation (sample 4204/5) 131
Figure 5.22 Void ratio against depth 133
Figure 5.23 Moisture content against depth 133
Figure 5.24 Matrix suction against void ratio 134
Figure 5.25 Matrix suction through the lower Lambeth Group and Thanet Sand 135
Figure 5.26 Drying curves for lower Lambeth Group and Thanet Sand Formation 136
Figure 5.27 Drying curves for the Lower Mottled Beds 138

Figure 5.28 SWRCs suction vs. saturation: sample 6908/3 139
Figure 5.29 SWRCs suction vs. volumetric water content: sample 6908/3 139
Figure 5.30 SWRCs suction vs. void ratio: sample 6908/3 140
Figure 5.31 Drying curves for the Upnor Formation 141
Figure 5.32 SWRCs suction vs. saturation: sample 4207/4 142
Figure 5.33 SWRCs suction vs. volumetric water content: sample 4207/4 142
Figure 5.34 SWRCs suction vs. void ratio: sample 4207/4 143
Figure 5.35 Drying curves for the Thanet Sand Formation 144
Figure 5.36 SWRCs suction vs. saturation: sample 5013/45 145
Figure 5.37 SWRCs suction vs. volume water content: sample 5013/45 145
Figure 5.38 SWRCs (drying and wetting) suction vs. void ratio: sample 5013/45 146
Figure 5.39 Gas monitoring at Borehole SA1066D 147
Figure 5.40 Gas flow at Borehole SA1066D 148
Figure 5.41 Gas monitoring at Borehole SR1031 149
Figure 5.42 Gas monitoring at NLFRS tunnel Borehole 278D/7 150
Figure 5.43 Gas flow at NLFRS tunnel Borehole 278D/7 150
Figure 5.44 Gas monitoring at TWRM Ext Borehole 773B/12 151
Figure 5.45 Oxygen depletion in pump-out test in Borehole SR4003 152
Figure 5.46 Observation of oxygen depletion in Upnor Formation (sample AM325) 155
Figure 5.47 Measured rate of oxygen depletion in the Upnor Formation 155
Figure 6.1 Evidence of green rust in Tideway Tunnel core samples 159

Tables

Table 2.1 The composition of air 18

Table 2.2 The effects of oxygen deficiency (Doyle, 2001) 18

Table 2.3 Average recorded values of dissolved oxygen 31

Table 3.1 Summary of soil classification tests 41

Table 3.2 A comparison of Upnor Formation lithofacies group terms 53

Table 3.3 Characteristic features of glauconite maturation (adapted from Amorosi, 1995) 70

Table 3.4 Origins of weathering by-products 81

Table 4.1 Schedule of receipt of rotary core samples 83

Table 4.2 Summary of U38 sampling at the Abbey Mills shaft 87

Table 4.3 Application of apparatus for laboratory testing 93

Table 4.4 Oxidised samples analysed using powder XRD 93

Table 4.5 Soil samples analysed using optical microscopy 96

Table 4.6 Analysis of U38 samples 98

Table 4.7 Samples analysed using position sensitive XRD 103

Table 4.8 Samples analysed using FTIR 105

Table 4.9 Rotary core samples for soil suction analysis 108

Table 4.10 The geology of gas sampled boreholes 112

Table 5.1 Mineral characterisation by XRD 117

Table 5.2 The chemical character of glauconite from the Abbey Mills shaft 124

Table 5.3 Summary of void ratio and moisture content 132

Table 5.4 Summary of matrix suction values 136

Table 5.5 Summary of matrix suction at residual saturation 146

Table 5.6 Summary of gas monitoring in the upper Lambeth Group 148

Table 5.7 Summary of gas monitoring in the NLFRS tunnel boreholes 149

Table 5.8 Summary of VHT permeability values 154

1 INTRODUCTION

1.1 Background

In August 1988, two engineers were asphyxiated by hypoxic (oxygen-depleted) gas during construction of a deep shaft within glauconite-bearing sediments of the lower Lambeth Group in Stoke Newington, north London. Since then, and based on the subsequent Crown Court inquest, the consensus within the construction industry is that oxidation of the mineral glauconite is the cause of oxygen depletion. However, this process has never been proved or quantified.

A number of other tunnel schemes within London have encountered hypoxic conditions during underground construction within the same lower Lambeth Group deposits, specifically the Upnor Formation. More recently, pressurised hypoxic gas was intercepted within this unit during construction of two boreholes for the current Thames Tideway Tunnel investigation (Newman and Hadlow, 2011) and there is now sufficient evidence to regard the Upnor Formation as a significant ground hazard during underground construction.

With continued foreseeable growth of London's urban infrastructure and the requirement for sub-surface construction to greater depths, major civil engineering schemes increasingly encounter the Upnor Formation, often with little or no precedent experience.

Ground gas (including hypoxia) is an infrequent hazard during tunnel construction, although it is a leading cause of injury and fatality (Critchfield, 1985) and usually results in costly delays. Current literature provides little information on the subject (Critchfield, 1985; Doyle, 2001; Shahriar et al., 2009), especially within the lower Lambeth Group. A better understanding and communication of this hazard will ensure a more efficient risk assessment by tunnel designers prior to excavation and more robust systems of control and mitigation.

1.2 Objectives

This research seeks to understand the processes leading to hypoxic gas within confined underground excavations, termed confined space hypoxia, in the lower Lambeth Group and to predict the likelihood of its occurrence during and after construction.

The research concentrates on two parallel but related themes. One is to assess the geochemical mechanisms leading to hypoxic gas and to gain an understanding of the key mineralogies and reaction pathways, in particular, the role of glauconite and pyrite or whether there are any other minerals in the lower Lambeth Group or Thanet Sand Formation that might cause hypoxic gas. The parallel theme will examine the physical processes that take place during dewatering and desaturation of soils that might influence the rates of reaction and gas exchange.

During dewatering, a soil becomes partly saturated and exposed to air and hence the effects of oxidation; increasing as the degree of saturation decreases. The development of Soil Water Retention Curves (SWRCs) enables characterisation of the partly saturated soil. A threshold is identified on the SWRC at a point where the desaturation (and hence oxidation) rate increases dramatically, allowing better prediction of the timing of confined space hypoxia events.

The first stage of this research is to investigate and collate literature records of cases of confined space hypoxia during tunnel or borehole construction in lower Lambeth Group deposits, to ascertain whether the strata here can be recognised as hazardous for tunnel construction. A primary aim is to verify the presence of unweathered glauconite within heavily oxidised soil samples from these deposits to test the widely assumed theory that it oxidises rapidly. This is achieved by use of optical microscopy, X-Ray diffraction and SEM techniques and X-Ray diffraction and infrared spectroscopy techniques to analyse changes in mineralogy during oxidation of fresh samples. In parallel, suction tests using the filter paper method characterise the partially saturated behaviour of soil samples, which influences their likely rates of oxidation and their potential for soil gas migration. The research is augmented with data gained from an analysis of long-term monitoring of borehole installations used for the Tideway Tunnel ground investigation.

1.3 Thesis structure

The thesis consists of six chapters. Following this introductory section (Chapter 1), Chapter 2 defines the term 'confined space hypoxia' and summarises the effects of oxygen depletion on the human body. The chapter continues by collating all the known literature on incidences of hypoxic air during tunnelling and borehole construction within lower Lambeth Group deposits in London, including a number of first-hand accounts that have never before been published.

The lower Lambeth Group deposits are characterised in Chapter 3, in terms of both their geology and geotechnical parameters relevant to this research, and the data are compared with published literature. A candidate list of minerals potentially causing confined space hypoxia is identified and discussed.

In Chapter 4, the test procedures for the research are described, including details of sample recovery and apparatus used. The results of the tests are presented and interpreted in Chapter 5, including suction characteristics and the potential for gas migration and top seal capabilities in the lower Lambeth Group deposits.

Finally, conclusions are drawn and recommendations are made for further research in Chapter 6.

2 LITERATURE REVIEW

2.1 Composition of breathable air

Normal air at ground level (Table 2.1) consists of 78.9% nitrogen (by volume, unless otherwise stated), 20.9% oxygen, 0.9% argon, together with lower concentrations of a number of gases (Doyle, 2001).

Table 2.1 The composition of air

Gas	Formula	% by volume	Density (kg m^{-3})
Nitrogen	N_2	78.08	1.25
Oxygen	O_2	20.95	1.42
Argon	Ar	0.93	1.44
Methane	CH_4	1.2 to 1.5 ppm	0.72
Hydrogen	H_2	0.4 to 1.0 ppm	0.09
Carbon dioxide	CO_2	200 to 400 ppm	1.98
Carbon monoxide	CO	Up to 0.20 ppm	1.25
Hydrogen sulphide	H_2S	0.002 to 0.02 ppm	1.54
Ammonia	NH_3	0.02 ppm	0.68

An oxygen-deficient, asphyxiating atmosphere will result when the level of oxygen falls below 20.9%.

Oxygen deficiency is a dangerous condition that arises when human tissue becomes deprived of oxygen, often with fatal consequences (Table 2.2). An oxygen concentration of less than 16% in air is considered immediately dangerous to life (Zugibe et al., 1987). In the UK, an underground excavation is oxygen-deficient if the oxygen concentration in the air falls below 19% (BSI, 2011) and if this occurs, an excavation must be evacuated immediately.

Table 2.2 The effects of oxygen deficiency (Doyle, 2001)

Concentration (%)	Effects
16 – 12	Increased breathing volume, accelerated heartbeat, impaired thinking and muscular co-ordination.
12 – 10	Intermittent breathing, very faulty judgement, rapid fatigue.
10 – 6	Nausea, vomiting, loss of strength, loss of consciousness.
<6	Spasmodic breathing, convulsions, cardiac arrest.

Michaelsen and Park (1954) state that 'no manhole should be considered safe (to enter) until it has been demonstrated to contain sufficient oxygen'.

2.2 Confined Space Hypoxia syndrome

The term "Confined Space-Hypoxia Syndrome" has been proposed for all confined space accidents occurring in mines and underground excavations, for example, resulting from oxygen-deficient atmospheres (Zugibe et al., 1987).

A confined space is defined as any space that has limited or restricted means of entry or exit but is large enough for a person to enter and perform tasks. It has the potential for dangerous atmospheric contamination – oxygen depletion amongst others (Zugibe et al., 1987) and applies especially to enclosed spaces underground, such as tunnels and shaft excavations.

The risk of encountering potentially hazardous gases or oxygen-depleted air within these is considered high, especially where the supply of air is inadequate, with implications for underground personnel being overcome and asphyxiated.

Zugibe et al. (1987) identified three categories of confined space based on the concentration of oxygen in the air:

Class A: immediately dangerous to life if the oxygen concentration in the air is 16% or less;

Class B: where the potential for causing injury and illness exists if preventative measures are not taken, i.e., the oxygen concentration in the air is between 16.1 and 19.4%;

Class C: not requiring any modification of work procedures where the oxygen concentration in the air is between 19.5 and 21.4%.

2.3 Case histories of deoxygenated air

2.3.1 General

Oxygen-depletion during underground excavation, within the Upnor Formation of the Lambeth Group, is a relatively new phenomenon within the tunnelling industry and there has been very little transfer of experiences of this from one construction project to another. Published records of occurrences of oxygen-depleted gas during underground excavation are limited, largely due to the legal and professional sensitivities (Critchfield, 1985).

There is little historic information on the occurrence of confined space hypoxia in underground excavations or oxygen depletion in boreholes, particularly within the Lambeth Group in London. Most of London's current tunnel infrastructure was constructed within the London Clay Formation, where ground gas has not been a subject of routine interest in subsurface exploration. Past events have often been poorly recorded or not documented at all; much of this literature review is based on anecdotal evidence or the author's own experiences.

This has led to a lack of practical information on gassy tunnelling conditions in civil engineering literature (Shahriar et al., 2009), despite incidences of ground gas (toxic, flammable and asphyxiating) being the second largest cause of fatalities in underground construction (Critchfield, 1985).

The problem has been exacerbated by a poor understanding of the nature of the Lambeth Group deposits within the civil engineering industry. This is the first detailed systematic study to address it, and a number of incidences of oxygen-depleted air in both underground excavations and boreholes have come to light (Figure 2.1).

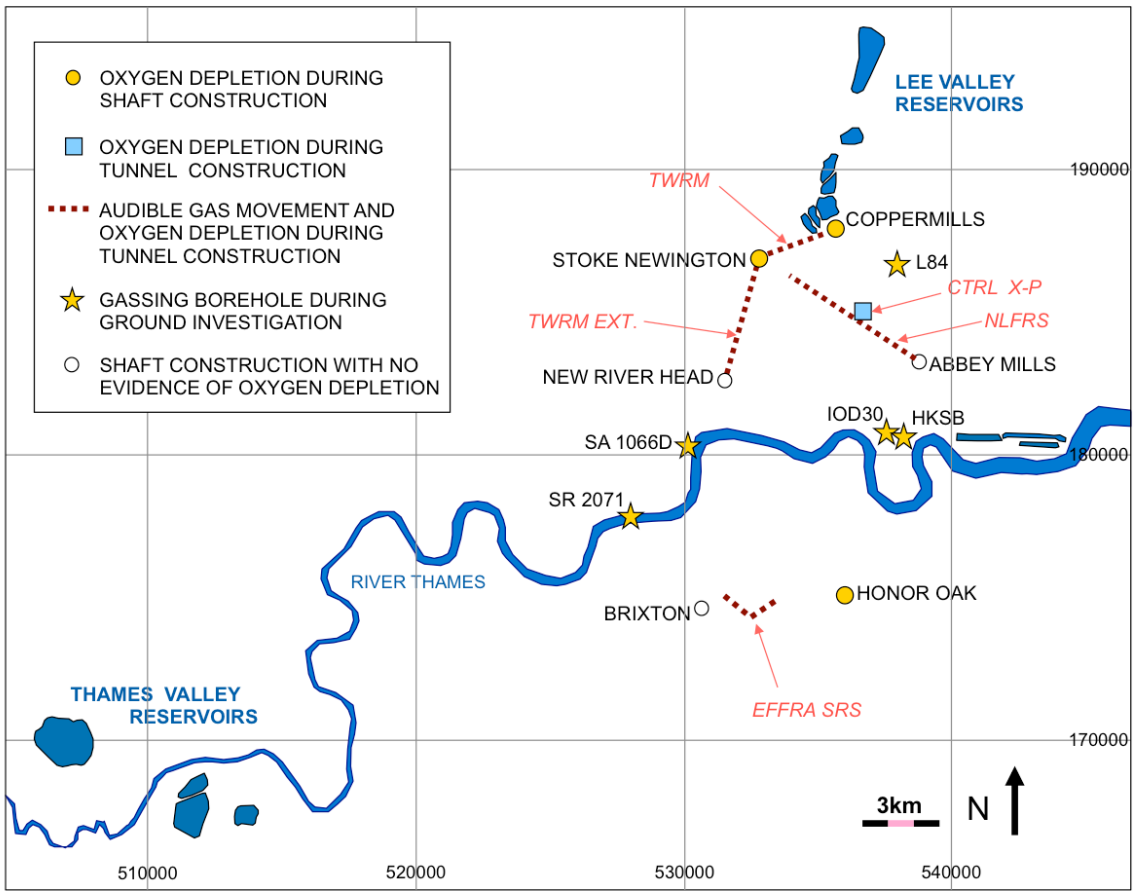


Figure 2.1 Location of occurrences of oxygen depletion

Figure based on Newman et al. (2013)

2.3.2 Underground excavations

One of the earliest recorded incidences of oxygen-depleted air in a tunnel beneath London was during construction of the London Underground Ltd (LUL) Victoria Line at Euston (Morgan and Bartlett, 1969), as discussed by Clark (1970). Here, the authors drew attention to the dangers of de-oxygenated air entering workings on structures from non-water bearing sand strata or pockets within the Woolwich and Reading Beds (now Lambeth Group).

Clark (1970) gave further account of an incident of oxygen depletion in the "Woolwich and Reading Beds", during construction of a cable tunnel beneath the Tottenham Court Road area

in 1951. The tunnel was evacuated upon the air becoming "highly de-oxygenated". It was concluded that this was due to dewatering of a previously water-bearing sand strata. It was also noted that the deoxygenated air entered the tunnel from the surrounding groundmass at times of low barometric pressure and exited again when the pressure was high.

In 1984, during construction of Thames Water's Effra Storm Relief Sewer Tunnel, in South London, personnel were evacuated when an oxygen-deficient atmosphere was encountered. Initially the tunnel was driven through the London Clay Formation as a day-works only contract, with the ventilation switched off at the end of each working day. No problems with oxygen deficiency were encountered at this stage. A short distance later, the tunnel intersected the Streatham Fault that had caused the vertical juxtaposition of Lambeth Group deposits, in particular the Upnor Formation, against the London Clay Formation (Figure 2.2). It was at this stage that oxygen deficiency was encountered at the start of each day shift (Newman et al., 2013), with levels restored only after a period of forced ventilation at the start of each morning.

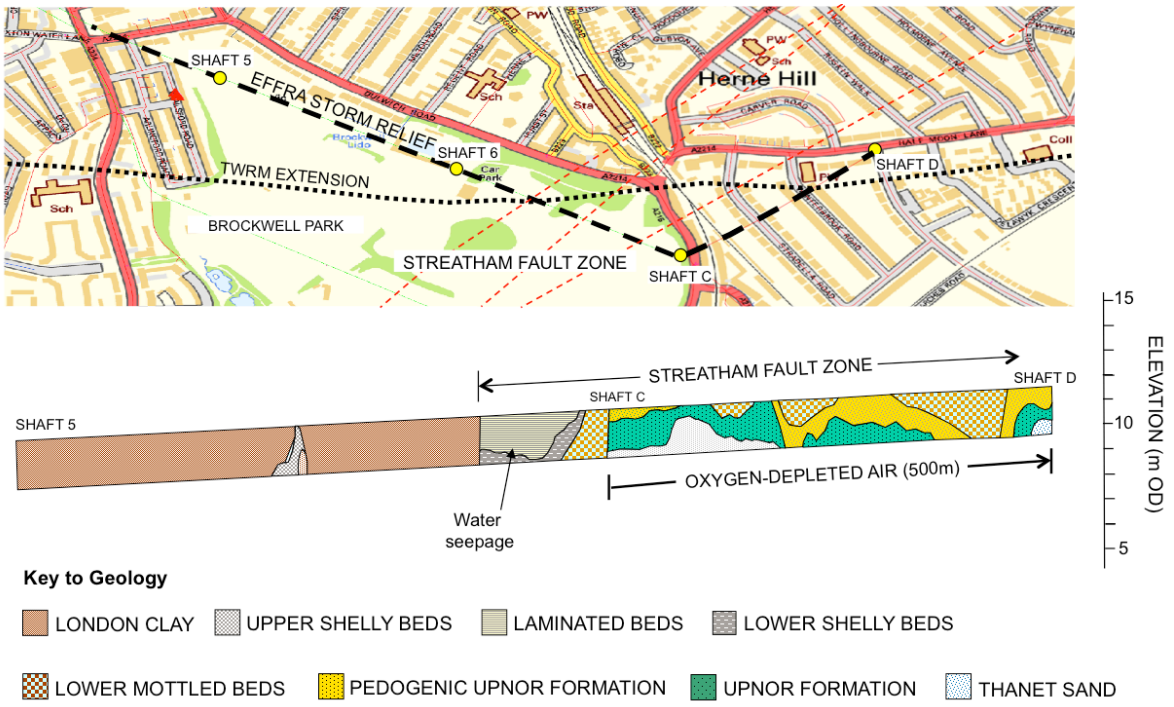


Figure 2.2 Schematic geological section through the Effra Storm Relief Sewer Tunnel

Figure based on Newman et al. (2013)

The most serious incident to date took place in August 1988 during construction of the Thames Water Ring Main (TWRM) shaft at Stoke Newington, North London (Thames Water, 1988; Newman et al., 2013). Two fatalities were suffered when an engineer and his assistant were asphyxiated within a sealed section of pipework, at the base of the 46.5 m deep, 11.9 m diameter shaft, excavated in the Upnor Formation. It was concluded at the subsequent Crown

Court inquest (CNPlus, 1991) that "rapidly oxidising" glauconite, within the soil groundmass, was the cause of hypoxia.

As part of the same TWRM project, a tunnel was constructed from Thames Water's Coppermills Water Treatment Works (WTW) to the shaft at Stoke Newington (Figure 2.3). Poor air quality was encountered as soon as the tunnel intersected the Upnor Formation, with as little as 11% oxygen recorded in the air (Newman et al., 2013). Prior to excavation of the tunnel, gas was witnessed escaping through the final invert of the shaft at Coppermills. This was visible in the form of bubbles, rising through ponded water on the shaft floor (Newman et al., 2013). Based on evidence from groundwater monitoring installations, the Upnor Formation was encountered above the groundwater table, in a dry condition.

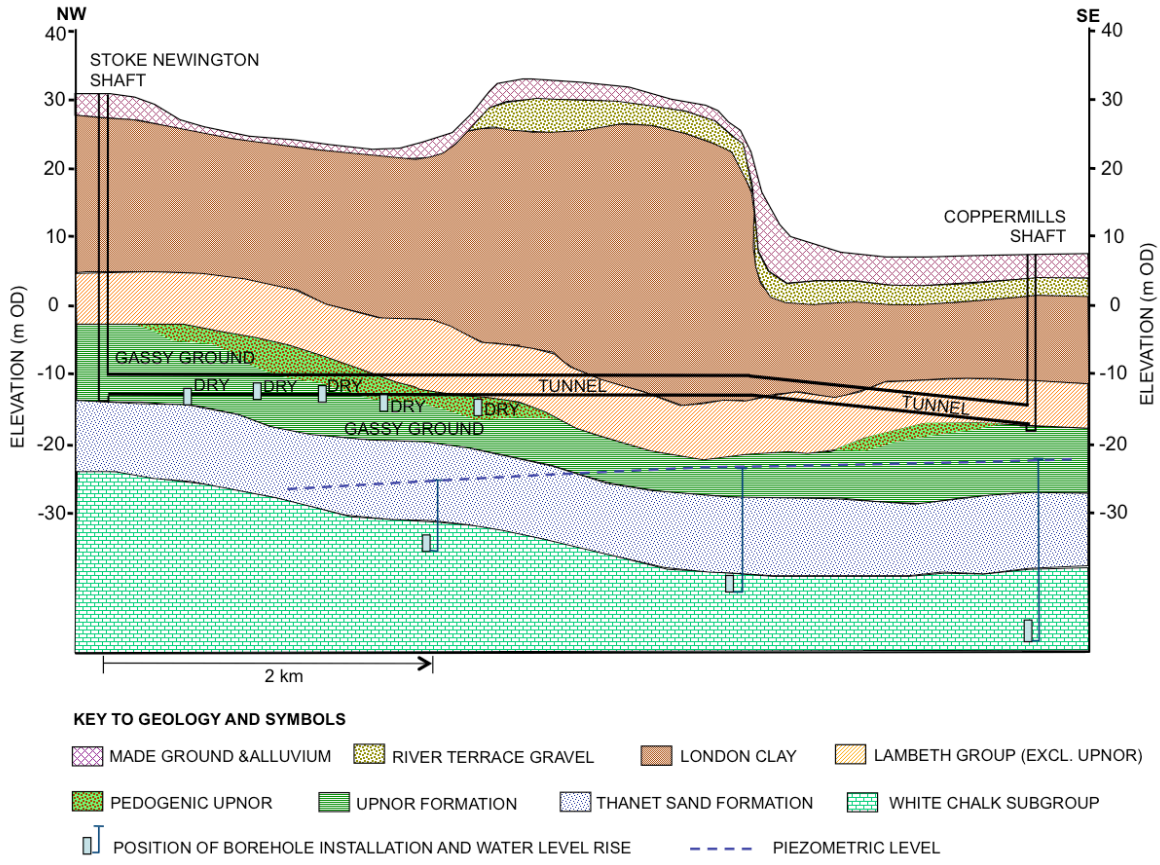


Figure 2.3 Schematic geological long section: Coppermills to Stoke Newington

Figure based on Newman et al. (2013)

Further incidences of oxygen depletion during underground construction in dewatered Upnor Formation deposits have been documented (Newman et al., 2013). The first of these was during construction of a cross passage for the Channel Tunnel Rail Link (CTRL). A 'near miss' was recorded when two personnel were partially overcome in oxygen-depleted air, requiring assistance in evacuating the tunnel. A second incident was recorded during caisson sinking for

Thames Water's Ring Main shaft at Honor Oak in South London (Newman and Wong, 2011) when the level of oxygen inside the excavation fell to below 17%.

2.3.3 Boreholes (and near-surface inspection chambers)

In light of the underground fatalities at Thames Water's TWRM Stoke Newington shaft, a rigorous borehole monitoring programme was implemented during ground investigation for their North London Flood Relief Sewer (NLFRS) in 1995, between Stratford, East London and Stoke Newington (Lewis and Harris, 1998). The tunnel was designed for construction almost entirely within the Upnor Formation and so a large number of borehole gas monitoring installations were scheduled at frequent intervals within this stratum (Figure 2.4).

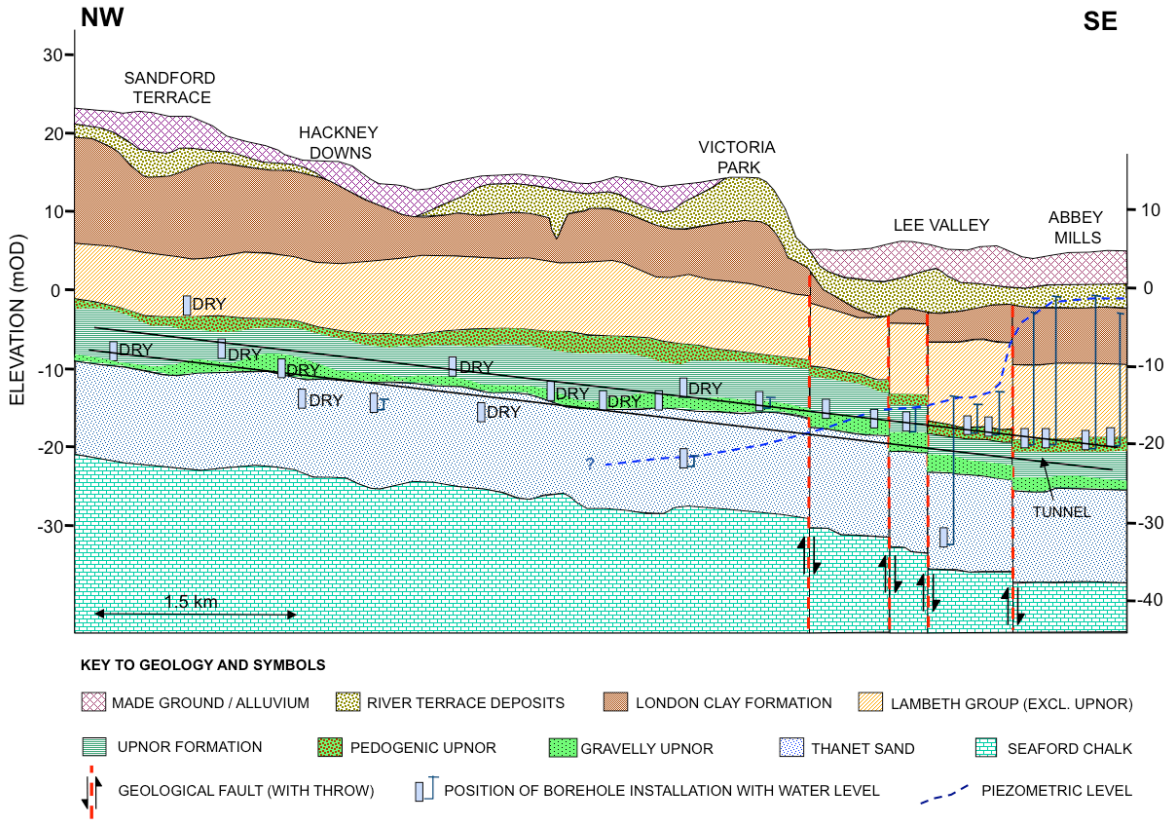


Figure 2.4 Schematic geological long section through the NLFRS tunnel

Figure based on Newman et al. (2013)

Samples of gas were taken from these for laboratory analysis, which were found to contain levels of nitrogen as much as 98% by volume, less than 1.2% oxygen and elevated levels of carbon dioxide, sometimes in excess of 1.0%. Rates of gas emission from each borehole were between 1.6 $m^3 s^{-1}$ and 5.0 $m^3 s^{-1}$, indicating a pressurised gas source. Monitoring of the boreholes continued for a year after their completion, over which time the levels of oxygen were recorded consistently below 1.0%, with levels of carbon dioxide between 1.0% and 2.0% (Figure 2.5). In mid-2011, the boreholes were recommissioned for monitoring as part of the

Tideway Tunnel ground investigation. Depleted levels of oxygen, together with elevated carbon dioxide, continue to be recorded within them at the time of writing.

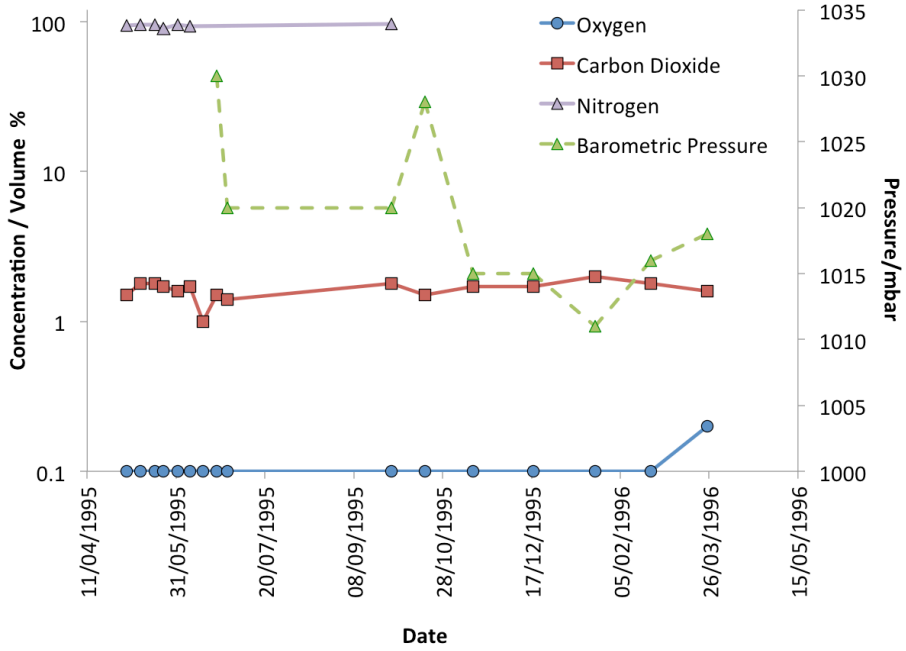


Figure 2.5 Gas monitoring data for Borehole 278D/2

Figure from Newman et al. (2013)

A more recent ground investigation for the TWRM Extension between Stoke Newington and Thames Water's New River Head site in central London (Newman et al., 2010) incorporated a number of gas-monitoring borehole installations within the Upnor Formation (Figure 2.6).

Results of monitoring, over a twelve-month period, indicated that the stratum lay above the water table and that significantly, less than 1.0% oxygen and up to 2.4% carbon dioxide was recorded. During construction of both tunnels, movement of gas passing through the tunnel lining was clearly audible (Lewis and Harris, 1998; Newman et al., 2013).

Information has been gained from other ground investigation schemes. In 1984 a cable percussion borehole in Leyton, East London (L84 in Figure 2.1), intercepted pressurised gas within dense clayey, sandy gravel at the junction between the Lower Mottled Beds and Upnor Formation, at 27.50 m below ground level (I. Hodgson, *pers. comm.*). The borehole was recorded as 'dry' at the time of the gas strike. The gas was estimated at an initial pressure in excess of 20 kPa above normal absolute atmospheric pressure (i.e., 101.3 kPa) and flowed up within the 150 mm diameter borehole casing for 5 hours prior to being sealed by a gas tap valve. Laboratory analysis on a single sample of the gas indicated 96% N_2, 1.1% O_2, 0.71% CO_2 and 630 ppm CH_4.

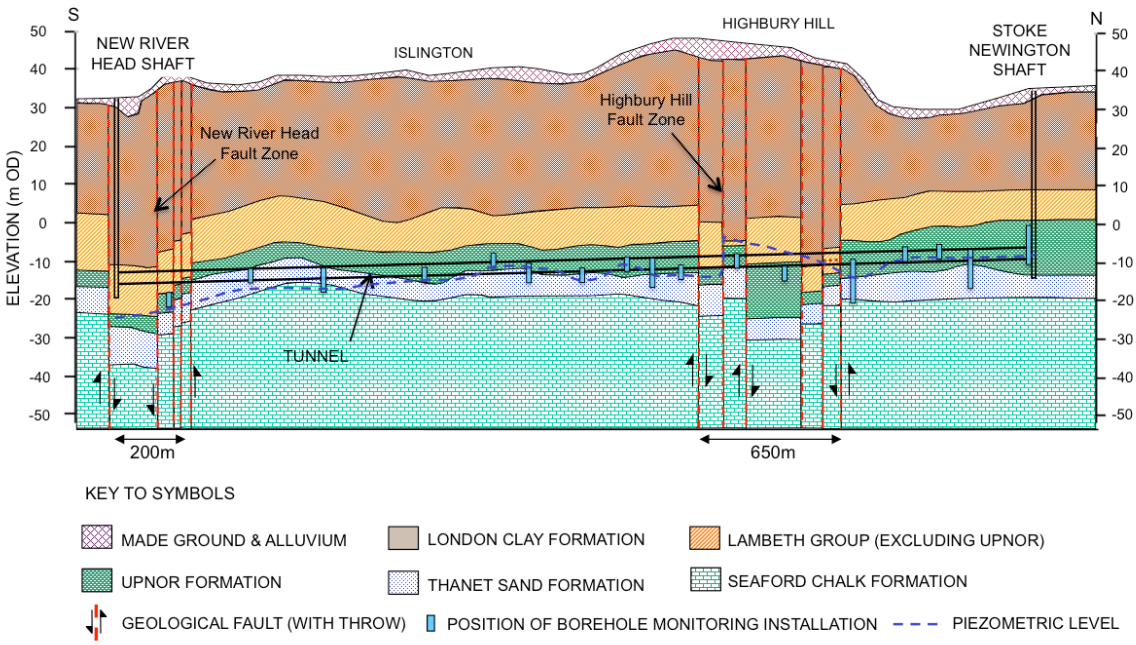


Figure 2.6 Schematic geological long section for the TWRM Northern Extension

Figure based on Newman et al. (2010)

In 1998 gas was witnessed bubbling within two boreholes (HKSB in Figure 2.1) within the Upnor Formation as part of the ground investigation for the Hong Kong Shanghai Bank (HKSB) in Canary Wharf (Hight et al., 2004). Initial flow rates were estimated up to 360 litres/min, reducing to 226 and then 180 litres/min over the next two days (D. Page, *pers. comm.*). Based on readings from gas-monitoring standpipes, gas emissions had ceased within four days. Prior to this, the composition of gas was measured using a site safety gas monitor, placed over the top of the casing of each borehole. Typically, concentrations were found to be:

- 0 to 9% oxygen,
- 8 to 10% Lower Explosive Limit (LEL, - whereby concentrations less than 20% are considered insignificant) methane,
- 0 to 4 parts per million volume (ppm) carbon dioxide,
- 0 ppm hydrogen sulphide

The gas was thought to have formed as localised 'pockets' within higher permeable zones in the Upnor Formation, as a result of construction dewatering for the adjacent LUL Jubilee Line Extension (JLE) station. Similar occurrences of gas had been noted in boreholes elsewhere in Canary Wharf.

In 2006, an investigation borehole (IOD30 in Figure 2.1), for the Crossrail tunnel scheme encountered "air escaping" from its casing at 26.15 m depth, within gravel material of the Upnor Formation. Prior to this, at 25.35 m and still within the Upnor Formation, the borehole suffered from a loss of drilling fluid into the surrounding ground that, from this, was evidently

dry. The borehole continued to lose drilling fluid until stiff, sandy clay material was intercepted. A gas-monitoring installation was inserted at this horizon and subsequently measured levels of oxygen as low as 0.1% by volume, with 98.1% N_2 and 1.5% CO_2 (M. Black, *pers. comm.*).

In 2009, boreholes SA1066D and SR2071 (Figure 2.1) intersected pressurised ground gas during investigations for Thames Water's current Tideway Tunnel scheme (Newman and Hadlow, 2011). Both boreholes were being advanced using cable percussive techniques at the time of the gas strike that, in either borehole, was encountered within clayey, sandy gravel at the junction between the Lower Mottled Beds and Upnor Formation. In the case of borehole SA1066D, the gas was escaping at an initial estimated flow of 120 litres/hour. A number of samples of the gas were taken for laboratory analysis during the ensuing two months (Figure 2.7a); these have been augmented by samples taken during the current monitoring programme (Figure 2.7b).

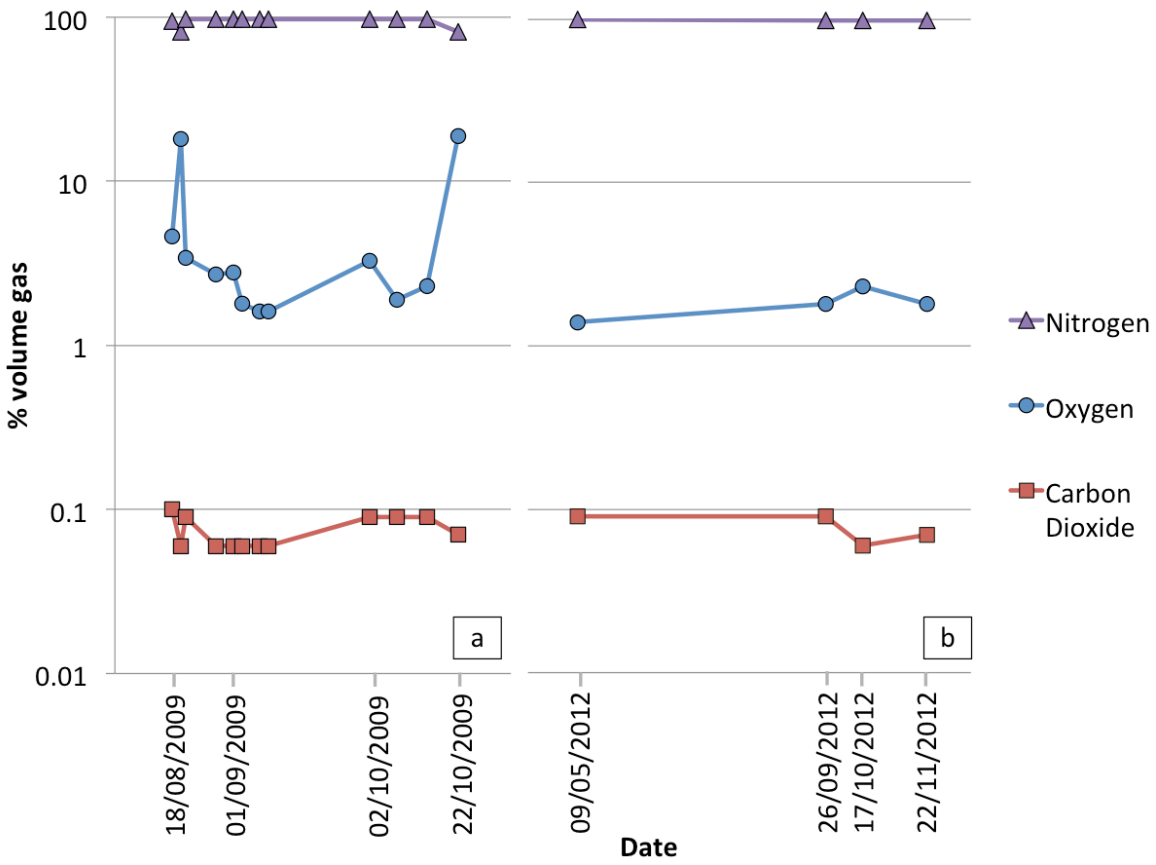


Figure 2.7 Gas quantities in Borehole SA1066D

Gas analysis indicates levels of oxygen almost always below 6% for most of the three-year monitoring period, whilst levels of nitrogen are typically above 95%, carbon dioxide below 0.09% and methane less than 0.02%. Results of monitoring show a similar theme with levels of oxygen less than 0.2%, carbon dioxide generally less than 0.1% and methane also less than 0.1% and with steady flow rates stabilising to between 20 and 30 litres/hour. Throughout the

monitoring period, however, the groundwater level has been recorded on average at 10.0 m above the level of the gas-monitoring response zone.

During overwater construction of borehole SR2071, a mini 'blow out' of pressurised gas was experienced, in which soil and drilling fluid was ejected to a height approximately 5.0 m above the top of the drilling platform (Figure 2.8). The gas was witnessed venting from the borehole casing for at least 30 minutes prior to the rig being evacuated by all personnel. This did not allow for any measurement of gas flow or composition and on returning to the drilling rig, approximately 24 hours later, the gas had ceased venting under any considerable flow. Owing to its overwater location with associated limitations on standing time, a monitoring and sampling programme was not possible for this borehole.



Figure 2.8 Evidence of pressurised gas blow-out in Borehole SR2071

2.3.4 Other case histories higher in the Lambeth sequence

Newman et al. (2013) discuss deoxygenated gas encountered in the Laminated Beds of the Woolwich Formation during a borehole investigation for a residential development scheme in Romford, Essex, in 2005. Two of the boreholes, BH3 and BH4, encountered an escape of pressurised ground gas at depths of 21.5 and 17.2 m respectively. The gas was clearly audible as bubbling noises in both boreholes and recorded as being significantly deoxygenated; less than 0.5% in either borehole. Elevated levels of carbon dioxide were recorded, at 1.7% in BH3 and between 2.3 and 2.6% in BH4, whilst less than 0.1% methane was detected in each borehole. In addition, a "rotten egg' odour was noted by the drilling operators at the level of gas strike in borehole BH4, although hydrogen sulphide gas (which can be smelt by humans at

sub-detectable levels) was not recorded at toxic amounts, being consistently below 1 part per million (ppm). Despite the available monitoring equipment being unable to measure the rate of gas flow, a large (45 litre capacity) bulk sample bag was fully inflated within one second of being placed over the top of the casing for each borehole. Significant positive flows of gas were noted for the following 24 hours, from either borehole, until they were backfilled and sealed.

Inspection of the borehole core showed the Laminated Bed material to contain up to 1% pyrite and visible grains of glauconite. In addition, a strong smell of pyrite/sulphur was particularly noticeable (RSA Geotechnics Ltd, 2005). Position Sensitive Detector X-Ray diffraction (XRD) was undertaken on recovered soil samples which showed that the pyrite and glauconite minerals were in an amorphous (broken-down) state and that each was previously present but had been oxidised and transformed into various by-products undetectable with the XRD equipment being used.

The ground investigation report for the scheme concluded that the gas was a result of oxidation of the pyrite and/or glauconite, following local dewatering by the nearby Ind Coope Brewery. Furthermore, the sample was dry and loose, consistent with the passage of gas through the sediment (RSA Geotechnics Ltd, 2005). The gas was trapped beneath the overlying, relatively impermeable, London Clay Formation, becoming increasingly pressurised during recovery of the groundwater table.

Oxidation of pyrite and/or glauconite was also suspected as the cause of pressurised, deoxygenated, ground gas during a borehole investigation for a residential construction scheme in Little Ilford in 2008 (Newman et al., 2013). Three separate cable percussion boreholes encountered audible inflows of ground gas, with a slight “bad eggs” odour upon intersection with the Laminated Beds of the Woolwich Formation. The gas was heard bubbling through groundwater by the drilling operators, at a depth of below 13 m. A hand-held gas detector was used to analyse the gas, which was found to comprise 0.0% oxygen, 0.9% carbon dioxide, 0.1% methane, 1 ppm carbon monoxide and 1 ppm hydrogen sulphide, with a noticeable odour of rotten eggs. The rate of gas flow was not recorded during site operations and this, together with the bad odour, was found to have diminished within 24 hours prior to backfilling and sealing of each borehole.

Elsewhere, oxygen depleted air has been recorded in borehole installations during remedial construction of a section of tunnel belonging to London Underground Limited (LUL) at Old Street, North London (Bird et al., 1989; Bracegirdle et al., 1996). The section of tunnel had been constructed through a relict channel feature, within the Lambeth Group Upper Mottled Beds. The feature comprised fine to medium sand that contained finely disseminated pyrite, constituting about 0.2% of the volume of the sand. A number of gas monitoring borehole

installations were placed within the sand channel feature, prior to commencement of the remedial construction work. During this, the channel was artificially drained of groundwater, by pumping, and exposed to aerobic conditions. Since then, the pyrite has been progressively oxidised under conditions fed by percolating groundwater from the consolidating London Clay Formation above and oxygen supplied through the permeable tunnel lining (Rainey and Rosenbaum, 1989). In addition to producing highly acidic, corrosive groundwater, a side effect of this has been oxygen depletion within the underground atmosphere. A strong flow of gas was detected emitting from some of the boreholes in response to very low barometric pressure (Bird et al., 1989; Bracegirdle et al., 1996). Analysis of the gas from the boreholes confirmed that it contained depleted levels of oxygen, as little as 0.5%, with elevated nitrogen and carbon dioxide, as much as 96.6% and 4.3% respectively (Bracegirdle et al., 1996). Hydrogen sulphide and methane, normally associated with reducing environments, were virtually absent. Furthermore, it was found that the lowest levels of oxygen coincided with a time of extremely low barometric pressure (965 mb).

The above cases of oxygen depletion are thought to have resulted from the oxidation of pyrite within granular subunits higher up in the Lambeth Group sequence. Unlike the Upnor Formation, these are not in hydraulic connection with the lower aquifer (Morrison et al., 2004); they are likely to represent confined aquifers and will not become aerated in response to underdrainage from the Chalk. Dewatering is, instead, usually provided by localised groundwater depressurising schemes.

The oxidation of pyrite within soil has been studied by a large number of authors (Nordstrom, 1982; Brown and Jurinak, 1989; Rainey and Rosenbaum, 1989; Bierens de Haan et al., 1994; Kinniburgh et al., 1994). There is much literature to indicate that this is ubiquitous in a wide variety of soils, with its oxidation leading to depleted levels of oxygen in the atmosphere.

2.4 Causal mechanisms

2.4.1 The introduction of air into the ground

Morgan and Bartlett (1969) suggested that abstraction and lowering of the Lower Aquifer groundwater table, during construction of the LUL Victoria Line, caused air to be drawn down through more than 30 m of overlying clay strata (presumably the London Clay Formation and cohesive members of the Lambeth Group), losing its oxygen content in the process. Alternatively, Flavin and Joseph (1983) suggested that the air is drawn down through inliers of more permeable Lambeth Group strata within the London Clay, or where the London Clay is thin and/or highly fissured. There are large inliers of these so-called 'windows' in east London (Figure 2.9), close to and/or surrounding the areas of known confined space hypoxia discussed earlier. In addition, hundreds of unbackfilled investigation boreholes and water

wells, excavated across London over the past 200 years, may have facilitated the direct introduction of air into the ground from the surface atmosphere (M. de Freitas, *pers. comm.*).

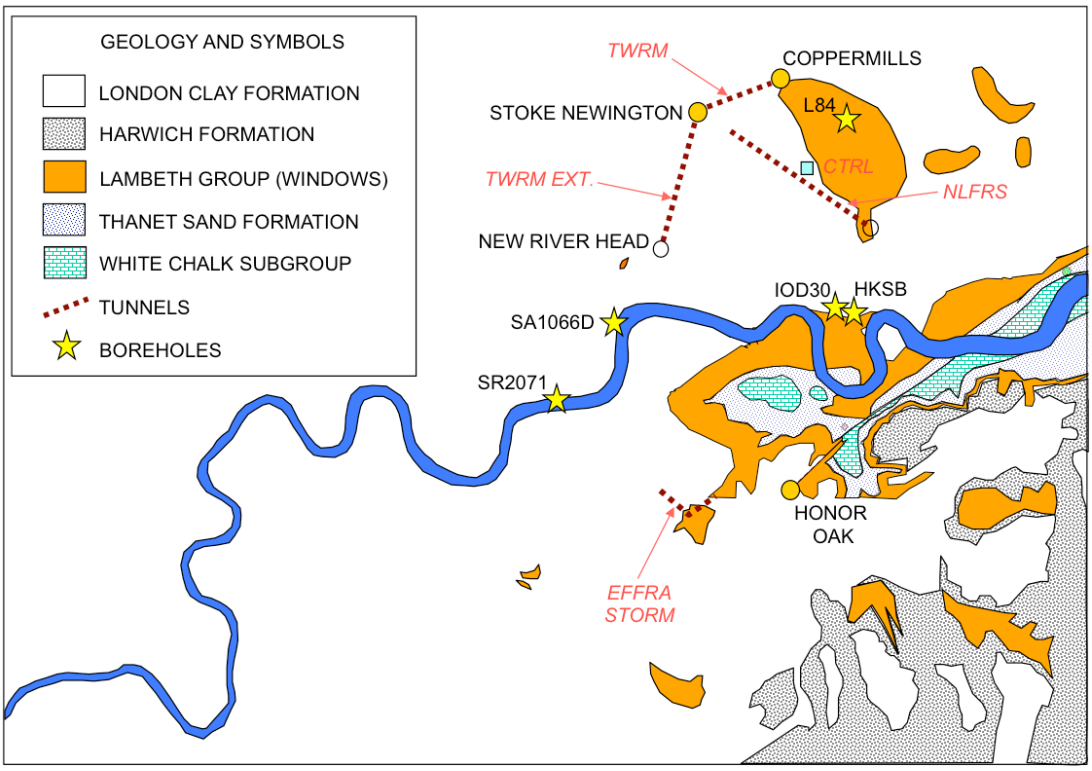


Figure 2.9 The 'Windows of London'

Figure based on Flavin and Joseph (1983)

Oxidised groundwater is introduced during recharge in northern and southern Chalk outcrops (i.e., The Chiltern Hills and North Downs respectively), flowing towards the central London area via a highly conductive fracture and fissure system (as opposed to the restrictive interstitial pore network). Elliot et al. (1999) suggest that during this migration water-rock interactions cause depletion of dissolved oxygen within the groundwater. However, replenishment of dissolved oxygen is likely to be gained (Table 2.3) during admixture of oxidising waters percolating through the Palaeogene cover, in particular the above-mentioned 'windows'.

Table 2.3 Average recorded values of dissolved oxygen

Borehole Reference	Oxygen (mg/litre)	Dissolved O_2 (% saturation)	% O_2 in cavitated air
SR6907	1.1	10.0	4.9
SR6908	5.4	47.0	20.0
SR6905	2.7	24.0	11.0
SR1055	1.0	9.5	4.4
SR1033H	3.4	27.0	12.6
SR3007	2.5	22.0	10.4
SR1028	3.8	33.0	15.0
SR4117	3.2	28.0	13.0
SR6902D	2.0	18.0	8.5
SR4114	3.8	33.0	15.0
SR4087	2.6	23.0	10.8

Data from the Tideway Tunnel ground investigation (Figure 2.10) shows a more complex pattern of dissolved oxygen with local depletions within partially to fully saturated groundwater.

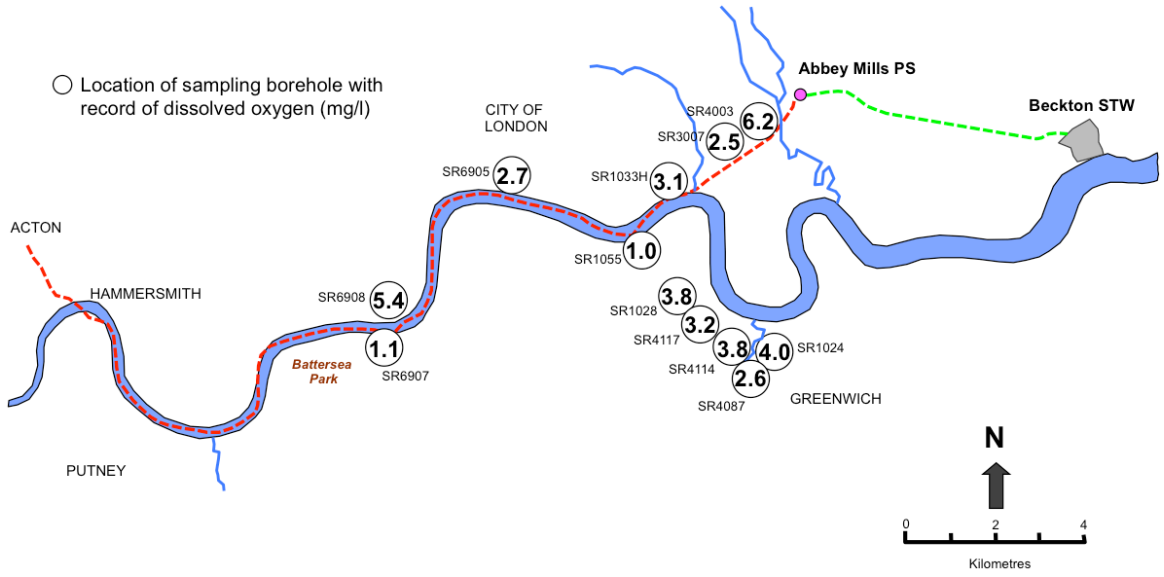


Figure 2.10 Location of Tideway Tunnel groundwater sampling boreholes

Recent research suggests that cavitation during drawdown of the lower aquifer releases air into the surrounding dewatered ground (Standing et al., 2013). Oxidation of minerals in the soil then consumes all the available oxygen so that the remaining cavitated gas is predominantly nitrogen.

The inquest into the fatalities at Stoke Newington (CNPlus, 1991) concurred that historic lowering of London's groundwater table was responsible as a mechanism in producing an oxygen-deficient atmosphere during underground construction. However, it was the first to propose that this caused oxidation of the mineral glauconite within the (dewatered) Upnor Formation. Although (to the author's knowledge) there has been no further research into this mechanism, the UK tunnelling industry accepts it to be the primary cause of confined space hypoxia in the Upnor Formation of the Lambeth Group.

This is reiterated in industry guidance (Hight et al., 2004) whereby:

> "There is a potential for oxygen depletion within sand-bearing strata especially those containing the clay mineral glauconite."
>
> "…..low oxygen contents have been encountered in the Upnor Formation where dewatered."
>
> "Glauconite rapidly oxidises on exposure to air and in a confined environment within a tunnel this may lead to the reduction of oxygen in the air."

Based on evidence gained during the investigation for the NLFRS, Lewis and Harris (1998) further suggested that the recovery of the groundwater table leads to a piston-like compression of the oxygen-depleted gas, beneath a continuous impermeable/low permeability stratum; in this case, the Lower Mottled Beds. There may even be localized concentrations of deoxygenated gas within structural traps such as anticlines or fault zones (horsts).

2.4.2 Fluctuations in the lower aquifer

Fluctuations in the level of the groundwater table appear to control the occurrence of confined space hypoxia. The Upnor Formation is known to be in hydraulic connection with the Chalk, via the Thanet Sand Formation. Together, these strata form London's 'lower aquifer' (Simpson et al., 1989). In its natural state, prior to any significant human influence, the lower aquifer was under artesian pressure (Figure 2.11a) and confined between the overlying Lower Mottled Beds and the Chalk Marl of the White Chalk Subgroup below.

Over-abstraction of the lower aquifer began in the early 1800s, rising steadily from approximately 9×10^6 m^3 a^{-1} to a peak of 83×10^6 m^3 a^{-1} by 1940 (Hurst and Wilkinson, 1986). This led to a significant lowering of the groundwater table and formation of a large cone of depression beneath west central London (Figure 2.11b), first recognised in 1820 and extensively developed by 1850 (Marsh and Davies, 1983). From 1940, the rate of groundwater abstraction from the lower aquifer reduced significantly following the destruction of a large number of abstraction wells during World War II and the control of abstraction by the 1945 Water Act (Wilkinson, 1985). Escalating costs, due to the increasing

depth of abstraction and a reduction in industrial requirement, limited the number of new wells constructed. Nonetheless, continued pumping had lowered the groundwater table by more than 70 m by 1965 (Figure 2.11c) in the centre of the cone of depression (Simpson et al., 1989). This was the lowest level on record and equated to 1.03×10^9 m^3 of water abstracted from the more than 1.2×10^{10} m^3 volume of the lower aquifer (Flavin and Joseph, 1983) over an area in excess of 200 km^2 (Marsh and Davies, 1983). The centre of this cone of depression was located close to Charing Cross and Trafalgar Square but a significant area of drawdown also occurred within the Lee Valley, near Thames Water's Abbey Mills Pumping Station site.

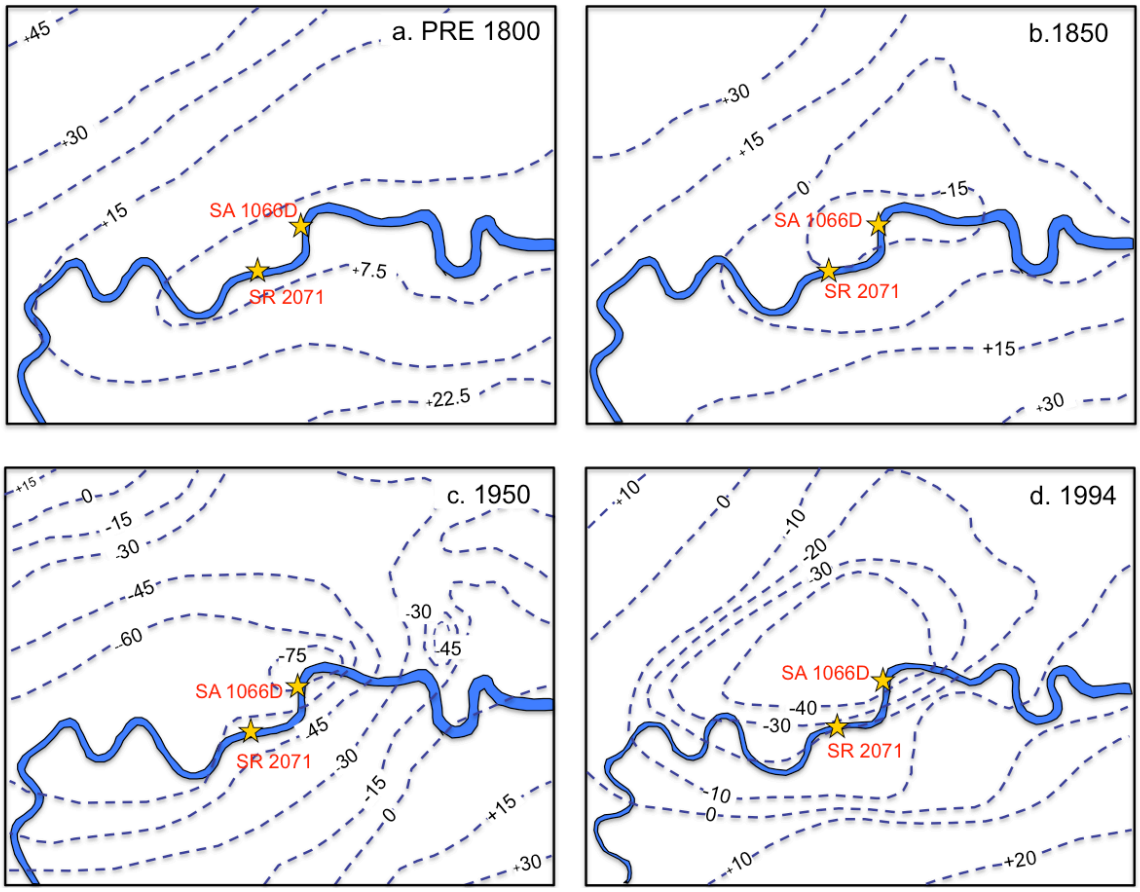


Figure 2.11 Changing groundwater table contours for the lower aquifer

a, b and c from Marsh and Davies (1983); d from Lucas and Robinson (1995); contours in metres OD.

From 1965, the rate of groundwater abstraction from the lower aquifer decreased by between 30 and 50%, from approximately 6.2×10^7 m^3 a^{-1} in 1965 to approximately 4.3×10^7 m^3 a^{-1} by 1982 (Wilkinson, 1985). This was due to the demise of heavy industry and resulted in a rise in the groundwater table. Estimates of the rate of rise vary, from 1.5 m a^{-1} (Simpson et al., 1989) to 2.5 m a^{-1} (Lucas and Robinson, 1995), to more recently 3.0 m a^{-1} (Jones, 2007). The greatest recovery is within the west central London cone of depression, which had risen 20 m by 1988. By 1994 the cone of depression had also significantly reduced its aerial extent, becoming confined to an area between Hammersmith and central London, mainly north of the River

Thames (Figure 2.11d). Most of the change between lowest recorded levels and highest rate of recovery encompasses an area between Hammersmith in West London and the section of the north bank of the River Thames between Chelsea and Victoria Embankments.

By the late 1980s the continued rise in groundwater level was recognised as a risk to deep tunnels and basements by changing the ground engineering properties and potentially causing flooding. In response, the GARDIT (General Aquifer Research Development and Investigation Team) strategy was launched in 1998 to control the rising groundwater by abstraction of 70 Ml per day (2.56×10^4 m^3 a^{-1}) on a schedule up to 2004. However, Thames Water and Environment Agency groundwater modelling demonstrated in 2000 that this rate was too high (Jones, 2007) and should be reduced to 50 Ml per day (1.83×10^7 m^3 a^{-1}). Continued monitoring demonstrates the success of GARDIT, with groundwater levels now broadly stable throughout central London.

2.4.3 Effects of barometric pressure

During the ground investigation for the NLFRS tunnel, Lewis and Harris (1998) noted that levels of oxygen depletion, within a number of the project boreholes, were greater during periods of lower barometric pressure. Based on this, a direct link between oxygen depletion and barometric pressure was suspected.

Prior to this, seasonal influences were investigated (Bell and Whaite, 1957; MacLean, 1966), whereby during cooler winter months air in a well would be relatively warmer than that at the surface and would tend to rise and mix with the outside atmosphere, resulting in higher values of oxygen. The temperature of the air in the bottom of the borehole must be at least 4.2˚C above outside air temperature for mixing to occur. In warmer summer months, the air in a well will be relatively colder than at the surface; there would be little or no tendency for the air to circulate that would therefore stagnate and result in low oxygen levels.

MacLean (1966) proposed a further correlation between barometric pressure and oxygen content within boreholes. An important contributing factor to this was that the borehole is unlined and situated above the groundwater table. When the barometric pressure falls below 1013 mb (i.e., normal atmospheric pressure) the air in soil pore spaces expands (according to Boyle's Law), resulting in the release of oxygen-depleted ("foul") air and the borehole "blowing". When barometric pressure is greater than 1013 mb the opposite occurs and air is sucked in from the atmosphere. The extent of this phenomenon in boreholes is widespread and overrides the effects of the ambient air temperature. In doing so, a borehole is able to communicate with the atmosphere as a huge air barometer.

The same mechanism was noted during a borehole investigation at the LUL tunnel at Old Street (Bird et al., 1989; Bracegirdle et al., 1996). Here, a strong flow of gas was recorded

exiting standpipe piezometers during low barometric pressure (965 mb). Furthermore, over the period of investigation, changes in barometric pressure resulted in the transfer of gas backwards and forward through the tunnel lining. It is suspected that this is the same principle applying to the transfer of gas through the NLFRS tunnel lining, as discussed previously in Section 2.3.3. The "blowing" of air from a borehole because of rising groundwater, for example during recovery after a pump test, is an entirely different mechanism (D. Nicholson, *pers. comm.*).

Most of the research by MacLean (1966) was based on observations of wells in chalk. It was noted that high levels of carbon dioxide are not characteristic of the atmosphere in chalk excavations, rather that the gas is emitted during falling barometric pressure and that the oxygen content is merely replaced within the confined space of the well. This observation was used to verify that gases mix freely in all proportions and dispel the theory that carbon dioxide would sink to the bottom of the well or shaft.

2.4.4 Chemical-oxygen demand

It has been suggested that changes in barometric pressure are relatively minor factors in altering the oxygen content of air in underground excavations (Michaelsen and Park, 1954). Of greater importance is the presence of organic matter and/or other extraneous materials within the soil that have a chemical-oxygen demand.

As mentioned in Section 2.4.1, the mineral glauconite has long been suspected as the potential cause of oxygen-depletion within the TWRM shaft at Stoke Newington (Thames Water, 1988; CNPlus, 1991). This was based on the proposals in a report by Soil Mechanics Ltd (1986) for Thames Water (Authority) that stated:

> "the presence of such materials (glauconite) presents a potential hazard to tunnelling: on exposure, glauconite rapidly oxidises and this can rob the tunnel atmosphere of oxygen."

It is not known what type of experiments were performed to base this conclusion on.

A similar theme has been proposed by Kohyama and Hayashi (1972) who report on "many accidents" in association with oxygen deficiency in confined, poorly ventilated sections of underground quarry workings in the Oya, Tochigi Prefecture in Japan. The quarrying extracts a tuffaceous volcanic rock, known locally as "Oya-ishi", for use as a building stone, with some of the workings extending up to 100 m underground. The Oya-ishi contains many volcanic rock fragments, known as "Miso" comprising a mixture of ferrous smectite compounds, likely to be green rust, which are stable within a reducing environment. They are dark blue-green in colour although, on exposure to air, oxidise first to black within a few hours and eventually brown after a few weeks in the laboratory. During this process, the ferrous smectitic

compounds alter to ferric smectitic compounds without any iron oxide impurities. Further experimental work by Kohyama and Hayashi (1972) indicated that as much as 105 ml of oxygen was consumed by a 10 g sample of the blue-green "Miso" within 48 hours, turning brown as an end result. During this process, the sample reduced in weight by up to 50% due to the expulsion of interlayer water.

A case report by Zugibe et al. (1987) investigated the cause of death of two meter readers who were found dead in the bottom of an underground manhole chamber. It was concluded that the deaths were as a result of asphyxiation, caused by depleted oxygen during microbial activity within the chamber. Evidence suggested that the chamber acted as a collection sump for surface run-off water contaminated with organic material from an adjacent refuse depot. It was deduced that microorganisms, within the water, fed on the organic material, consuming oxygen and producing carbon dioxide during the process of decomposition. Based on the results of air quality tests, it was probable that the level of oxygen within the chamber reduced to below 15% whilst that of carbon dioxide increased to 2.5%. There was no evidence of either methane or hydrogen sulphide.

2.5 Containment of ground gas by an impermeable barrier

In the case of the NLFRS and recent Tideway Tunnel investigation boreholes, it is suspected that the deoxygenated, pressurised, gas within the Upnor Formation has been contained by a 'cap rock' or 'top seal' (Kaldi et al., 2010) that prevents leakage of the buoyant gas into the overlying strata or to the ground surface.

Many effective top seals are mud rocks and clays (Ingram and Urai, 1999) that, if water saturated, will act as a significant barrier to fluid and gas migration (Harrington and Horseman, 1999). Within the London Basin geological sequence, the cohesive Lower Mottled Beds are considered to act as an effective top seal to the oxygen-depleted gas produced in the underlying granular Upnor Formation (Lewis and Harris, 1998).

A perfect top seal will have: (i) very small pores, (ii) be ductile so that it will not yield by brittle fracturing, and (iii) be thick and laterally continuous (Schowalter, 1979).

Because of its low permeability and correspondingly high capillary entry pressures, gas is unlikely to enter the top seal by Darcy flow (Schlömer and Krooss, 1997; Ingram and Urai, 1999). It must be thick enough to maintain an effective seal across faults that might have displaced it and be of sufficient lateral extent, usually basin-wide, to cover the gas storage reservoir (Kaldi et al., 2010).

Experimental research (Standing et al., 2013) has shown that these conditions exist in the Lambeth Group sediments beneath London. The Lower Mottled Beds in particular have significant air-entry values (similar to the London Clay Formation) and hence prevent upward

migration of gas from the more granular underlying beds during dewatering. In addition, the lower air-entry values of the underlying granular beds allow cavitation to occur at lower suction values in these beds.

An estimate of the air-entry value (AEV) is gained through construction of a soil water retention curve (SWRC) which defines the relationship between soil suction and water content (Barbour, 1998; Vanapalli et al., 1999). This comprises a primary drying curve (PDC), formed from drying a soil from a slurry form to the residual condition and a primary wetting curve (PWC) from wetting from the residual point (Figure 2.12). All other curves (i.e., scanning) are assumed to lie within the envelope between the PDC and PWC (J. Standing, *pers. comm.*). The AEV represents the point at which air begins to enter the soil voids upon desaturation and is obtained by extending the constant slope portion of the drying curve to intersect the suction axis at 100% (Vanapalli et al., 1999). The beginning of residual conditions are at the degree of saturation where the liquid phase becomes discontinuous and is obtained by extending the constant slope portion of the drying curve to intersect a line tangential to the end section of the drying curve.

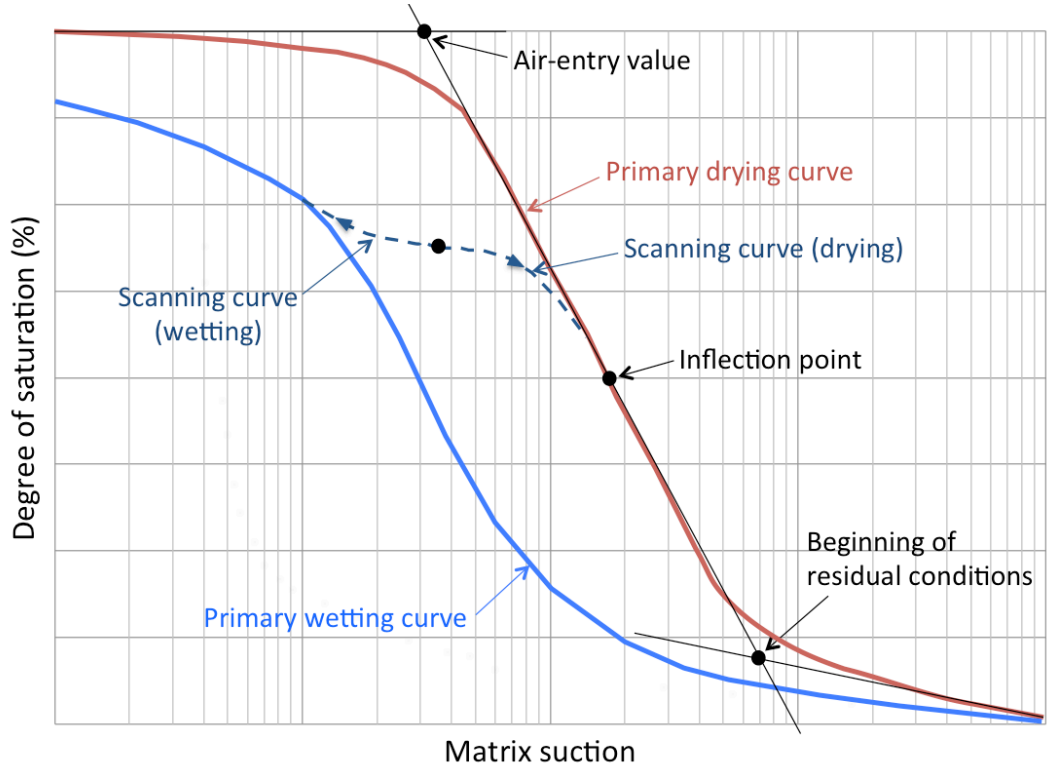


Figure 2.12 Example of a soil water retention curve (SWRC)

Seal failure is unlikely for top seals with high capillary entry pressures. Usually, seals are partially or fully saturated and no hydrodynamic flow exists (Watts, 1987). However, if forces that drive migration exceed the resistance of a barrier, gas and fluids will move by exploiting 'preferential pathways' (Harrington and Horseman, 1999) and an interconnected flow-path forms across the pore system of the top seal (Schlömer and Krooss, 1997); this occurs when:

- Tectonic fault displacements occur in excess of seal thickness. In addition, faults could act as conduits to flow through a seal and where a high density of faults exist, a permeable network of dilatant faults and fractures will exist;
- There is tensile fracturing under extreme fluid pressure conditions; and/or
- There is a network of juxtaposed thin leaky beds across sub-seismic faults, i.e., seals may leak if faults are sufficiently numerous and their throws great enough to create a connected network of juxtaposed leaky beds (Ingram and Urai, 1999).

Alternatively, if the driving force (buoyancy) exceeds the retarding forces (displacement pressure), gas will displace water from the confining pore throats of the rock/soil (Schowalter, 1979) and leakage will take place along the largest interconnected pore throats (Watts, 1987).

3 THE LOWER LAMBETH GROUP DEPOSITS

3.1 Introduction

This research forms part of the wider ground investigation for the engineering design of Thames Water's 25 km long Thames Tideway Tunnel (hereafter referred to as the Tideway Tunnel). The tunnel is planned for construction between Acton, West London and Abbey Mills in Stratford, East London (Newman and Hadlow, 2011) and is part of the overall London Tideway Tunnels (LTT) scheme (Figure 3.1). This also incorporates the Lee Tunnel, currently under construction between Abbey Mills and Beckton Sewage Treatment Works (STW) in the Thames Gateway area (Jewell and O'Conner, 2012).

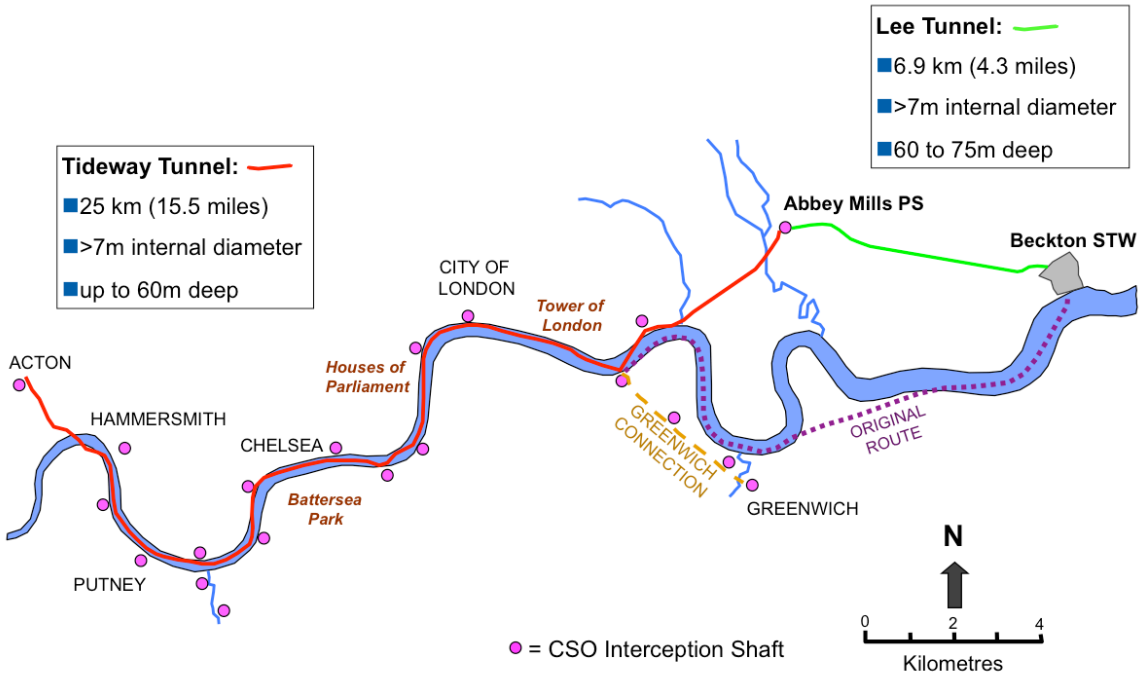


Figure 3.1 The London Tideway Tunnels alignment

To date, ground investigation for the Tideway Tunnel has included (but not been limited to) six phases of intrusive borehole investigations (series 1000 to 6000 inclusive). These have amounted to 301 rotary core and cable percussion boreholes and two trial sonic drill boreholes, of which 194 have intersected Lambeth Group deposits (Figure 3.2). Experience gained through these in understanding the geotechnical nature of the deposits has been supplemented by borehole investigations for the Lee Tunnel (Skipper et al., 2008) and previous investigations for the TWRM north and south extensions, from Stoke Newington to New River Head (Newman et al., 2010) and Brixton to Honor Oak (Newman and Wong, 2011) respectively. Further experience has been gained during construction phases of these tunnelling projects.

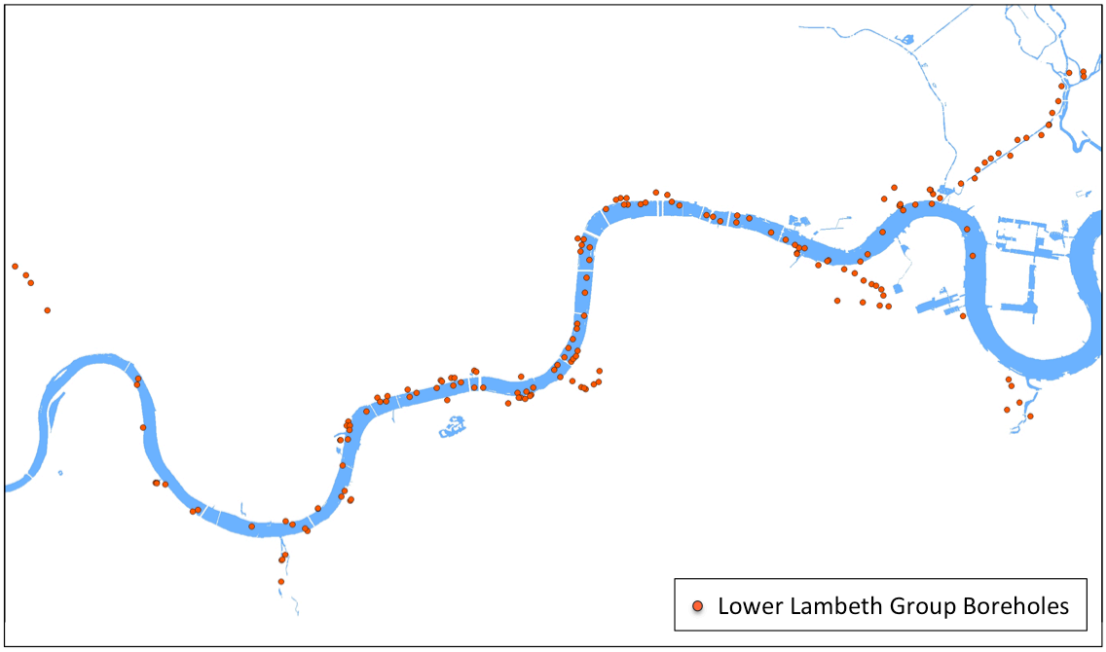


Figure 3.2 Tideway Tunnel boreholes intersecting the Lambeth Group

In this chapter the Lower Mottled Beds and Upnor Formation of the Lower Lambeth Group, together with the underlying Thanet Sand Formation, are discussed based on findings from the Tideway Tunnel investigation, with comparisons made to published literature. A number of geotechnical classification tests, such as Atterberg Limit and Particle Size Distribution (PSD) tests, have been undertaken to characterise the respective deposits.

The Atterberg Limit tests were used to identify the soil water contents at the boundaries of the liquid limit (LL) and plastic limit (PL), where the soil exists as liquid and solid states respectively. The range between these is referred to as the plasticity index (PI), in which the soil exists in a plastic state. A plasticity index below 10 is found in soils of low plasticity, 10 to 20 is medium plasticity, 20 to 40 is high plasticity and above 40 it is very highly plastic.

The Activity (A) of a soil can be gauged on the ratio between its clay content and plasticity index. The Activity provides an indication of how much wetting or drying would be required to move a soil from one state to another, for example across the liquid limit. Normally, soils fall within an Activity range of between 0.75 and 1.25. Soil below this range is inactive.

The uniformity coefficient (C_u) is derived from the PSD test and is an expression of the uniformity in the grain size of a soil, reflecting the ratio between values of D_{60} and D_{10}. A soil is considered uniform when it is not well graded, i.e., does not possess a wide range in particle sizes. A soil with a uniformity coefficient of less than 2 is considered 'uniform' (Lambe and Whitman, 1979). For gravels and sands, a uniformity coefficient of less than 4 and 6 respectively indicates uniform soil.

A summary of the geotechnical parameters is outlined in Table 3.1 although these will be discussed in further detail where appropriate.

Table 3.1 Summary of soil classification tests

Parameter	LMB	UPN	TSF
LL (%)	24 – 85	26 – 80	30 – 55
PL (%)	10 – 33	14 – 33	15 – 31
PI (%)	5 - 65	4 – 47	7 - 32
A	0.58 – 0.64 (typical)	0.72 – 1.33	N/a
Class	CI – CV (west) CI – CH (east)	CL - CI	N/a
C_u	N/a	32 – 210 (PB) 33 -140 (GS)	<4.5

LMB = Lower Mottled Beds; UPN = Upnor Formation; TSF = Thanet Sand Formation; PB = Pebble Bed; GS = Glauconitic Sand. For Class, 'C' indicates clay of: 'L' low plasticity; 'I' intermediate plasticity; 'H' high plasticity; 'V' very high plasticity.

3.2 The Lambeth Group

The Lambeth Group deposits comprise the Woolwich, Reading and Upnor formations (Figure 3.3) and underlie much of southern England, particularly the London and Hampshire Basins. They form a complex and highly variable sequence of clays, sands and gravels of Palaeogene age (Hight et al., 2004).

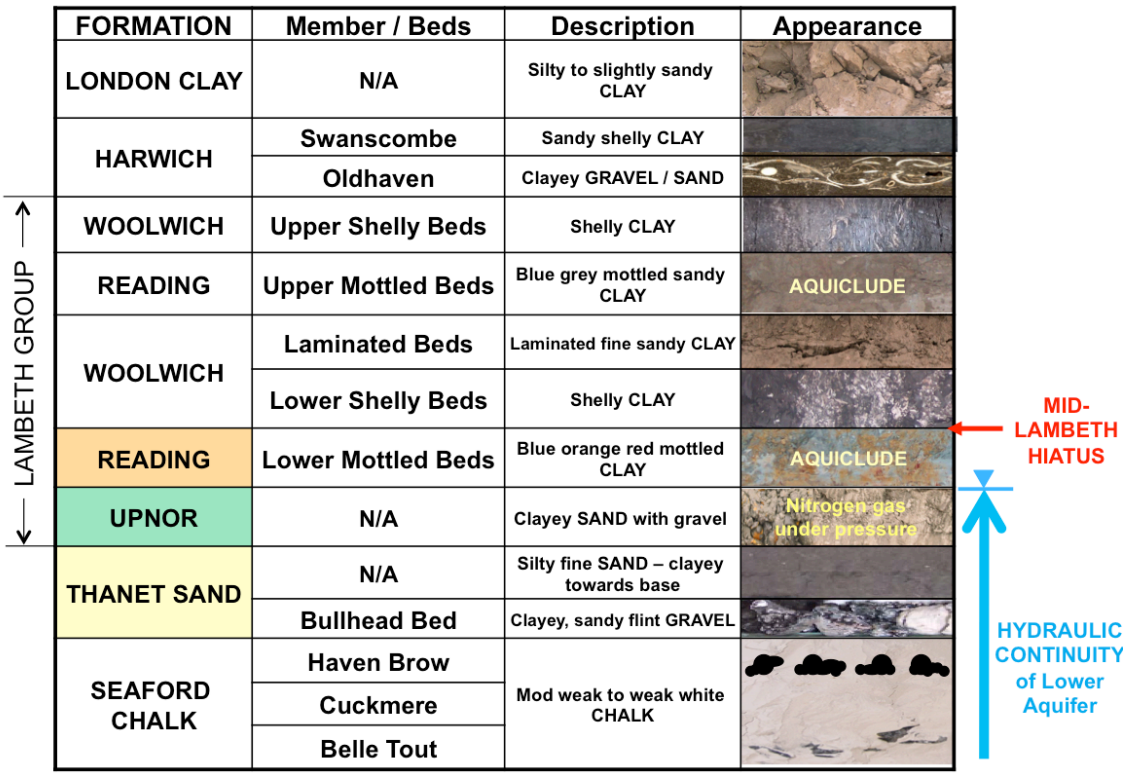


Figure 3.3 The geological succession for London

Figure from Newman et al. (2013)

The group lies unconformably on the Thanet Sand Formation throughout the entire London Basin and to the west, oversteps this onto the Chalk (Ellison, 1983; Ellison et al., 1994; Ellison et al., 1996; Page and Skipper, 2000). The maximum thickness occurs in Chertsey, Surrey, where up to 30 m has been encountered (Hester, 1965). However, across the Tideway Tunnel scheme within central London, where construction is anticipated to intersect the group, the thickness is typically between 16.2 and 21 m (Figure 3.4), increasing slightly towards the west. The deposits are expected at between 20 and 66 m beneath the surface, respectively between Acton in the west and Abbey Mills in the east of the scheme, as displayed by the geological model in Figure 3.5.

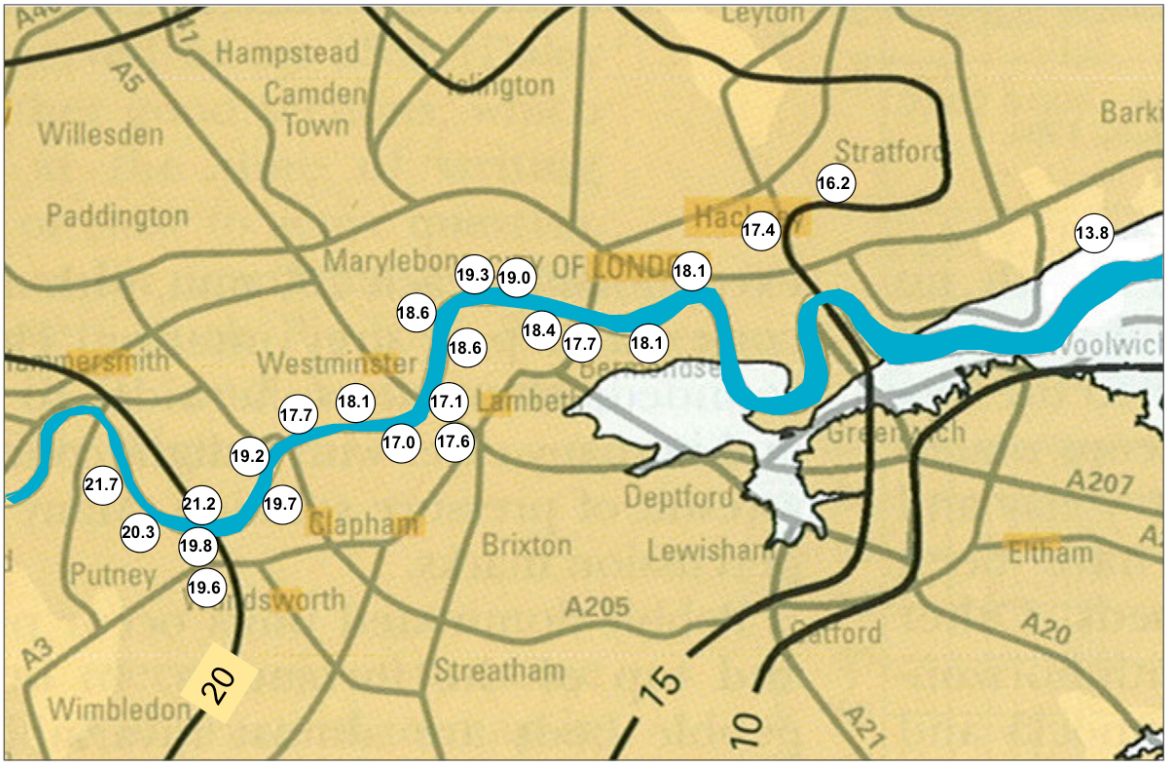


Figure 3.4 **The thickness of the Lambeth Group deposits in London**

Figure based on Ellison et al. (2004)

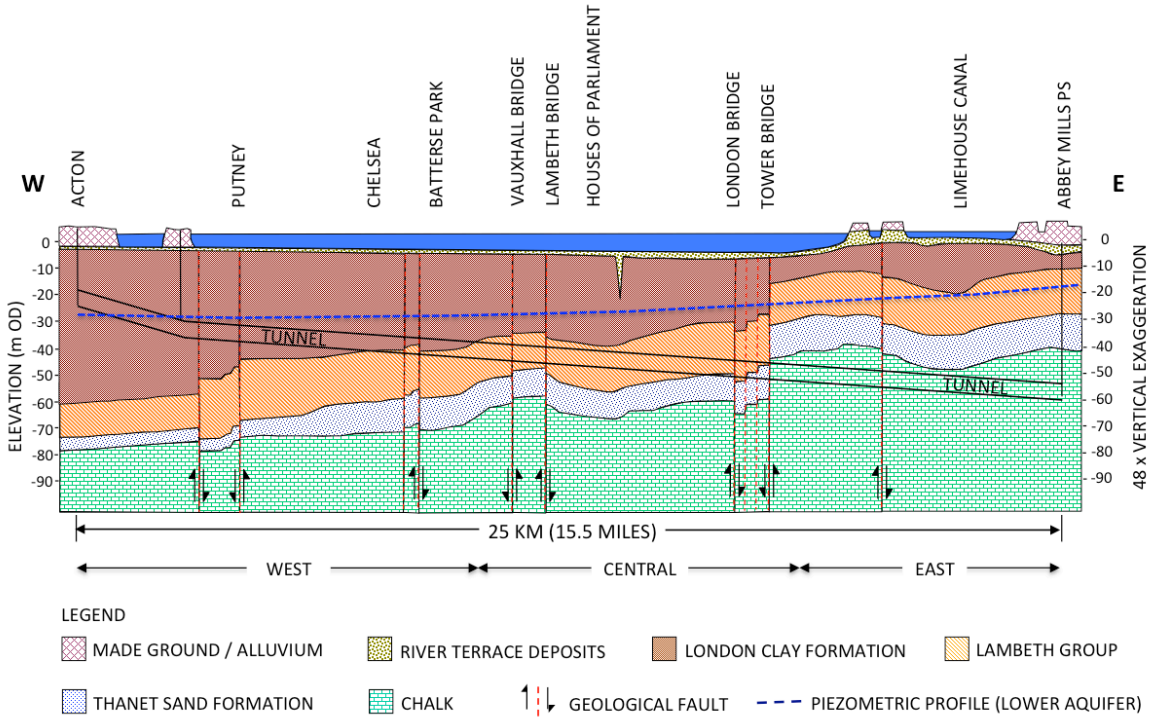


Figure 3.5 **The Thames Tideway Tunnel – geological model**

The term Lambeth Group was introduced in 1994 under a revised classification scheme by Ellison et al. (1994). Prior to this, the group was referred to as the 'Woolwich & Reading Beds', in which the Upnor Formation was known as the 'Bottom Bed' (Hester, 1965). Page and

Skipper (2000) recognised a poor understanding of the Lambeth Group deposits within the civil engineering industry and suggested that no other group of sediments within the UK displays such a range of textures and fabrics within such a small stratigraphic thickness. The deposits are likely to be encountered more frequently during future underground construction in London.

3.2.2 Environment of deposition

The Lambeth Group sediments were deposited in the London and Hampshire Basins approximately 56 to 55 Ma ago, on the western edge of a fault-bound, rapidly subsiding, deep-water marine basin, centred on the present North Sea (Ellison, 1983; Page and Skipper, 2000; Hight et al., 2004). During deposition, a highland area lay to the northwest, in the present day area of Wales, with a broad, topographically low-lying, alluvial and coastal plain area to the southeast. This gave way to restricted brackish lagoons, separated from the open sea to the east by a barrier of littoral sands and pebble beds, with limited input of terrigenous sediment from the hinterland (Ellison, 1983). Three distinct facies have been deciphered from the palaeogeographical setting (Figure 3.6):

- Reading Formation sediments (mainly fluviatile)
- Woolwich Formation sediments (lagoonal)
- Upnor Formation ('Bottom Bed') sediments (marine)

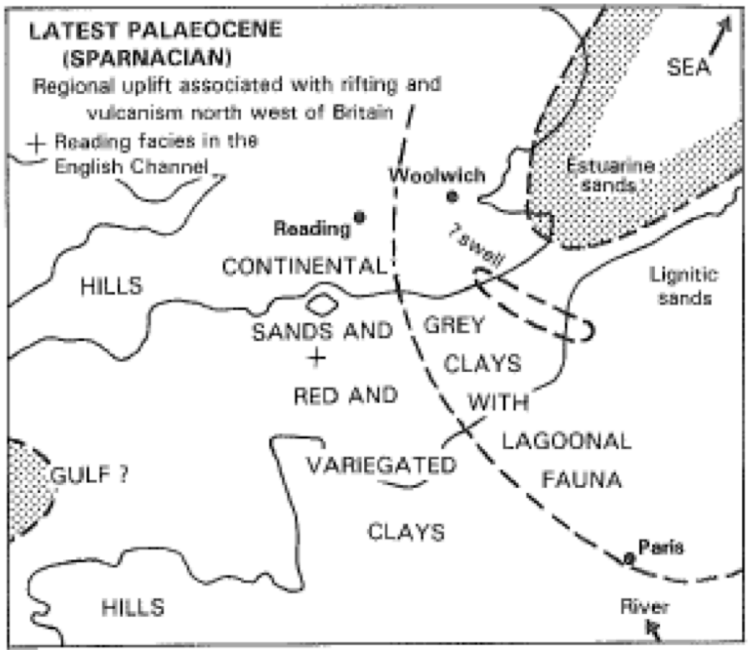


Figure 3.6 The palaeogeographical setting during deposition of the Lambeth Group

Figure from Curry (1992)

These facilitated a wide variety of Lambeth Group sediments (Figure 3.7) including marine sands, brackish lagoonal muds and pedogenic horizons (Hester, 1965; Ellison, 1983; Ellison et al., 1996).

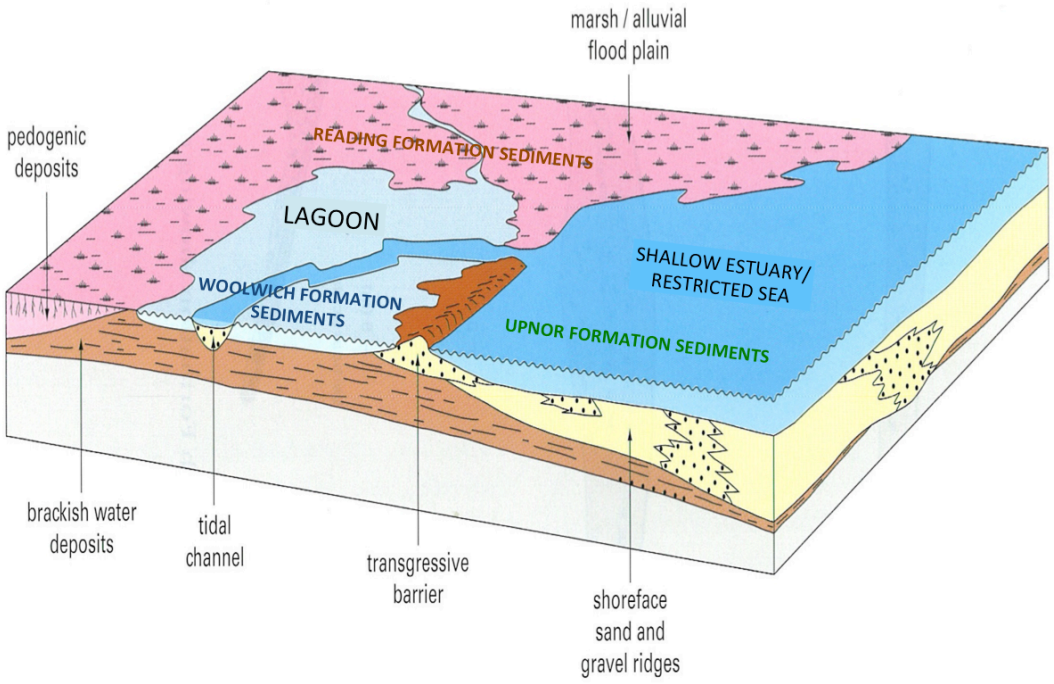


Figure 3.7 Palaeofacies setting during deposition of the Lambeth Group

Figure based on Ellison et al. (2004)

The sea level fluctuated and the shoreline periodically advanced and retreated across the region (Ali and Jolley, 1996). A sea level fall caused a shift in the alluvial sediments eastward, whilst a sea level rise caused a shift in marine sediments westward, i.e., towards land, resulting in diachronous boundaries (Figure 3.8) between the contemporaneous Lambeth Group formations and sharp lateral changes in facies (Knox, 1996; Page and Skipper, 2000).

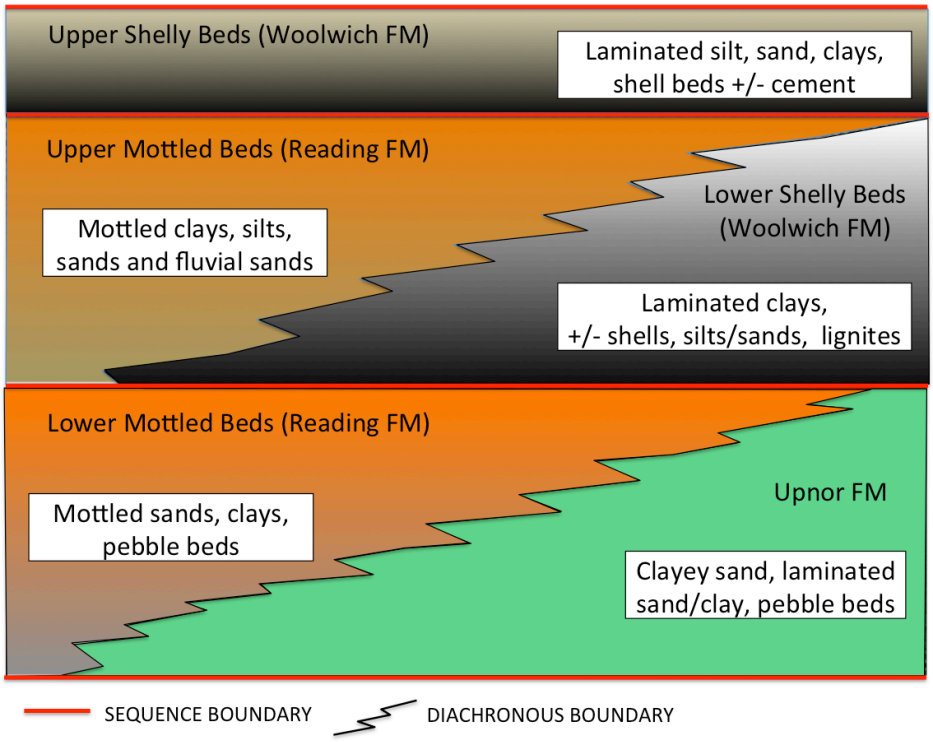


Figure 3.8 Diachronous boundaries between Lambeth Group strata

Figure based on Page and Skipper (2000)

Climatic conditions were sub-tropical, with distinct wet and dry seasons (Hight et al., 2004), similar to present-day South East Asia (Page and Skipper, 2000). Following sea level fall, formerly marine sediments were exposed to sub aerial weathering and pedogenic (soil forming) processes, producing 'palaeo-landsurfaces'.

3.2.3 Thanet Sand Formation

The Thanet Sand Formation is the oldest Palaeogene deposit beneath central London (Ellison et al., 2004) and was deposited in an inner-shelf to coastal marine environment (Ali and Jolley, 1996). It extends across the entire Tideway Tunnel scheme, although reducing in thickness from at most 15 m in the east to 5 m in the west (Figure 3.9), at depths from 35 to 80 m below ground level respectively (Figure 3.5).

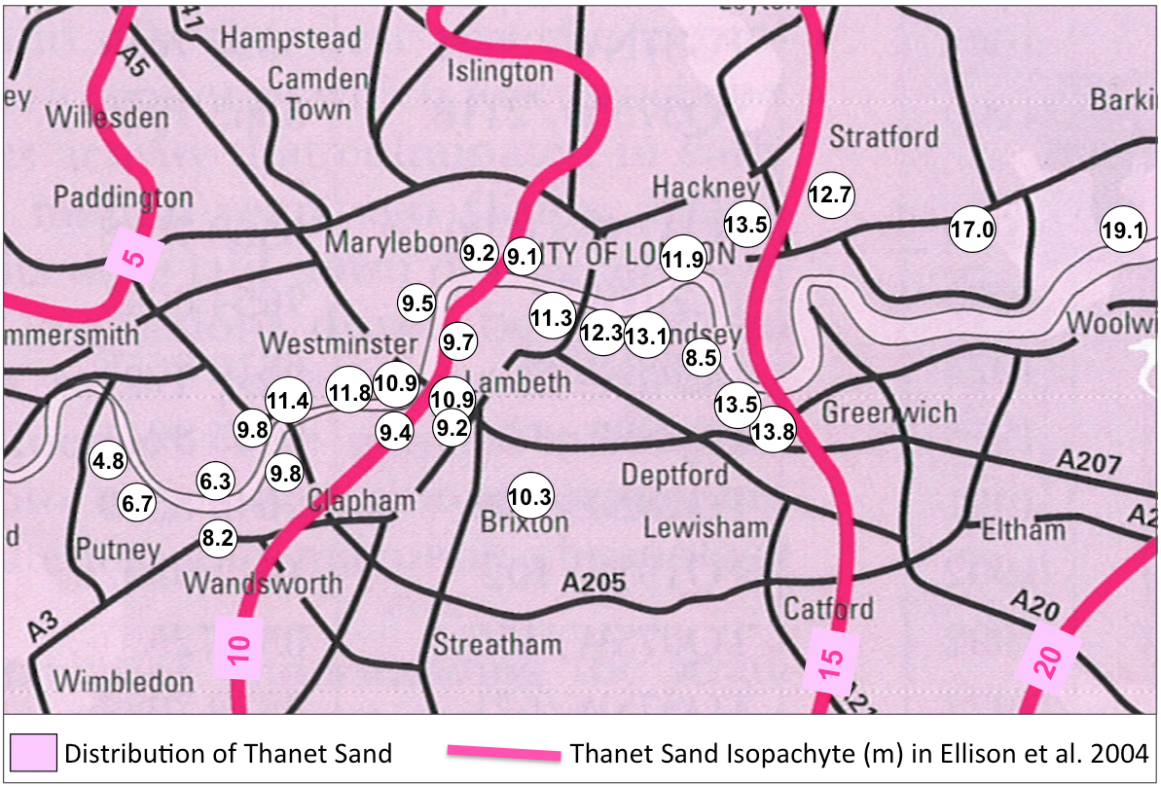


Figure 3.9 Thickness of the Thanet Sand Formation across London

Figure based on Ellison et al. (2004)

The formation lies unconformably over the White Chalk Subgroup and is frequently demarcated at its base by the Bullhead Bed Member (Figure 3.10). This is typically 0.2 to 0.5 m thick, comprising angular to sub-rounded, fine to coarse, to occasionally cobble size, black flint gravel within a fine to coarse sandy clay matrix. The flints are frequently coated in a thin veneer of green glauconite, giving an indication of the prevailing marine conditions (Ali and Jolley, 1996).

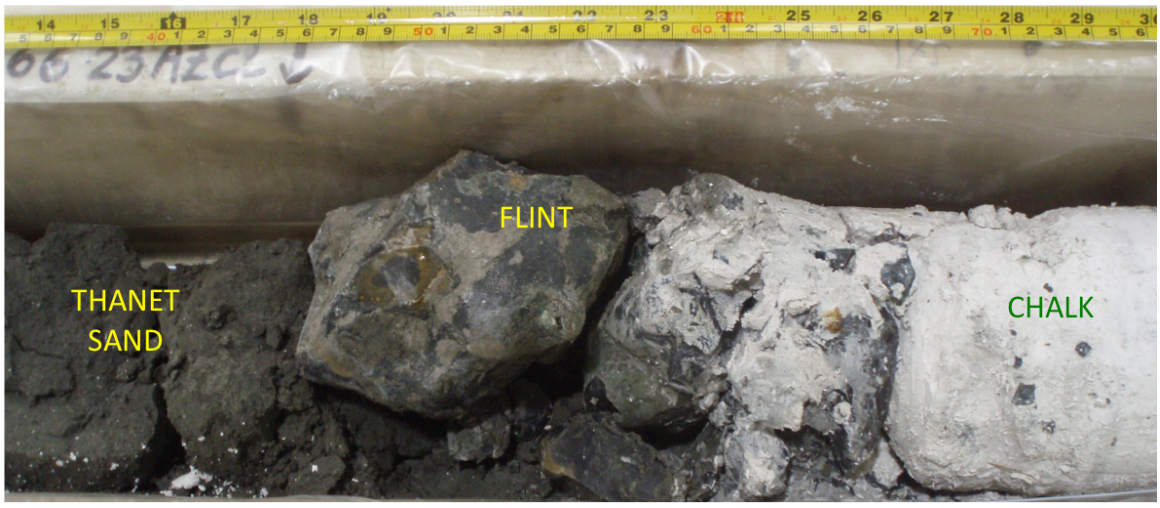


Figure 3.10 Core sample of the Bullhead Bed

Field Description and Geotechnical Character

In the Tideway Tunnel boreholes, the Thanet Sand Formation typically comprises medium to dark grey, silty fine sand (Figure 3.11), weathering to a pale yellowish grey. A coarsening-upward sequence, in which it is noticeably more clayey and silty in the bottom several metres, is prevalent towards the east end of the scheme.



Figure 3.11 Core sample of the Thanet Sand (sample 5015/51)

A very small range in particle size distribution is derived from PSD tests, confirming the material as predominantly silty fine sand (Figure 3.12a), although not including the Bullhead Bed. The Tideway Tunnel PSD data is very similar to that from the British Geological Survey (BGS) Memoir for the Geology of London (Ellison et al., 2004) (Figure 3.12b). Based on the data, the uniformity coefficient (C_u) ranges between 2 and 17, although is nearly always less than 4.5, indicative of a uniform sand.

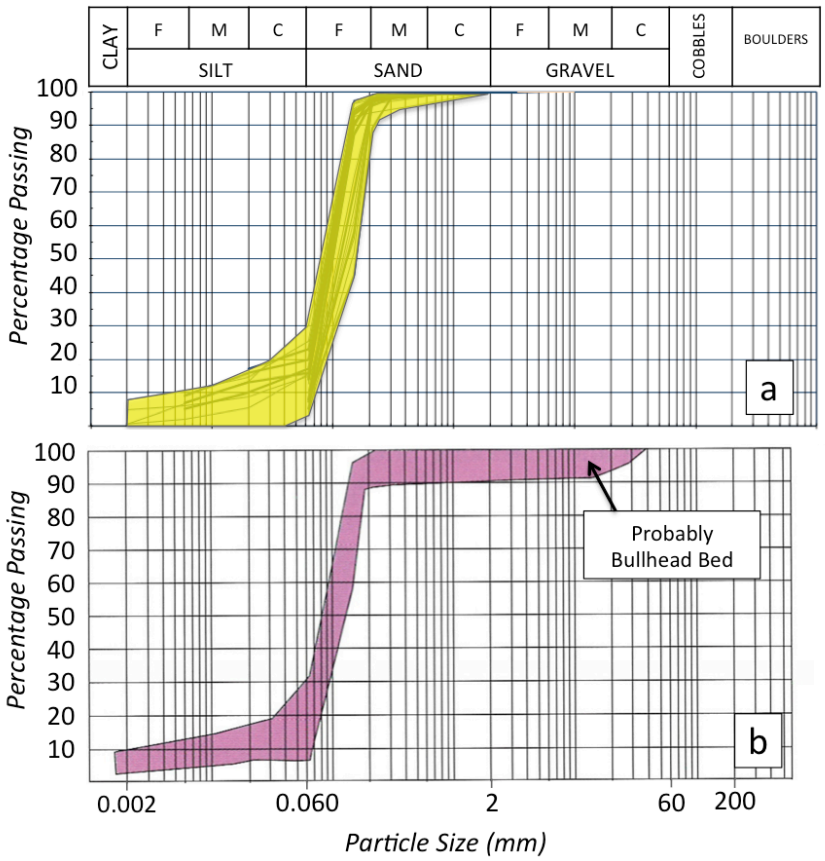


Figure 3.12 Particle Size Distribution for the Thanet Sand

a from Tideway Tunnel; b from Ellison et al. (2004)

The Thanet Sand is intensely bioturbated, resulting in primary sedimentary structures being usually absent. Authigenic pyrite and glauconite are rare, as are detrital glauconite grains and nodules of pyrite, less than 5 mm across, which are sparsely distributed throughout (Ellison et al., 2004).

The top of the Thanet Sand Formation represents a sub-aerial erosion surface whereby the uppermost 4 m of the Thanet Sand was eroded prior to deposition of the younger Lambeth Group sediments. This occurred because of uplift, regression and exposure of the formation approximately 56 Ma ago, resulting in the absence of the magnetostratigraphic polarity unit, Chron C25n, from the stratigraphic record across almost all of southern England (Ali and Jolley, 1996). The duration of this hiatus is estimated to have been between 0.5 Ma (Ali and Jolley, 1996) and 0.6 Ma (Aubry et al., 1986). The top of the remaining Thanet Sand was subjected to decalcification and depletion of heavy mineral assemblages (Morton, 1982).

3.2.4 Upnor Formation

The Upnor Formation forms the basal unit of the Lambeth Group and occurs throughout the London Basin (Hester, 1965). The formation is thickest in the east but generally between 3.5 and 7.0 m thick over the Tideway Tunnel scheme (Figure 3.13), similar to published values of

between 5.0 and 7.0 m in central London (Ellison et al., 1994; Hight et al., 2004). The stratum is between 70 m below ground level (bgl) in the west and 32 m bgl in the east of the scheme (Figure 3.5).

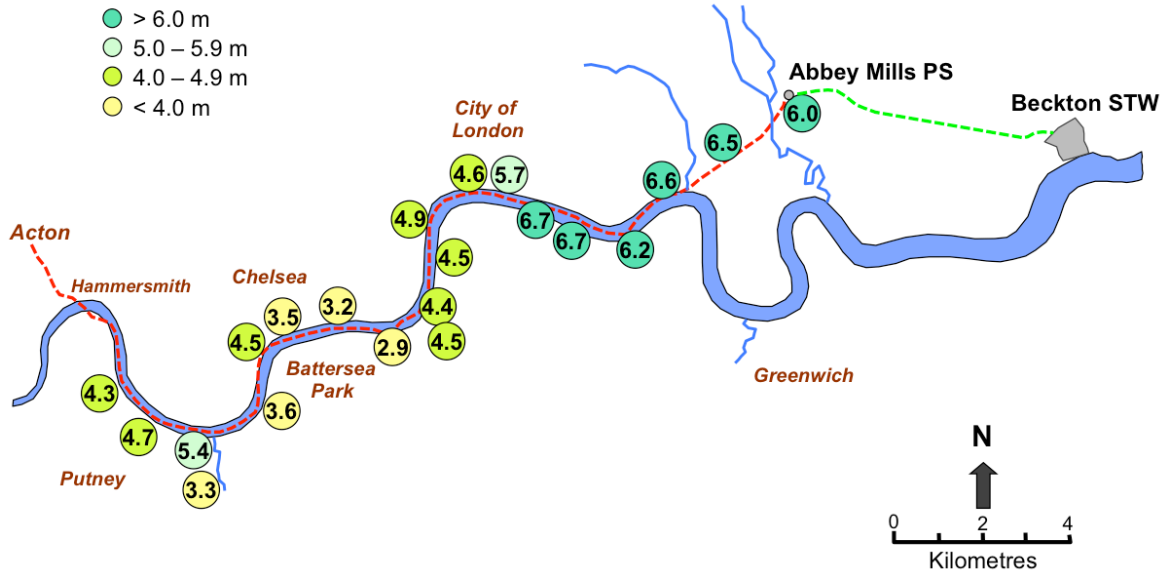


Figure 3.13 Thickness of the Upnor Formation across London

Environment of deposition

The Upnor Formation represents the transgressive stage of the Lambeth Group (Knox, 1996; Ellison et al., 2004) and was deposited in a tidally influenced, shallow marine environment in which the rate of sea level rise was faster than sediment input (Hester, 1965; Ellison, 1983; Skipper, 1999). At the same time, the London Basin (Thames Valley) syncline extended by fault-controlled deepening, rather than uplift of the surrounding areas (Hester, 1965). The formation transgressed over the whole of south-east England during the Chron C25n period, approximately 56 Ma ago (Ali and Jolley, 1996), creating a connection between the Atlantic Ocean and North Sea (Skipper, 1999).

Field Description

The Upnor Formation comprises clayey, silty, fine to medium-grained sands with one or more beds of flint gravel and is rich in glauconite (Hester, 1965; Ali and Jolley, 1996; Skipper, 1999; Page and Skipper, 2000). It is highly variable and may consist of one or all of the above constituents (Hester, 1965), as shown by the wide range in sample descriptions identified during investigation for the Tideway Tunnel. The following three categories, however, predominate:

- Stiff to very stiff, greenish grey to brownish grey, sandy, slightly gravelly to gravelly clay (Figure 3.14a).

- Dense to very dense, greyish green, silty, slightly gravelly to gravelly sand (Figure 3.14b).
- Very dense, sandy, clayey gravel (Figure 3.14c).

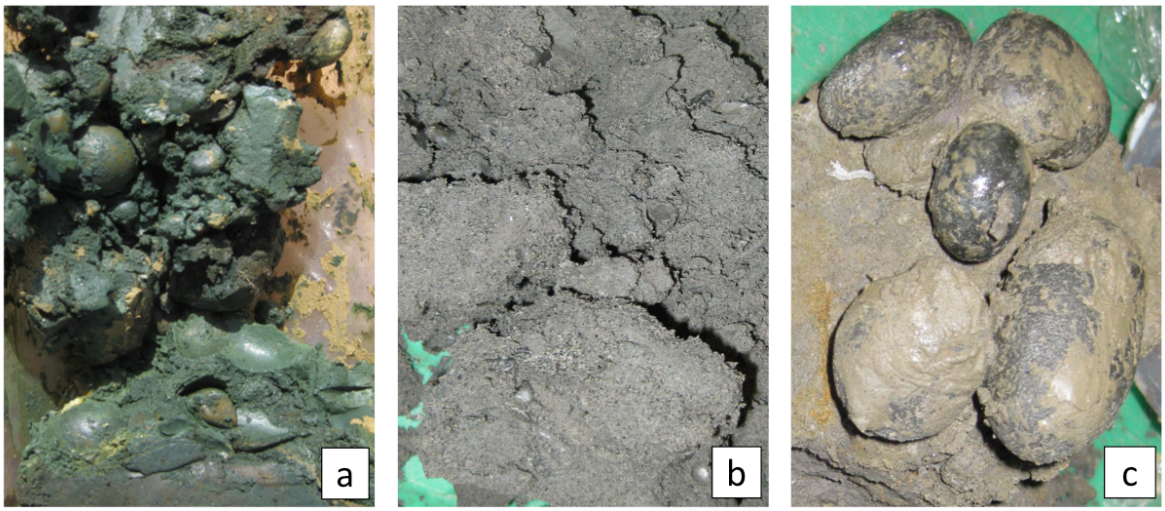


Figure 3.14 A selection of Upnor Formation lithologies

In all of the above descriptions, the sand is recorded as fine to medium whilst the gravel is fine, medium and coarse, sub rounded to rounded black flint.

The base of the Upnor Formation is associated with an inshore, intertidal, wave-cut platform that was swept clear of sediment and commonly affected by glauconite-filled burrows within the top 2 m of the underlying Thanet Sand Formation (Hester, 1965; Ellison et al., 2004).

The abundance of bioturbation (Figure 3.15) and glauconite implies a low sedimentation rate during its deposition; burrowing organisms would otherwise have been continuously buried and unable to feed (Skipper, 1999; Page and Skipper, 2000; Ellison et al., 2004).

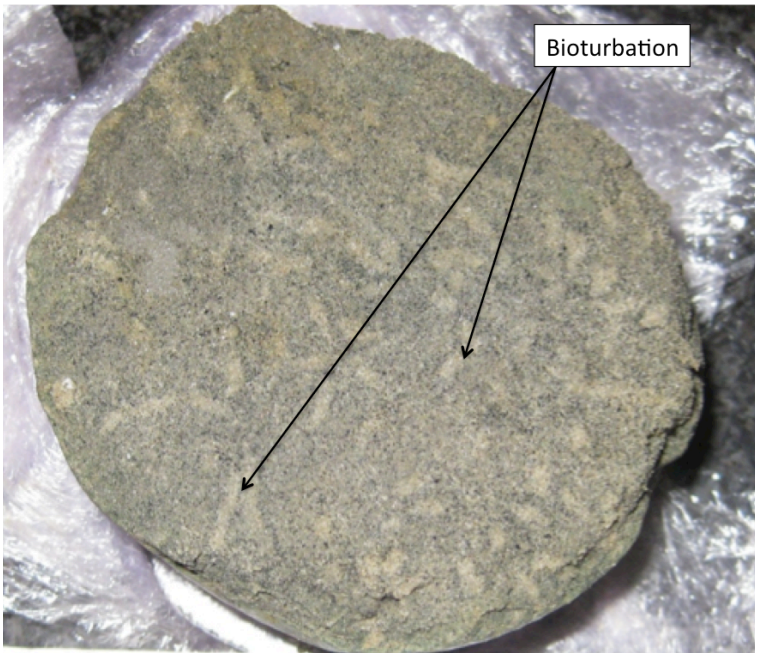


Figure 3.15 Bioturbation structures (sample 5015/44)

On the basis of erosion surfaces and the presence of matrix-supported flint gravel (Figure 3.16), Skipper (1999) proposed that much of the glauconite has been winnowed and concentrated, indicating a high energy environment and degree of reworking.

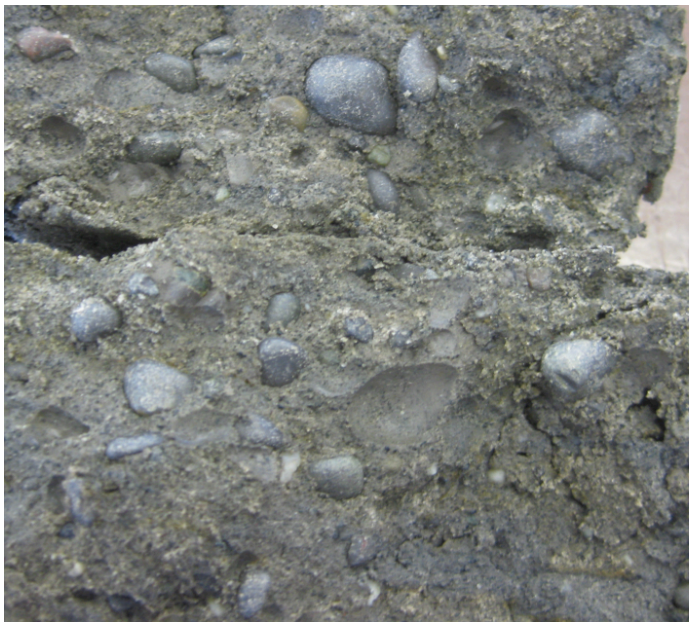


Figure 3.16 Matrix-supported flint gravel (sample 4208/5)

Ellison (1983) identified two main lithofacies groups within the Upnor Formation: the Glauconitic Sand (GS) and the Pebble Beds (PB). These are analogous to the respective Transgressive Pebble Beds and Sands (TPBS) and Pebbly Bedforms (PB) identified by Skipper (1999), as outlined and compared in Table 3.2. An additional two lithofacies groups were identified by Skipper (1999): the Laminated Sands (LS) and Sandy Bedforms (SB). The latter

has not been encountered during recent Thames Water borehole investigations and will not be discussed further.

Table 3.2 A comparison of Upnor Formation lithofacies group terms

Ellison (1983)	Skipper (1999)
Glauconitic Sand	Transgressive Pebble Beds and Sands
Pebble Beds	Pebbly Bedforms
	Laminated Sands
	Sandy Bedforms (cross-bedded sands)*

** not encountered during the Tideway Tunnel investigation*

Glauconitic Sand

The Glauconitic Sand (GS) forms the predominant lithology of the Upnor Formation and is thought to be reworked sediment, transported by rivers flowing from the south (Ellison, 1983). In the Tideway Tunnel boreholes, it is typically green-grey, medium-grained sand and clayey sand with variable amounts of glauconite grains of fine to medium sand grade (Figure 3.17), similar to a number of published descriptions (Ellison, 1983; Ellison et al., 2004; Hight et al., 2004).



Figure 3.17 Glauconitic Sand (TWRM Honor Oak shaft)

Beds and stringers of well-rounded, matrix-supported, black flint gravel are frequently recorded in the Tideway Tunnel core samples and published accounts (Ellison et al., 1994; Ellison et al., 1996).

Ellison et al. (2004) identified non-clay minerals within the Glauconitic Sand as predominantly sub angular, well sorted, quartz, with variable amounts of glauconite, some alkali feldspar, chert, minor mica and traces of calcite.

A number of glauconite 'pulses' are recognised within the Upnor Formation, characterised by a high concentration of the mineral, up to 25% (30% in Entwisle et al. (2013)), and resulting in a stronger green colour. These occurred during flooding events in which there was winnowing and low sediment input (Ellison et al., 1994; Ellison et al., 1996; Hight et al., 2004).

The Glauconitic Sand weathers to pale grey brown or yellow brown, displaying a characteristic speckled "salt and pepper" appearance due to the glauconite remaining dark green-black (Ellison, 1983; Ellison et al., 1994; Ellison et al., 1996; Ellison et al., 2004; Hight et al., 2004).

The clay content within the Upnor Formation is variable, with laminae and local beds of grey clay, up to 300 mm thick, frequently encountered (Figure 3.18) interdigitating with the Glauconitic Sand (Ellison et al., 2004; Hight et al., 2004). These are likely deposited by small rivers that emptied into the shallow sea and may contain carbonaceous material (Hester, 1965).



Figure 3.18 Clay layer within the Glauconitic Sand (sample 5018/60)

In the absence of basal gravel, it may be difficult to distinguish the Glauconitic Sand from the underlying Thanet Sand because of a zone of bioturbation in the top 2 m of the latter, in which the two lithologies are mixed. This was encountered in many of the boreholes across the Tideway Tunnel scheme, where differentiation was based on a colour change from grey Thanet Sand to green-grey Glauconitic Sand. In addition, the Glauconitic Sand has a slightly coarser grade than the Thanet Sand, but with a higher clay percentage. In many of the Tideway Tunnel core hand specimens, it imparted a distinctly 'gritty' feel, as also noted by Ellison et al. (1994) and Hight et al. (2004).

Morton (1982) proposed that the sand content of the Thanet Sand has a Scottish provenance to the north, whilst the Upnor Formation is either from the Armorican or the Ardennes-

Rhenish massifs to the southeast. Regardless, the Upnor Formation has a more diverse heavy mineral assemblage than Thanet Sand Formation.

Laminated Sands

The Laminated Sands, as defined by Skipper (1999), succeed the Transgressive Pebble Beds and Sands (Glauconitic Sand) and comprise parallel laminations of clay and silt or fine sand (Figure 3.19).



Figure 3.19 Laminated Sediments (TWRM northern extension – tunnel face)

Figure from Newman et al. (2010)

They contain very few fossils (mostly pieces of lignite), representing a change to lower energy sedimentation from the Transgressive Pebble Beds and Sands (Glauconitic Sand). Very small amounts of glauconite implies that this was still not a deeper marine environment; the high quantity of plant material indicates a shallow marine environment under tidal influence, most likely at the proximal end of a large estuarine complex, with marine influence lessening with falling sea level. Alternation of sand or silt and clay laminations reflects deposition at rising (higher energy) and ebbing (lower energy) tides.

Skipper (1999) identified a maximum development of this sub-facies in Islington, north London, where up to 7 m have been detected. This was verified during construction of the Thames Water Ring Main extension between Stoke Newington and New River Head (Newman et al., 2010).

Notwithstanding, the Laminated Sands are recorded only sporadically within the Tideway Tunnel core and no pattern of its occurrence is evident.

Pebble Beds

The Pebble Beds (PB) are encountered as sporadic horizons or stringers of well-rounded fine to coarse flint gravel in beds from one clast thick up to about 5 m thick (Page and Skipper, 2000), with the thickest beds usually encountered at the base and top of the formation. They are frequently recorded in Tideway Tunnel boreholes and typically consist of well-rounded, elongate, black flint gravel (Figure 3.20), with a clast size usually between 20 and 30 mm (see Page and Skipper, 2000; Ellison et al., 2004; Hight et al., 2004). The gravel constitutes up to 75% of the sediment (Ellison, 1983), although it is often supported by a very glauconitic pale green to dark green sandy clay or sand matrix containing common *Ostrea bellovacina* fossils (Skipper, 1999).



Figure 3.20 Pebble Bed material recovered in rotary core

A pebble bed is often present at the base of the Upnor Formation (Ellison, 1983), comprising matrix-supported, rounded, black flint gravel where the matrix ranges from glauconitic, dark green sandy clay to clayey sand. The gravel is derived from the erosion of the Chalk, exposed as a wave-cut platform by a period of uplift between the Thanet Sand Formation and Lambeth Group (Ellison, 1983). This is not always observed in the Tideway Tunnel boreholes, but where it is, it often displays evidence of percussion marks indicating an extremely high energy, transgressive, shallow marine environment (Skipper, 1999). The thickness of the basal pebble-bed decreases eastwards, with distance from the old Thanet shoreline, until it disappears and the junction between Upnor and Thanet Sand formations becomes more difficult to define (Hester, 1965).

Several authors have recognised a persistent ('upper') pebble bed, up to 3 m thick, at the top of the formation across central and southeast London (Ellison et al., 1994; Ellison et al., 1996; Skipper, 1999; Ellison et al., 2004; Hight et al., 2004). It occurs in the majority of Tideway Tunnel boreholes (Figure 3.21) and ranges in thickness between 0.2 and 4.5 m and is evident as far west as Putney, more than 5 km west of the boundary interpreted by Ellison et al. (2004). It is thickest in the central London area, between London Bridge and Shad Thames, where up to 4.5 m has been recorded, but its thickness is not always reliably recorded in boreholes, since it is frequently lost during core recovery. In view of this, it is likely that the data in Figure 3.21 may be under-representative.

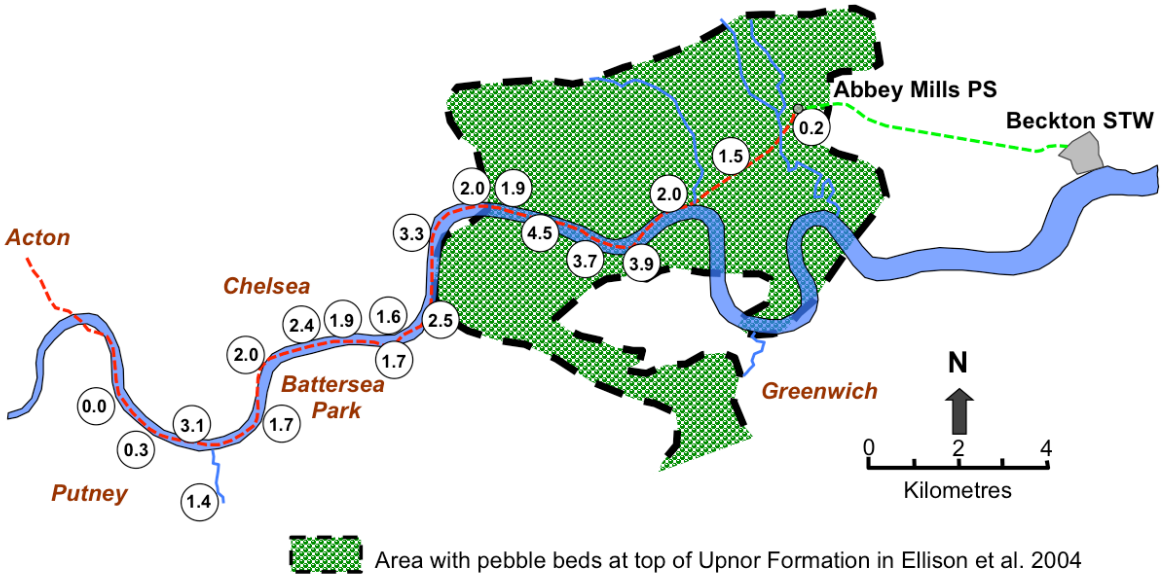


Figure 3.21 Thickness of the upper Pebble Bed across London

As with the basal pebble bed, the source of the gravel in the upper pebble bed is erosion of the underlying Chalk due to tectonic uplift of the landmass to the west and Chilterns to the north, leading to a sudden influx of large quantities of clastic (flint) material. Transgression after this tectonism led to development of fast-flowing, tidal, estuarine channels with a heavy bed-load of Chalk-derived flint gravel that scoured through the Glauconitic Sand or led to the removal of a large proportion of this earlier deposit (Ellison, 1983; Skipper, 1999; Ellison et al., 2004). The same tectonic activity led to severance of the connection with the Atlantic (Skipper, 1999).

Geotechnical character

The PSD grading envelope obtained from the Tideway Tunnel is compared to the grading envelope in Ellison et al. (2004), in Figure 3.22a and Figure 3.22b respectively. The envelopes show a very similar large range of soil types from clayey, slightly gravelly, fine and medium

sand to slightly clayey, sandy coarse gravel, corresponding to the respective Glauconitic Sand and Pebble Bed lithofacies groups.

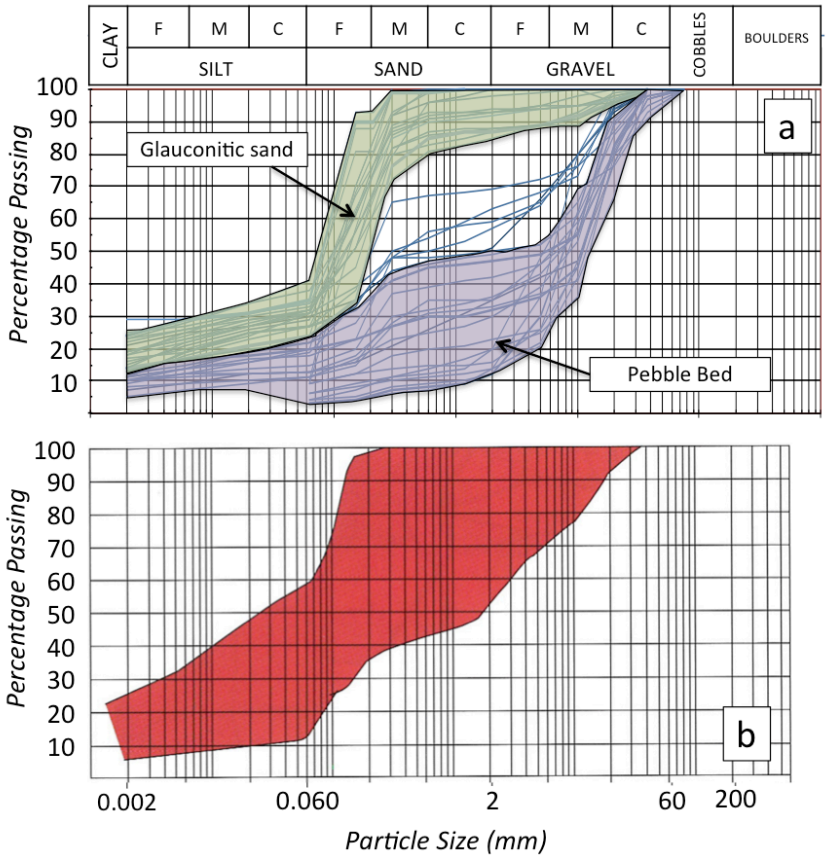


Figure 3.22 PSD grading envelopes for the Upnor Formation

a from Tideway Tunnel; b from Ellison et al. (2004)

The uniformity coefficient (Cu) ranges approximately between 33 and 140 for the Glauconitic Sand material and between 38 and 210 for the material constituting the Pebble Beds, indicating that both are well graded and non-uniform. A value of up to 500 has been calculated for the gravelly, sandy, silty clay material that lies between these two main lithofacies group components, as indicated on the PSD plots (Figure 3.22a and Figure 3.22b).

Atterberg Limit tests have been undertaken on selected samples from discrete layers in which there was sufficient clay material to perform the test. Results of the tests (Figure 3.23) indicate that the layers comprise sandy silty clay material, possessing a low range in plasticity and reflecting its predominantly granular nature. The moisture content shows a wide variation, from values close to or even below the plastic limit, to considerably higher, with no discernible pattern with depth (Figure 3.24). Values of Activity for the clay material within the formation range between 0.72 and 1.33, indicating relatively high activity.

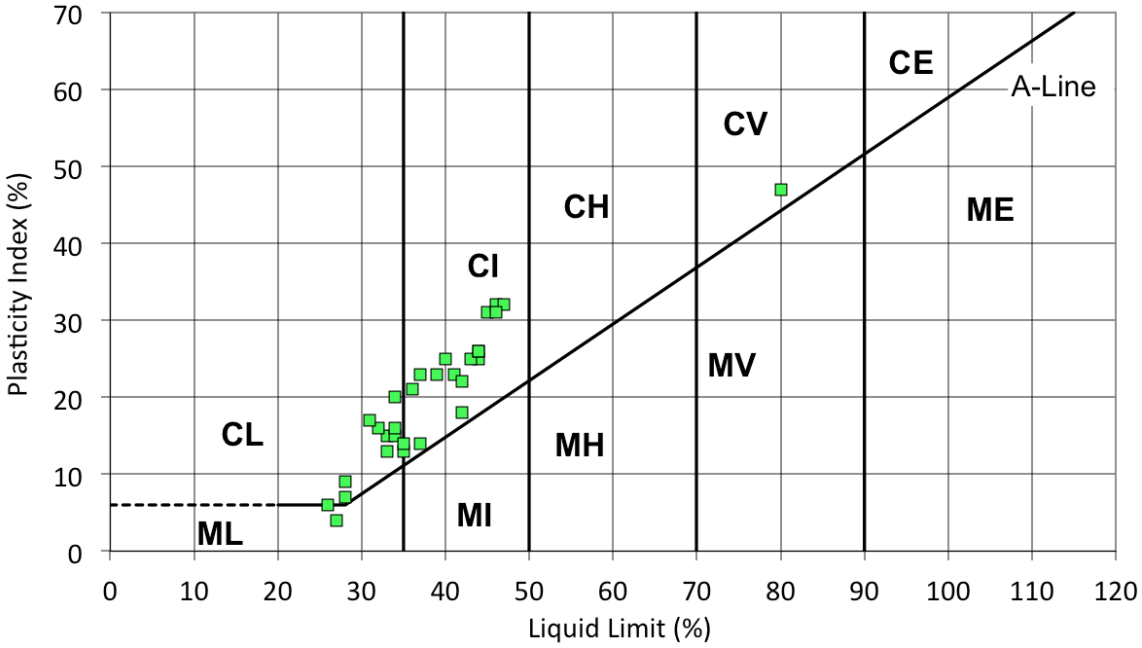


Figure 3.23 Soil classification of the Upnor Formation

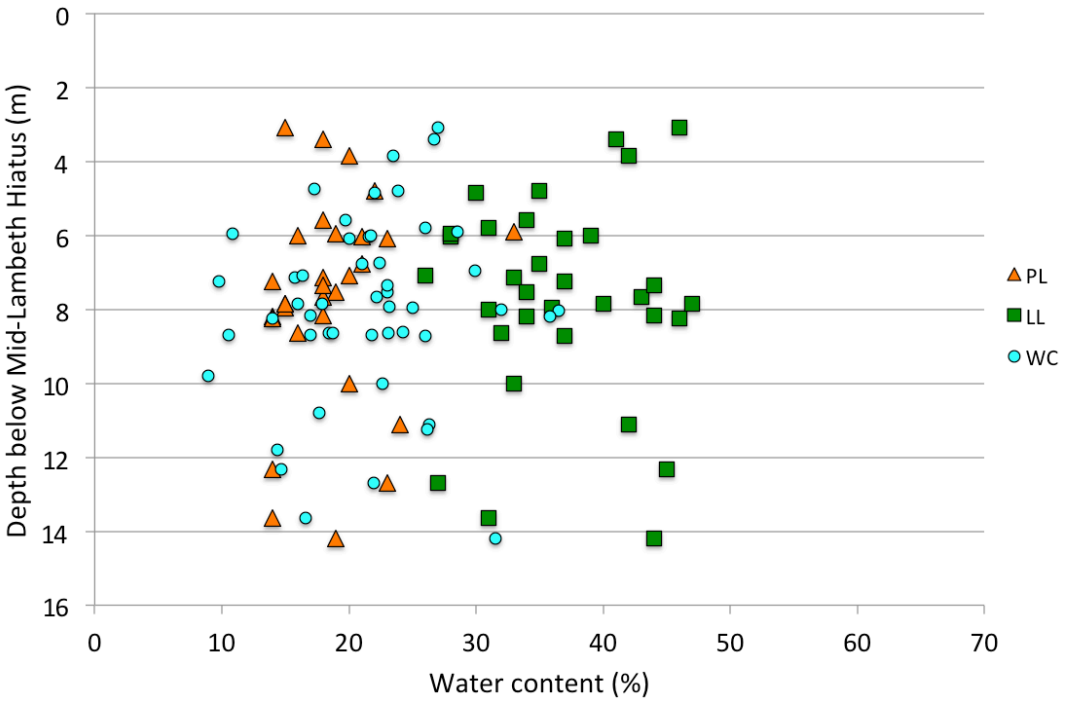


Figure 3.24 Plasticity within the Upnor Formation

3.2.5 Lower Mottled Beds

Following deposition of the Upnor Formation, tectonic uplift to the west of the London Basin led to a fall in sea level and emergence and establishment of a terrestrial environment. A very broad delta system of distributaries was formed over the current London area, comprising marshy mudflats crossed by river channels and incised by tidal creeks (Hester, 1965; Ellison, 1983; Page and Skipper, 2000; Hight et al., 2004). Initially, much of the underlying Upnor

Formation was removed by fluvial erosion, over which the Lower Mottled Beds were deposited as alluvial fines, transported from the west. During hiatuses in sedimentation the deposits were exposed to sub-aerial weathering and soil forming (pedogenic) processes. The rate of subsidence of the alluvial plain was slightly slower than deposition, resulting in pedogenic alteration of all sediments prior to burial (Hester, 1965; Skipper, 1999).

The regional groundwater level was lowered for long periods but often fluctuated over several metres. Above the lowest groundwater table, alternating reduction and oxidation caused leaching of iron, leaving residual aluminium-rich minerals and resulting in a mottling effect of the respective orange-brown and greyish colours (Buurman, 1980). Occasional surface flooding resulted in perched water tables that stagnated on impermeable subsurface layers. This led to the development of dark grey, saturated, gley soils (pseudogleys), formed in reducing conditions. (Buurman, 1980; Skipper, 1999).

The Mid-Lambeth Hiatus (MLH)

Eventually, a major fall in sea level lead to the development of a series of mature soils and planation of the land surface during a significant hiatus called the Mid-Lambeth Hiatus (Page and Skipper, 2000). This forms a regional marker horizon across London, easily recognised in borehole logs and excavation exposures by the abrupt change in colour from the dark grey of the overlying Lower Shelly Beds, to the mottled reddish orange, oxidised, Lower Mottled Beds (Figure 3.25a and Figure 3.25b).

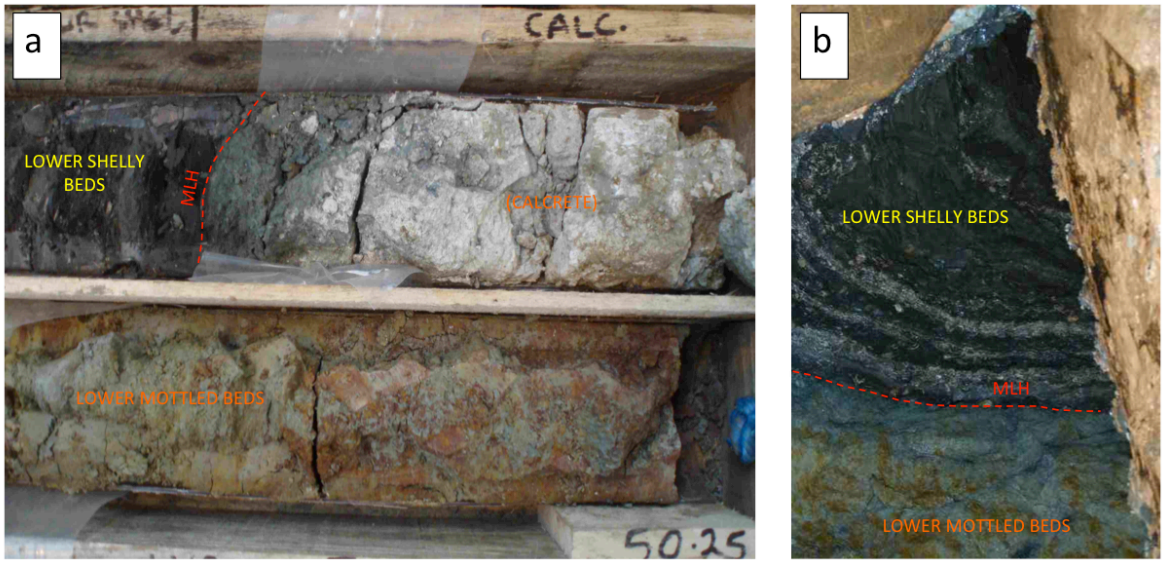


Figure 3.25 The Mid-Lambeth Hiatus

a in core sample; b in tunnel face exposure (courtesy of R. Margerison)

Following the Mid-Lambeth Hiatus, the sea level rose slowly, leading to deposition of the transgressive Lower Shelly Beds.

Field Description and Geotechnical character

The base of the Lower Mottled Beds overlies clayey sands and coarse flint pebble beds of the Upnor Formation. The thickness of the stratum increases from approximately 2.0 m in the east to 10.2 m in the west (Figure 3.26).

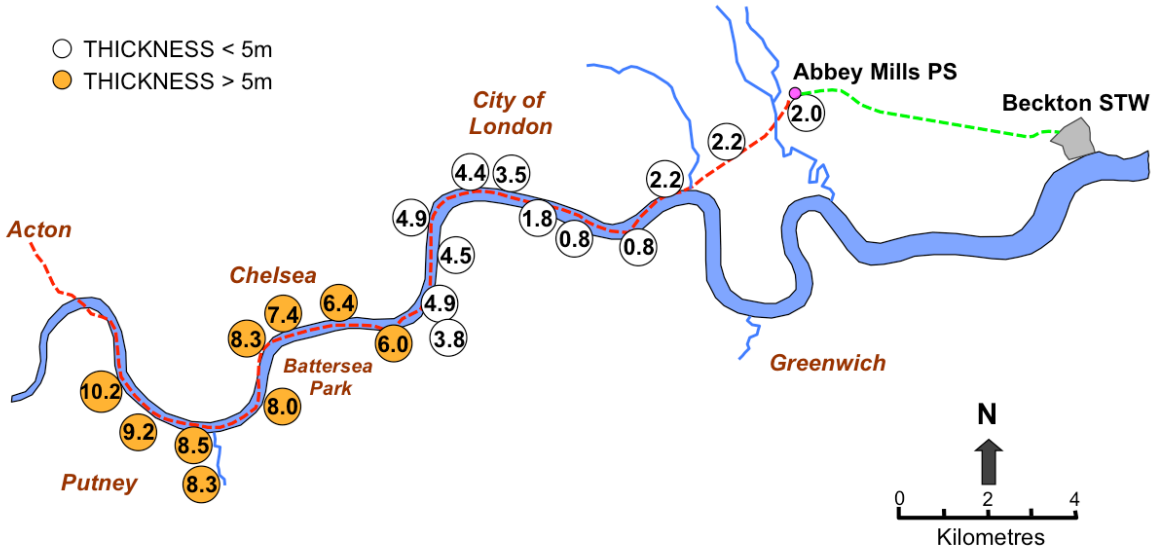


Figure 3.26 Thickness of the Lower Mottled Beds across London

The Lower Mottled Beds in the Tideway Tunnel boreholes are stiff to very stiff to occasionally hard, silty clay and clay. They are mainly unbedded and display a wide range of mottled colours, depending on oxidation state, including pale grey-blue, dark brown, red-brown and purple. The material frequently possesses a blocky texture caused by numerous very closely spaced, listric-shaped, polished and striated (slickensided) fissures. These are the result of syndepositional desiccation during seasonal changes in ground moisture in the mottled clays (Hight et al., 2004). They are more clay rich in the west of the Tideway Tunnel scheme (Figure 3.27a), becoming increasingly sandier towards Abbey Mills in the east (Figure 3.27b) as also noted by Skipper (1999) and Hight et al. (2004).

Buurman (1980) reported that the Lower Mottled Beds become redder upon greater dehydration and that the mottling of colours disappears above the highest groundwater table. At this level, the soil becomes a homogenous reddish brown colour, with complete removal of organic material by oxidation (Page and Skipper, 2000; Hight et al., 2004). Smectite (mostly montmorillonite), smectite-rich illite, kaolinite, illite and minor chlorite form the dominant clay mineralogy (M. Black and J. Huggett, *pers. comms.*), with smectite increasing from low concentrations at the base of the stratum to high concentrations at the top (Buurman, 1980).



Figure 3.27 Rotary core samples from the Lower Mottled Beds

The material possesses a high range in plasticity, between low and very high, reflecting the variation between sandier and more clayey types. More typically, the material possesses intermediate to mainly high plasticity, as displayed in the Atterberg Limit tests (Figure 3.28), in which most of the data from the east of the Tideway Tunnel scheme is classified as low to intermediate plasticity, confirming earlier field logging observations.

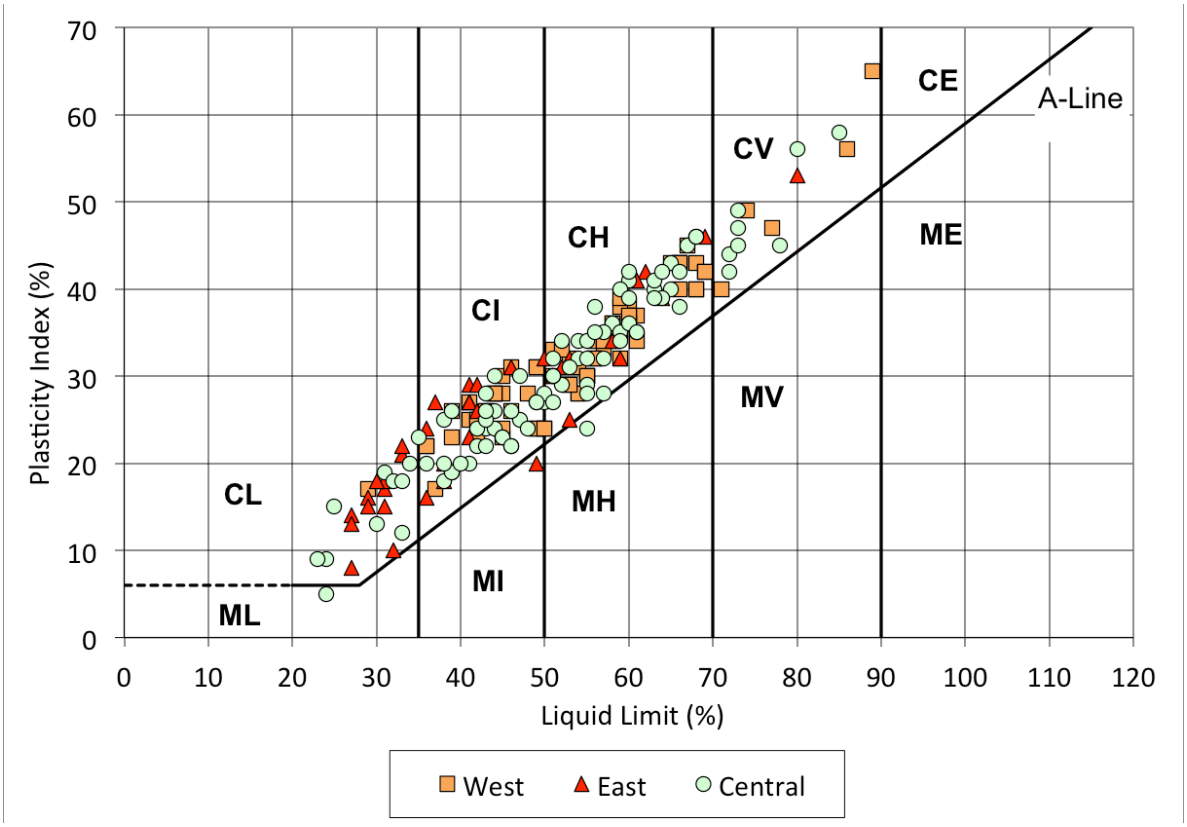


Figure 3.28 Soil classification of the Lower Mottled Beds

A slight decrease in plasticity occurs with depth (Figure 3.29), reflecting the increase in sand content. In addition, the moisture content lies close to and in many cases, below the plastic

limit and values of Activity range between 0.39 and 0.90, although more typically between 0.58 and 0.64, indicating inactive clay.

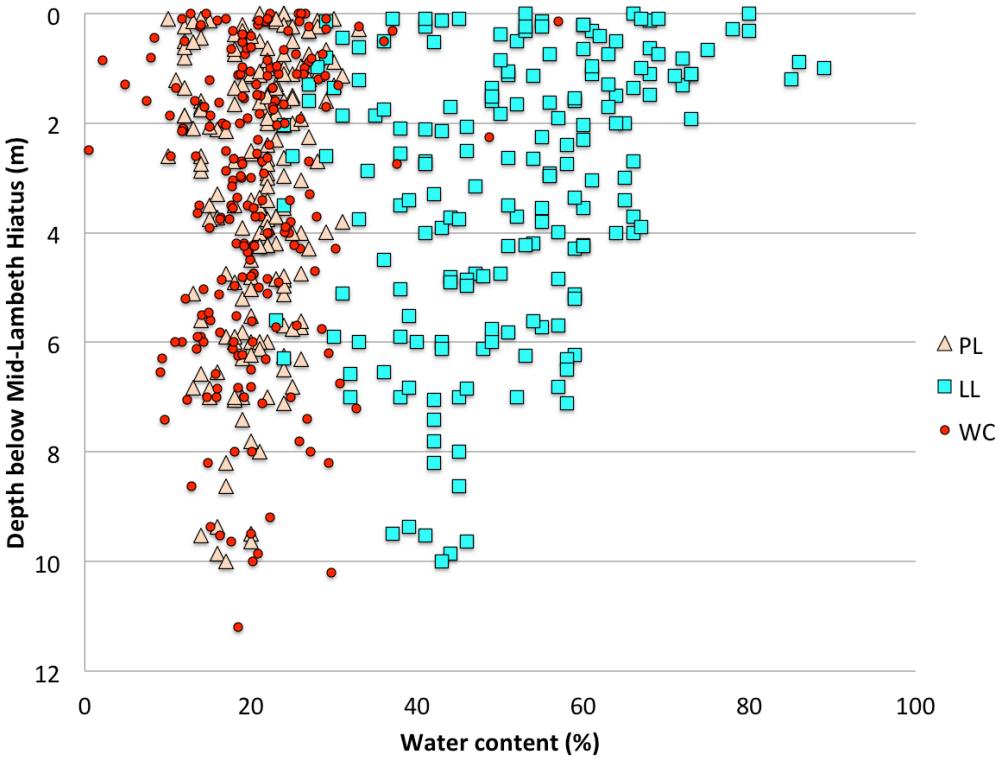


Figure 3.29 Plasticity within the Lower Mottled Beds

The silty clay nature of the material is indicated in the PSD plot in Figure 3.30.

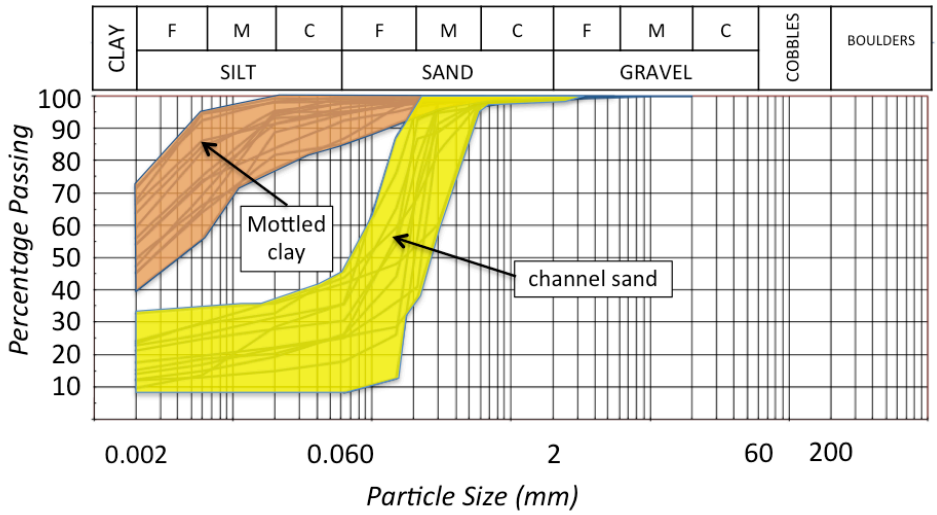


Figure 3.30 PSD grading envelope for the Lower Mottled Beds

Relict Sand Channels

Relict river channel features occur irregularly throughout the Lower Mottled Beds (Hight et al., 2004). These are up to 200 m wide and 4 m deep and contain light brown to yellowish brown, slightly silty, fine to medium sand, as demonstrated on the PSD plot (Figure 3.30).

Calcrete

Calcrete nodules are commonly found at the top of the Lower Mottled Beds, formed by precipitation of carbonate derived from the dissolution of shells (Hight et al., 2004) during pedogenesis (see below). In the sandier Lower Mottled Beds in east London, the nodules coalesce to form a massive limestone unit (Figure 3.31a). To the west of London, where the Lower Mottled Beds are more clay-rich and hence less permeable, pore fluids are unable to migrate (Page and Skipper, 2000) and the calcretes have developed as fine grained or coarse gravel size nodules (Figure 3.31b).

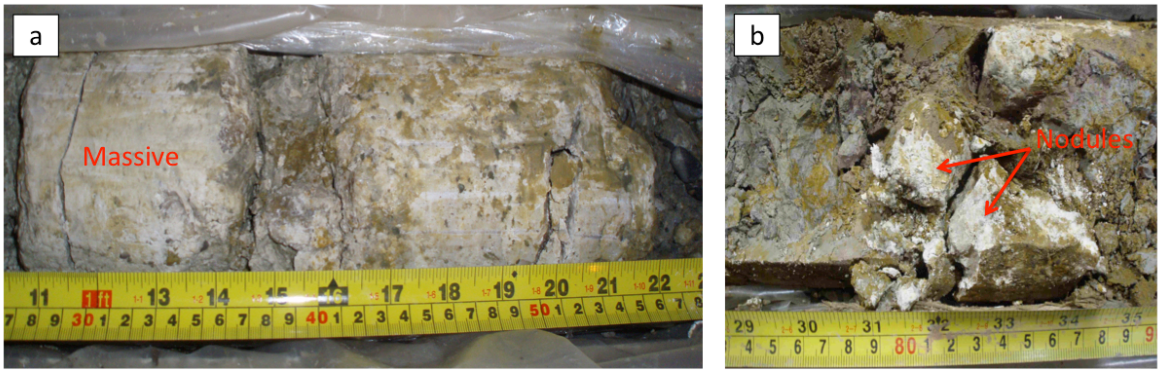


Figure 3.31 Examples of calcrete in Tideway Tunnel core

3.2.6 Pedogenic alteration of the Upnor Formation

Pedogenic processes occurred across London during formation of the Lower Mottled Beds and extended into the top of the underlying Upnor Formation, where it was close enough to the surface (Ellison et al., 1994; Skipper, 1999; Hight et al., 2004; Aldiss, 2012), causing extensive oxidation and alteration from dark, green-grey sediment to a range of brown, orange, red and purple colours.

The Pebble Bed at the top of the Upnor Formation, in particular, was strongly altered (Figure 3.32) with development of a clay matrix from the transport of fines downward, through the overlying soil profile during periods of lowered water table. The shiny black flint pebbles were pedogenically altered, changing to matt yellow-brown to white and became brittle, shattering into numerous sharp shards (Ellison et al., 1996; Skipper, 1999).



Figure 3.32 Pedogenic effects seen in the upper Pebble Bed

The depth of pedogenic alteration of the top of the Upnor Formation is between 1.3 and 4.8 m (Figure 3.33), but there is no obvious pattern or trend to this. The remaining thickness of unoxidised (fresh) Upnor Formation, unaffected by pedogenic processes, is between 1.2 and 4.5 m, with a slight increase towards the east (Figure 3.34).

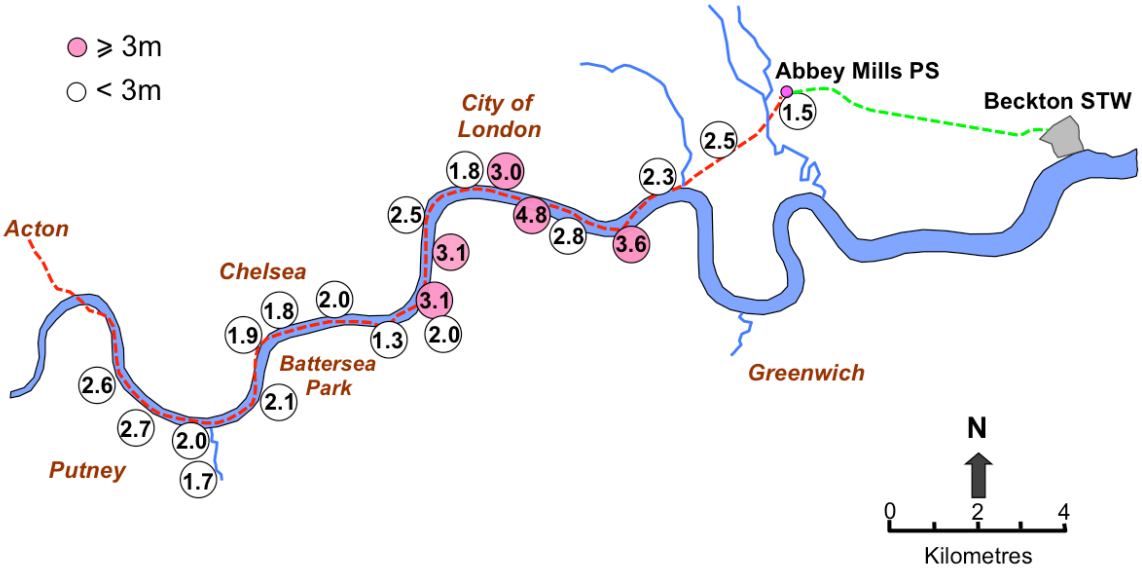


Figure 3.33 Depth of pedogenic alteration across London



Figure 3.34 Thickness of unaltered (fresh) Upnor Formation across London

The Pebble Beds contain clasts of mottled clay, less than 10 mm in diameter, from syndepositional deposits of the Lower Mottled Beds to the west (Ellison et al., 1996) indicating emergence and a hiatus in deposition between the Upnor Formation and succeeding Lower Mottled Beds. The contact between the Lower Mottled Beds and the pedogenically altered upper Pebble Bed of the Upnor Formation is recognisable by virtue of the contrast in lithology, despite the uniform mottled colours (Figure 3.35).

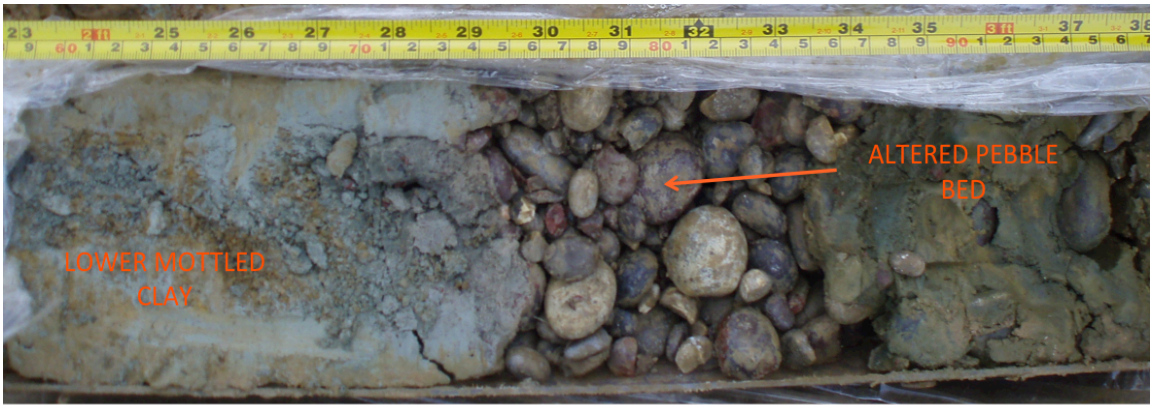


Figure 3.35 Contrasting Lower Lambeth Group lithologies

Pedogenically altered Upnor Formation contains unweathered (fresh) glauconite in many of the Tideway Tunnel cores (Figure 3.36a and Figure 3.36b), the glauconite remaining dark green or green-black within a weathered red-brown clay or pale grey to yellow brown sandy matrix.

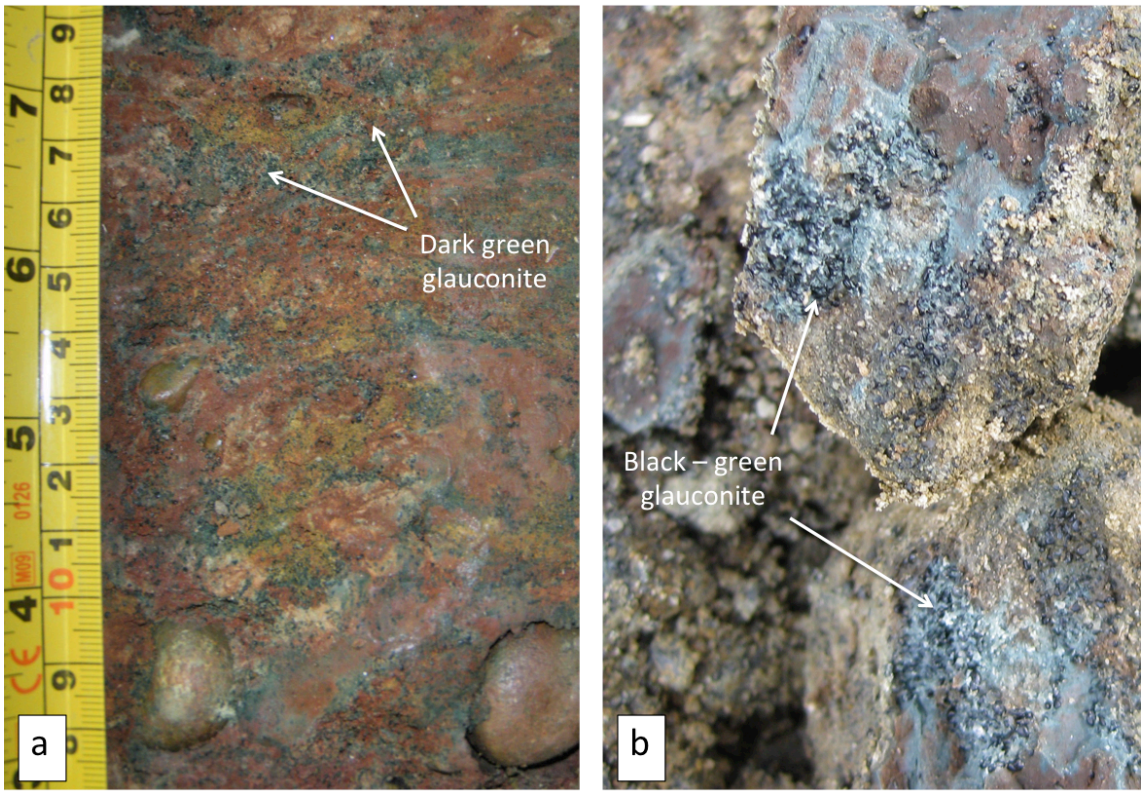


Figure 3.36 Unweathered glauconite in pedogenically altered Upnor Formation

Figure a based on Newman et al. (2013)

3.3 Glauconite

3.3.1 Introduction

Glauconite is a potassium and iron phyllosilicate, belonging to the mica group of minerals with aluminium, magnesium and calcium often present. It has a monoclinic crystal system, similar to that of mica and has the general formula of:

$(K, Na)(Fe^{3+}, Al, Mg)_2(Si, Al)_4O_{10}(OH)_2$

(Read, 1970).

It is usually of marine origin and contains up to 9% potassium (K_2O) which is the main reason why glauconite-bearing soils are so favourable for crop growth (Tedrow, 2002).

Granules of glauconite are often coarser than quartz sand grains (Odin and Lamboy, 1988), although they are made up of relatively stable clay-sized crystallites, ranging from no more than 0.5 mm to less than 1 µm in diameter; the latter being able to float in water (Tedrow, 2002).

A number of authors have distinguished between the terms ‘glaucony’ and ‘glauconite’. The former applies to the facies for formation of small, spherical, earthy green glauconite-rich

pellets whilst the latter is a mineralogical term for pure end-member glauconite (Burst, 1958; Bentor and Kastner, 1965). The use of the facies term 'glaucony' instead of mineral name 'glauconite' was proposed where the clay has not been analysed and may contain glauconite-smectite mixed layer clay and some detrital components left over from the original pseudofaecal pellet (J. Huggett, *pers. comm.*). Glaucony is a very stable component in the sea, with which it is in thermodynamic equilibrium (Odin, 1988) and it is particularly abundant in the Upnor Formation (Huggett and Knox, 2006).

3.3.2 Environment of deposition

Glaucony facies are typically open marine environments, at the shelf break, namely outer shelf and upper slope settings, between 60 and 300 m depth. Here conditions are cool, with temperatures below 15˚C and a pH around 8 (Harder, 1980; Odin and Fullagar, 1988; Amorosi, 1995; Jimenez Millan et al., 1998; Eder et al., 2007), low sedimentation rates leading to condensed stratigraphic sequences, often in association with hiatus surfaces (Huggett and Gale, 1998; Eder et al., 2007), and abundant fossils in intensively burrowed sediments (Amorosi, 1995). In this setting, glauconite forms a few centimetres below the sediment-water interface (Odin, 1988; Eder et al., 2007), at the boundary between reducing and oxidising zones (Harder, 1980). It is one of the most reliable indicators of low sedimentation rates in marine settings and is diagnostic of marine transgressions because of its presence at the base of transgressive/regressive cycles (Amorosi, 1995).

3.3.3 Formation and growth

The initial substrate is usually granular and highly porous, facilitating a specific, partially isolated, microenvironment known as a semi-confined environment (Odin, 1988; Jimenez Millan et al., 1998). This consists of mineral debris but more commonly biogenic carbonate particles, foraminiferal tests and faecal pellets (Odin and Matter, 1981; Odin and Fullagar, 1988; Jimenez Millan et al., 1998), particularly within burrows (Huggett and Gale, 1998). The inside of the test or faecal pellet has a favourable, semi-restricted, physio-chemical microenvironment and there is no link between the nature and composition of the substrate to that of the glauconite grain (Odin and Lamboy, 1988).

Glauconite forms by progressive alteration and replacement of in situ smectite and illite and latterly by authigenic growth of crystals in the pores of the substrate (J. Huggett, *pers. comm.*). The process involves absorption of potassium from the sea water with an end member, potassium-rich glauconite mica, properly termed 'glauconite', developing from an initial potassium-poor glauconite smectite at the start of the evolutionary process (Amorosi, 1995). The chemistry and redox conditions of the pore water are the controlling factors in glauconite growth (Harder, 1980), rather than pressure and temperature (depth of burial), in which

borderline reducing conditions prevail due to consumption of available oxygen through the bacterial decay of organic matter (J. Huggett, *pers. comm.*). This is only possible where the rate of sediment input is low (Amorosi, 1995; Jimenez Millan et al., 1998) but no specific climatic conditions are required (Odin and Matter, 1981). The mineral is iron-rich, with available iron being derived from weathering of adjacent continental landmasses (Eder et al., 2007), even when the surrounding sediment is iron-deficient (Odin and Fullagar, 1988).

3.3.4 Maturation

Maturation of glauconite follows a complex process of chemical evolution, related to progressive equilibrium with the seawater (Sánchez-Navas et al., 2008). If the rate of sedimentation increases, burial will preserve glauconite in the initial, immature, state before it has had a chance to attain maturity. However, if unburied, glauconite grains remain exposed to the open marine environment for a sufficiently long period of time for continued absorption of potassium and maturation (Odin and Matter, 1981; Odin and Fullagar, 1988; Huggett and Gale, 1998).

Odin and Matter (1981) and Amorosi (1995) proposed four stages of evolution as follows (Table 3.3):

i) nascent,

ii) slightly evolved,

iii) evolved,

iv) highly evolved.

During maturation there is a change in colour from pale yellow-green to light green in nascent and slightly evolved grains, to dark blue-green to black-green in highly evolved grains. In addition to the changes in colour there is a change in mineralogy, in which Al, Si, Mg, Ca and Na are replaced by an increase in Fe and K and in particular the ratio of Fe^{2+} to Fe^{3+} (Fanning et al., 1989; Eder et al., 2007; Sánchez-Navas et al., 2008).

In the latter stages of maturation, glauconite begins to grow by displacement. The confined internal portion of the test and/or pellet favours maturation more than the periphery, resulting in the central part of the grain becoming more evolved than the external layer. Normally, there is zero or slow growth on the grain surface whilst the inside is expanding, leading to cracks developing in the outer less-evolved layer due to the differential growth rate between this and the expanding centre (Odin, 1988; Odin and Lamboy, 1988). Thus the grain surface texture is a good indicator of maturity (Figure 3.37). Nascent grains are rounded with smooth surfaces, followed by cracks appearing in the slightly evolved grains, developing into

deep cracks in even more evolved grains. Finally, mature grains develop well rounded, smooth surfaces. (Odin and Lamboy, 1988; Amorosi, 1995; Huggett and Gale, 1998).

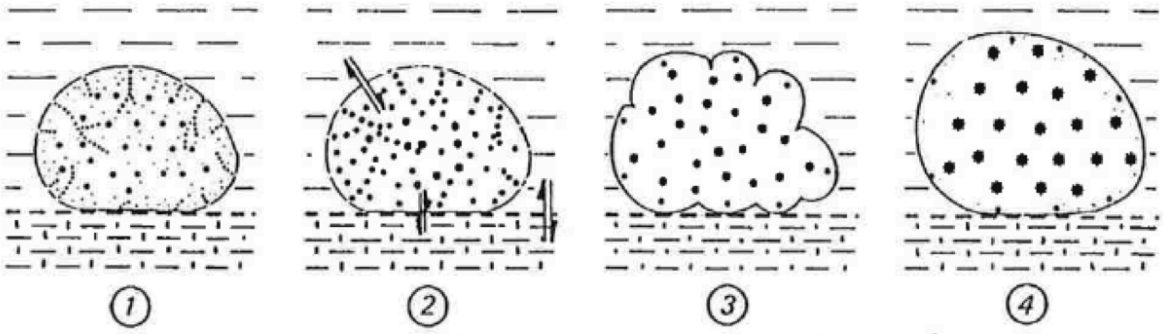


Figure 3.37 Schematic representation of the stages of growth of a glauconite grain

Figure from Odin and Matter (1981) in which 1 = nascent to 4 = highly evolved

With progressive replacement of the initial substrate and subsequent evolution, the grains become increasingly green and dense. The structure evolves from heterogeneous, pore-rich pellets toward homogeneous dense pellets in the oldest and deepest sediments (Odin, 1988). The greener the glaucony, the higher the density, to the extent that highly evolved grains may have a density of 2950 kg m^{-3} (Odin and Matter, 1981; Odin and Lamboy, 1988).

Table 3.3 Characteristic features of glauconite maturation (adapted from Amorosi, 1995)

Glaucony	Nascent	Slightly evolved	Evolved	Highly evolved
Maturity	Low	Moderate	High	Very high
Colour	Pale green	Light green	Green	Dark green
Morphology	Smooth and rounded	Swellings and local cracking	Deep cracks	Smooth and well-rounded
K_2O Content	<4%	4 – 6%	6 – 8%	>8%
Specific gravity	2.2	2.5	2.7	2.95
Mineral Structure	Smectite	→	→	Mica

The time required for formation of the initial glauconitic smectite is estimated at between 10 and 1000 years and maybe 10^5 to 10^6 years for highly evolved glauconitic mica (Odin and Matter, 1981).

3.3.5 Characterisation by X-Ray diffraction

The potassium content is the most reliable indicator for the stage of maturity of glauconite but it is only detectable using X-ray analysis and bulk chemical analytical methods (J. Huggett,

pers. comm.). Highly evolved grains contain up to 9% K_2O, indicated by sharp, narrow XRD peaks, whereas less evolved grains contain as little as 3% K_2O with a greater presence of smectite and Al_2O_3, indicated by broader XRD peaks (Amorosi, 1995; Jimenez Millan et al., 1998).

3.3.6 Weathering and alteration

Whilst glauconite grains mature from the centre outward, they weather from the outside in, during a progressive process that is the reverse of glauconitisation (Courbe et al., 1981).

Weathering alteration of glauconite grains by oxidation produces brown coloured rims, formed by the leaching of K and Fe and resulting enrichment in Al (Figure 3.38). The core of the grain usually displays a yellow-green colour, but remains considerably richer in K and Fe than the brown rim (Eder et al., 2007; Sánchez-Navas et al., 2008).

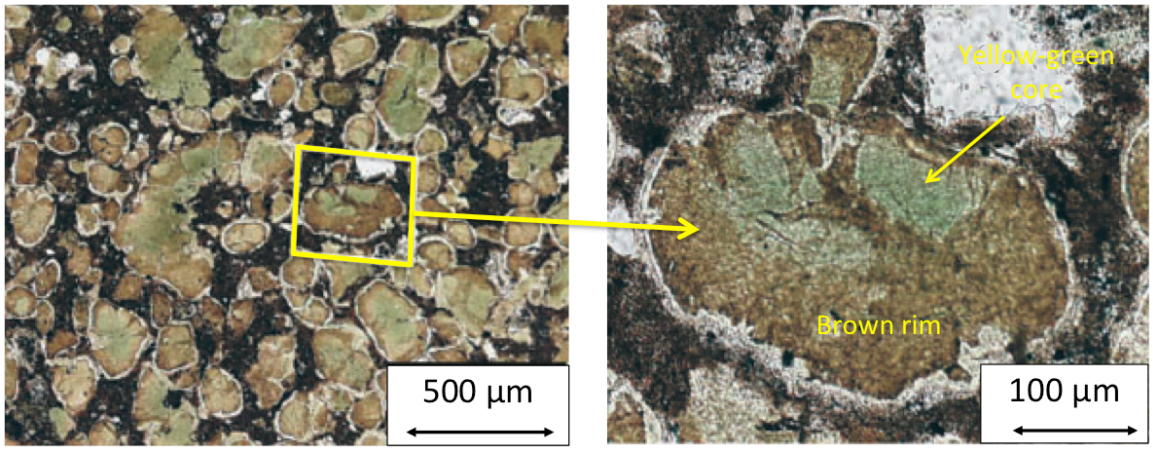


Figure 3.38 Partially weathered glauconite

Figure from Eder et al. (2007)

The colour change from yellow-green cores to brown rims arises from partial transformation to goethite, a common alteration product of glauconite (Bentor and Kastner, 1965; Odin and Fullagar, 1988; Sánchez-Navas et al., 2008). Other products of alteration are kaolinite and smectite (Courbe et al., 1981).

Altered grains show significant textural complexity, are of variable roundness and frequently cerebroid in shape. Cracks develop from the periphery of the grain, towards the core and fill with Fe-(Al) oxyhydroxides (Eder et al., 2007; Sánchez-Navas et al., 2008), most commonly goethite. Subsequent sediment transport may result in the mixing of highly evolved and altered grains within a particular stratum (Eder et al., 2007).

Mild alteration is associated with well-oxygenated, intertidal marine water, but sub-aerial exposure is required for more significant weathering (J. Huggett, *pers. comm.*). Even then, glauconite has been observed to persist for months to years in hand specimens.

3.3.7 Field evidence

In the weathered (oxidised) zone of a soil profile, altered glauconite displays a yellow-green colour rather than the blue-green colour observed in reduced zones (Fanning et al., 1989), and is often associated with significant kaolinite, smectite and iron oxide concretions (Courbe et al., 1981). These cannot always be recognised under the binocular microscope but are obvious in thin section and XRD (Bentor and Kastner, 1965).

Monroe (1947) conducted a number of observational experiments on samples of New Jersey Greensand. It was found that glauconite within the samples retained its characteristic green colour and hardness, even after several years of exposure to air whilst in storage. Similar observations by Tedrow (2002) showed very little alteration of glauconite within field exposures of the New Jersey Greensand, demonstrating that glauconite is more resistant to pedogenesis than other greensand soils in the region and requires a longer time to reach a moderately advanced stage of podsolic development. Huggett (*pers. comm.*) observed unaltered glauconite grains in a number of cliff exposures in southeast England that appear to have resisted weathering for many years. Tedrow (2002) did observe dark brown or yellow-brown colours in some glauconites as a result of oxidation of iron within the mineral structure, but such alteration is not detectable in either chemical analysis or XRD, implying limited chemical transformation (Courbe et al., 1981).

3.3.8 Hand specimen – observational experiment

A relatively simple observational experiment was conducted on a core specimen of fresh Upnor Formation. The sample was extracted from Borehole 5012A (Figure 3.39a) in June 2011, at a depth of 43.40 m, from dark grey-green, slightly gravelly, fine to medium sandy clay (Figure 3.39b). The aim of the test was to monitor the sample during exposure to atmospheric conditions to test the existing theory on “rapid oxidation” and breakdown of glauconite that would be manifested by a change in colour from green to brown.

No colour change has been observed in the two years of continuous exposure to atmospheric conditions (Figure 3.39c after 1 year and Figure 3.39d after 2 years), indicating that there has been no “rapid oxidation” or superficial alteration of the mineralogy.



Figure 3.39 Observation for colour change during oxidation of the Upnor Formation

3.4 Pyrite

3.4.1 Formation

Pyrite originates from bacterial reduction of naturally occurring sulphate in sediment pore water, resulting in the formation of hydrogen sulphide (H_2S). Some of the H_2S escapes to the atmosphere, whilst some reacts with dissolved ferrous iron to form FeS, evolving with time to pyrite (FeS_2) (Bierens de Haan, 1991). Pyrite formation is entirely limited to the reducing zone, in the presence of organic matter (Berner, 1981; Fanning et al., 1989; Huggett and Gale, 1998).

3.4.2 Shape and morphology

Most pyrite in Lambeth Group sediments is invisible to the naked eye in core material and hand specimens and is not abundant in the Thanet Sand or Upnor Formations in which its concentration is estimated at less than 1% (Bierens de Haan et al., 1994). It is rarely observed in polished thin sections under the binocular microscope; examination of discrete grains requires the use of a scanning electron microscope (SEM).

Although pyrite varies in grain size and morphology (Nordstrom, 1982), a number of common forms prevail (Bierens de Haan et al., 1994; Hawkins, 2012):

- Euhedral cubes/lumps.
- Framboids (clusters of "seed" resembling raspberries).
- Cryptocrystalline pseudomorphs of biogenic debris.

Framboidal pyrite is common in argillaceous organic-rich sediments of marine and brackish environments and is usually accompanied by disseminated euhedral pyrite (Bierens de Haan, 1991). The size of framboids ranges from 3-20 µm (Hawkins, 2012) but can be as small as 0.05 to 1 µm (Bierens de Haan, 1991).

Pyrite often occurs as aggregates within sediments and has a very large specific surface area exposed to pore fluids, in particular framboids which are weakly aggregated and porous (Nordstrom, 1982; Bierens de Haan, 1991; Bierens de Haan et al., 1994; Hawkins, 2012). Aggregates of discrete crystals are found in the ranges 0.5 to 5 µm (Hawkins, 2012) and 5 to 50 µm in diameter (Bierens de Haan, 1991). Aggregates of fine crystals can also form within cracks in glauconite grains (Fanning et al., 1989; Sánchez-Navas et al., 2008) (Figure 3.40).

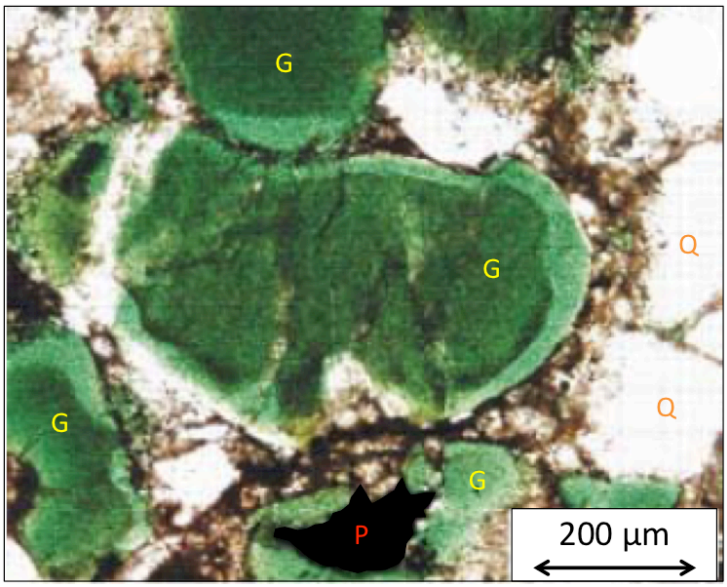


Figure 3.40 Fine crystal of pyrite within crack in a glauconite grain

Figure from Sánchez-Navas et al. (2008) in which G= glauconite; P= pyrite and Q = quartz

3.4.3 Oxidation and alteration

Pyrite is oxidised in a complex biogeochemical process on exposure to water and air (Nordstrom, 1982). Chemical reactions may occur within sediments containing as little as 0.1% pyrite (Hawkins, 2012). Using SEM, McKibben and Barnes (1986) observed that weathering attack on pyrite grains is non-uniform and concentrated at grain edges and corners. The rate of pyrite oxidation depends on (Bierens de Haan, 1991):

i. Surface area of a sample;
ii. Concentration of the oxidising agent; and
iii. pH of the leaching medium.

However, grain size differences may exert the greatest control. For example, framboid pyrite reacts more quickly than euhedral 'lumps' (Rimstidt and Vaughan, 2003; Hawkins, 2012). The rate of oxidation is significantly increased in the presence of *Thiobacillus ferrooxidans* bacteria, which can accelerate the reaction by a factor of 10^5 to 10^6 (Bierens de Haan, 1991; Bracegirdle et al., 1996; Hawkins, 2012). They are most active in the pH range 1 to 2.5 at temperatures between 20° and 55°C (Brown and Jurinak, 1989; Bierens de Haan, 1991), with the rate of oxidation doubling for every 10°C rise (Nordstrom, 1982). This rate is further accelerated on exposure to solar ultraviolet radiation (Bierens de Haan, 1991).

Oxidation of pyrite produces sulphuric acid as a by-product (Kinniburgh et al., 1994) which dissolves calcium carbonate in fossil shell debris in the sediment and precipitates calcium sulphate, typically as selenite gypsum (Nordstrom, 1982; Banks et al., 1996; Bracegirdle et al., 1996; Hawkins, 2012). Glauconite is also highly susceptible to the sulphuric acid by-product (Bentor and Kastner, 1965) although it is more resistant to weathering oxidation than pyrite, which will usually oxidise in air within days or weeks.

3.4.4 Cause of oxygen depletion: LUL Old Street

The occurrence of oxygen-depleted air within gas-monitoring boreholes at LUL Old Street was discussed in Chapter 2. Based on that event, Bracegirdle et al. (1996) and Rainey and Rosenbaum (1989) proposed that the oxidation process of pyrite proceeds as follows:

The first step is the bacterial oxidation of pyrite and release of sulphuric acid (H+) given by:

$$FeS_2 + 3.5\ O_2 + H_2O = Fe^{2+} + 2\ SO_4^{2+} + 2\ H^+ \qquad \text{(eq. 1)}$$

The second step involves bacteria catalysing further oxidation of ferrous to ferric ions and is given by:

$$Fe^{2+} + 0.5\ O_2 + 2\ H^+ = 2\ Fe^{3+} + H_2O \qquad \text{(eq. 2)}$$

In a third step, the ferric ions produced by the above equation initiate abiotic oxidation of further pyrite given by:

$$FeS_2 + 14\ Fe^{3+} + 8\ H_2O = 15\ Fe2 + 2\ SO_4^{2-} + 16\ H^+ \qquad \text{(eq. 3)}$$

The ferrous ions generated in the above reaction are then oxidised by the reaction in equation 2, instigating a cyclic process that is dependent on the activity of *Thiobacillus ferrooxidans* bacteria.

In a final step, ferric hydroxide may be precipitated with the release of more acid, given by:

$$Fe^{3+} + 3\ H_2O = Fe(OH)_3 + 3\ H^+ \qquad \text{(eq. 4)}$$

It was deduced that the Old Street tunnel facilitated entry of oxygen into the underground environment, resulting in oxidation of pyrite in the sand. Furthermore, Bird et al. (1989) estimated that there was sufficient pyrite left to continue the reaction at a similar level for a very long time and that oxidation would continue until all the available pyrite is consumed (Rainey and Rosenbaum, 1989).

3.5 Green Rust

3.5.1 Introduction

Green rust (GR) is a unique class/family of Fe(II) and Fe(III) layered double hydroxides (LDH) within the pyroaurite group of minerals (Chaves, 2005; Zegeye et al., 2005; Kwon et al., 2007; O'Loughlin et al., 2007; Mazeina et al., 2008; Christiansen et al., 2009; Ahmed et al., 2010; Davesne et al., 2010; Zegeye et al., 2012). It has a structure (Figure 3.41) consisting of positively charged brucite-type layers of Fe(II) and Fe(III), alternating with negatively charged interlayers of anions and water molecules (Hansen, 1989; Trolard et al., 1997; Ona-Nguema et al., 2001; Parmar et al., 2001; Simon et al., 2003; Legrand et al., 2004; Feder et al., 2005; Zegeye et al., 2005; Bearcock et al., 2006; Kwon et al., 2007; O'Loughlin et al., 2007; Nagata et al., 2009; Ahmed et al., 2010; Zegeye et al., 2012). Sulphate, carbonate and chloride are the most common interlayer anions (Schwertmann and Fechter, 1994; Hansen and Bender Koch, 1998).

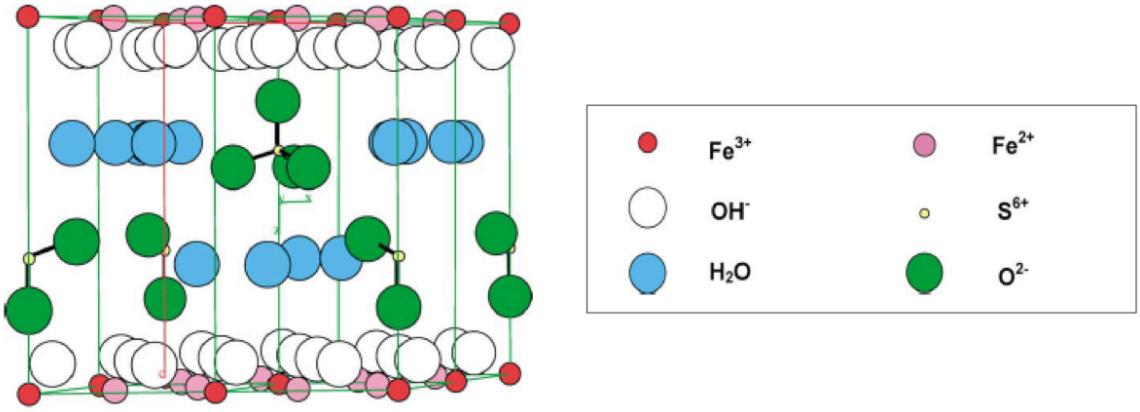


Figure 3.41 General view of an ordered representation of a green rust 2 lattice (not to scale) containing sulphate interlayer anions

Figure from Simon et al. (2003)

Various general formulae have been proposed for green rust:

$[Fe^{II}_{(1-x)}Fe^{III}_{x}(OH)_2]^{x+} \cdot [(x/n)A^{n-} \cdot (m/n)H_2O]^{x-}$ (Zegeye et al., 2012).

$Fe_4^{II}Fe_2^{III}(OH)_{12}SO_4 \cdot \approx 8H_2O$ (Simon et al., 2003).

$Fe_2(OH)_5$ or $[Fe^{(II)}Fe^{(III)}(OH)_4]^+ \cdot [OH]^-$ (Trolard et al., 1997).

Two types of green rust have been identified; GR1 incorporating planar or spherical anions such as carbonate or chloride and GR2 incorporating anions with a more three-dimensional structure such as sulphate (Pantke et al., 2011). In addition, GR2 differs from GR1 in that it has two adjacent planes of anions and water molecules, instead of a single one as in GR1 (Simon et al., 2003).

The ratio of Fe(II) to Fe(III) has been described as variable (Taylor, 1980) although most authors agree on 2:1 (Hansen, 1989; Drissi et al., 1995; Zegeye et al., 2005; Bearcock et al., 2006; Bearcock and Perkins, 2007). However, in some cases, a maximum of 4:1 has been interpreted (Bearcock et al., 2006; Bearcock and Perkins, 2007).

Green rust is characterised by distinctive, platy, hexagonal crystals (Figure 3.42) in SEM and transmission electron microscopy (Hansen and Bender Koch, 1998; Ona-Nguema et al., 2001; Parmar et al., 2001; Legrand et al., 2004; Génin et al., 2005; Zegeye et al., 2005; Bearcock et al., 2006; Trolard et al., 2007; Ahmed et al., 2010).

The crystals are very fine grained, typically from just 0.4 μm (Trolard et al., 2007) to 10 μm (Ona-Nguema et al., 2001) in diameter, resulting in a very high surface area (Mazeina et al., 2008; Christiansen et al., 2009). It is characteristically blue-green in colour (Legrand et al., 2004; Feder et al., 2005; O'Loughlin et al., 2007; Trolard et al., 2007), although this can range from bright to dark shades depending on the ratio of Fe(II) to Fe(III) (Taylor, 1980; Trolard and Bourrié, 2006).

Most observed green rust is produced synthetically under laboratory conditions (Ona-Nguema et al., 2001) but it is believed to occur naturally within soils and sediments in many locations throughout the world (Bender Koch and Morup, 1991; Parmar et al., 2001; Génin et al., 2005; Christiansen et al., 2009; Pantke et al., 2011) in anoxic, hydromorphic (waterlogged), weakly acidic to alkaline (Schwertmann and Fechter, 1994; O'Loughlin et al., 2007) gley soils (Bearcock et al., 2006; Ruby et al., 2006; O'Loughlin et al., 2007; Trolard et al., 2007). The optimal pH is 6.5 to 7.5 (Parmar et al., 2001). In addition, it can also occur as free colloidal-size particles within natural groundwater (Christiansen et al., 2009). Trolard et al. (1997) suspect that green rust is present in very small amounts, where present within a soil, but Feder et al. (2005) suggest that iron distribution in soil is a consequence of oxido-reduction processes and that green rust formation is a reversible process.

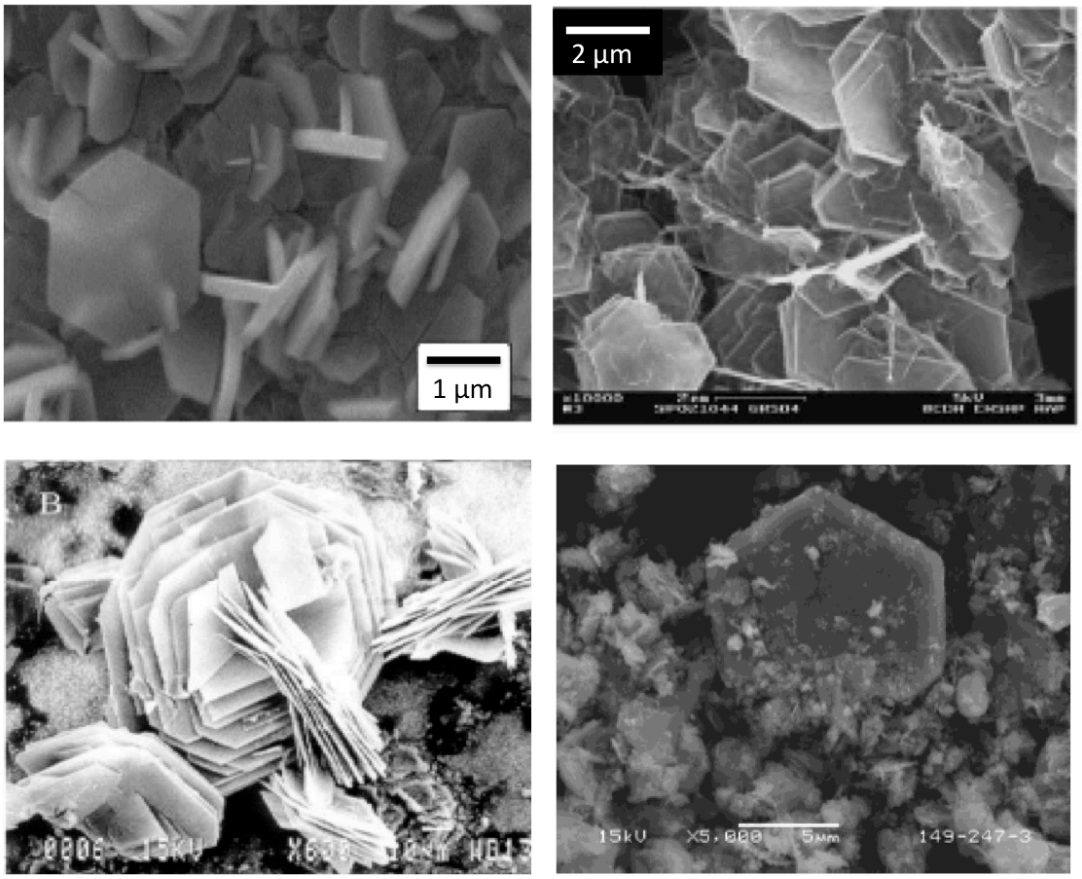


Figure 3.42 Hexagonal green rust crystals

Figures from clockwise top left; Legrand et al. (2004); Peulon et al. (2003); Su and Puls (2004); Parmar et al. (2001)

3.5.2 Formation by reduction

Based on a number of laboratory synthesis experiments, green rust forms as a result of bioreduction of iron (FeIII) oxyhydroxides, such as lepidocrocite (γ-FeOOH) and goethite (α–FeOOH). The process involves the activity of dissimilatory iron-reducing bacteria (DIRB), namely *Shewanella putrefaciens*, in which ferric oxyhydroxides are gradually dissolved into Fe(II) ions (Ona-Nguema et al., 2001; Legrand et al., 2004; Génin et al., 2005; Zegeye et al., 2005; Ruby et al., 2006; O'Loughlin et al., 2007; Davesne et al., 2010; Pantke et al., 2011; Zegeye et al., 2012). The transition is observed by the change in colour from the orange of lepidocrocite to a dark blue-green, commensurate with increasing Fe(II) concentration (O'Loughlin et al., 2007). Furthermore, Ona-Nguema et al. (2001) demonstrate that green rust is only a transient state during bacterial reduction of ferric iron to more stable forms (such as magnetite and siderite) upon cessation of microbial activity.

In the natural environment, the process is assumed to involve bacterial action in an anoxic aquifer, facilitating the anaerobic transformation of organic matter that plays a major role in the reduction of ferric compounds (Bender Koch and Morup, 1991; Ruby et al., 2006).

3.5.3 Formation by oxidation

Green rust also forms a transient state during microbial Fe(II) oxidation (Pantke et al., 2011), as observed during laboratory synthesis by partial oxidation of Fe(II) to Fe(III) (Ahmed et al., 2010). The end products of green rust oxidation are iron oxides such as magnetite (Fe_3O_4), goethite (α-FeOOH) and lepidocrocite (γ-FeOOH) (Olowe and Genin, 1990; Lewis, 1997; Phillips et al., 2003; Feder et al., 2005; Mazeina et al., 2008; Davesne et al., 2010).

Oxidation of iron(II) compounds involves a two step process in which the first step produces Fe(II)-Fe(III) green rust in the form of nanocrystalline particles shaped as hexagons. The second step produces nanocrystalline particles of iron(III) oxyhydroxides, such as lepidocrocite and goethite and is accompanied by a significant reduction in pH.

A number of laboratory experiments have confirmed this two-stage process (Kwon et al., 2007; Popov et al., 2010) in which the initial oxidation of Fe(II) is accompanied by growth of the green rust crystal structure, in the form of nano-size hexagonal-shaped crystals. The transformation process is dependent upon conditions such as temperature, heat and residual oxygen (Nagata et al., 2009) and is accompanied by a significant reduction in pH (Kwon et al., 2007; Popov et al., 2010). During the experiments, green rust oxidised after only a few minutes on exposure to air, visible as a rapid change in colour from the characteristic blue-green to various hues of yellow-brown and orange (Taylor, 1980; Taylor and McKenzie, 1980; Schwertmann and Fechter, 1994; Trolard et al., 1997; Ona-Nguema et al., 2001; Legrand et al., 2004; Bearcock et al., 2006; Trolard and Bourrié, 2006; Bearcock and Perkins, 2007; Christiansen et al., 2009). Continued oxidation leads to a gradual disappearance of the hexagonal crystals and growth of iron oxyhydroxides, seen as aggregates of needles of lepidocrocite or anisotropic platelets of goethite. Lepidocrocite is usually derived from chlorine-containing suspensions whilst goethite is derived in the presence of sulphate ions (Popov et al., 2010).

An intermediary stage, ferrihydrite, was identified by Schwertmann and Fechter (1994) and Lewis (1997) during the formation of green rust, when oxidation is so rapid that crystallization of stable forms cannot occur (Refait et al., 2003; Génin et al., 2005).

3.5.4 Environment of formation

The reversible reactions involved in the formation of green rust and iron oxides are typically found within a pedogenic environment, at the water table surface in soils (Taylor, 1980), within a redox front that follows the fluctuating water levels (Ruby et al., 2006), similar to conditions within the Upnor Formation at the present time.

During drier periods and a low water table, oxidized soil profiles contain Fe in the form of goethite or lepidocrocite (Taylor, 1980). However, in more humid periods, under a rising

water table, there is a supply of organic matter and water saturation, resulting in a change from ferric to ferrous iron, accompanied by a colour change from ochrous to blue-green (Ruby et al., 2006; Trolard et al., 2007).

Based on field observations, Feder et al. (2005) noted fast and reversible mineralogical transformations of iron oxides within a soil profile. During these, it was evident that green rust completely oxidised in summer to lepidocrocite, whilst a fresh supply of organic matter and water saturation during autumn caused the lepidocrocite to reduce.

3.5.5 Difficulties in sample analysis

A number of researchers have discussed the difficulties in identifying or characterising green rust because it is so susceptible to rapid oxidation (Hansen, 1989; Bender Koch and Morup, 1991; Lewis, 1997; Bearcock et al., 2006; Mazeina et al., 2008; Ahmed et al., 2010). Green rust will transform to Fe(III) oxyhydroxides within minutes of exposure to air, often before it can be observed, sampled, or analysed (Christiansen et al., 2009; Davesne et al., 2010). This is the main reason why green rust is often unnoticed in natural environments (Christiansen et al., 2009).

Green rust is very dilute within a soil, constituting as little as 2 to 3.9% by volume (Bearcock et al., 2006; Trolard and Bourrié, 2006). In addition, its nano particle size and the difficulties in separating it from other minerals (Trolard and Bourrié, 2006) mean that it may not be captured in samples for laboratory testing.

If successful sampling for green rust is accomplished, oxidation can still easily occur when adequate care is not undertaken during sample preparation, even within anaerobic conditions (Phillips et al., 2003).

3.6 Summary

The lower Lambeth Group deposits comprise a complex, wide-ranging sequence of soil types. At the top are the Lower Mottled Beds, consisting of very stiff clays of generally low Activity and variable plasticity, depending on local increases in sand. Beneath these is the Upnor Formation which is predominantly sand but with frequent clay-rich and gravel-rich horizons. The underlying Thanet Sand Formation is uniform fine silty sand.

Glauconite is locally abundant within the Upnor Formation and is indicative of a marine origin of the stratum. The mineral matures during an evolutionary process of up to 1 Ma and in a reversal of this process, becomes altered to goethite, kaolinite and smectite during sub-aerial weathering (Table 3.4).

Table 3.4 Origins of weathering by-products

Weathering by-product	Glauconite	Green Rust	Pyrite
Iron oxide (goethite)	✓	✓	✓
Kaolinite	✓		
Smectite	✓		

Note that gypsum may also occur as an indirect by-product from the reaction between sulphuric acid – produced from pyrite – and calcium carbonate in fossil shells.

The top of the Upnor Formation was subjected to sub-aerial weathering and pedogenic processes during deposition of the overlying Lower Mottled Beds, in a terrestrial environment. Alteration is evident in colour and lithological changes, reflected in transformation from green-grey to mottled orange and brown, and an increase in clay content. Changes in mineralogy are not obvious and several authors have reported the presence of unaltered glauconite within the pedogenically altered Upnor Formation.

Pyrite occurs in very small quantities within the Upnor Formation, although it too is altered to goethite during sub-aerial weathering (Table 3.4).

Green rust is a highly reactive Fe(II) and Fe(III) layered double hydroxide and forms as a transitory stage between reduced and oxidised end products, in a reversible reaction. It has a nano particle size, may comprise only a few percent of the soil mass, and rapidly oxidises making it very difficult to detect. When fully oxidised, it alters to goethite (Table 3.4).

4 EXPERIMENTAL METHODOLOGY

4.1 Laboratory testing

The aim of the laboratory tests is to identify the mineral composition in various oxidised soil samples, principally the pedogenically altered Upnor Formation and Lower Mottled Beds, to verify the end product of oxidation. More specifically, the presence of glauconite is sought, to test the assertions discussed in Chapter 2 that it "oxidises rapidly" (on exposure to air). In addition, attempts are made to identify the presence of green rust in fresh (unoxidised) soil samples, principally from the Upnor Formation, and register the mineralogical transformation to iron oxide (goethite and/or lepidocrocite) during a controlled period of exposure and oxidation.

A second aspect of laboratory testing is to undertake partially saturated soil analysis experiments on samples of the Lower Mottled Beds, Upnor and Thanet Sand formations. These determine the capacity of the Lower Mottled Beds to act as an impermeable barrier to gas migration from the underlying Upnor and Thanet Sand formations.

4.2 Field sample recovery

Field samples for laboratory analysis were recovered over most of the London Tideway Tunnels scheme; these were obtained from rotary core boreholes during ground investigation for the Tideway Tunnel or from hand-dug samples during shaft excavation, as part of the Lee Tunnel construction. There were a number of phases to the borehole investigation and improved sample preservation techniques were developed and tested on site, together with practice and improvement in sub-sampling procedures within the laboratory.

4.2.1 Rotary core samples

Rotary core samples were recovered during three of the six phases of borehole investigation for the Tideway Tunnel, namely series 4000, 5000 and 6000 (Figure 4.1). Series 4000 and 6000 boreholes were drilled from land-based locations whilst series 5000 boreholes were drilled from jack-up platforms within the River Thames.

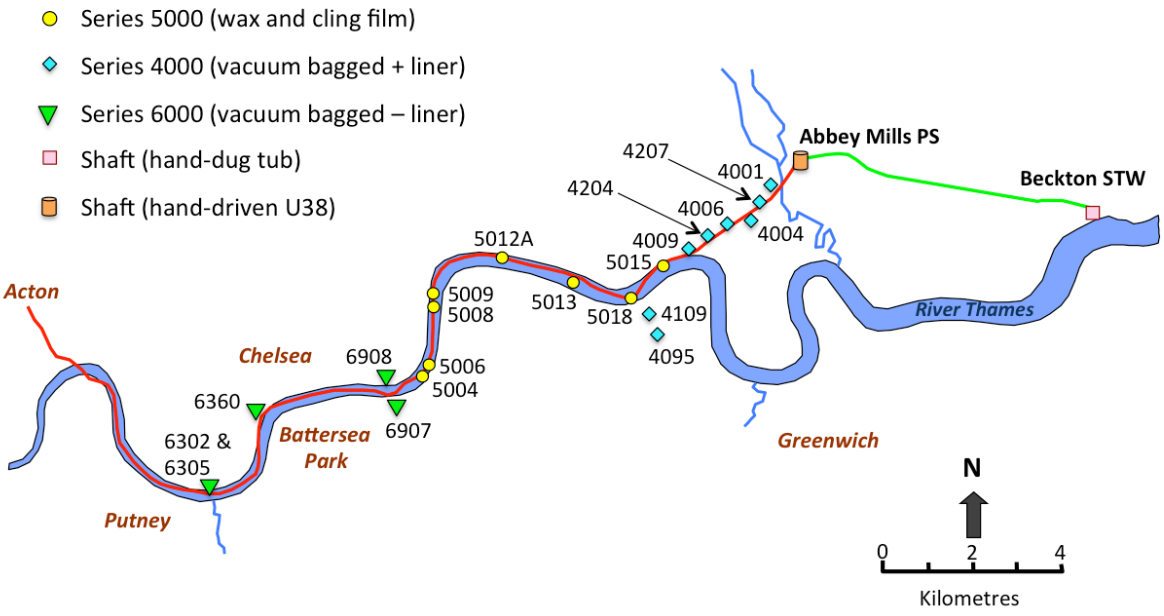


Figure 4.1 Borehole sample location plan

The boreholes were excavated using a Geobore 'S' wireline system with either mud (polymer mix) or potable water used as the drilling fluid for the land-based boreholes or river water for those in the River Thames. Table 4.1 summarises the date of receipt of samples from the various phases of borehole investigation.

Table 4.1 Schedule of receipt of rotary core samples

Borehole phase/series	Dates of laboratory receipt
4000	March to May 2012
5000	April to June 2011
6000	June 2012 to April 2013

During borehole construction, nominally 100 mm diameter core was brought to surface within a plastic liner to keep the core intact. Whilst still within the liner, 100 mm length samples were cut at 0.50 m intervals. The Mid-Lambeth Hiatus was used as a reference marker; sampling commenced two metres below this and continued at 0.5 m spacing until two metres into the Thanet Sand Formation.

Waxing and cling film preservation

The first samples were obtained from the series 5000 boreholes. Once cut, each core sample was immediately coated in hot liquid wax at either end (Figure 4.2a) and then wrapped in at least one layer of cling-film (Figure 4.2b). Plastic core liner caps were then placed over each

end and the sample was again wrapped in at least one more layer of cling-film (Figure 4.2c). Finally, the sample was sealed using adhesive duct tape, labelled and then sealed again within a clear plastic bulk bag (Figure 4.2d). All samples were delivered to Imperial College and stored in a temperature-controlled laboratory, prior to further sub sampling and analysis.



Figure 4.2 Core waxing and cling film preservation

The on site process was not fast enough to prevent oxidation of any green rust exposed to the atmosphere. Laboratory analysis also indicated that the heat from the wax may have destroyed any green rust within them. In addition, wax had penetrated planes of weakness in some samples, rendering them ineffective for partially saturated soil analysis.

Freezing preservation

A review of the literature indicated that the samples should be frozen, or at least kept below a temperature of 4°C, as soon as possible after recovery (Hansen, 1989; Bender Koch and Morup, 1991; Bearcock et al., 2006). On freezing, water in the liquid phase within the soil pores expands in volume, preventing air entry and oxidation of the sample. Furthermore, the lower temperature reduces the oxidation rate of a mineral.

Vacuum seal preservation

A revised sample preservation technique was administered on samples obtained from the series 4000 boreholes. As previously, 100 mm length samples were cut within the plastic

liner, at 0.5 m spacing, using the Mid-Lambeth Hiatus as the starting reference (Figure 4.3a). However, after cutting, each sample was immediately placed within a clear, gas-proof (high barrier) vacuum pouch, impermeable to oxygen, nitrogen and water (Figure 4.3b). The pouched sample was placed in an Audionvac VMS 163 vacuum-sealing machine (Figure 4.3c), which removed the air and hermetically heat-sealed the pouch (Figure 4.3d). Each vacuum-sealed sample was thus given rapid, long-term, oxygen-free protection. Following recommendations by Dr. S. Shaw, samples were placed in a plastic cool box, packed with ice during transit to Imperial College and then transferred into a chest freezer for storage at – 18°C.



Figure 4.3 Vacuum seal preservation of rotary core sample

In some of the first batch of vacuum-sealed samples, the vacuum was lost because the pouch had been punctured by the sharp cut edges of the plastic liner. Subsequently, therefore, the liner was filed and smoothed after cutting and the sample sealed using two stages of vacuum bagging. Later, the liner was dispensed with altogether so that the pouch formed a tighter, more efficient, seal around the soil sample during the vacuuming process.

4.2.2 Hand-dug tub samples

A total of six hand-dug soil samples were recovered during construction of the 25 m internal diameter drive shaft at the Beckton Sewage Treatment Works (STW). The shaft is located in

Beckton, east London, at the east end of the Tideway Lee Tunnel (Figure 4.1). The samples were taken in October 2011, as excavation intersected the Upnor Formation at approximately 38 m below ground level.

In each case, a small pit was dug into the shaft invert, using a machine excavator, to ensure that each sample would be as free as possible from exposure to the atmosphere and the effects of oxidation. The sample was then taken using a small hand trowel and immediately placed within a small plastic tub with a sealable, air-tight, lid.

4.2.3 Hand-driven U38 tube samples

A sequence of hand-driven, stainless steel U38 sample tubes were taken throughout the entire Upnor Formation during construction of the 25 m internal diameter reception shaft at the Abbey Mills Pumping Station (PS). The shaft, referred within the LTT design team as 'Shaft F', is located in Stratford, east London, at the west end of the Lee Tunnel (Figure 4.1).

The U38 samples were taken over a two-week period in June 2012, during excavation between 27 and 33 m bgl (Figure 4.4a to d).

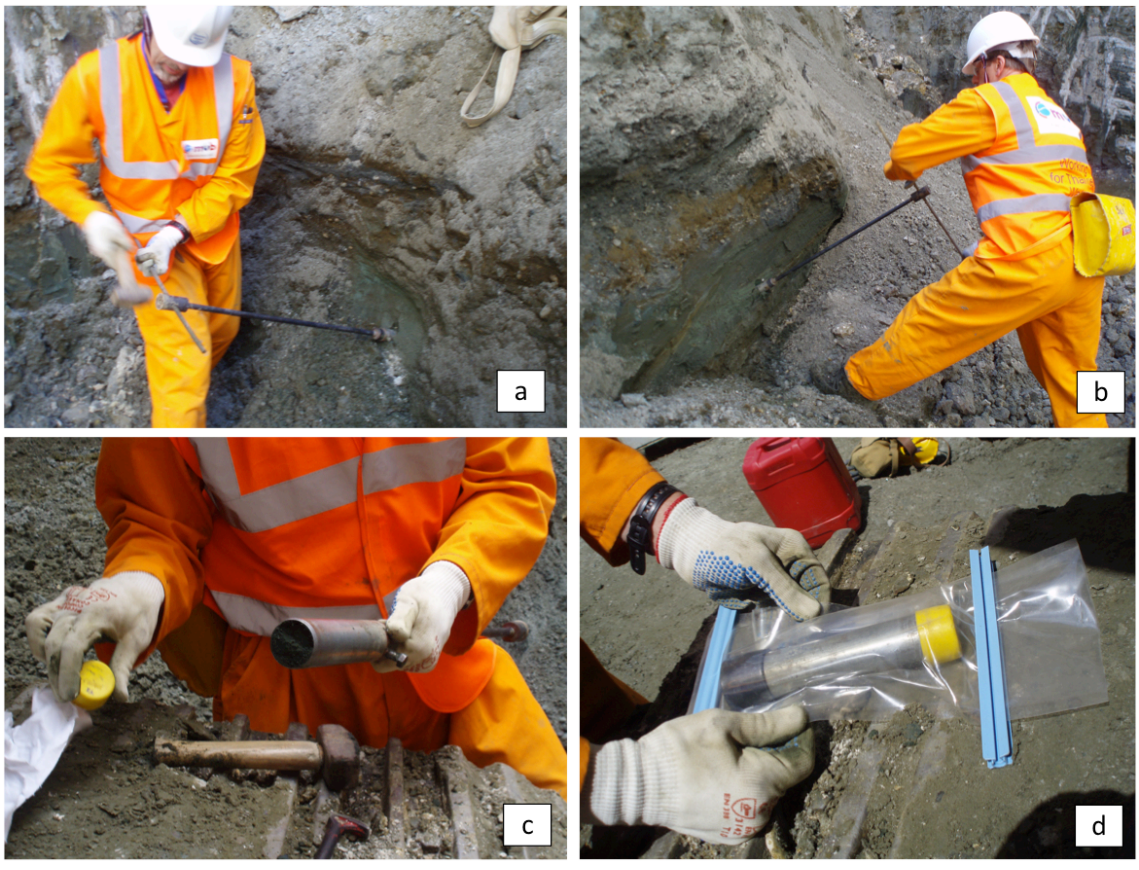


Figure 4.4 U38 sampling at Abbey Mills

The tube was attached to a rod extension and manually hammered into the ground until full of soil (Figure 4.4a), then extracted from the ground (Figure 4.4b), released from the rod extension, and sealed with plastic caps on either end (Figure 4.4c). Following this, the samples

were immediately placed within a hermetically sealed, gas-proof (high barrier) pouch (Figure 4.4d) prior to transportation to freezer storage in the laboratory.

Table 4.2 summarises the number, depth and basic description of the samples taken within the Abbey Mills shaft; a schematic geological logging section (Figure 4.5) through the Upnor Formation shows the location of these samples.

Table 4.2 Summary of U38 sampling at the Abbey Mills shaft

Sample reference	U38 or Grab	Depth (mbgl)	No. taken	Basic soil description
AM270	U38	27	1	Grey white mottled grey green silty fine sand with abundant calcrete.
AM280	U38	28	1	Dark blue green, silty, fine to medium sand.
AM290	U38	29	2	Dark green slightly clayey fine to medium sand.
AMG290	Grab	29	2	Dark green slightly clayey fine to medium sand.
AM295	U38	29.5	3	Greyish green clayey, gravelly, fine to medium sand.
AM305	U38	30.5	1	Greyish green brown, clayey, fine to medium sand.
AM320	U38	32	1	Greyish green, slightly clayey, fine to medium sand.
AMG320	Grab	32	1	Greyish green, slightly clayey, fine to medium sand.
AM325	U38	32.5	3	Greyish brown, very sandy, gravelly clay.

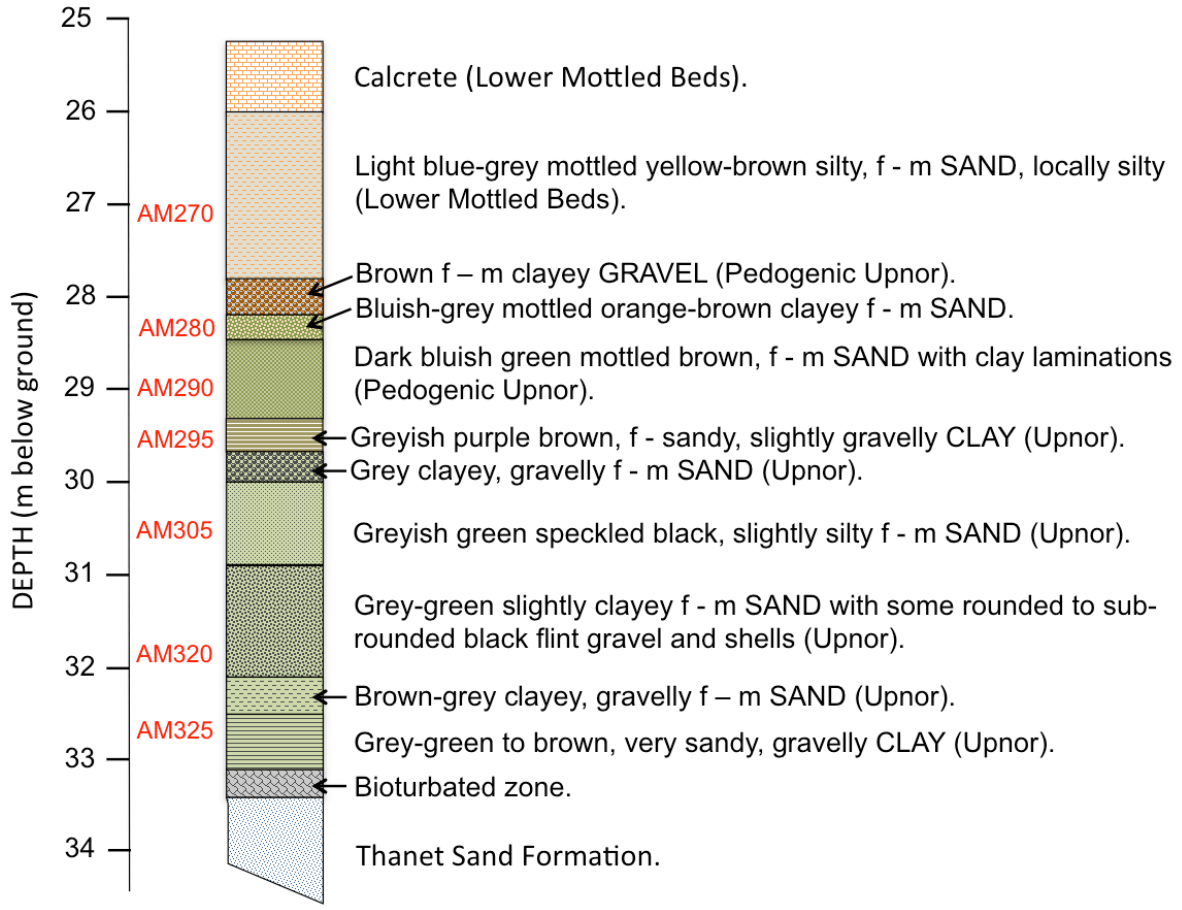


Figure 4.5 Geological log of the Abbey Mills shaft (sample locations in red)

During the sampling exercise at Abbey Mills, a number of observations were made that verified the statements made in the literature guidance in Chapter 3 and confirmed the predictions made based on the Tideway Tunnel borehole logs.

The top of the Upnor Formation is pedogenically altered, displaying characteristic brown mottle and grading downward into yellow-green (Courbe et al., 1981) slightly weathered material (Figure 4.6).

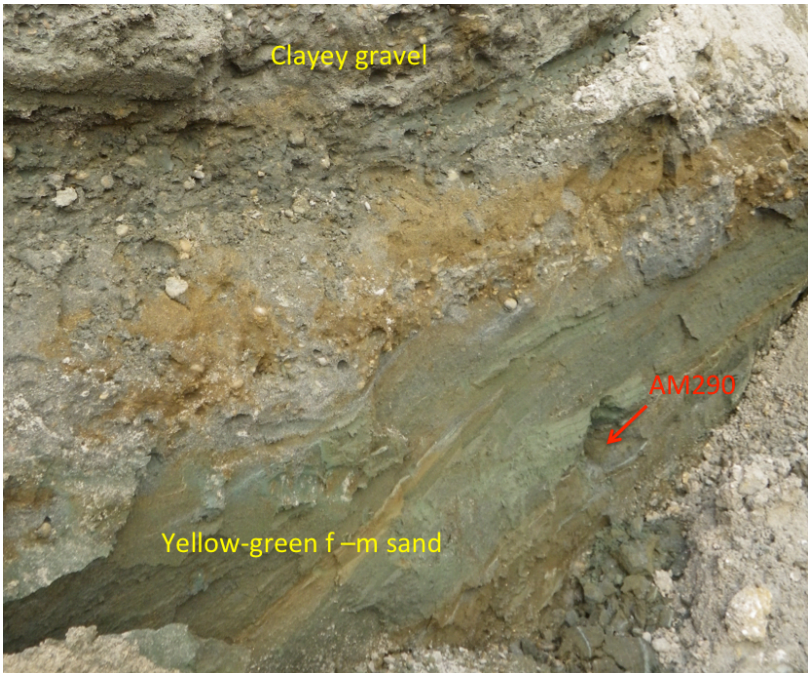


Figure 4.6 The top of the Upnor Formation, showing effects of slight weathering

In places, the gradation is less evident where, instead, a more abrupt interface between pedogenically altered and fresh Upnor Formation is observed (Figure 4.7); the latter a greyish purple-brown sandy, gravelly clay, as noted in the shaft log (Figure 4.5) between samples AM290 and AM295.

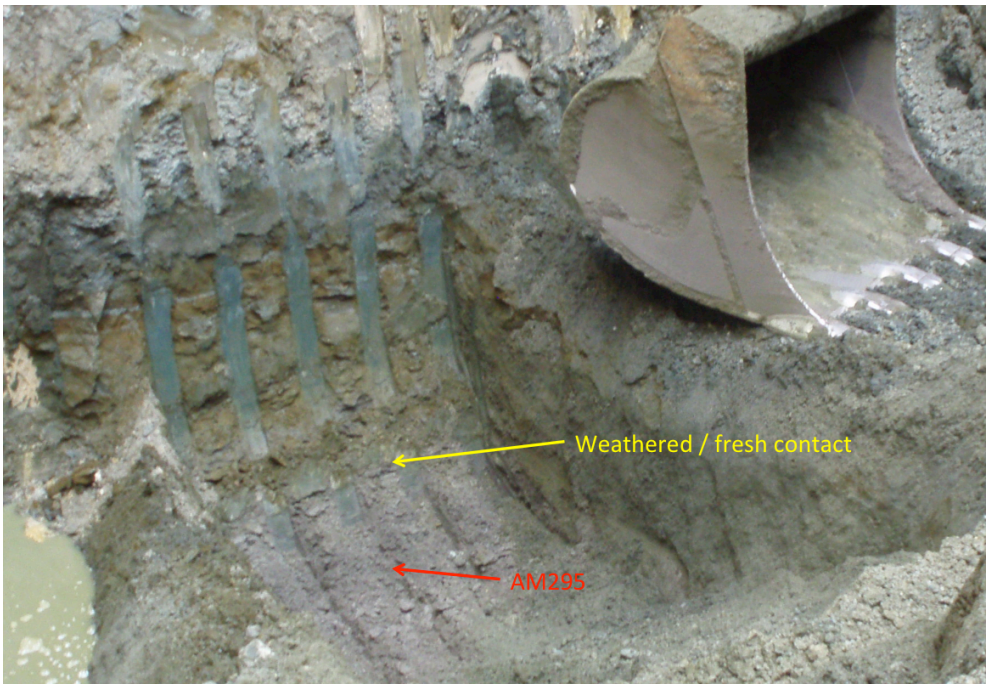


Figure 4.7 Contact between pedogenically altered and fresh Upnor Formation

The colour difference between the yellow-green, slightly weathered material and the darker greyish green fresh material was even more obvious during inspection of the 'muck pile' on the surface (Figure 4.8).



Figure 4.8 Pedogenically altered and fresh Upnor Formation on muck pile

Further down the sequence, fresh Glauconitic Sand was recorded as typically greyish green clayey, fine to medium sand (Figure 4.9).



Figure 4.9 Glauconitic sand exposed during excavation

A gravelly, clay-rich band, up to 200 mm thick, was recorded in the basal 1.0 m of the formation (Figure 4.10). This contained *Ostrea bellocovina* shells and was cemented by $FeCO_3$ (siderite), resulting in an increase in strength of the material (J. Huggett, *pers. comm.*).

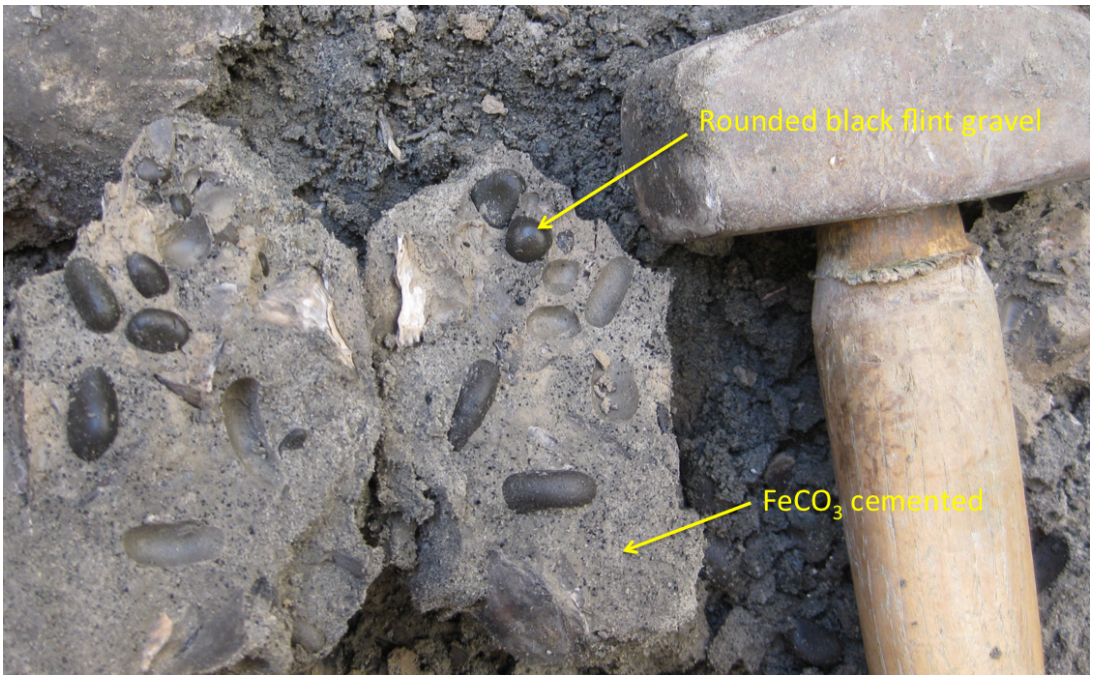


Figure 4.10 Clay-rich band towards the base of the Upnor Formation

The contact between the Upnor and Thanet Sand formations (Figure 4.11) was observed as sharp, with no evidence of bioturbation.

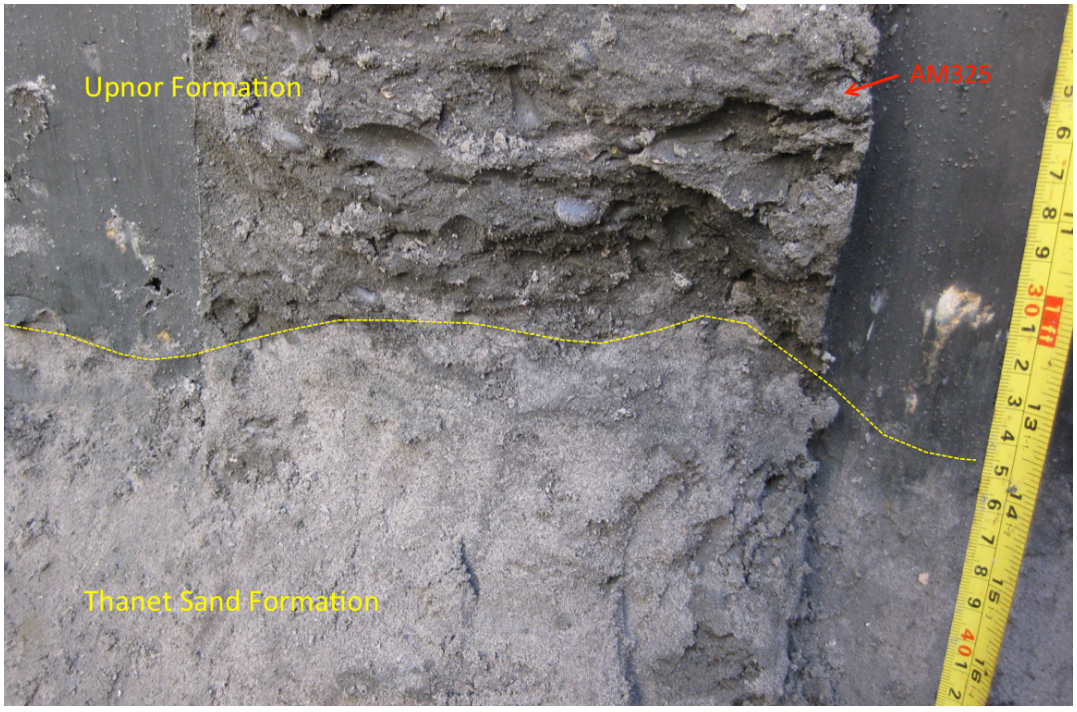


Figure 4.11 Contact between Upnor and Thanet Sand formations

During inspection of the 'muck pile', a gravel-size iron-type nodule was found within the stockpile of yellow-green weathered Upnor material. When unearthed it displayed a distinctive turquoise-blue colour (Figure 4.12a) that transformed to yellow-brown within 1 hour of exposure to the atmosphere (Figure 4.12b).

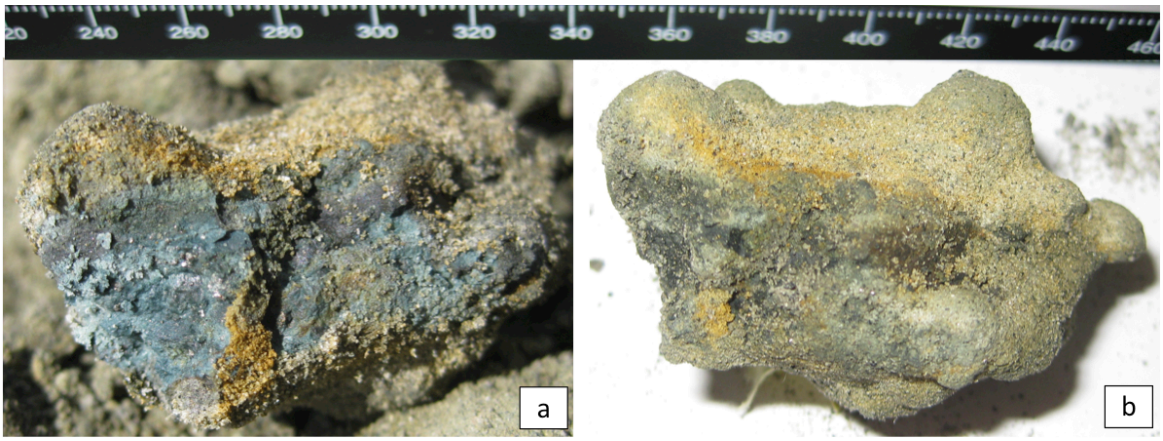


Figure 4.12 Probable nodule of green rust from Abbey Mills

During construction through the top part of the Upnor Formation, the author, excavator operator and excavation foreman, experienced significant fatigue and light-headedness and a sulphurous odour was sensed by the excavation foreman. This was treated as a recorded incident to the Lee Tunnel site management team and Health & Safety officer. Four gas monitors were in use at various points within the shaft diameter but none recorded any significant fall in the level of atmospheric oxygen during the incident. It is possible that green rust within the ground oxidised upon exposure to the atmosphere during excavation and that the human body was sensitive enough to react to the initial symptoms of oxygen depletion in the air when the gas monitors were not. The sulphurous odour may also indicate oxidation of dispersed nanoparticles of pyrite.

4.3 Apparatus

4.3.1 Introduction

A selection of X-ray diffraction (XRD), Fourier transform infrared (FTIR) spectroscopy and optical techniques, such as thin section (TS) petrography and scanning electron microscopy (SEM), were used to help identify the mineralogy of samples in the reduced and oxidised state. In addition, soil suction tests, using the filter paper (FP) technique, were undertaken to ascertain the soil water retention curves (SWRC).

Each of the techniques is described below. Table 4.3 summarises the application of each during laboratory testing.

Table 4.3 Application of apparatus for laboratory testing

Technique	Sample condition	
	Reduced	***Oxidised***
XRD	✓	✓
FTIR	✓	✓
TS		✓
SEM		✓
FP		✓

4.3.2 Identification of oxidised mineralogy

Powder X-ray diffraction – point detector method

One hundred and twenty eight oxidised soil samples from the Tideway Tunnel series 1000 and 5000 phase borehole investigations, plus a further six tub samples from the Beckton connection shaft, were subjected to powder XRD analysis (Table 4.4). The samples from the series 1000 boreholes were analysed as part of an initial interpretation of ground conditions for the Tideway Tunnel, prior to the current research. The series 1000 samples were recovered between January and August 2009.

Table 4.4 Oxidised samples analysed using powder XRD

Stratum	Series 1000	Series 5000	Beckton
Lower Mottled Beds	15	16	-
Pedogenic Upnor	8	27	-
Upnor (unaltered)	7	24	6
Thanet Sand Formation	7	24	-

The aim of the analysis was to characterise the bulk mineralogy of soil samples in an oxidised condition. Analysis was undertaken using a Phillips 1820 automated X-ray diffractometer (Figure 4.13). This was located in and owned by the Natural History Museum (NHM) and operated by Dr J. Huggett (Consultant, Petroclays).

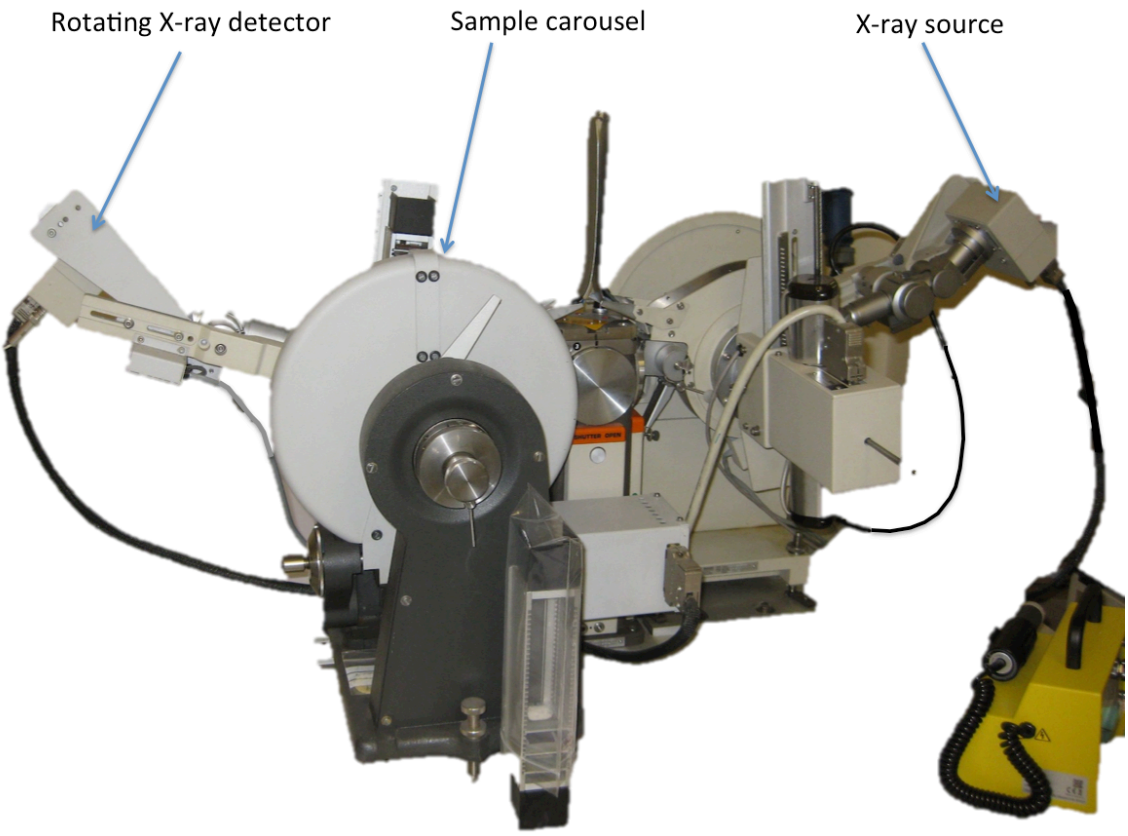


Figure 4.13 Phillips 1820 automated X-ray diffractometer

X-ray diffraction is a widely used technique to identify clay minerals, their crystal structure and chemical composition. X-rays have wavelengths ranging between 10^{-12} and 10^{-8} m (Mitchell, 1993) and are generated by a cathode ray tube, filtered to produce monochromatic radiation, further collimated, concentrated and directed as a beam towards a sample.

Elastic scattering of waves is produced when the incident X-rays strike the particle electron and a number of constructive waves are reflected in a few directions as determined by Bragg's Law ($n\lambda=2d \sin \theta$). In this manner, atomic planes (cleavage faces) at a spacing *'d'* within a crystal, produce a reflection of X-ray beams (Figure 4.14) at certain angles of incidence, θ, in which λ is equal to wavelength and *n* is an integer. This law relates the wavelength of electromagnetic radiation to the diffraction angle and the lattice spacing in a crystalline sample (Moore and Reynolds, 1997; Pecharsky and Zavalij, 2009). X-rays produce useful diffraction patterns because the wavelength λ is typically the same order of magnitude as the spacing, *d*, between the atomic planes in crystalline materials (Mitchell, 1993).

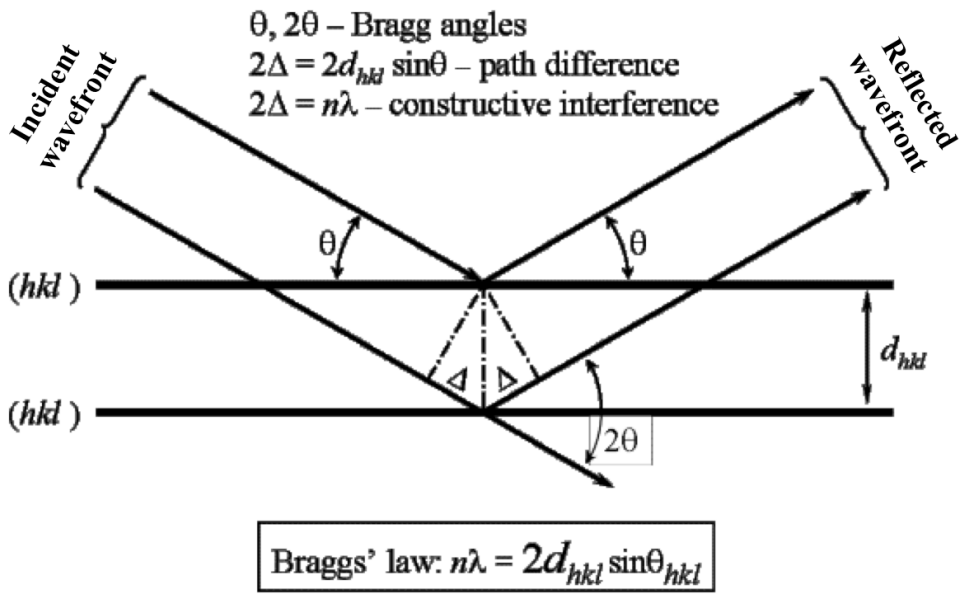


Figure 4.14 Geometric conditions for X-ray diffraction according to Bragg's Law

Figure from Pecharsky and Zavalij (2009)

The diffracted X-rays are detected, processed and counted and by scanning the sample through a range of 2θ angles, all possible diffraction directions of the lattice are attained by the random orientation of the powdered material. Conversion of the diffraction peaks to *d*-spacings allows identification of the mineral because each mineral has a set of unique *d*-spacings from which standard reference patterns are derived for comparison.

In preparation for XRD analysis, each soil sample is mixed with distilled water and gently crushed in a McCrone micronizing mill, with a few drops of ammonia added to act as a dispersant. The resulting slurry is placed in an ultrasonic bath for 30 minutes to release the maximum amount of clay into suspension and then centrifuged (at 1000 revolutions/minute) for 4 minutes to leave only the <2 μm fraction in solution. The clay suspension is then decanted off from the >2 μm fraction and centrifuged, at higher speed (4000 revolutions/minute) for 20 minutes until all of the clay is removed from suspension.

Using a pipette each sample is mounted on a heated silicon wafer (Figure 4.15), used to negate potential background interference, and loaded into the X-ray diffractometer. The samples are scanned using Ni-filtered Cu Kα radiation, at a rate of 15 seconds per 0.15° step width, using 3 mm slits, from 5 to 70° θ.

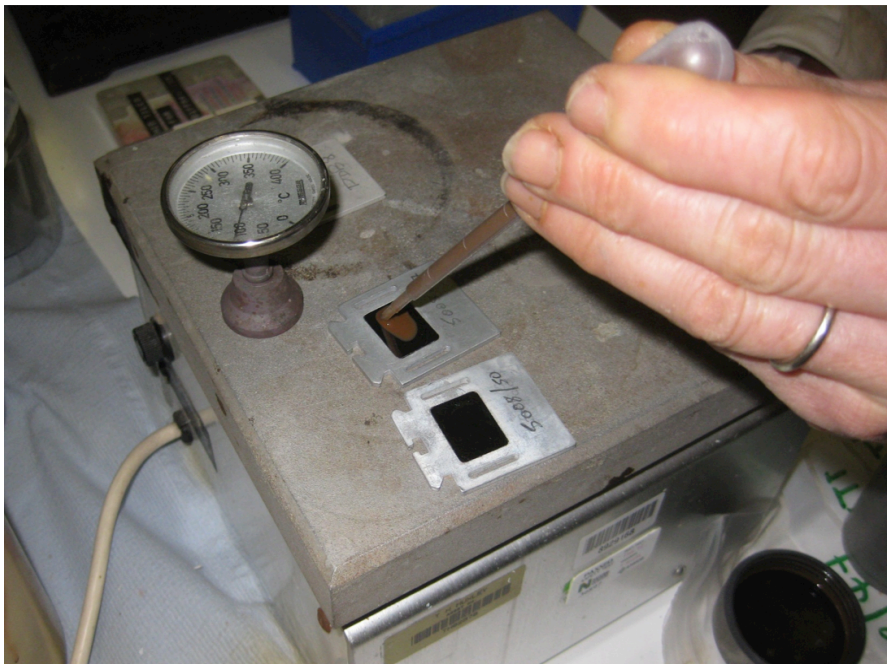


Figure 4.15 Mounting of sample via pipette onto a silicon wafer

Optical microscopy

Seventy seven oxidised soil samples from the Tideway Tunnel series 5000 phase borehole investigation, plus four tub samples from the Beckton Connection shaft, were subjected to optical microscopic analysis, as summarised in Table 4.5.

Table 4.5 Soil samples analysed using optical microscopy

Stratum	Series 5000	Beckton
Lower Mottled Beds	14	-
Pedogenic Upnor	20	-
Upnor (unaltered)	20	4
Thanet Sand Formation	19	-

The aim of the analysis was to identify specific mineral types within oxidised sediment, in particular, the presence of pyrite, goethite and glauconite. Oxidised soil samples were prepared as thin section mounts and analysed with an Olympus EX41 optical microscope and point counter (Figure 4.16), owned and operated by Dr J. Huggett.

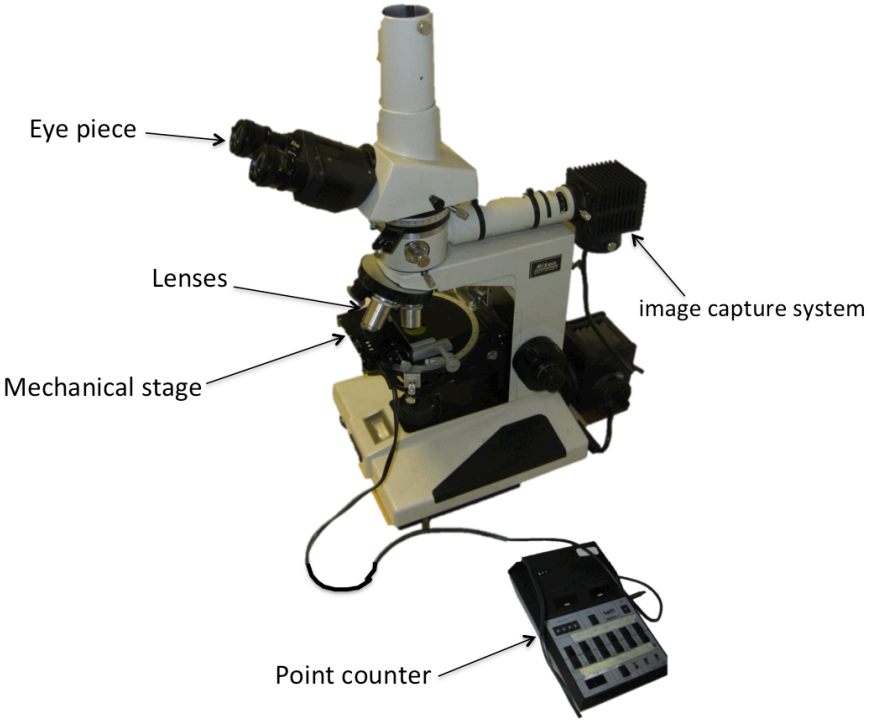


Figure 4.16 Olympus EX41 optical microscope

Optical microscopy involves the use of an optical petrological microscope to view minerals in thin section that otherwise cannot be seen with the naked eye. The technique involves passing visible light, transmitted through or reflected from the thin section sample, through single or multiple lenses to produce a magnified view that allows individual minerals to be observed through the eyepiece. The apparatus includes a manually operated mechanical stage and point counting mechanism to enable modal analysis of various minerals in the thin section, and an image capture system to take snapshot photographic images.

In preparation for thin section analysis, a small teaspoon-size sample of soil is consolidated by injection of epoxy resin and then cut to an appropriate size for advanced preparation. The sample is further reduced in size by grinding with abrasive discs and then smoothed, using silicon carbide slurry (Figure 4.17a), before being mounted on a glass slide (frosted side for increased bonding) using Loctite 358 UV resin (Figure 4.17b) and compressed in a mechanical press for 5 minutes. The slide is cured in an oven, using ultraviolet light and then thinned using a circular diamond cutting saw (Figure 4.17c). More precise thinning is then attained using a thin sectioning system, incorporating a rotating grinder and LED micrometer for thickness detection. Accurate measurement of the slide is undertaken using a caliper gauge, until the required thickness is reached (Figure 4.17d).



Figure 4.17 Preparation of petrographic thin section

Scanning electron microscopy (SEM)

All the U38 soil samples obtained from the Abbey Mills shaft logging exercise were subjected to SEM analysis (Table 4.6).

Table 4.6 Analysis of U38 samples

Sample Ref	Sam Shaw/Christine Rogers	Jenny Huggett
AM270		✓
AM280	✓	✓
AM290	✓★	✓
AM295	✓	✓
AM305	✓	✓
AM320	✓	✓
AM325		✓

★ *includes an additional grab sample*

Six samples were despatched to Dr S. Shaw and Dr C. Rogers at Leeds University (School of Earth, Atmospheric and Environmental Sciences), for analysis using a Quanta FEG 650 scanning electron microscope (Figure 4.18) and a further seven samples were analysed by Dr J. Huggett, at the Natural History Museum, as part of a semi-independent study (Huggett et al., *in preparation*). The location of each sample is shown in Figure 4.5. The aim of the SEM analysis was to obtain a visual perspective of the oxidised mineralogy of the samples and, if possible, to identify the presence of green rust in the reduced state or hexagonal goethite pseudomorphs of oxidised crystals. Additional images of pyrite and glauconite were sought.

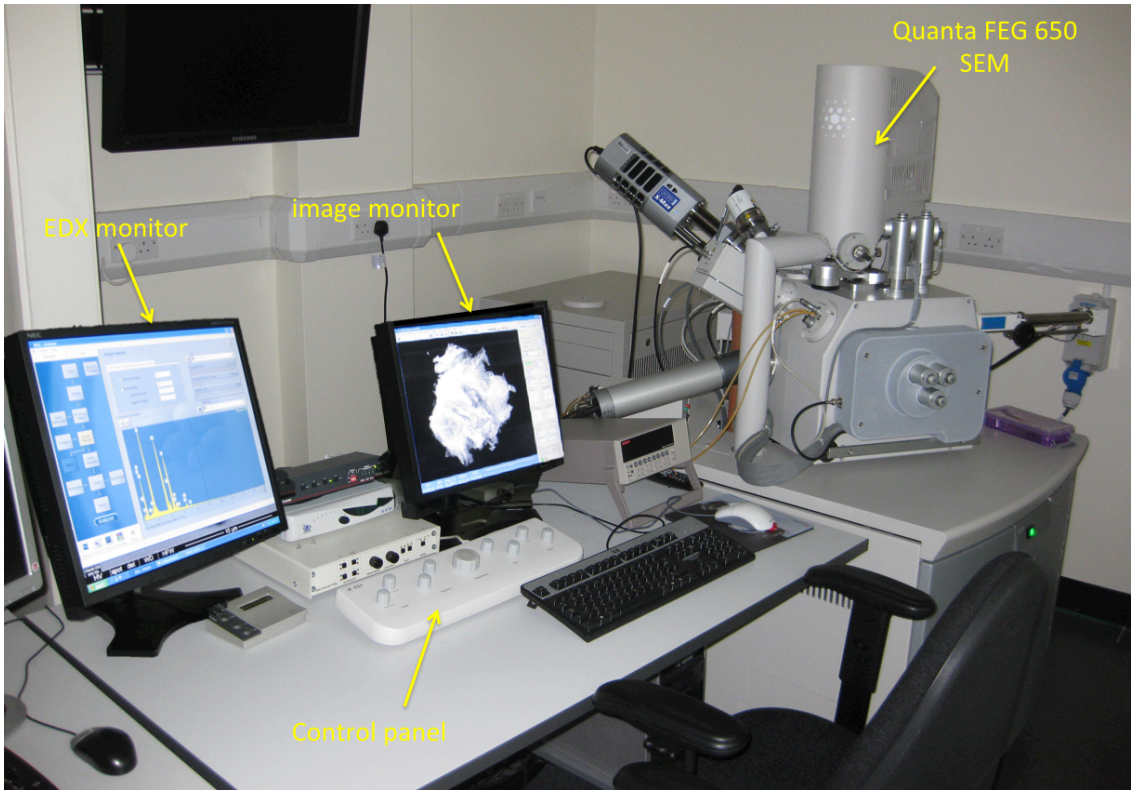


Figure 4.18 Quanta FEG 650 Scanning Electron Microscope

Scanning electron microscopy was first developed in the 1930s as a solution to the limitations in magnification and resolution using optical microscopy. The latter relies on the transmission of optical photons, whilst SEM uses an electron gun to emit a steady/continuous beam of electrons at a much shorter wavelength that permits a magnification approximately 250 times greater than the most powerful optical microscope, resolving details less than 1 nm in size. The apparatus uses a series of electromagnetic coils, firstly to compress the beam to increase its focus and precision and then to bend it, producing a scanning-type motion in the x and y axes, across the mineral specimen. The specimen is held within a vacuum chamber as electrons do not travel very far within air due to interference from atmospheric particles. The electron beam is reflected off the mineral specimen with the resulting scatter of electrons being electronically amplified by a detector and registered as variations in brightness on a

computer monitor. The image seen on the monitor represents a distribution map of the intensity of the signal being emitted from the scanned area.

The Leeds University SEM contained an Energy-Dispersive X-ray spectroscopy (EDX) capability, to characterise the chemistry of the mineral being scanned. The action of the electron beam on the mineral specimen releases X-rays that can be measured by the energy-dispersive spectrometer, to identify the atomic structure and composition of the mineral.

In preparation for the SEM, 100 g of sediment was stirred with 400 ml of deoxygenated water in a sonic bath for 30 minutes, resulting in a suspension of fines. After one week, the fines were removed using a pipette and placed on absorbent paper to remove excess water. The resulting residue was placed on a sticky carbon pad, adhered to an aluminium SEM stub (Figure 4.19a) and further coated in a layer of carbon within a carbon evaporation coating device (Figure 4.19b). The carbon is used to drain the electron current during the SEM process, to prevent excessively large intensity readings being recorded for the aluminium. The carbon-coated sample stubs are then loaded into the SEM machine (Figure 4.19c and Figure 4.19d).

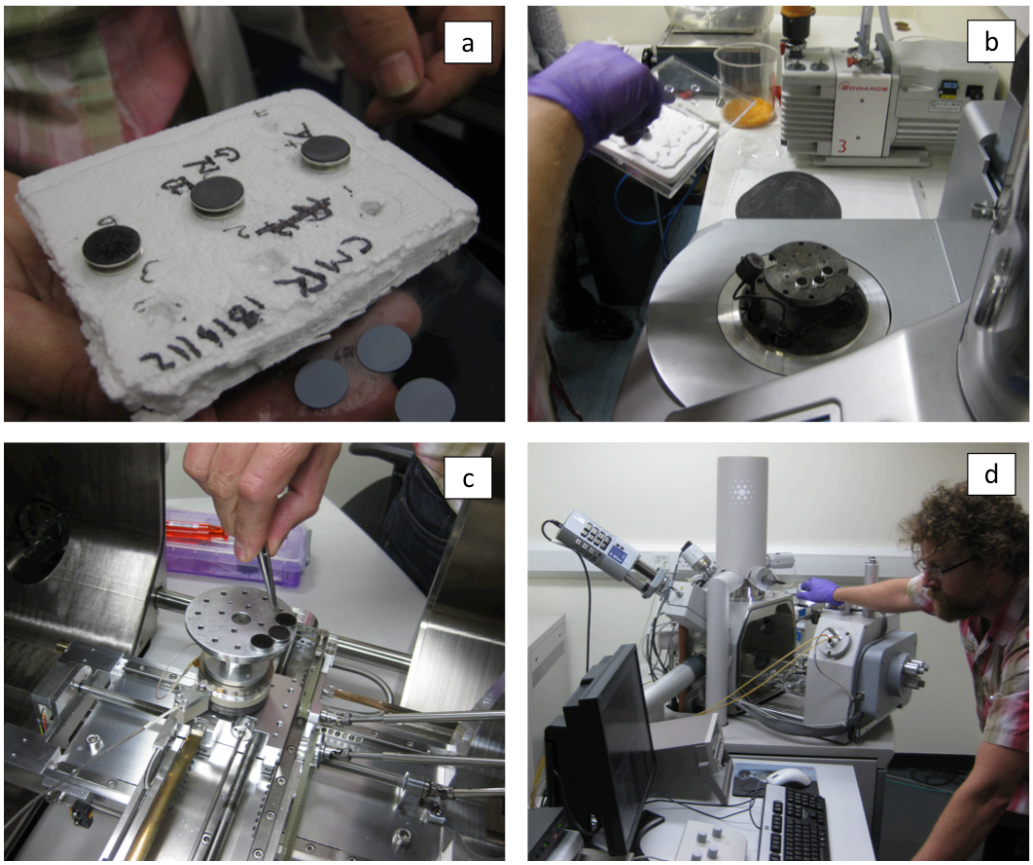


Figure 4.19 Preparation of samples for SEM analysis

4.3.3 Identification of reduced to oxidised transformation

Bespoke anaerobic chamber (glove box)

A number of authors have emphasised the need for laboratory analysis of samples containing green rust as soon as possible after collection (Phillips et al., 2003; Feder et al., 2005) because green rust oxidises very rapidly in air and care is needed to prevent it from oxidising (Drissi et al., 1995; Lewis, 1997; Feder et al., 2005). This is commonly achieved by undertaking sample preparation within a sealed anaerobic chamber (informally known as a glove box). An anoxic atmosphere is created within the chamber by purging the oxygen with an inflow of inert gas, usually nitrogen but sometimes argon (Lewis, 1997; Parmar et al., 2001; Refait et al., 2001; Feder et al., 2005; Nagata et al., 2009).

A glove box was constructed in the Soils Laboratory using teak wood and glass materials (Figure 4.20a and Figure 4.20b). The box is cuboid in shape, with internal dimensions measuring 760 mm across, 385 mm in depth and 290 mm in height.

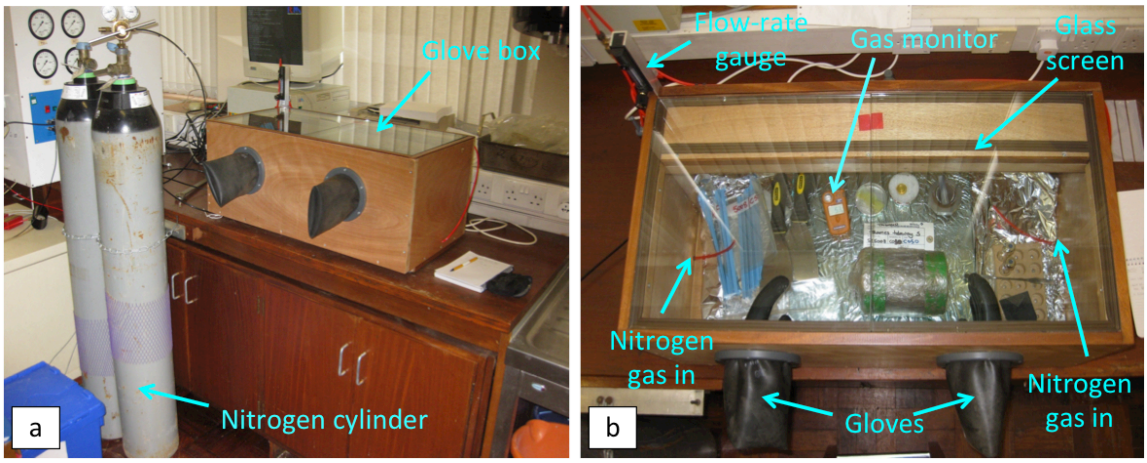


Figure 4.20 Anaerobic chamber (glove box)

Teak wood was used for construction of the base and all four sides, as it is dense and only slightly porous, yet permits modifications to be made easily and cheaply, thus allowing for progressive improvements in design. A 10 mm thick glass panel is positioned over the top as a viewing screen. The rear side of the box is hinged, to allow it to be opened for sample input. Two 110 mm diameter holes, cut into the front side, with sealed attachment of heavy-duty rubber gloves allow sample handling within the box. Finally, a small electric fluorescent light was fixed inside the top of the box for illumination during operation. The box is connected to a nitrogen cylinder via two 5 mm diameter plastic tubes inserted through both sides. Nitrogen is fed into the box via a pressure gauge regulator at a controllable rate of up to 30 l/min. Soil samples are placed within the glove box, still within their cling-film or gas-proof bag preservation wrapping, prior to closing the back door and turning on the nitrogen supply. A Crowcon gas detector (Ref: W164558) is placed within the glove box to monitor the level of

oxygen at all times during sample handling. The sample is not taken out of the protective cling-film or vacuum-sealed bag until the level of oxygen falls below 2%, a level similar to that measured in situ within the ground.

It is never possible to lower the oxygen level to below 1% per volume, even by increasing the time and flow rate of nitrogen to the glove box. At first this was assumed to be from leakage that was part of the glove box design (to allow for a positive pressure from continuous nitrogen flow) but later research showed that hydrogen and a heated palladium catalyst are required to eliminate oxygen altogether (S. Shaw, *pers. comm.*). At best, the lowest level achieved was 1.2%, which quickly rose to above 2% (typically 3 to 5%) upon removal of the cling-film or vacuum-sealed bag from air trapped within the pore spaces in the sample. With continued inflow of nitrogen, the level of oxygen was again reduced to between 1.5 and 3.0% during sample dissection.

Although the glove box was designed to facilitate gas leakage, to allow for the purge of oxygen, a number of checks were undertaken to record whether these might hinder the process of achieving anoxia internally. To enable this, the box was filled with nitrogen, as far as possible (usually to 1.2% oxygen content), with no sample inside. The nitrogen flow was then turned off and the gas detector monitored over an ensuing period of time. The resulting rate of oxygen 'recovery' was then monitored. The results were similar for each test, with oxygen content increasing at 1% per 25 minutes (the usual time taken to sub-sample one soil sample). This implies that the glove box leakage is not detrimental to achieving anoxic conditions for soil sub-sampling, particularly given that a low rate of positive nitrogen flow is maintained throughout the sub-sample preparation.

Application of glycerol for protection from oxidation

In addition to the use of a glove box, Hansen (1989) proposed that wetting a sample containing green rust with compounds containing hydroxyl groups, such as glycerol or ethylene glycol, offers protection from rapid oxidation. Glycerol does not penetrate the interlayer region of the pyroaurite structure but does reduce the diffusion rate of oxygen into the sample. This process has since been adopted by a number of authors during laboratory experiments to characterise green rust (Lewis, 1997; Refait et al., 2001; Phillips et al., 2003; Mazeina et al., 2008; Nagata et al., 2009). In particular, Mazeina et al. (2008) found that samples containing green rust remained unoxidised for 1.5 hours when covered in glycerol. Application of glycerol or ethylene glycol was therefore undertaken on samples obtained from the Tideway Tunnel series 4000 boreholes.

Powder X-ray diffraction - position sensitive detector (XRD-PSD) method

Green rust has been identified in XRD-PSD (Hansen and Bender Koch, 1998; Phillips et al., 2003; Bearcock and Perkins, 2007; Christiansen et al., 2009; Popov et al., 2010) which is particularly effective in recording the transformation of green rust into iron oxides, such as goethite and/or lepidocrocite, during oxidation (Taylor, 1980; Taylor and McKenzie, 1980; Bender Koch and Morup, 1991; Drissi et al., 1995; Kwon et al., 2007; Ayala-Luis et al., 2008; Popov et al., 2010). In such experiments, the transformation caused a change in the XRD pattern, typically with peak spacings shifting to lower values accompanied by a colour change of the sample from blue-green to yellow-brown.

Similarly, XRD techniques have been used to characterise the growth of green rust during reduction of FeOOH lepidocrocite (Ona-Nguema et al., 2001), indicating that green rust is an intermediatory phase in a reversible chemical reaction. These experiments also used an anaerobic chamber and glycerol coating to prevent oxidisation of the evolving green rust.

One limitation in using XRD-PSD is that it is inappropriate for identifying a minor mineral component within a sample (Ruby et al., 2006) and green rust often constitutes only a minor percentage of the total soil volume (Bearcock et al., 2006). In addition, it is diffuse, scattered and mixed with other mineral compounds, making it difficult to distinguish (Refait et al., 2001; Trolard et al., 2007). Bender Koch and Morup (1991) concluded that for green rust to be detected by XRD techniques, it must be present in the soil in a higher concentration.

Sixty six soil samples from the Tideway Tunnel series 4000 and 5000 phase borehole investigations, plus a further three tub samples from the Beckton connection shaft, were subjected to position sensitive XRD-PSD analysis (Table 4.7).

Table 4.7 Samples analysed using position sensitive XRD

Stratum	Series 5000	Series 4000	Beckton
Lower Mottled Beds	2	-	-
Pedogenic Upnor	22	6	-
Upnor (unaltered)	14	15	3
Thanet Sand Formation	4	3	-

All core samples were prepared within the glove box to extract a thimble-size quantity of soil from the centre of the core (Figure 4.21a), which is assumed to be furthest from the external oxidation front. The sample is ground in a mortar and pestle to ensure randomness of the crystal atomic planes and avoid any preferred orientation (Figure 4.21b).

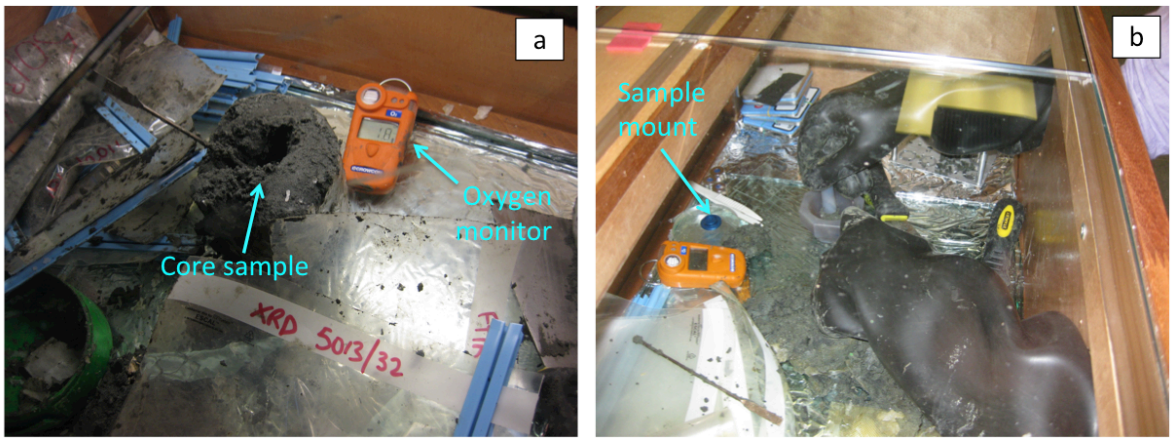


Figure 4.21 Sample preparation for XRD-PSD analysis

Grinding also reduces the particle size and so increases the number of particles likely to be included in the diffraction process. After grinding, the sample is placed in a 1 mm deep x 13 mm diameter sample mount and carefully smoothed flush with the top of the mount, using a glass slide. The sample mount is then placed in a protective casing and sealed in a gas-proof pouch prior to despatch for XRD-PSD analysis.

The analysis used an Enraf Nonius Powder XRD-PSD machine (Figure 4.22), located in and owned by the Natural History Museum (NHM) and operated by Dr Jens Najorka (X-Ray Laboratory Manager, Mineral Sciences).

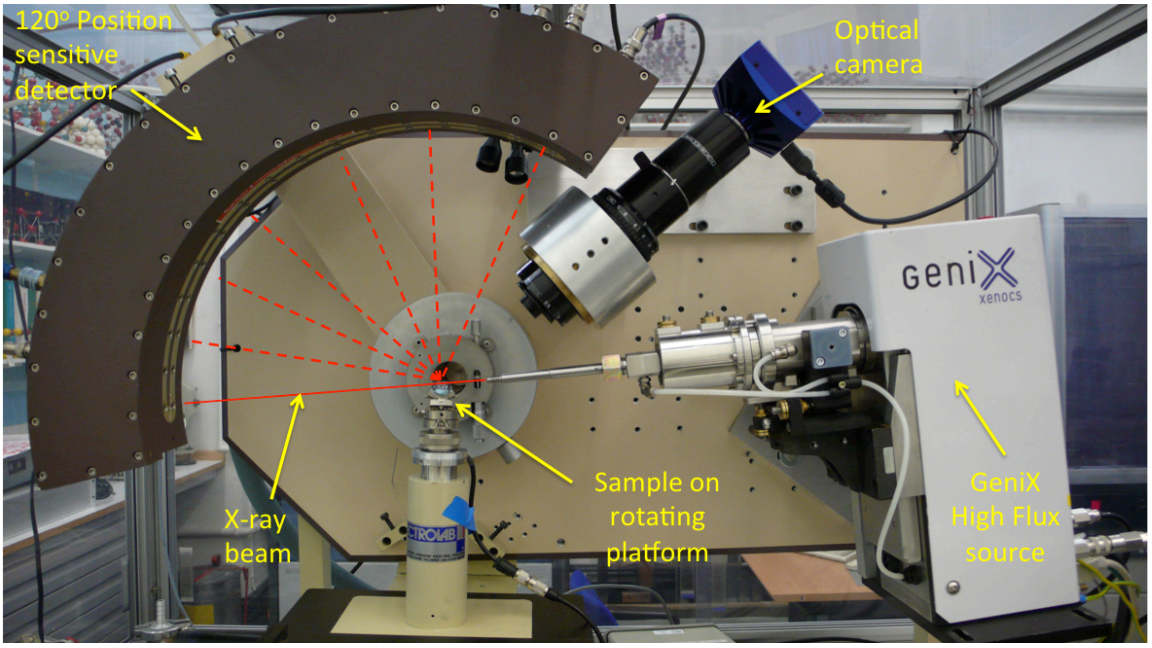


Figure 4.22 Enraf Nonius Powder XRD-PSD machine

For each analysis the sample mount is placed on a sample platform within the XRD-PSD machine as quickly as possible after removal from the air-tight packaging; usually in less than one minute. An X-ray beam is directed at the sample using a GeniX High Flux source equipped

with a FOX 2D focussing mirror. The diffracted beams are collected by an INEL 120˚ curved position sensitive detector (PSD), capable of simultaneously recording diffracted X-ray intensities over a 2θ range of 120˚. Each analysis lasts for one hour, during which a total of 60 one-minute snapshots are recorded. The sample is exposed to the atmosphere for the entire period, with the intention of observing the transformation in XRD pattern during the oxidation of the green rust. Throughout the analysis, the sample is rotated on the holder, to improve the particle counting statistics.

Attenuated Total Reflection (ATR) Fourier Transform Infrared (FTIR) Spectroscopy

FTIR is a form of Internal Reflection Spectroscopy and was first developed/commercialised in the late 1950's to obtain an infrared spectrum of absorption of a solid (soil) sample. It is a powerful tool for characterising the distribution of different chemicals in heterogeneous materials (Chan and Kazarian, 2003). Every mineral has its own unique identity (Povarennykh, 1978), although many are very similar.

FTIR has been used to differentiate and quantify iron oxides and oxyhydroxides and, in particular, the spectra for goethite and lepidocrocite are well established (Namduri and Nasrazadani, 2008). The infrared spectra of iron (II) hydroxide and green rust were first obtained by Misawa et al. (1969), who found that its spectral intensity decreased during oxidation at the same time as absorption spectra, characteristic of goethite (αFeOOH), appeared.

Forty nine soil samples from the Tideway Tunnel series 4000 and 5000 phase borehole investigations, plus a further three tub samples from the Beckton connection shaft, were subjected to FTIR analysis, as summarised in Table 4.8.

Table 4.8 Samples analysed using FTIR

Stratum	Series 5000	Series 4000	Beckton
Lower Mottled Beds	2	-	-
Pedogenic Upnor	9	5	-
Upnor (unaltered)	11	16	3
Thanet Sand Formation	3	3	-

In preparation for analysis, each sample was divided into a set of reduced and oxidised specimens. The reduced samples were prepared within the glove box (Figure 4.23a), in which a thimble-sized quantity of soil was inserted into a screw-top glass vial (Figure 4.23b) and placed within a sealed gas-proof pouch.

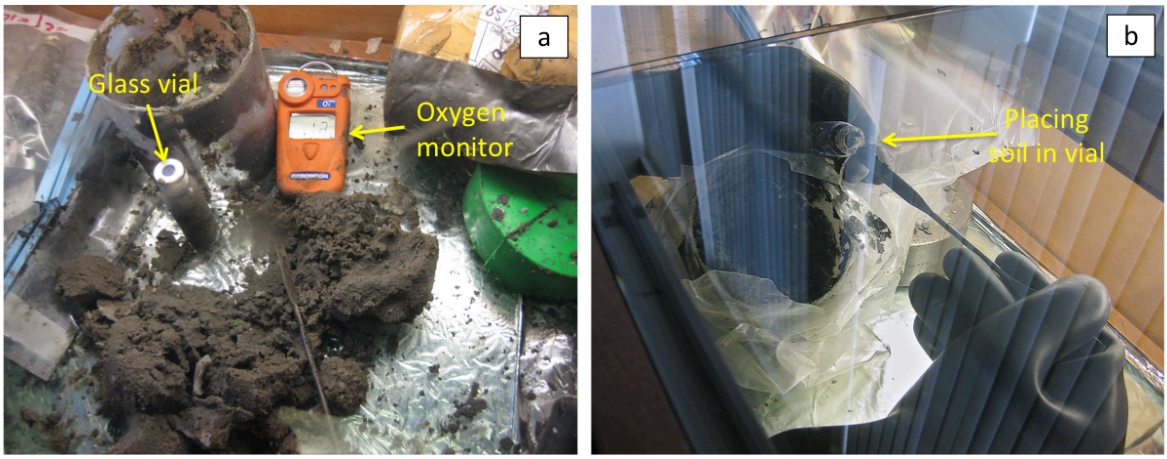


Figure 4.23 Sample preparation for FTIR analysis

The oxidised samples were baked on a sample tray in an oven at a constant temperature of 105˚C for 24 hours. The analysis used a Thermo-Nicolet 5700 Fourier Transform Infrared (FTIR) spectrometer (Figure 4.24), housed in the Department of Earth Science and Engineering that was operated by the author, initially with the assistance of Dr Richard Court.

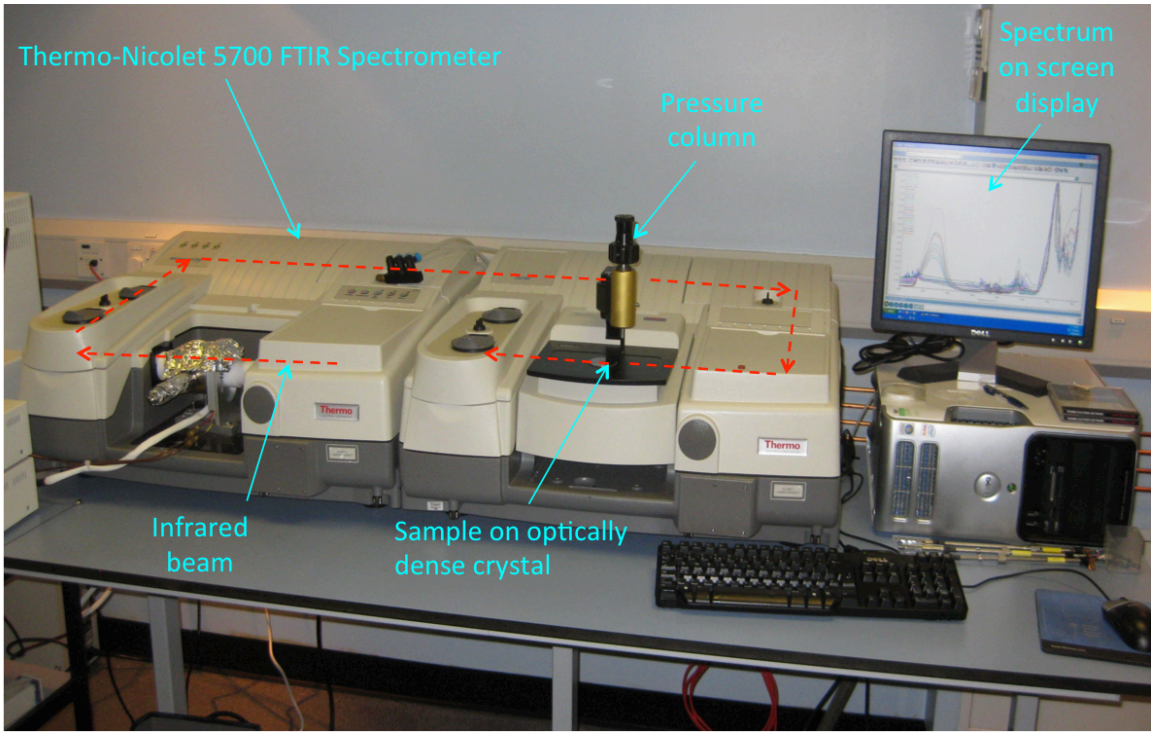


Figure 4.24 Thermo-Nicolet 5700 Fourier Transform Infrared (FTIR) spectrometer

The aim of the analysis was to compare the differences in Infrared (IR) absorption spectra between the fresh and baked samples. An additional glycerol-coated, fresh sample was prepared from most of the series 4000 samples, for further comparison and to test its usefulness in preventing oxidation.

A beam of infrared light is passed through an optically dense but transparent crystal (typically diamond or germanium), possessing a high refractive index in which it is reflected at least once off the internal surface. This results in an evanescent wave extending no more than 0.5 µm beyond the crystal surface. When a soil sample is placed in contact with the crystal surface, total reflection is destroyed (Harrick, 1967) and the evanescent wave protrudes into the sample by as much as 2.0 µm (Figure 4.25). The wave is then attenuated (altered) where it is absorbed by the sample and partially reflected back into the IR beam, exiting at the other end of the crystal and then through a detector. The reflectivity is a measure of the interaction of the evanescent wave and soil sample and is output as an infrared spectrum for the attenuated beam (Harrick, 1967). In all cases, an initial background reading is taken for air in contact with the crystal, prior to generating a second spectrum for the soil sample. The final result is the sample spectrum minus the background spectrum, to correct for any atmospheric effects (R. Court *pers. comm.*).

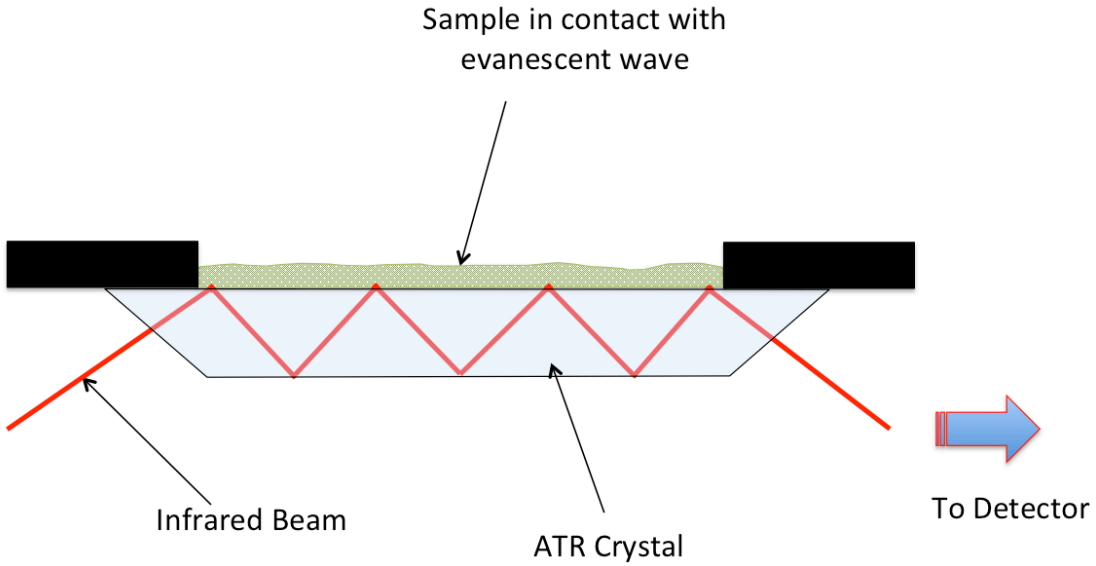


Figure 4.25 Production of an evanescent wave

Figure based on PerkinElmer (2005)

4.3.4 Soil suction filter paper test equipment

One hundred and forty three rotary core soil samples were prepared in the Department of Civil and Environmental Engineering Soils Laboratory for soil suction tests using the Filter Paper technique. Table 4.9 indicates the number and stratigraphic level of the samples analysed using this technique.

Table 4.9 Rotary core samples for soil suction analysis

Stratum	Series 4000	Series 5000	Series 6000	Total
Lower Mottled Beds	3	27	35	65
Pedogenic Upnor Formation	2	13	3	18
Upnor Formation	7	14	3	24
Thanet Sand Formation	6	29	1	36

The purpose of the filter paper tests was to differentiate between the soil suction characteristics of the Lower Mottled Beds and those of the Upnor and Thanet Sand formations.

Soil suction is found in all partially saturated soils above the groundwater table (Chandler et al., 1992; Hu et al., 2010). The filter paper method is a relatively simple and inexpensive soil suction experiment, used to measure total and matrix suction. Matrix suction of a soil is the difference between air and water pressure within its pores and can be expressed by:

$$s = (u_a - u_w) \qquad \text{Equation 4.1}$$

which can be inferred from the contact filter paper method (Bicalho et al., 2007). The test works by placing absorbent filter paper in contact with a soil surface. Water in the liquid phase exchanges freely from the soil to the filter paper until both come into equilibrium (Fredlund and Rahardjo, 1993; Hu et al., 2010) and the soil and filter paper have the same suction value. The water content of the filter paper is measured and converted to suction using a filter paper calibration curve (Fredlund and Rahardjo, 1993; Bicalho et al., 2007).

For each filter paper test, a core sample is removed from its protective wrapping and cut to an appropriate size (according to ASTM D 5298-92), typically 100 mm diameter by 20 mm thick for clay samples (Figure 4.26a) and 100 mm by 60 mm for sandier samples to prevent disintegration during cutting. Each end of the sample is smoothed to provide an intimate contact with the filter paper (Whatman No.42), which is placed dry on either end, using tweezers, and covered with a perspex disc (Figure 4.26b and Figure 4.26c). The sample and perspex discs are then wrapped in and sealed by several layers of cling film to prevent evaporation (Figure 4.26d), placed in two sealable plastic sample bags and stored in a temperature-controlled laboratory for seven days to allow the soil and filter paper to reach equilibrium.

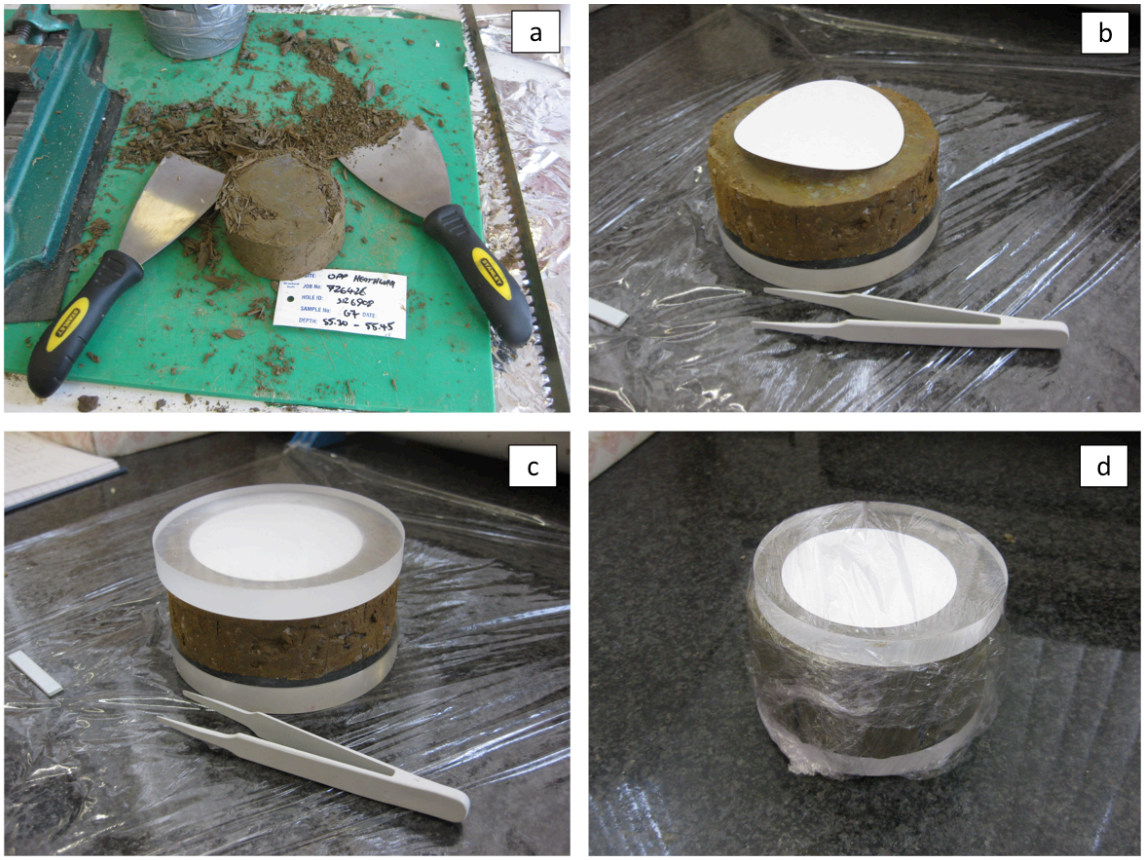


Figure 4.26 Sample preparation for the filter paper test

The sample is then unwrapped and the moisture content of the filter paper calculated by comparing its weight when wet and dry, after a minimum of 4 hours oven-drying at 105˚C. At the same time, the soil sample is weighed and measured using a caliper gauge, to calculate changes in volume, void ratio and saturation and thus enable the soil matrix suction to be obtained using previously established correlations (Chandler and Gutierrez, 1986; Chandler et al., 1992).

The Soil Water Retention Curves are derived by continuation of the filter paper method until the soil is dry (or the residual moisture content is achieved). The relationship between the volumetric water content and soil suction is usually plotted graphically as the soil water retention curve, or SWRC (Barbour, 1998; Fredlund et al., 2002; Péron, 2007). Soil is initially saturated until air begins to enter the pores at a point called the air-entry value (AEV) and drying begins at an equivalent value of suction. A decrease in the soil grain size leads to an increase in the AEV of suction (Barbour, 1998; Fredlund et al., 2002), so that a soil with a greater percentage of clay fraction and hence smaller pore sizes exhibits the highest suction values (Cumbers et al., 2008) .

4.4 Field Tests

4.4.1 Borehole gas monitoring

During the ground investigation for the Tideway Tunnel, a number of boreholes were constructed to incorporate gas-monitoring installations within the Upnor Formation. This was partly in response to the ground gas incidences encountered during construction of boreholes SR2071 and SA1066D but is also standard procedure, whereby all strata within the London Basin geological sequence are targeted for ground gas monitoring.

The installations are constructed by insertion of a length of 50 mm diameter UPVC pipe into the open borehole, upon its completion to the required depth. The pipe contains a slotted section through the stratum of interest (also known as the 'response zone') and is embedded in sand over this interval through the application of a "geowrap" membrane to prevent ingress of the sand. Elsewhere, it is sealed in place with bentonite, in the annulus between its outside diameter and the borehole wall. A plastic seal cap, containing a gas release tap, is placed over the top of the pipe at ground level. In this way, any gas emanating from the response zone will collect in the pipe and will be released and recorded when the gas tap is opened.

The aim of the borehole gas monitoring exercise is to manually record the concentration of different gases within specific boreholes using a Geotechnical Instruments GA2000 gas-monitoring device. This contains a suction attachment to extract any gas accumulation in the borehole and records the concentrations of the following gases:

- Oxygen (O_2)
- Carbon dioxide (CO_2)
- Methane (CH_4)
- Carbon monoxide (CO)
- Hydrogen sulphide (H_2S)

The gas monitor records the flow of gas from the borehole, as volume in litres per hour. In addition, a record of the barometric pressure is taken during each monitoring visit.

The monitoring boreholes are predominantly from the series 1000 borehole investigation, constructed in the period between January and August 2009 (Figure 4.27). These were augmented by a number of investigation boreholes recommissioned from the NLFRS tunnel and TWRM southern extension; both having previously encountered oxygen-depleted air during construction in the Upnor Formation (Lewis and Harris, 1998; Newman and Wong, 2011).

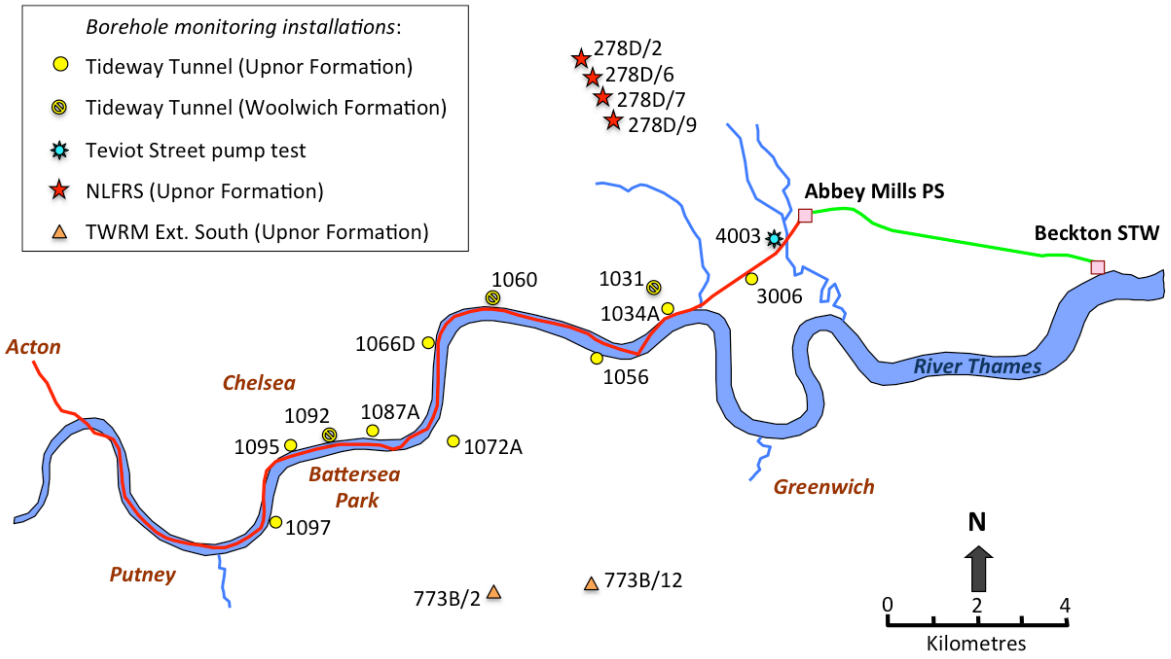


Figure 4.27 Location of gas monitoring boreholes

In addition, a small selection of boreholes containing gas-monitoring installations within the Woolwich Formation Upper Shelly and Laminated Beds were selected for observation, as part of this research (Figure 4.27). Monitoring of the boreholes commenced in April 2011 and is planned to continue at least until tunnel construction. Significant budgetary constraints affected the Tideway Tunnel project between September 2009 and April 2011 and no borehole monitoring was undertaken during this period.

4.4.2 Borehole gas sampling

Sampling of ground gas from the Upnor Formation was undertaken at two borehole locations (Figure 4.27):

- SA1066D (Tideway Tunnel)
- 773B/12 (TWRM Southern Extension)

The aim of the sampling exercise is to quantify additional elements within the gas, undetected by site operated apparatus and compare the quantities of gas to those obtained from the monitoring exercise. The numbers of sampling visits for each of the above boreholes are summarised in Table 4.10.

Table 4.10 The geology of gas sampled boreholes

Borehole	Target stratum	Logging description	No. sampling visits
SA1066D	Pedogenic Upnor	Very stiff mottled light bluish grey and orange brown sandy, slightly gravelly clay, locally clayey and very gravelly sand. Gravel is sub angular to rounded, fine and medium flint.	16
773B/12	Upnor	Dark greenish brown, slightly clayey sand with occasional rounded, fine to medium flint and abundant fine to medium black glauconite sand.	1

A method statement describing the process of gas sampling is given in Appendix A.

4.4.3 Borehole pump-out test

A relatively small-scale pump-out test was conducted as part of the Tideway Tunnel ground investigation (Series 4000) incorporating one pump-out borehole and two adjacent observation boreholes. The test site, on the south bank of the Limehouse Cut, was located in Teviot Street, Bromley, in the London Borough of Tower Hamlets. A detailed site location plan and design cross section of the boreholes is included in Appendix B.

The 305 mm diameter pump-out borehole (SR4003) was drilled to a depth of 45.5 m, using rotary percussion techniques and terminated in the Thanet Sand Formation. The observation boreholes (SR4206 and SR4207) were drilled at 127 mm diameter, using rotary coring, at a distance of 10.0 m either side of SR4003. Borehole SR4206 was excavated to a depth of 80.0 m whilst Borehole SR4207 was excavated to 76.2 m; both terminating in the Seaford Chalk Formation.

The Upnor Formation was measured as 6.0 m thick, between 32 and 38 m below ground level. The piezometric level of the lower aquifer was recorded, prior to the test, at 28 m below ground, indicating that the Upnor Formation is saturated and under 4.0 m of piezometric head pressure.

A small Grundfos SP8A submersible pump was placed in Borehole SR4003, within a 14.5 m section of 150 mm internal diameter, plastic slotted well screen. This extended from the base of the borehole, through the top 7.0 m of the Thanet Sand Formation. A 5.0 m section of 25 mm diameter plastic slotted pipe, with geotextile wrap, was installed entirely within the Upnor Formation in both observation boreholes (Figure 4.28).

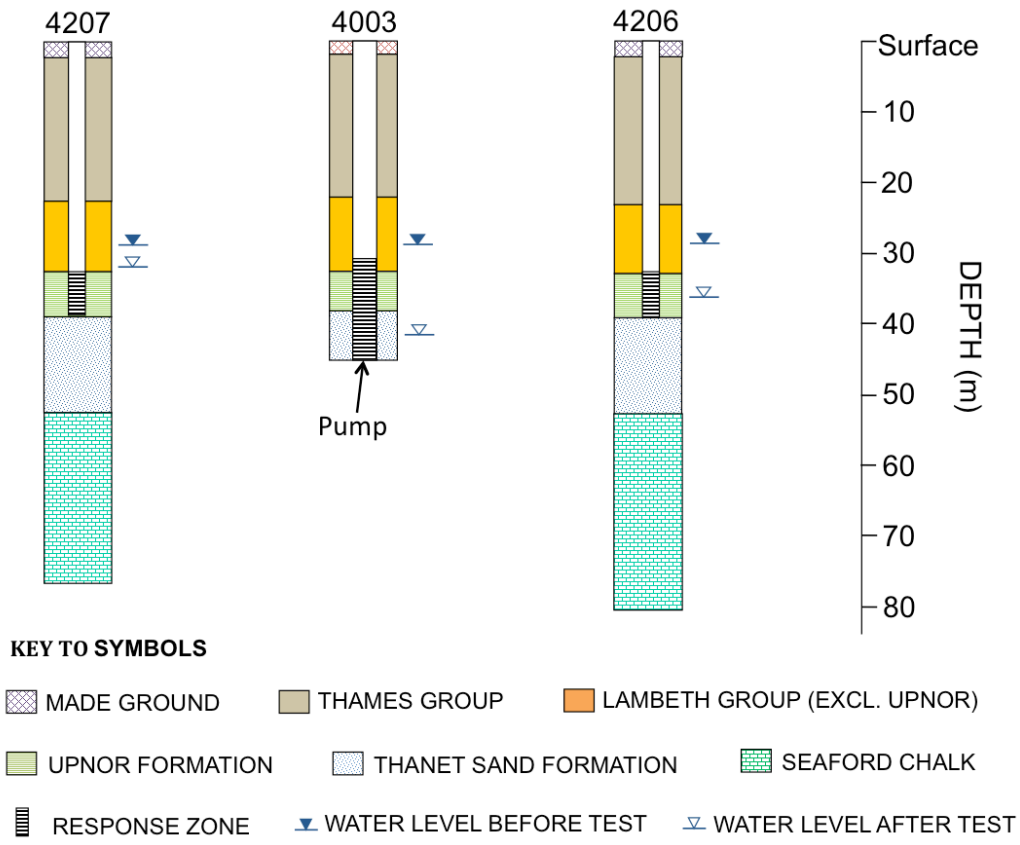


Figure 4.28 Schematic cross section through pump out test boreholes

The aim of the pump out exercise was to draw down the lower aquifer water table, below the Upnor Formation, to change the in situ subsurface environment from reducing to oxidising conditions. The submersible pump is capable of extracting groundwater at a rate of between 3.3 to 3.6 m^3 per hour (0.92 to 1.0 litres/second). At the same time, the installations in all three boreholes were monitored for any resulting change in gas concentrations, particularly oxygen depletion.

Severe time constraints were placed on both drilling and pumping operations because the site was located within an active demolition compound (Figure 4.29). Strict environmental controls needed to be satisfied in advance of the planned 24 hour pumping operations.



Figure 4.29 Borehole pump out test site

The regulatory consents granted limited pumping operations to 105 hours (just under 4.5 days), commencing at 14:00 on Thurs 16th August 2012 and running continuously for 105 hours to 23:00 on the 20th August 2012, during which 378 m^3 of groundwater was discharged to the wastewater network.

5 EXPERIMENTAL RESULTS

5.1 Identification of oxidised mineralogy

5.1.1 X-Ray diffraction

XRD was used to identify the mineralogical character of oxidised sediment samples as outlined in Chapter 4. The aim was to identify the presence of glauconite through the succession of lower Lambeth Group deposits and Thanet Sand Formation, particularly within the pedogenic Upnor Formation, and any weathering products, e.g., goethite. As XRD is unable to differentiate between glauconite, illite and mica in the presence of quartz (J. Huggett, *pers. comm.*), the data for glauconite must be regarded as an estimate and an error of >20% is assumed.

Glauconite/illite is concentrated below the Mid-Lambeth Hiatus (Figure 5.1) in the Lower Mottled Beds and in both the pedogenically altered and fresh Upnor Formation, but it is nearly absent in the Thanet Sand Formation except towards its clay-rich base. In some samples, glauconite/illite is also absent from the pedogenically altered Upnor Formation and Lower Mottled Beds, but it is always present in fresh Upnor Formation.

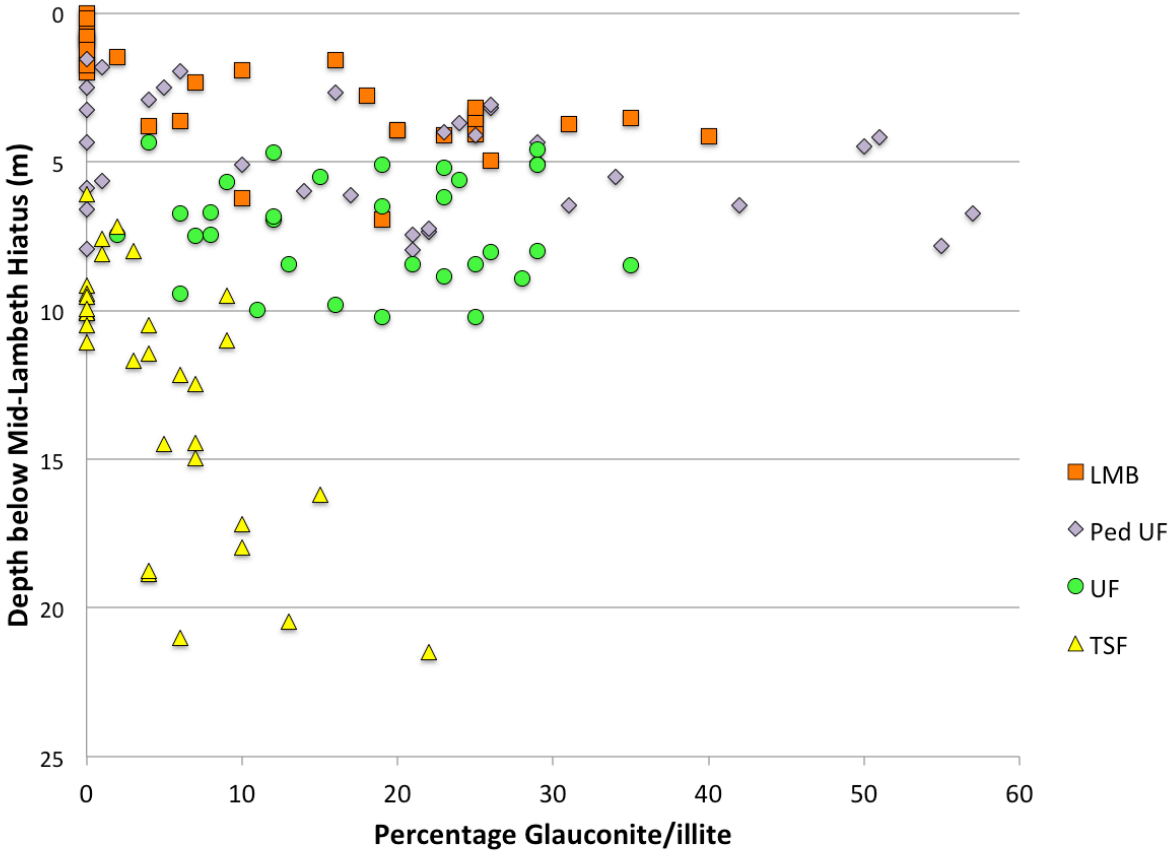


Figure 5.1 Identification of glauconite/illite by XRD

Symbols used from hereon: LMB = Lower Mottled Beds; Ped UF = Pedogenically altered Upnor Formation; UF = Upnor Formation; TSF = Thanet Sand Formation.

The XRD patterns for goethite are distinct and not confused with any other mineral, so the data give an accurate trend in its distribution. Goethite is prevalent within the Lower Mottled Beds and pedogenically altered Upnor Formation, where as much as 12% to 15% respectively has been detected (Figure 5.2). Conversely, goethite has been detected in only a few samples of fresh Upnor Formation, in concentrations no greater than 5%. It is absent in all of the 31 samples of the Thanet Sand Formation.

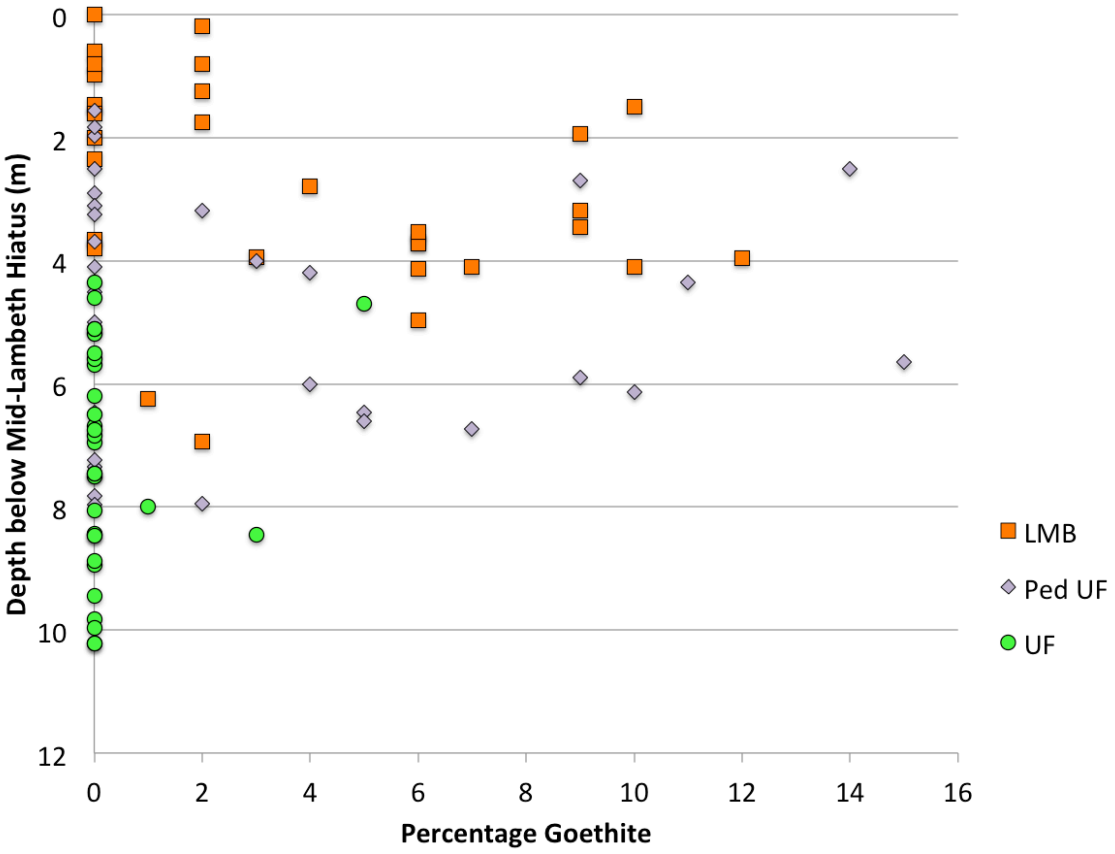


Figure 5.2 Identification of goethite by XRD

Kaolinite also has a distinctive XRD signature and occurs in the majority of samples from the Lower Mottled Beds, at up to 18% (Figure 5.3); it is absent in only a small number of samples from this stratum. Kaolinite is frequently observed in the pedogenically altered and to a lesser extent, fresh Upnor Formation samples at up to 9% and 5% respectively. It was detected in only five of the thirty-one samples of Thanet Sand Formation, at up to 3%.

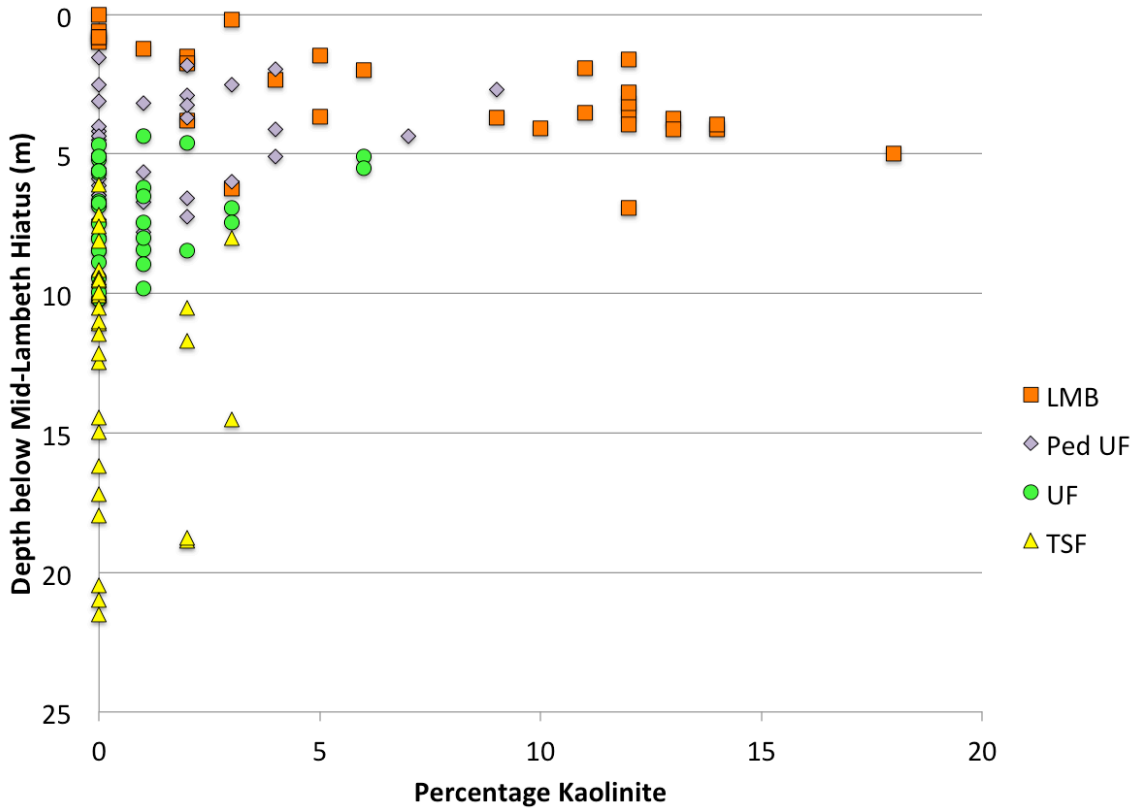


Figure 5.3 Identification of kaolinite by XRD

The pedogenic deposits contain a higher proportion of alteration products of oxidation, namely goethite, kaolinite and smectite (Table 5.1). Conversely, the proportion of glauconite/illite is greatest in both the pedogenic and fresh Upnor Formation, indicating that glauconite resists pedogenic alteration of the Upnor Formation. Pyrite was detected in only four samples, at no more than 2% concentration. Gypsum, a by-product of the reaction between calcite and sulphuric acid (from weathering alteration of pyrite), was not observed in any of the samples analysed and is therefore not shown in the tables.

Table 5.1 Mineral characterisation by XRD

Stratum	No. samples	Number of samples detecting:				
		Glauc/ill	Pyrite	Goethite	Kaolinite	Smectite
LMB	31	20 (12)	0 (0)	21 (4)	26 (7)	29 (32)
Ped' UPN	34	27 (19)	2 (0)	14 (3)	17 (1)	15 (11)
UPN	37	37 (17)	2 (0)	3 (0)	19 (1)	12 (5)
TSF	31	22 (5)	0 (0)	0 (0)	5 (0)	8 (2)

Average percentages in brackets. LMB = Lower Mottled Beds, Ped' UPN = Pedogenic Upnor Formation, UPN = Upnor Formation, TSF = Thanet Sand Formation

5.1.2 Optical microscopy

The image of each slide was carefully studied to identify the evidence of glauconite and other minerals, commenting on unusual features. Quartz grains are typically angular and white in colour. Goethite forms rounded, dark brown grains, sometimes as pseudomorphs of glauconite; whilst smectite is observed as an amorphous, light brown speckled black material, often within the sample matrix. Glauconite is easily recognisable in thin section as rounded, dark to olive green coloured grains and is nearly always present in the Upnor Formation (Figure 5.4) but in a few pedogenically altered samples is absent. These samples contain a higher than normal concentration of kaolinite (up to 9%) and to a lesser extent, goethite, implying loss of original glauconite during pedogenesis and not during recent drawdown of the lower aquifer.

Glauconite is absent in the majority of Lower Mottled Beds, being observed in only 15% of the samples. The glauconite is likely to originate from occasional periods of marine flooding during deposition of the Lower Mottled Beds (Section 3.2.5.). However, the Lower Mottled Beds do contain relatively high quantities of kaolinite (up to 18%) and goethite (up to 12%) that may imply weathering/pedogenic alteration of original glauconite. Glauconite is present in low quantities throughout the Thanet Sand Formation, largely in agreement with the XRD results, with a slight increase in the basal clay-rich zone (Figure 5.4).

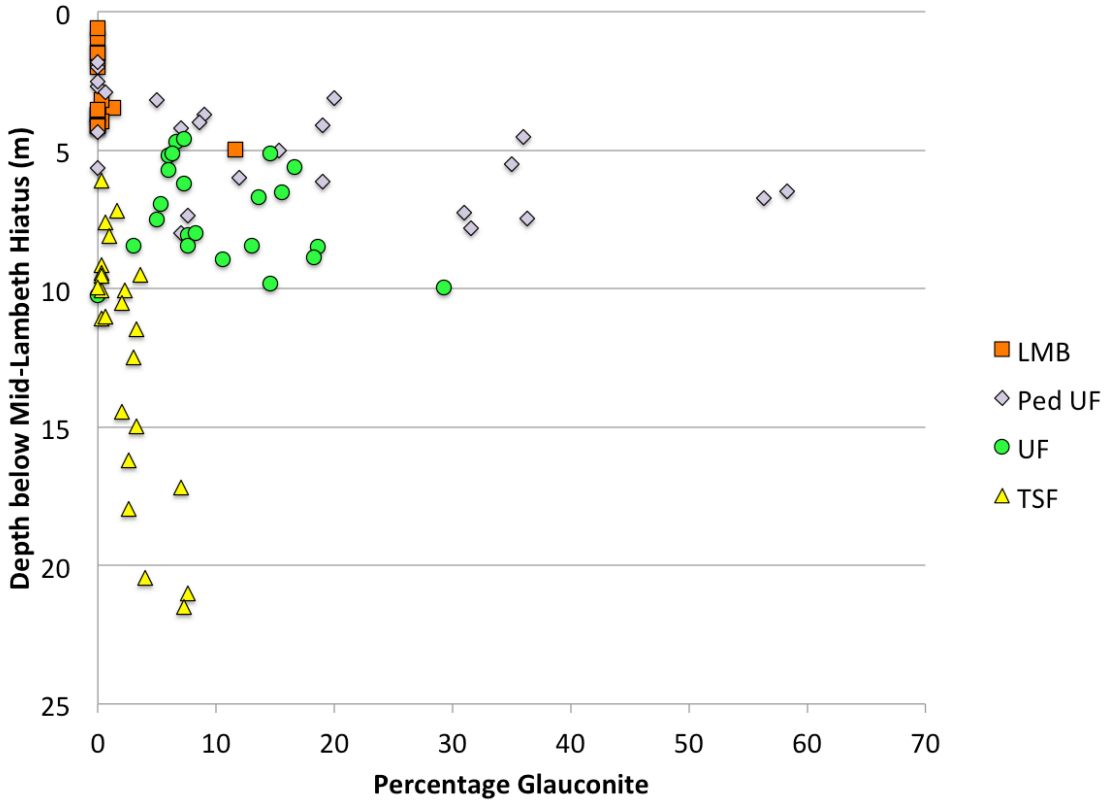


Figure 5.4 Identification of glauconite by optical microscopy

The following observations have been made from the full set of petrographic thin sections (Appendix C):

- Glauconite grains are usually bigger than the quartz grains.
- Glauconite grains are rounded whilst quartz grains are usually sub-angular.
- Goethite (iron oxide) is recognised as a homogeneous darker brown colour, whilst smectite/kaolinite displays a lighter, speckled brown colour.
- Goethite is often present as replacement pseudomorphs of glauconite.

These observations are illustrated in the clearest images as demonstrated in the following samples:

Sample 5004/39 – Lower Mottled Beds

In the hand specimen, oval shaped glauconite grains are present in very stiff, light blue grey, mottled orange-brown slightly fine sandy clay (Figure 5.5a). In thin section (Figure 5.5b), one of the grains, marked 'x', is relatively unweathered whilst another, marked 'y', is at an advanced stage of alteration by weathering. This grain is dark brown, with a less altered, lighter orange-brown, cracked rim. Oxidising fluids may have penetrated the grain via these cracks and preferentially weathered the core.

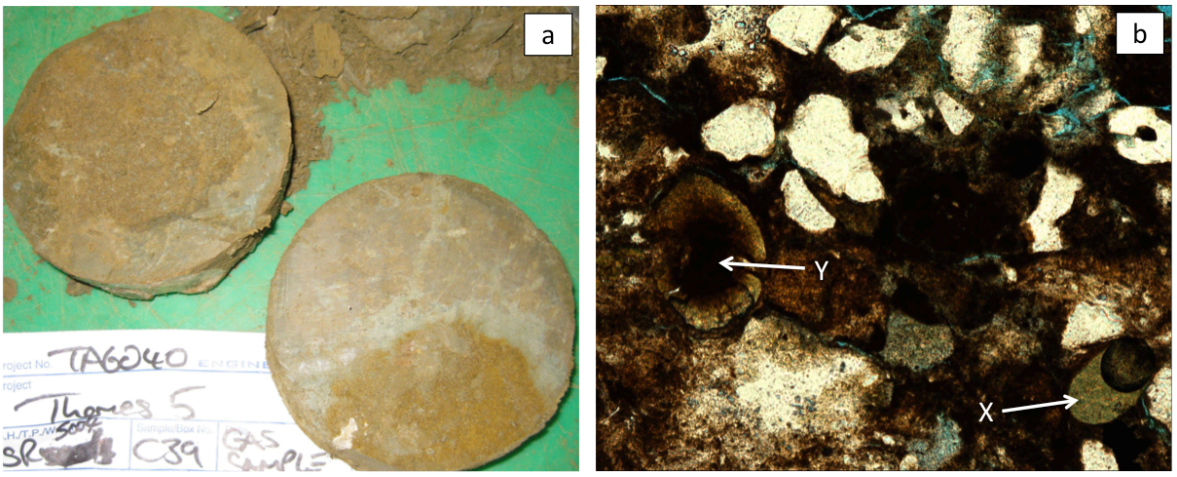


Figure 5.5 Partially weathered glauconite identified in the Lower Mottled Beds

Sample 5006/37 – Pedogenically altered Upnor Formation

The hand specimen (Figure 5.6a) contains fine black, sand size, grains of glauconite within a heavily oxidised brown and orange fine to medium sand. In thin section (Figure 5.6b), the

grains have not been altered by weathering and are sub-rounded to rounded, olive green, alongside white, sub-angular quartz grains within a goethite/smectite clay matrix.

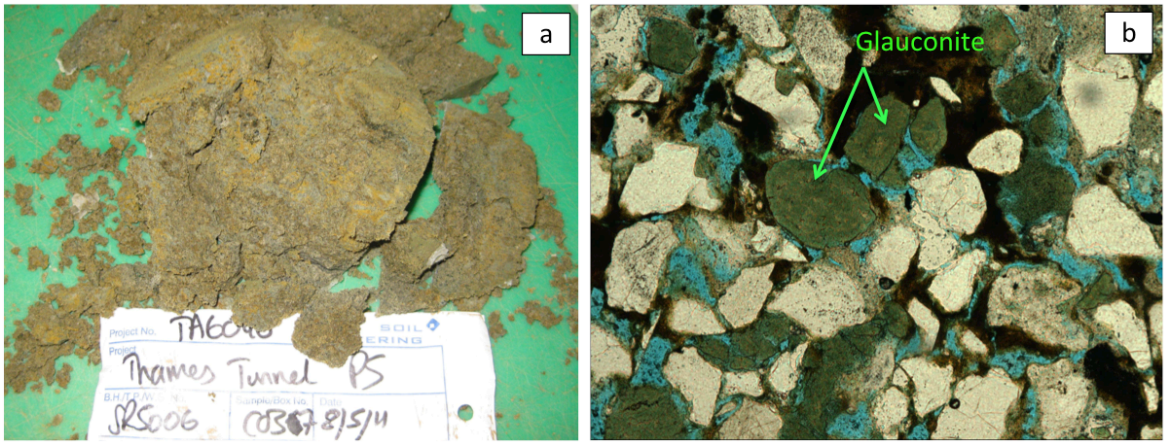


Figure 5.6 Unweathered glauconite identified in pedogenically weathered sediment

Sample 5015/39 – Pedogenically altered Upnor Formation

In the hand specimen (Figure 5.7a), light blue grey, silty fine to medium sand displays distinct orange-brown weathering mottle, whilst in thin section (Figure 5.7b), glauconite is dark blue-green, indicating resistance to weathering.

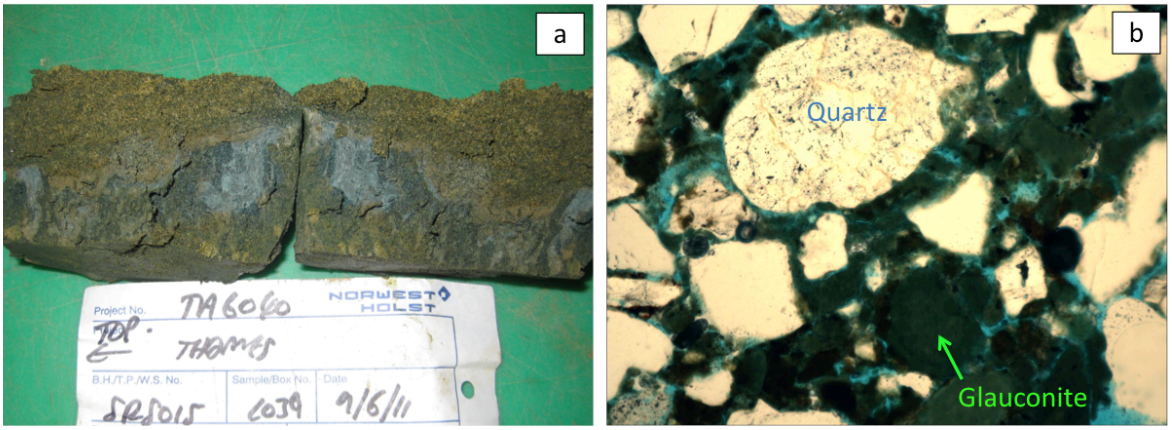


Figure 5.7 Unweathered glauconite identified in pedogenically weathered sediment

Sample 5006/38 – Fresh (unaltered) Upnor Formation

The hand specimen (Figure 5.8a) consists of green grey slightly silty, fine to medium, sand that is typical of the unit. In thin section (Figure 5.8b) there is an abundance of rounded, unaltered, green glauconite grains.

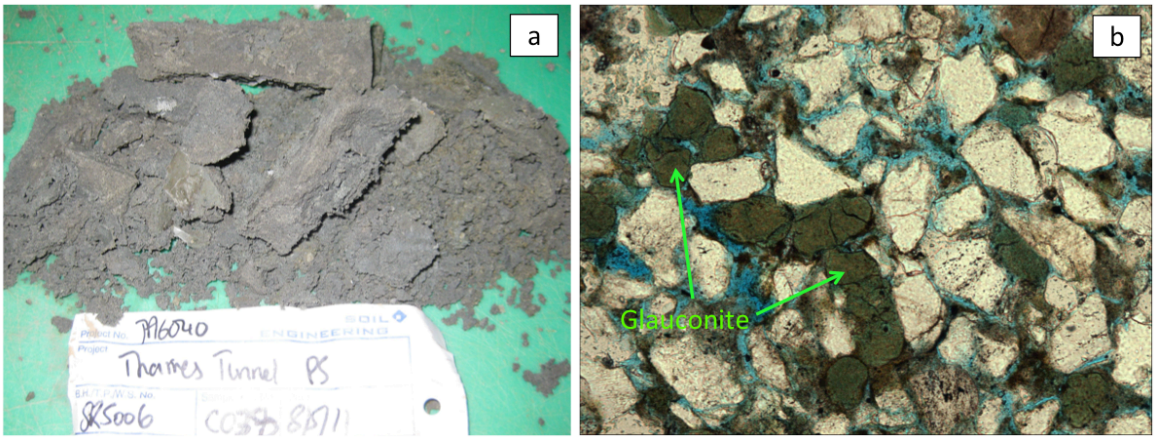


Figure 5.8 Unweathered glauconite identified in fresh Upnor Formation

Sample 5013/33 – Thanet Sand Formation

The hand specimen (Figure 5.9a) is from the top 1.0 m of the Thanet Sand Formation and is characteristically grey, silty fine sand. In thin section (Figure 5.9b), rounded grains of glauconite (marked 'G') and a few minor particles of chert are distributed randomly within the predominantly angular quartz grain material.

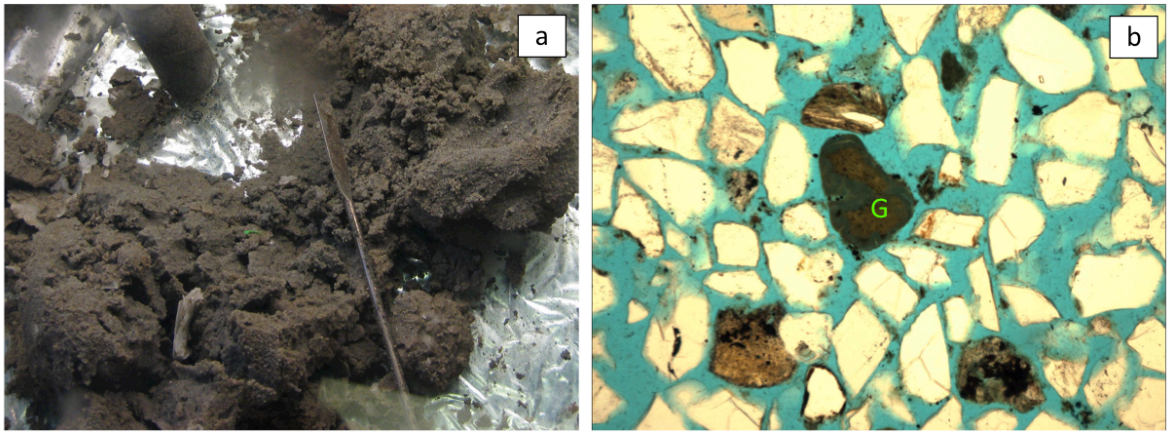


Figure 5.9 Thanet Sand in thin section

Sample 5015/76 – Thanet Sand Formation

The hand specimen (Figure 5.10a) is from the bottom 1.0 m of the Thanet Sand Formation, recorded as distinctly more 'clayey' than the remainder of the formation, although this is not obvious from the sample photograph. An increase in smectite is apparent in thin section (Figure 5.10b) and a decrease in the size of the quartz grains when compared to the sample at the top of the formation, consistent with the coarsening upward of grain size within the Thanet Sand Formation (Ellison et al., 2004).

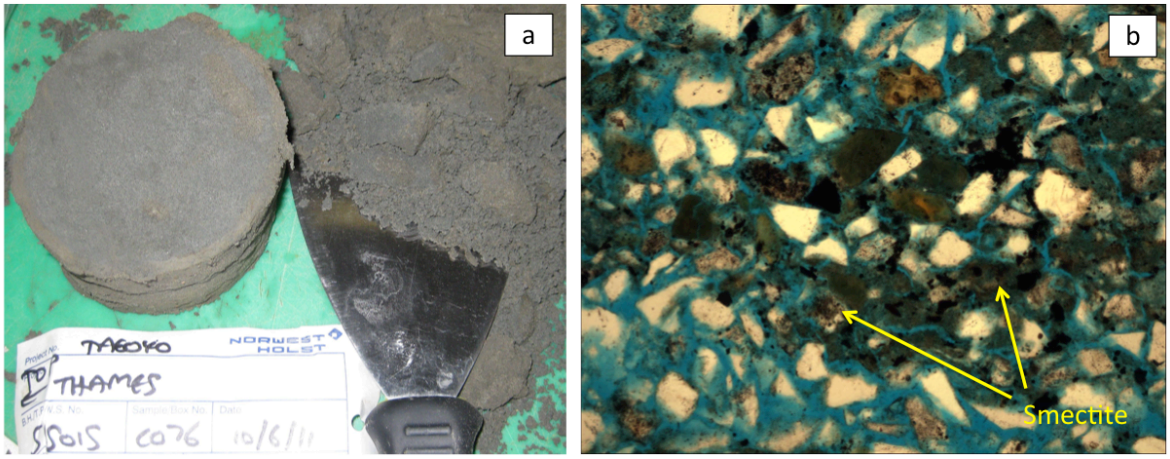


Figure 5.10 Evidence of clay enrichment in the basal Thanet Sand

5.1.3 Scanning Electron Microscopy (SEM)

SEM analysis of six samples from the Upnor Formation, taken during construction of the Abbey Mills shaft, was undertaken by Dr Sam Shaw and Dr Christine Rogers at Leeds University (Appendix D). The key results are as follows.

Sample AM280 – Pedogenically altered Upnor Formation

Both the SEM image and EDX data pattern (Figure 5.11) indicate iron oxide that may have been derived from the oxidation of green rust.

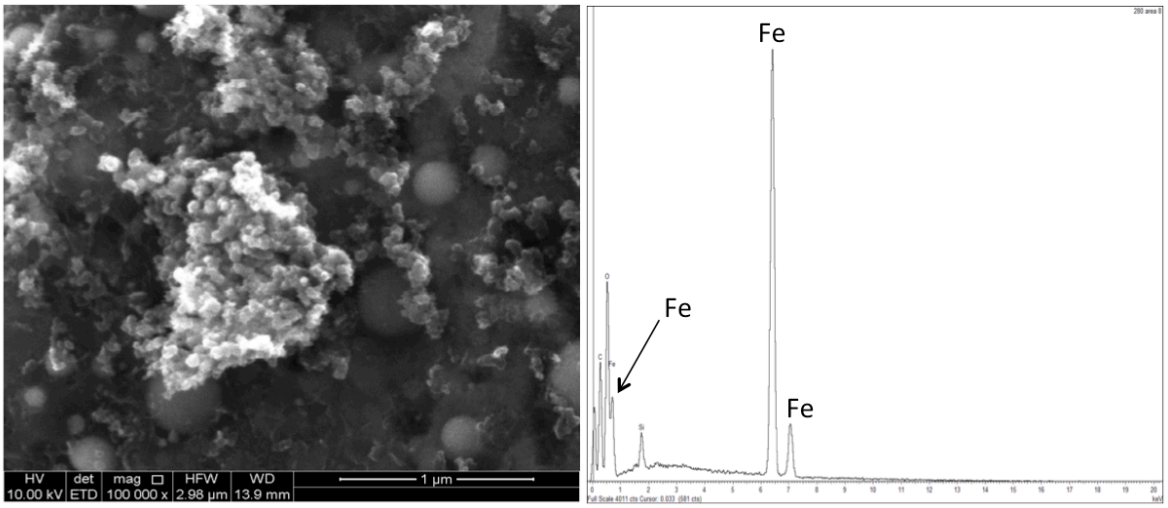


Figure 5.11 Identification of iron oxide in pedogenically altered Upnor Formation

Zinc was also detected (Figure 5.12) and, as a known to substitute for Fe(II) in the green rust lattice (Ahmed et al., 2008), its presence supports the inference of a green rust precursor for the iron oxide detected.

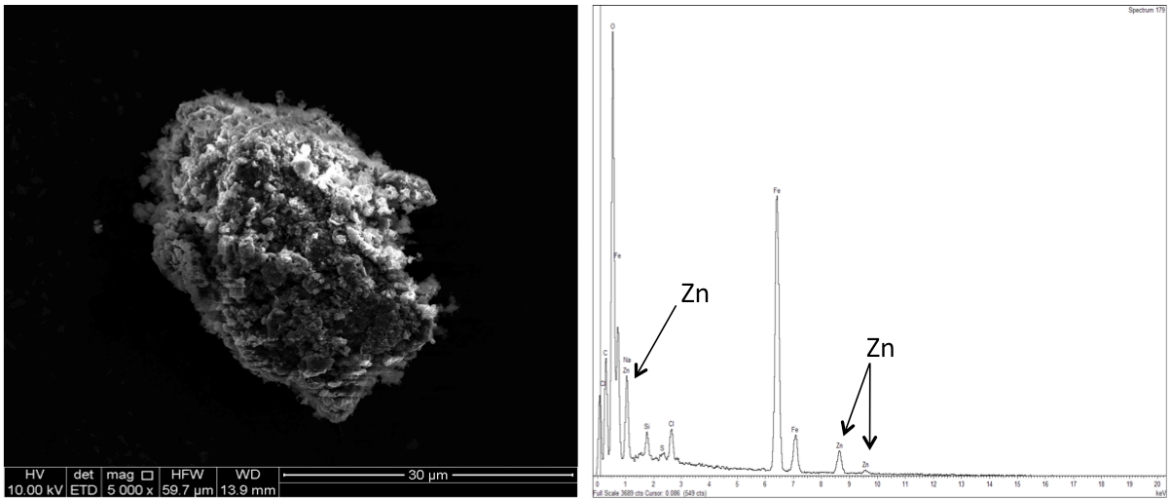


Figure 5.12 Identification of zinc in pedogenically altered Upnor Formation

Sample AM290 – Pedogenically altered Upnor Formation

The detection of glauconite (Figure 5.13) demonstrates its resistance to pedogenesis and later oxidation, in contrast to the inferred green rust.

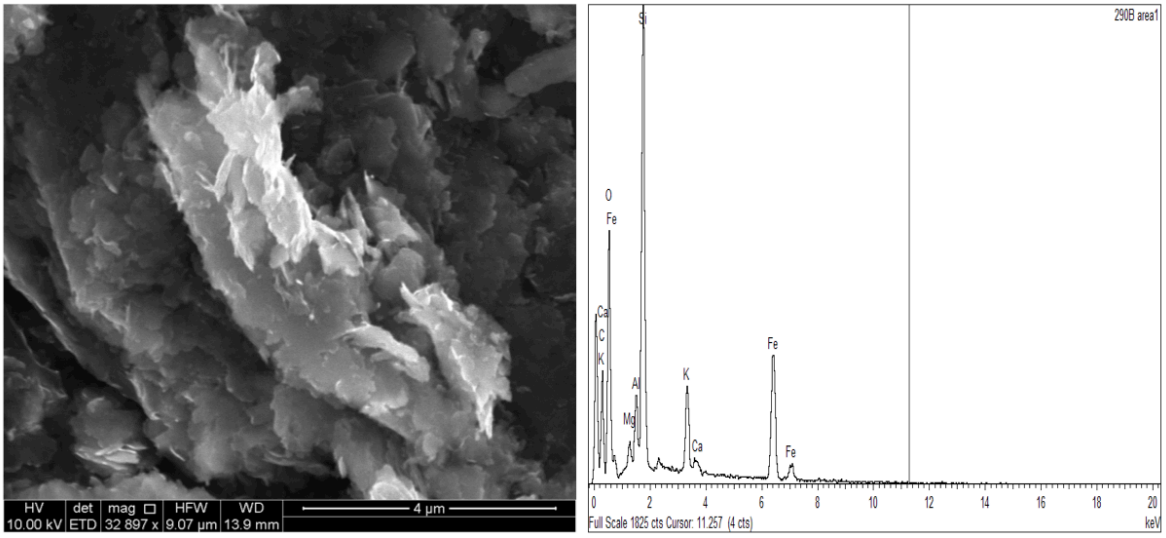


Figure 5.13 Identification of glauconite in pedogenically altered Upnor Formation

Sample AM305 – Fresh Upnor Formation

The presence of framboidal pyrite in this sample (Figure 5.14) is consistent with its occasional detection in the XRD data. While potentially an important reducing agent, its low concentration demonstrates that it cannot be the major cause of oxygen loss within the Upnor Formation. Furthermore, the survival of such small crystals without any obvious alteration, indicates that pyrite oxidation is a relatively slow process.

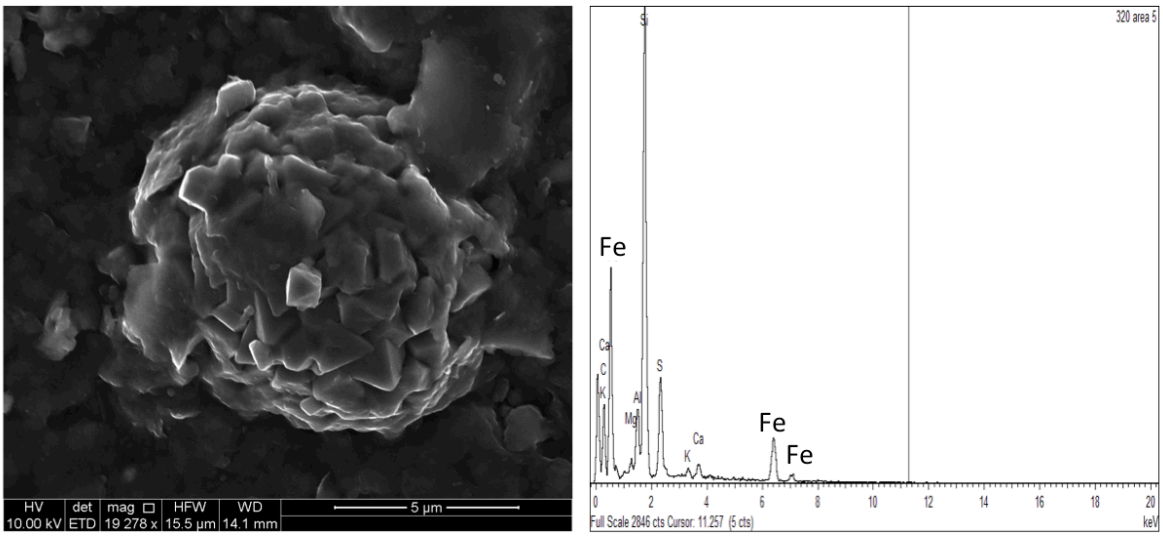


Figure 5.14 Identification of pyrite within fresh Upnor Formation

The concentration of any mineral cannot be determined using SEM but the images do imply the former presence of green rust, and the resistance of both pyrite and glauconite to oxidation.

Further SEM analysis was undertaken on samples of glauconite, taken through the entire sequence of the Upnor Formation at Abbey Mills, by Dr J. Huggett to investigate the chemical character of the glauconite grains and the extent of weathering oxidation.

The results of the analysis are summarised in Table 5.2, which shows that the concentration of potassium is quite consistent, between 7.08 and 6.68% throughout the Upnor Formation. Similarly, levels of Fe_2O_3 and Al_2O_3 are consistent throughout the sequence, indicating that there has been no weathering-induced alteration, even within the top, pedogenically altered section as noted by Courbe et al. (1981) and discussed in Section 3.3.7.

Table 5.2 The chemical character of glauconite from the Abbey Mills shaft

Sample	Mineral (%)					
	S_iO_2	Al_2O_3	Fe_2O_3	CaO	MgO	K_2O
AM275	45.25	4.24	26.36	0.36	2.67	7.05
AM280	44.79	4.08	25.80	0.31	2.66	6.97
AM290	46.62	5.00	24.80	0.39	2.76	7.19
AM295	46.79	4.85	24.34	0.35	2.87	7.07
AM305	47.20	5.41	23.84	0.46	2.99	7.08
AM320	47.64	5.33	23.83	0.48	2.96	6.80
AM325	46.59	4.56	23.94	0.43	2.80	6.68

5.2 Identification of reduced to oxidised mineral transition

5.2.1 Position Sensitive X-Ray diffraction

Only 40 of the 69 samples analysed using XRD-PSD (Appendix E) gave reliable results. No meaningful results were obtained from the first 29 samples because of unsuitable sample preparation; improved preparation techniques were used for the following 40 samples.

No significant changes in mineralogy were recorded during any of the 1 hour-long XRD experiments, with the exception of dehydration of smectite, involving the loss of interlayer water and shrinkage of the smectite lattice and resultant shift in XRD peak patterns, and no green rust or pyrite were detected.

Almost all samples contained numerous quartz grains that cause a large peak in the XRD response, obscuring the smaller responses of goethite, lepidocrocite and other oxidation products of green rust.

Green rust, and its oxidation products, may be detectable with improved sample extraction and preparation techniques, particularly the removal of quartz grains. However, it is possible that XRD-PSD is not sensitive enough to detect green rust at the low concentration expected (<10%) in the Upnor Formation (Ruby et al., 2006).

5.2.2 ATR FTIR spectroscopy

ATR-FTIR analysis was undertaken on 49 samples in the Department of Earth Science Engineering (Appendix F). To begin with, tests were undertaken on pure samples of the following minerals for background data (Figure 5.15) in addition to glycerol and ethanol glycol with additional data sourced for silica and montmorillonite :

- Pyrite
- Goethite
- Lepidocrocite
- Glauconite
- Gypsum
- Kaolinite
- Haematite
- Calcite

The FTIR signature of green rust has never been detected because it is so reactive with oxygen that it always oxidises before analysis. Therefore, data from reduced samples (which

nonetheless will have lost any green rust prior to testing) are compared to those from baked, oxidised samples to identify any significant changes in mineralogy during the oxidation process that may arise from reducing agents other than green rust, such as pyrite or organic material. However, no such changes were detected.

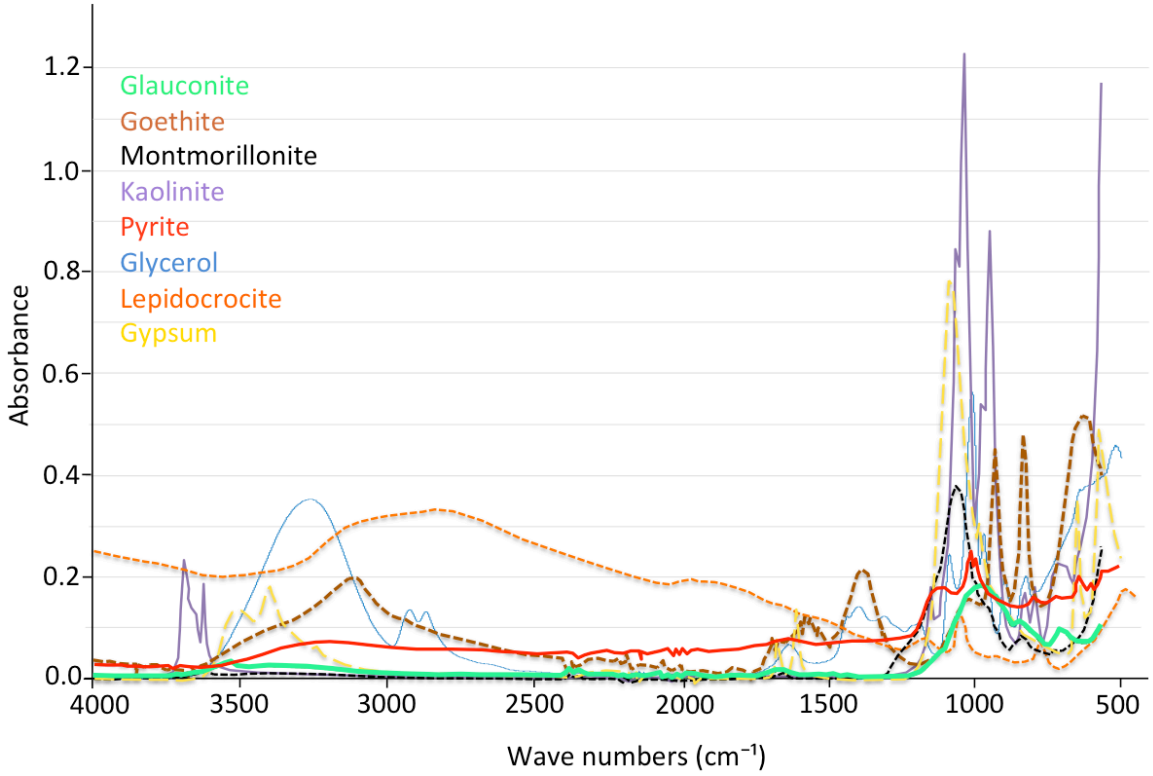


Figure 5.15 Background mineral data for FTIR analysis

Lower Mottled Beds

Two samples produced very similar spectra (Figure 5.16), indicating a predominance of kaolinite and montmorillonite, as would be anticipated in this material, although the presence of other minerals is not distinguished.

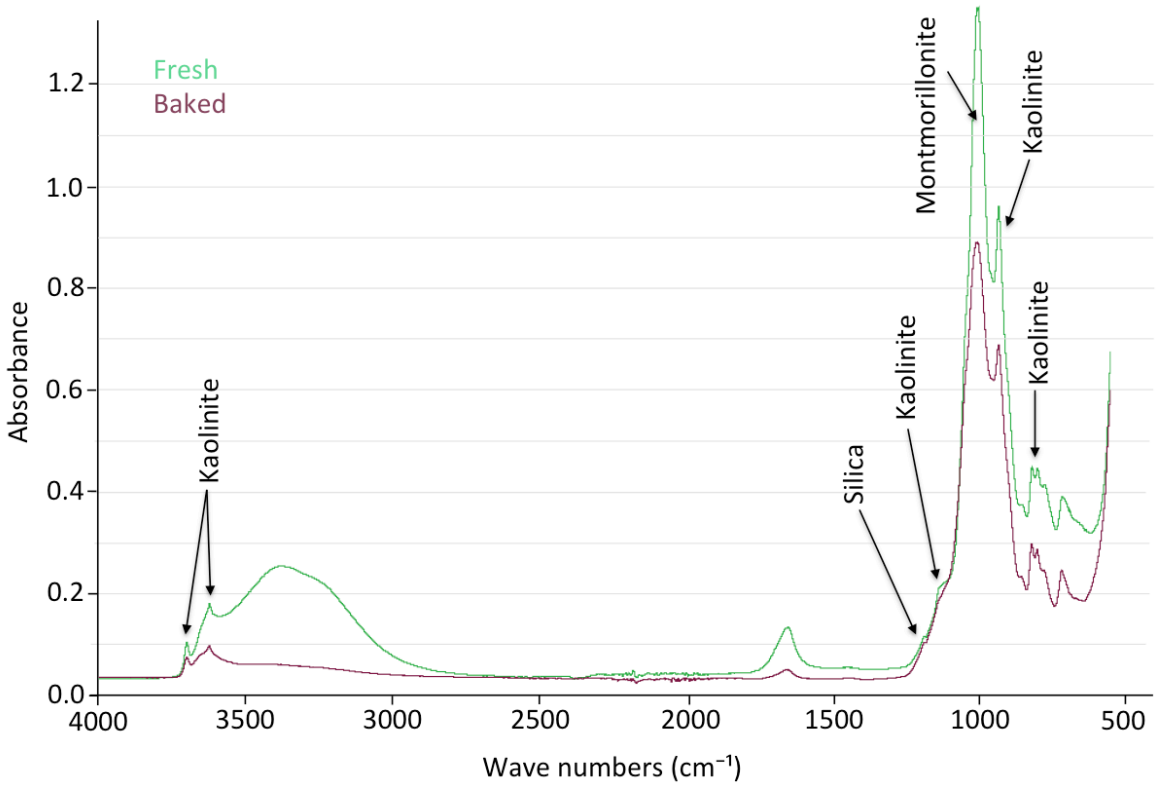


Figure 5.16 FTIR spectra for the Lower Mottled Beds (sample 5006/36)

Upnor Formation

Similarities are observed between the spectra for fresh and pedogenically-altered samples, in particular, bands for kaolinite and montmorillonite (Figure 5.17). A broad rounded band between 3000 and 3600 and a smaller sharper band, at around 1650 cm^{-1} in all of the fresh samples, indicate water. Both bands are significantly reduced in the baked spectra, verifying dehydration of the sample as detected in the previous PSD-XRD analysis. In some experiments, the band at 1650 cm^{-1} did not reduce significantly, indicating that water and other hydrated phases can survive baking (R. Court, *pers. comm.*). Spectra for the fresh samples coated in glycerol and those that were not were usually almost identical; the only differences being in the glycerated samples where small bands were noted at 2960, 2890, 1300-1400 and 880 cm^{-1} (Figure 5.17).

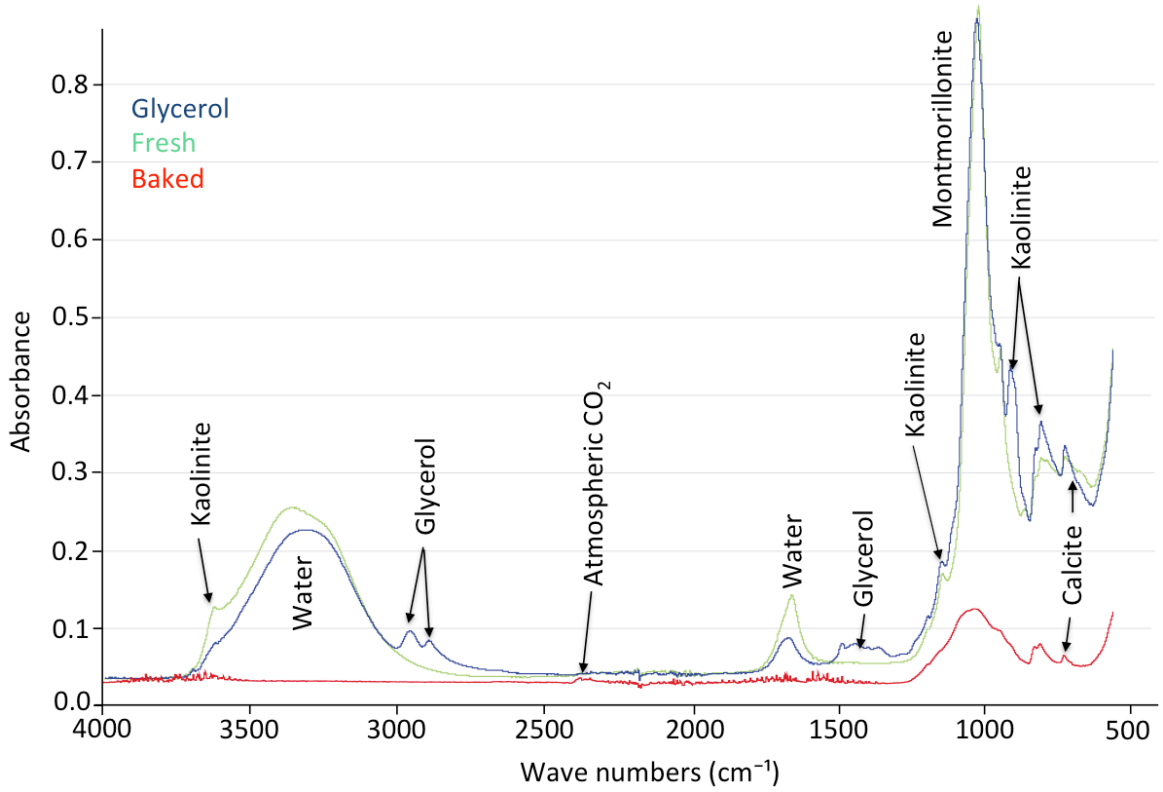


Figure 5.17 FTIR spectra for the Upnor Formation (sample 4207/3)

Goethite was not detected in any of the samples, whether from the baking process or pre-existing within pedogenically altered specimens but it is likely that it was obscured by atmospheric carbon dioxide, which shares a similar band position at around 2350 cm^{-1}.

It is possible that goethite is represented by the band at 3150 cm^{-1} in a sample of baked Upnor Formation (Figure 5.18) but this is inconclusive as many hydrated minerals have a broad water band around this location.

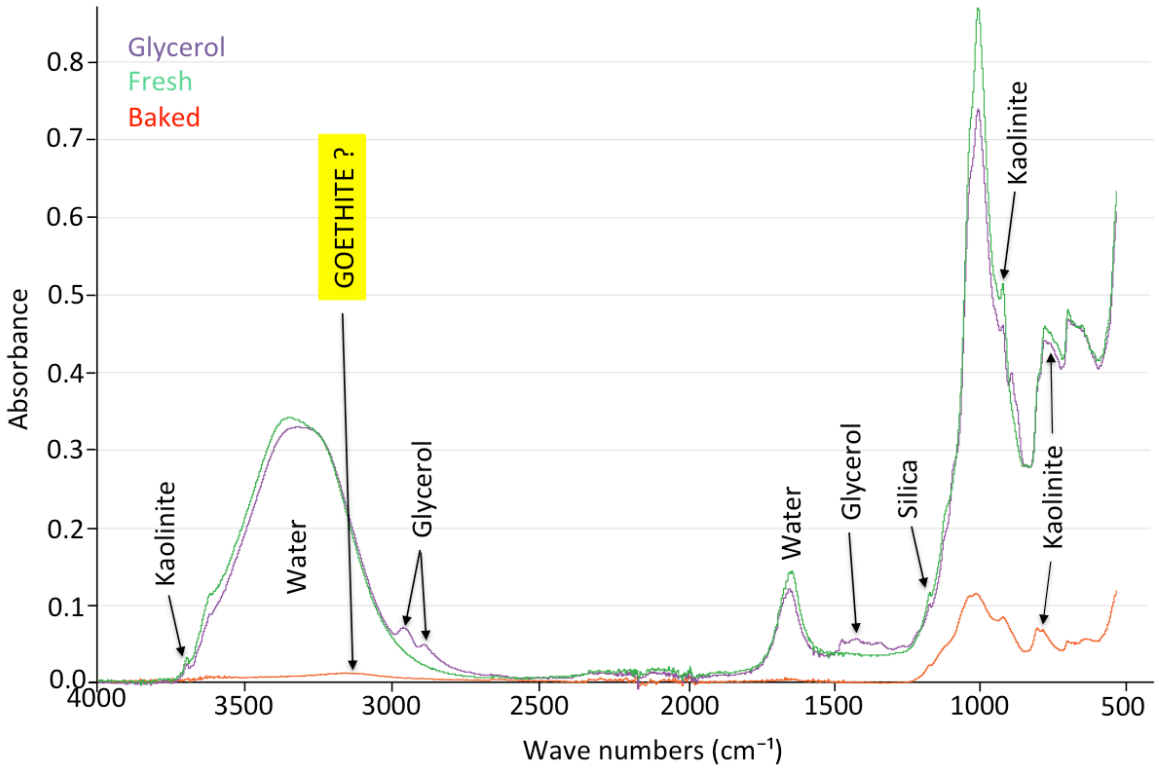


Figure 5.18 Possible goethite in pedogenic Upnor Formation (sample 4009/2)

Glauconite, however, is clearly present in the spectra for many of the baked samples (Figure 5.19), indicating that it has survived oxidation during baking. It is also indicated in a number of pedogenically altered samples, therefore having survived pedogenic alteration. Calcite is clearly visible in the spectra for many of the more shelly samples (Figure 5.20), from which it is evident that it too survives the baking process.

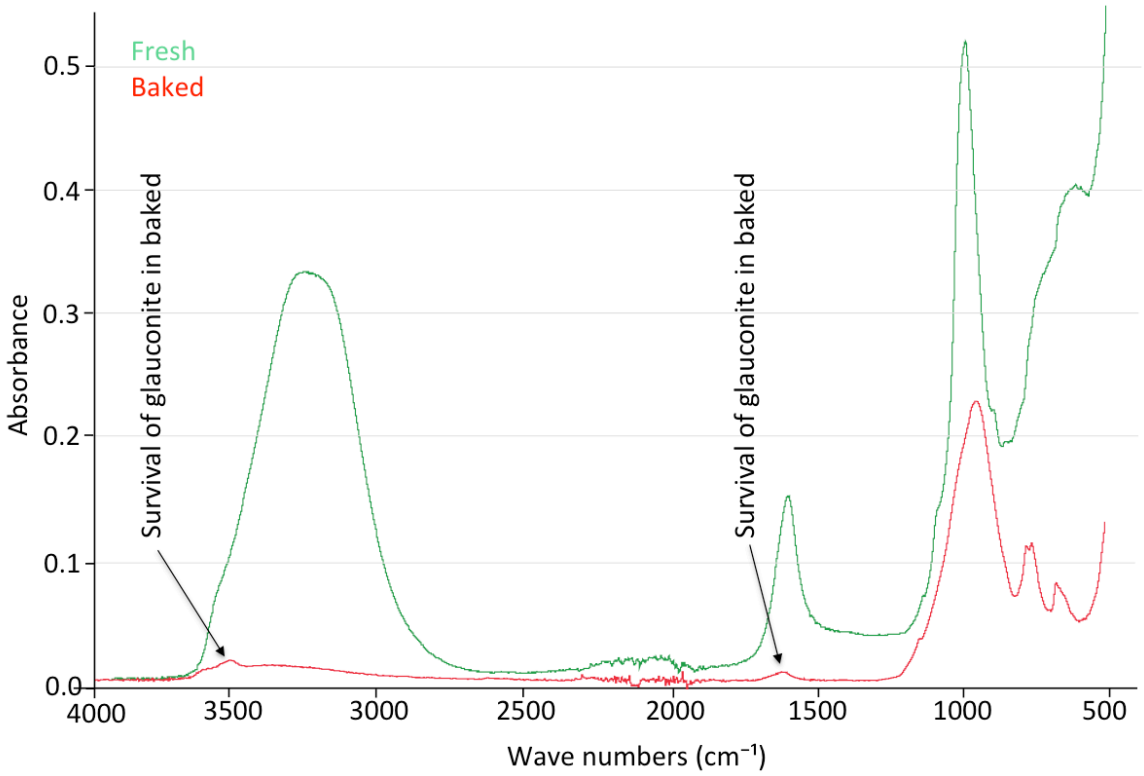


Figure 5.19 Survival of glauconite in baked, oxidised sediment (sample 5018/61)

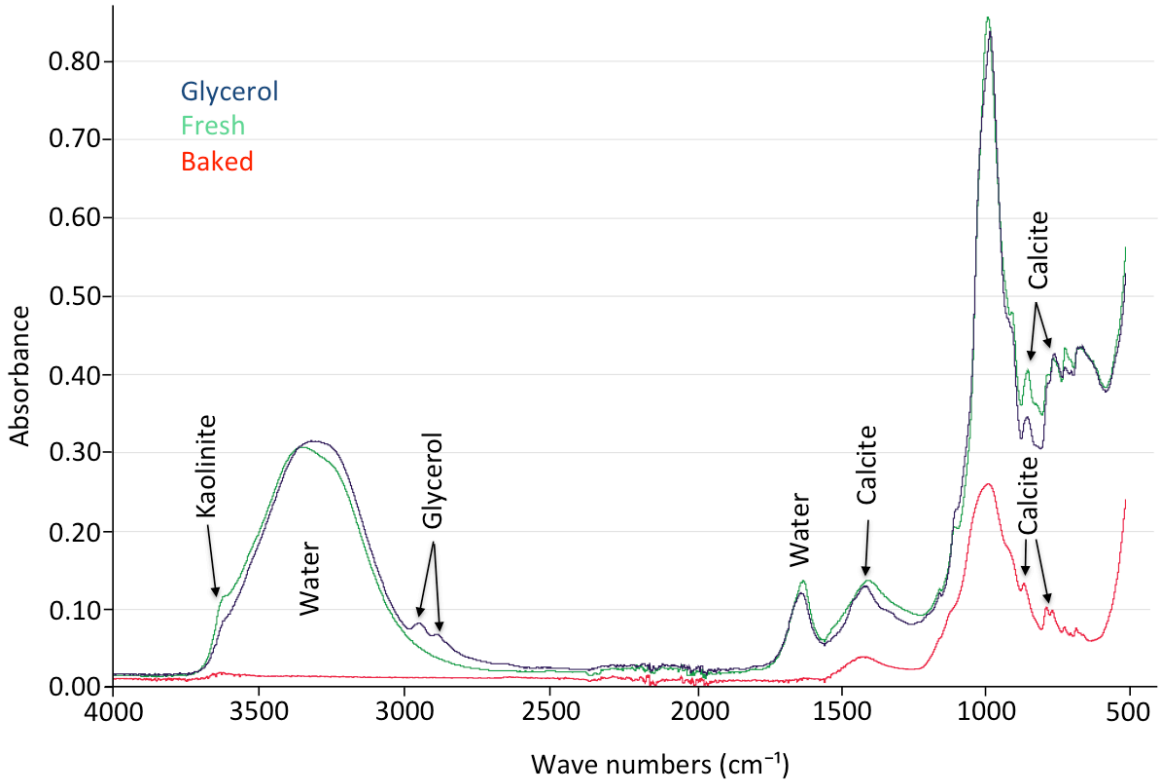


Figure 5.20 FTIR spectra of shelly Upnor Formation (sample 4204/3)

Thanet Sand Formation

Kaolinite and montmorillonite are less obvious than in the Upnor Formation and most spectra were dominated by prominent bands indicating silica at around 1163, 800 and 780 cm^{-1} (Figure 5.21).

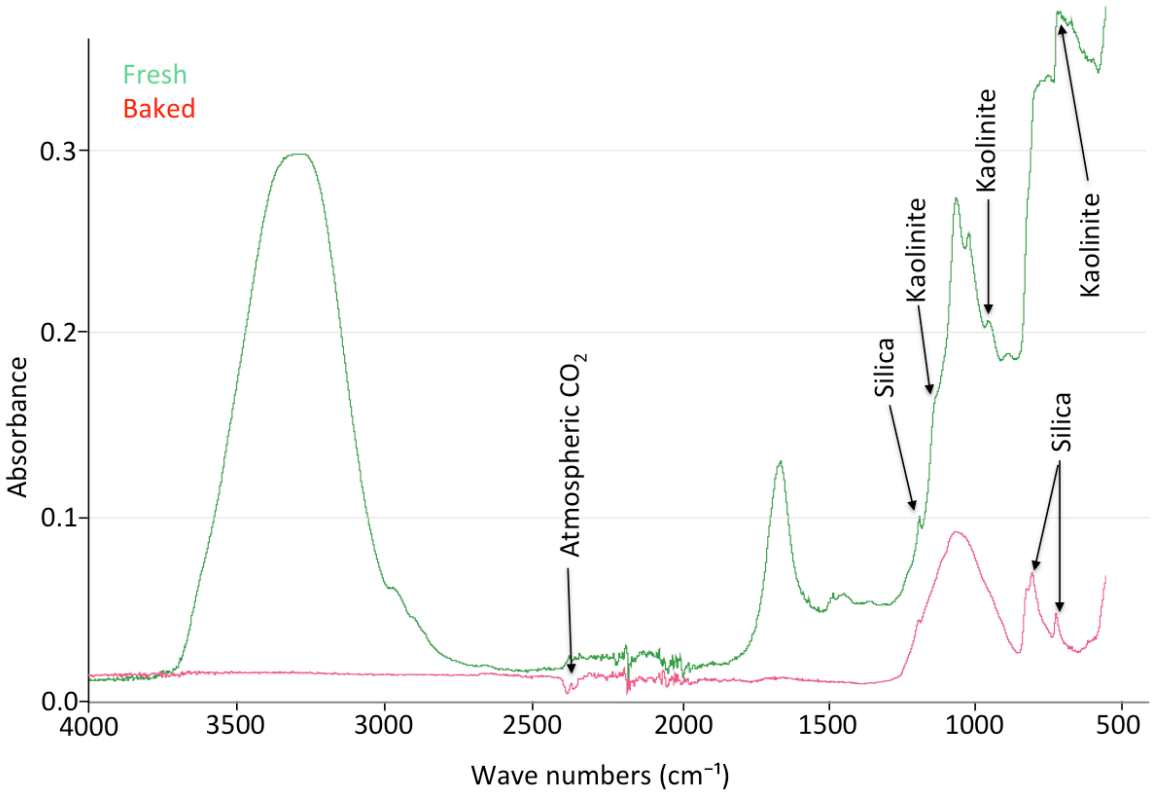


Figure 5.21 FTIR spectra for the Thanet Sand Formation (sample 4204/5)

Various difficulties were encountered when analysing the spectra. The baked sample data are noisy, particularly between 1200 and 2400 cm^{-1}, which is strongly affected by atmospheric carbon dioxide (R. Court, *pers. comm.*). In addition, the peak positions of a number of key minerals, such as goethite and glauconite, are close to one another, especially within the 600-1100 cm^{-1} region, resulting in overlapping or obscured mineral spectra. This severely limits the usefulness of FTIR for this study. In addition, the small scale of the sample renders it vulnerable to the effects of rapid oxidation in the time taken to load it onto the apparatus. Any green rust in the sample will oxidise before the analysis and it is assumed that application of glycerol has not given adequate protection against this.

5.3 Soil suction filter paper test results

5.3.1 Introduction

Stiff clay of the Lower Mottled Beds is well suited for the filter paper test, and a disproportionately larger data set exists for this material when compared with the coarse

gravelly Upnor Formation and wet, collapsible Thanet Sand samples which are mostly unsuitable. Significantly fewer samples of Upnor Formation were available for testing due to frequent core loss of the more gravelly material during borehole recovery. This material is not represented by the results from the filter paper technique, and there is a bias of the data towards the more cohesive, clayey, sub-units within the formation.

Additional data for void ratio (e) and moisture content (w) are gathered as part of the filter paper test procedure (Table 5.3), which clearly show an increase with depth through the lower Lambeth Group sequence, consistent with increasing grain size.

Table 5.3 Summary of void ratio and moisture content

Stratum	Range			
	Void ratio	Average	Moisture content (%)	Average
Lower Mottled Beds	0.40 – 0.63	0.52	9 - 24	17.3
Pedogenic Upnor	0.49 – 0.73	0.56	10 – 27	17.9
Upnor Formation	0.54 – 0.75	0.62	10 – 30	21.6
Thanet Sand Formation	0.63 – 0.87	0.78	20 – 35	26.2

The Lower Mottled Beds possess relatively low values of void ratio and moisture content, with no apparent increase in depth for either (Figure 5.22 and Figure 5.23). In the fresh Upnor Formation, a slight decrease in both void ratio and moisture content reflects the more clay-rich nature towards the base of the stratum and corroborates the findings discussed in Section 3.2.4. The void ratio in the Thanet Sand is mostly between 0.74 and 0.86, although there is no evidence for the increase in clay towards the base of the stratum.

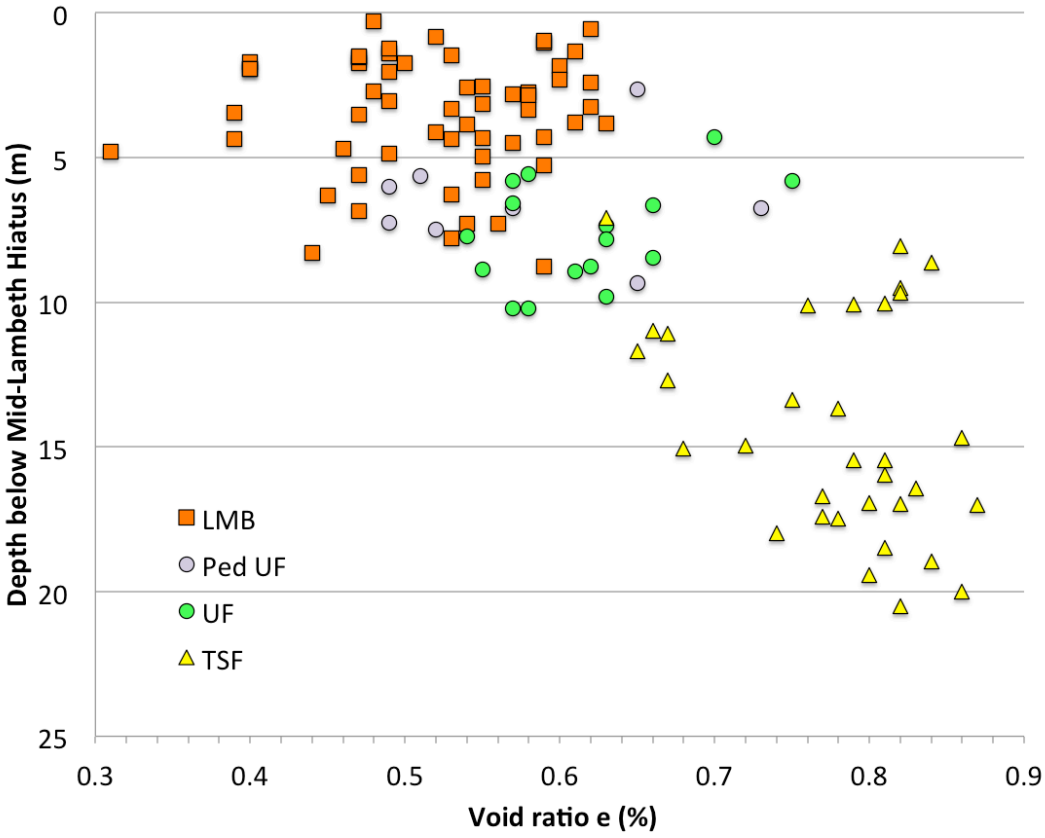


Figure 5.22 Void ratio against depth

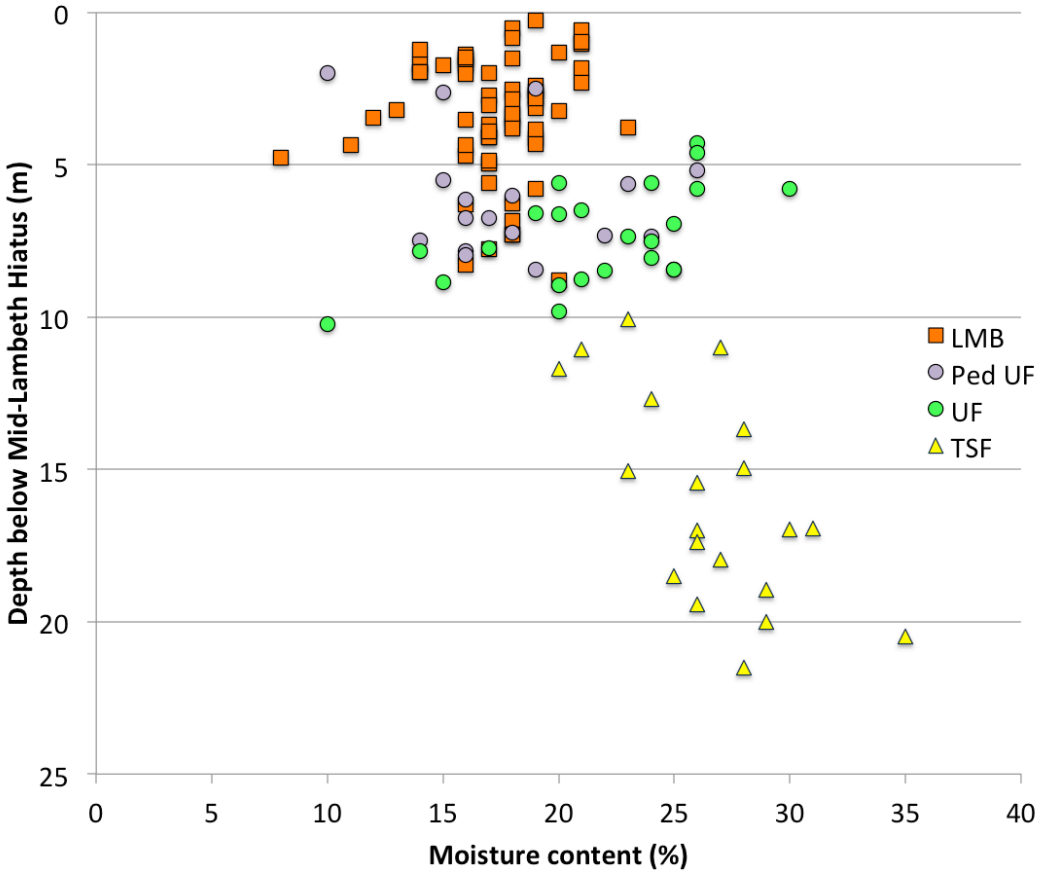


Figure 5.23 Moisture content against depth

5.3.2 Matrix suction

A distinct correlation is inferred between a decrease in void ratio and increase in matrix suction (Figure 5.24). The small void ratios (0.40 to 0.63) in the Lower Mottled Beds correspond with greater values of matrix suction, between 100 and 1500 kPa, whilst the relatively larger void ratios (0.63 to 0.87) in the Thanet Sand Formation are associated with very low matrix suction, mostly less than 20 kPa. Similarly very low values of matrix suction, typically less than 10 kPa, are found in the Upnor Formation, indicating the sandy nature of the stratum. However, larger values of up to 99 kPa are derived from a small number of samples, coinciding with slightly lower void ratios, reflecting the variability within the stratum as discussed in Section 3.2.4. A wide range in matrix suction, between 4 and 500 kPa, is derived from samples of pedogenically-altered Upnor Formation, coinciding with the wide range in void ratio and reflecting the highly variable nature of this deposit.

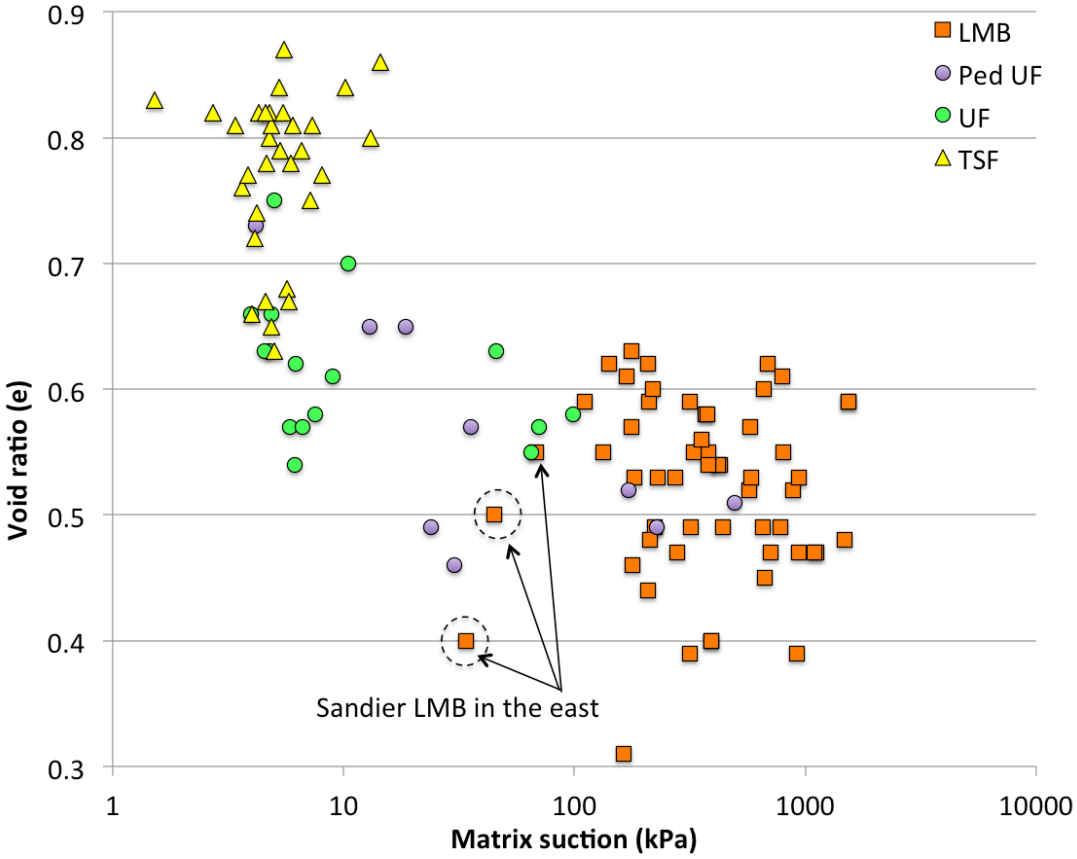


Figure 5.24 Matrix suction against void ratio

Lower Mottled Beds

A very slight decrease in matrix suction is apparent with depth through the Lower Mottled Beds (Figure 5.25), associated with an equally slight increase in sand content. Values below 100 kPa are inferred for three sandier samples from the east of the Tideway Tunnel scheme, as discussed in Section 3.2.5.

Upnor Formation

An increase in matrix suction occurs at the base of the Upnor Formation, as much as 99 kPa, indicating the presence of clay-rich layers, as discussed in Section 3.2.4. These values deviate from the otherwise uniformly low values at higher elevations (Figure 5.25). A wide range in data exists for the pedogenically altered Upnor Formation, although a very slight increase in suction with depth is evident, as a result of the downward migration of clay fines during the pedogenic process, discussed in Section 3.2.6.

Thanet Sand Formation

Most of the matrix suction data for the Thanet Sand Formation lie within a very narrow range below 10 kPa, indicating that the deposit is largely uniform in nature, except for the slight increase in values to 16.5 kPa marking the clay-rich base of the stratum (Figure 5.25), as discussed in Section 3.2.3.

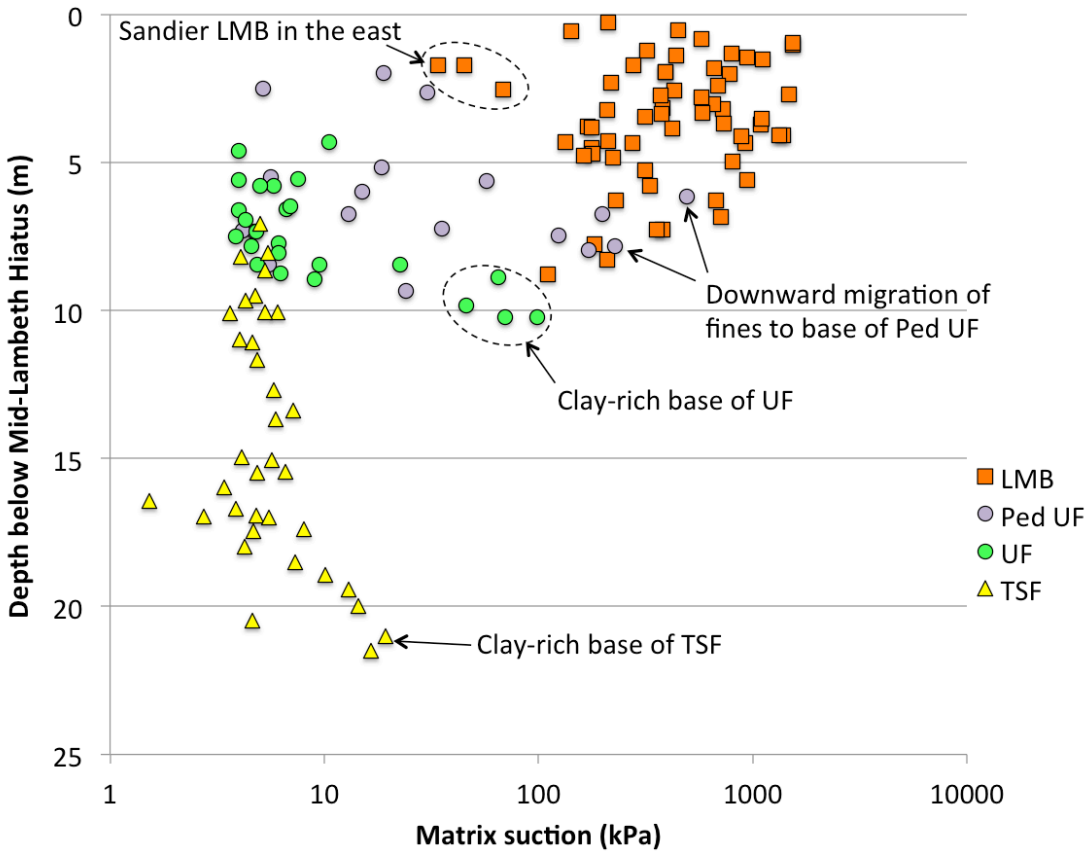


Figure 5.25 Matrix suction through the lower Lambeth Group and Thanet Sand

Results of the filter paper tests indicate that the value of matrix suction decreases with depth through the lower Lambeth Group and Thanet Sand Formation (Table 5.4).

Table 5.4 Summary of matrix suction values

Stratum	Suction range (kPa)	Average suction (kPa)
Lower Mottled Beds	133 – 1531	557.9
Pedogenic Upnor Formation	4.1 – 492	80.5
Upnor Formation	3.8 – 99	17.4
Thanet Sand Formation	1.5 – 16.5	6.3

Note: Data for the three sandy samples of Lower Mottled Beds have been omitted, as they are not considered representative of the material across the majority of the Tideway Tunnel alignment.

5.3.3 Soil Water Retention Curves (SWRCs)

SWRCs for the lower Lambeth Group and Thanet Sand Formation were derived from the filter paper technique (Appendix G). Samples of pedogenically altered Upnor Formation were not tested because no suitable samples were available during experimentation. Drying curves developed for a selection of lower Lambeth Group and Thanet Sand samples further demonstrate the increase in matrix suction through the sequence (Figure 5.26).

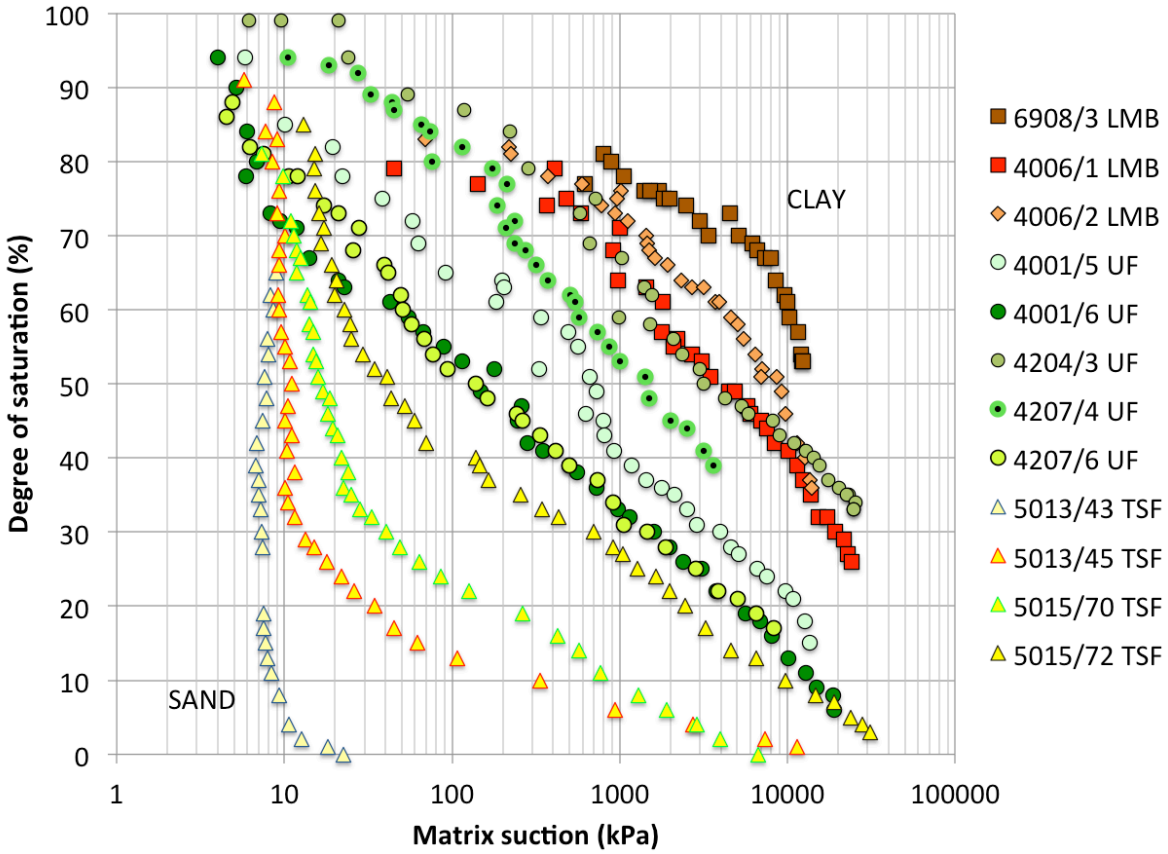


Figure 5.26 Drying curves for lower Lambeth Group and Thanet Sand Formation

LMB = Lower Mottled beds; UF = Upnor Formation; TSF = Thanet Sand Formation

There are very clear differences between the SWRCs relating to the granular soils of the Thanet Sand Formation and the high plasticity clays of the Lower Mottled Beds, as evident from Figure 5.26, with the SWRCs for the Upnor Formation lying between the two. Of particular note are the air-entry values (AEVs) with those of the Thanet Sand Formation being of the order of 10 kPa whilst those for the Lower Mottled Beds are nearer to about 1 MPa. AEVs for the Upnor Formation again lie between these values and are more variable because of the reduced homogeneity in this stratum. Standing et al. (2013) propose that cavitation is closely linked to AEV. They demonstrated this with a series of simple laboratory tests simulating the dewatering and consequent cavitation processes that took place historically in the Thanet Sand and Upnor formations and the Lower Mottled Beds. It was concluded that cavitation occurs at low suctions for coarser soils such as the Thanet Sand Formation, which has greater pore sizes than the Upnor Formation and Lower Mottled Beds, as evident in Figure 5.22. The SWRC results indicate clearly that cavitation is highly likely to occur in the Thanet Sand Formation, even at very low suction values, while it is very unlikely to occur in the Lower Mottled Beds based on the recorded levels of drawdown of the lower ground water table. This means that the air derived from cavitation will rise and become trapped beneath the Lower Mottled Beds (especially during recovery of lower water table levels). Moreover, the high AEVs of the Lower Mottled Beds means that even when the trapped air is pressurised beneath the stratum from the recovery of water table levels, the air will be prevented from permeating vertically into it.

The curves can be modelled mathematically as proposed by Van Genuchten (1980) and attempts have been made in the past to relate the Van Genuchten coefficients to soil characteristics such as PI and Activity (Melgarejo Corredor, 2004) with limited success. This technique was not considered appropriate for application to samples derived from the Upnor Formation, given the variability of materials within this stratum.

Lower Mottled Beds

SWRCs were developed for three samples (Figure 5.27). Sample 6908/3 was recorded as very stiff, light blue-grey mottled orange-brown clay in the west of the Tideway Tunnel scheme. The other two samples, 4006/1 and 4006/2, were recovered from stiff, green-grey mottled orange-brown, slightly fine sandy clay in the east of the scheme.

The SWRC for 6908/3 indicates a large increase in matrix suction, accompanied by a relatively small decrease in saturation, thus implying a high air entry value (AEV), despite an initial saturation at 82%. The rate of increase in suction becomes less pronounced at around 1000 kPa, at which point the rate of desaturation appears to increase. The drying curve for

sample 6908/3 was stopped at 12.3 MPa because of time constraints on the testing programme.

A greater rate of desaturation during drying is indicated by the drying curves for 4006/1 and 4006/2, caused by the higher void ratio of the material discussed previously. The drying curve for sample 4006/1 was also terminated prematurely. Drying of sample 4006/2 continued until the capacity of the filter paper was reached at about 33 MPa, at a residual saturation of 17%. This indicates that, although not as great as sample 6908/3, significantly high AEVs can also be sustained by this sandier material.

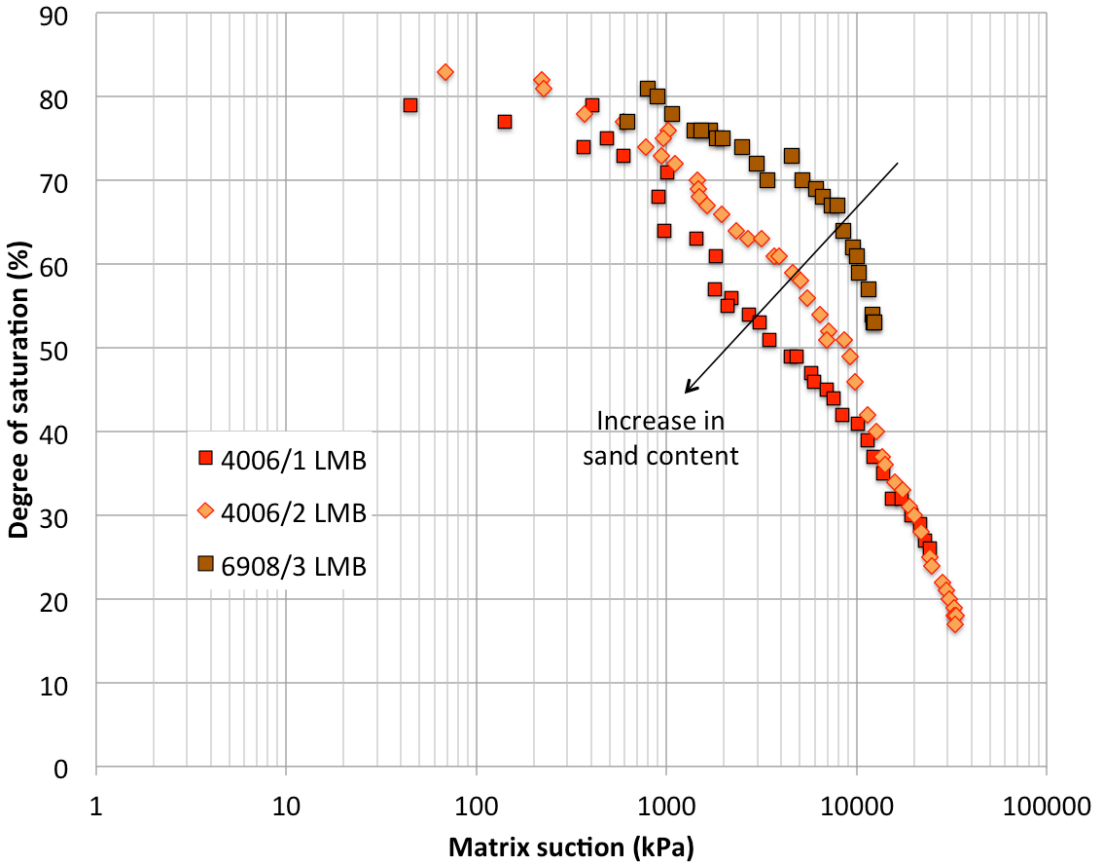


Figure 5.27 Drying curves for the Lower Mottled Beds

Based on the wetting cycle for 6908/3, significant hysteresis develops between the wetting and drying curves. A significantly lower degree of saturation is recorded by the wetting curve when compared to equivalent values of matrix suction on the drying curve (Figure 5.28), reflected in a significantly lower volumetric water content during wetting when compared to equivalent values of matrix suction during drying (Figure 5.29). Some sample shrinkage (and reduction in pore size) took place during the drying cycle, indicated by the smaller void ratios for the wetting curve when compared to equivalent values of matrix suction on the drying curve (Figure 5.30). However, there is no evidence of the shrinkage limit being encountered.

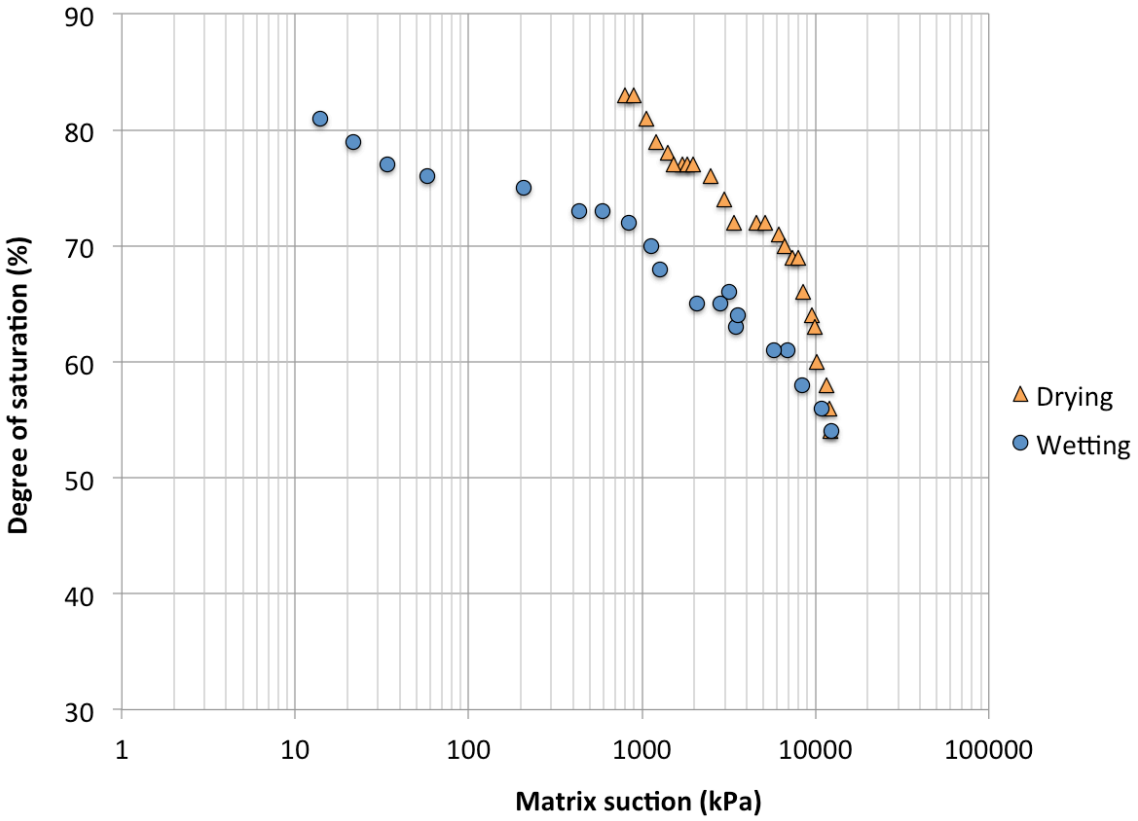


Figure 5.28 SWRCs suction vs. saturation: sample 6908/3

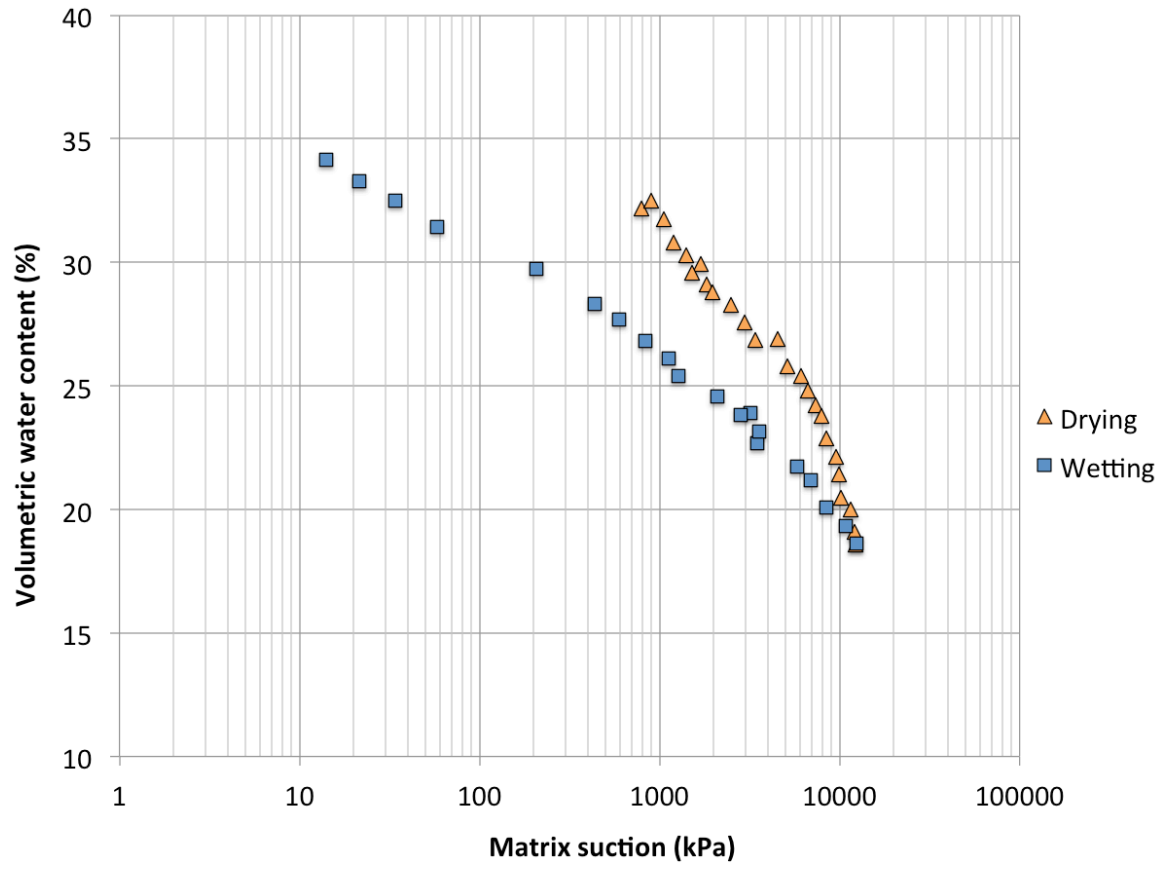


Figure 5.29 SWRCs suction vs. volumetric water content: sample 6908/3

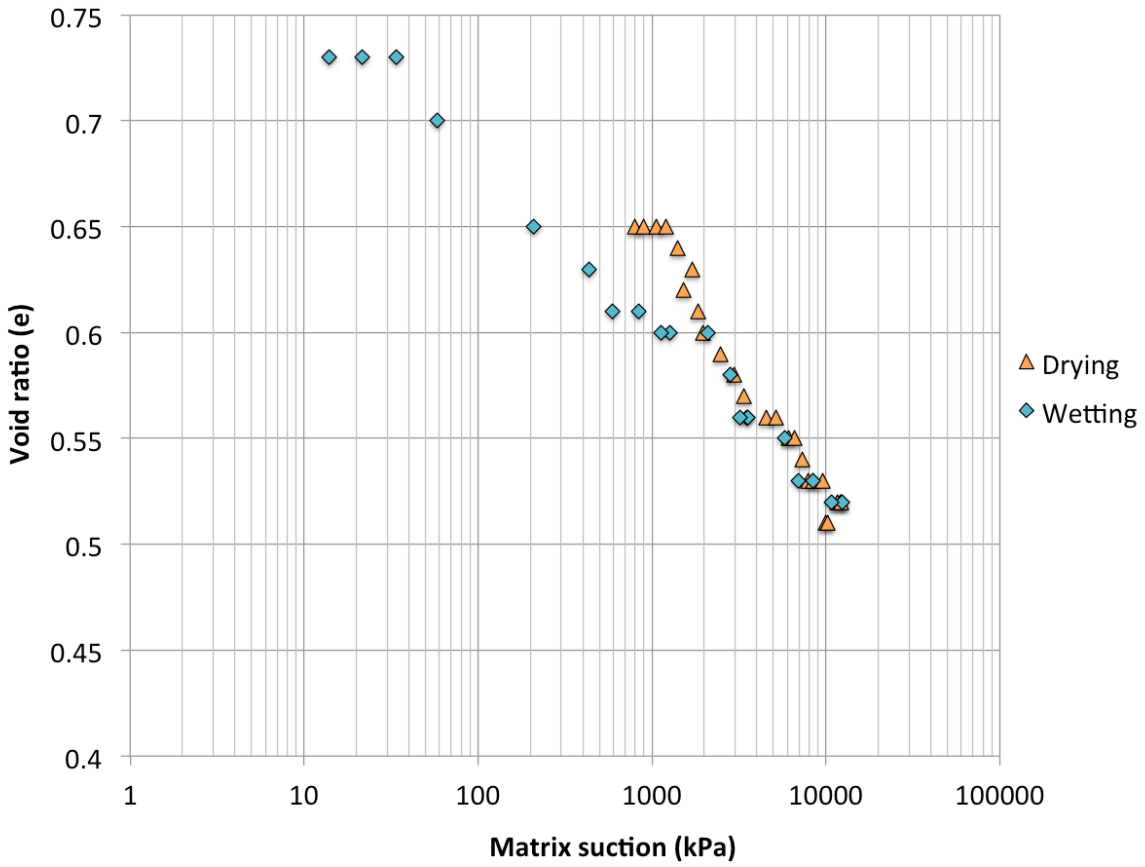


Figure 5.30 SWRCs suction vs. void ratio: sample 6908/3

Upnor Formation

SWRCs were developed for five samples from the Upnor Formation. A similar material description of green-grey, slightly clayey to clayey, slightly gravelly, fine to medium sand was recorded for each. The drying curves follow a similar rate of increase in matrix suction with desaturation for all of the samples (Figure 5.31). Only two of the samples, 4001/6 and 4207/6, continued their drying curves to the point of residual saturation; both indicative of a clayey sand material (as noted in Section 3.2.4). Time constraints again caused premature termination of the drying cycle for the remaining three samples.

All five samples indicate low values of matrix suction, 10 kPa or less, near the start of the drying curve. A greater rate of increase in matrix suction and lower rate of desaturation is recorded by samples 4204/3 and 4207/4 when compared to the other three samples, indicating higher clay content in these. The drying curves show a slight divergence and indicate the variable ratios between clay and sand within the respective Upnor Formation samples (Figure 5.31). Nevertheless, all of the data indicate significantly lower AEVs when compared to the sandy clay samples from the Lower Mottled Beds.

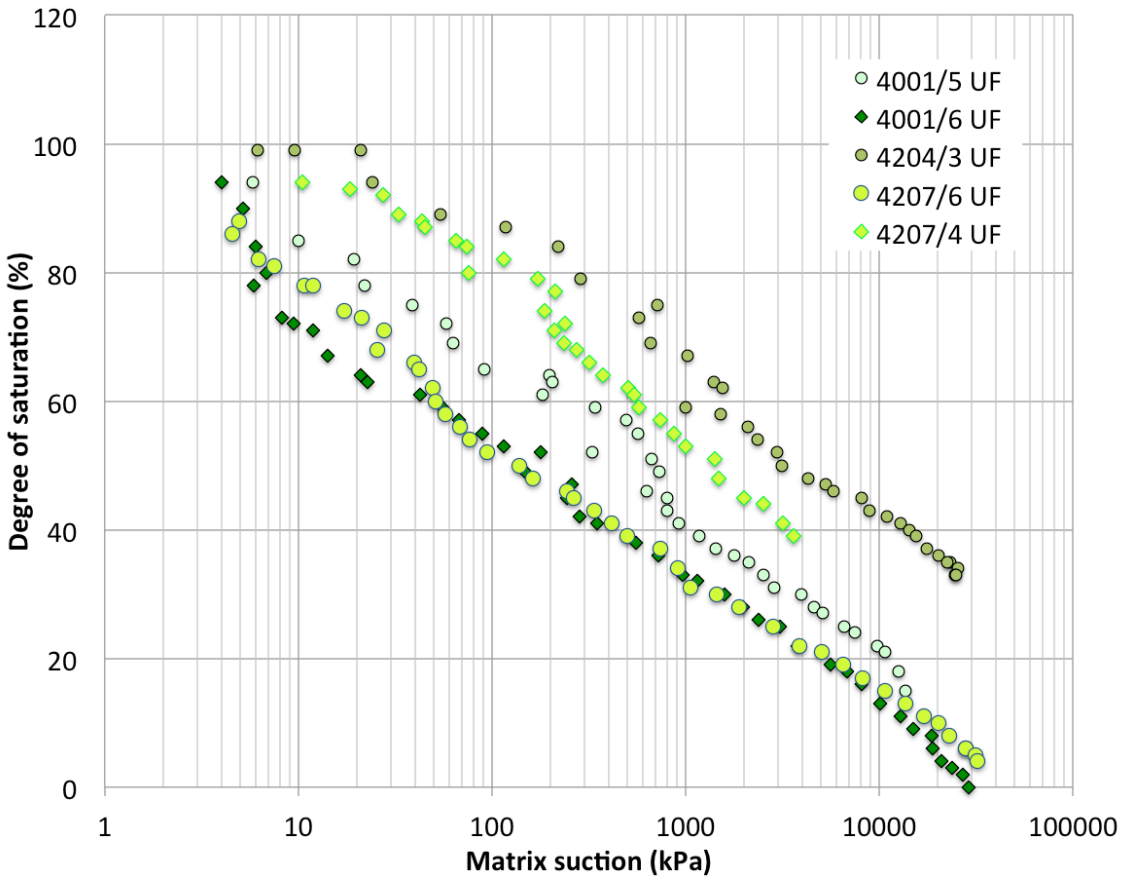


Figure 5.31 Drying curves for the Upnor Formation

There is significant hysteresis between the drying and wetting curves for sample 4207/4 (Figure 5.32) in which a significantly lower degree of saturation is apparent on the wetting curve when compared to equivalent values of matrix suction on the drying curve. This is reflected in significantly lower volumetric water contents during wetting when compared to equivalent values of matrix suction during the drying cycle (Figure 5.33). Slight shrinkage of the sample occurred during the drying cycle, indicated by a slightly lower void ratio during wetting when compared to the equivalent value of matrix suction during drying (Figure 5.34).

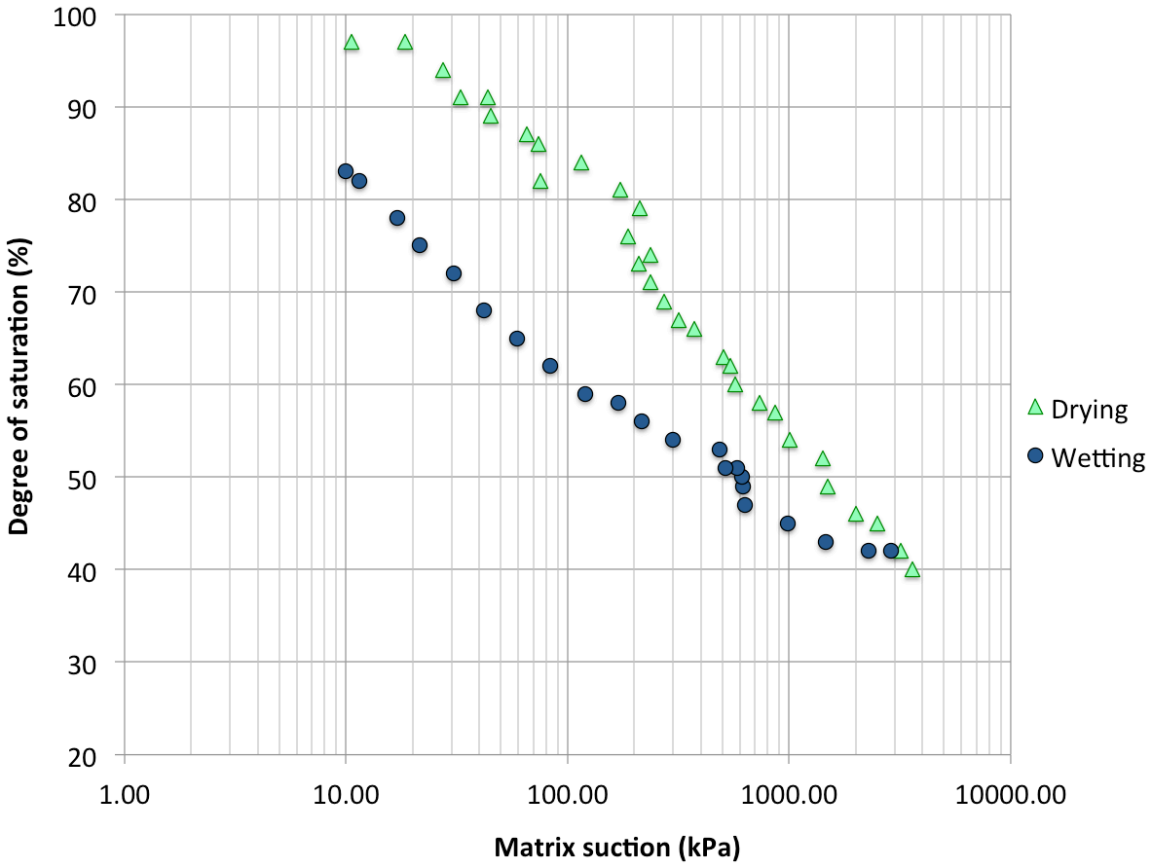


Figure 5.32 SWRCs suction vs. saturation: sample 4207/4

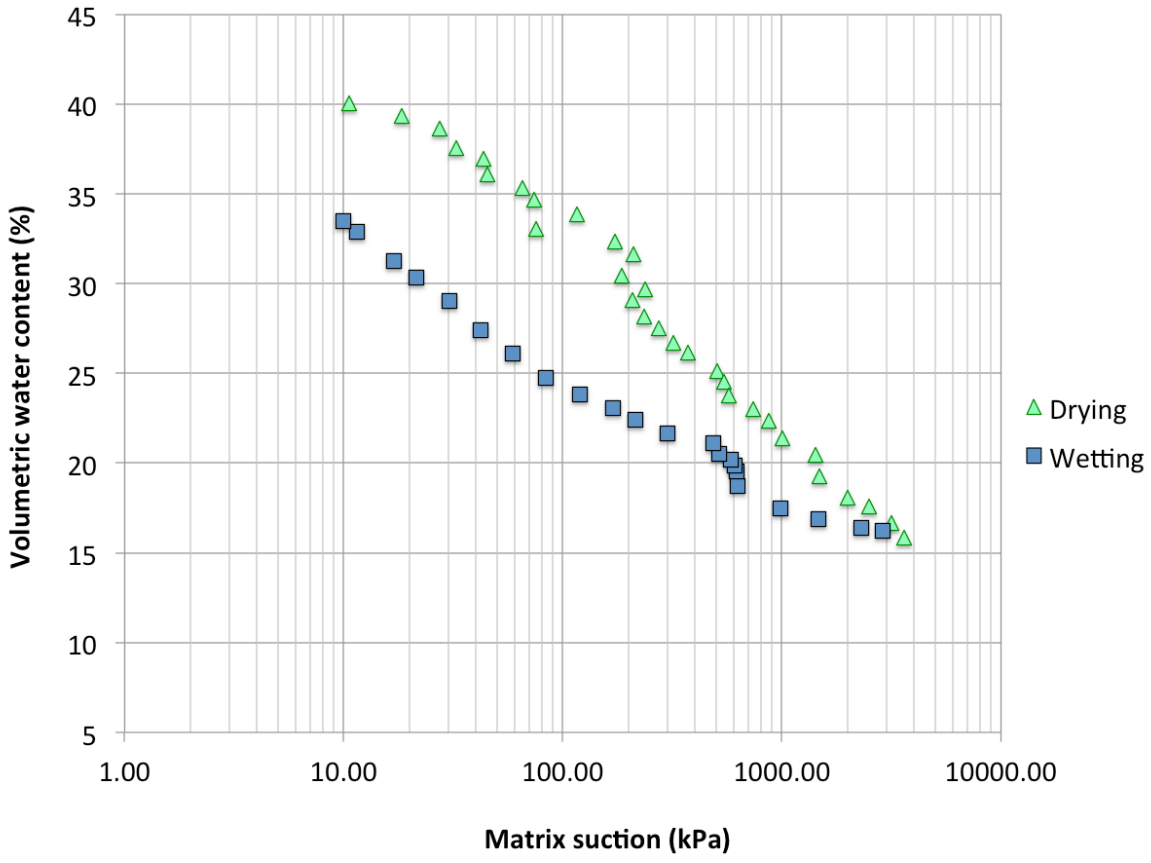


Figure 5.33 SWRCs suction vs. volumetric water content: sample 4207/4

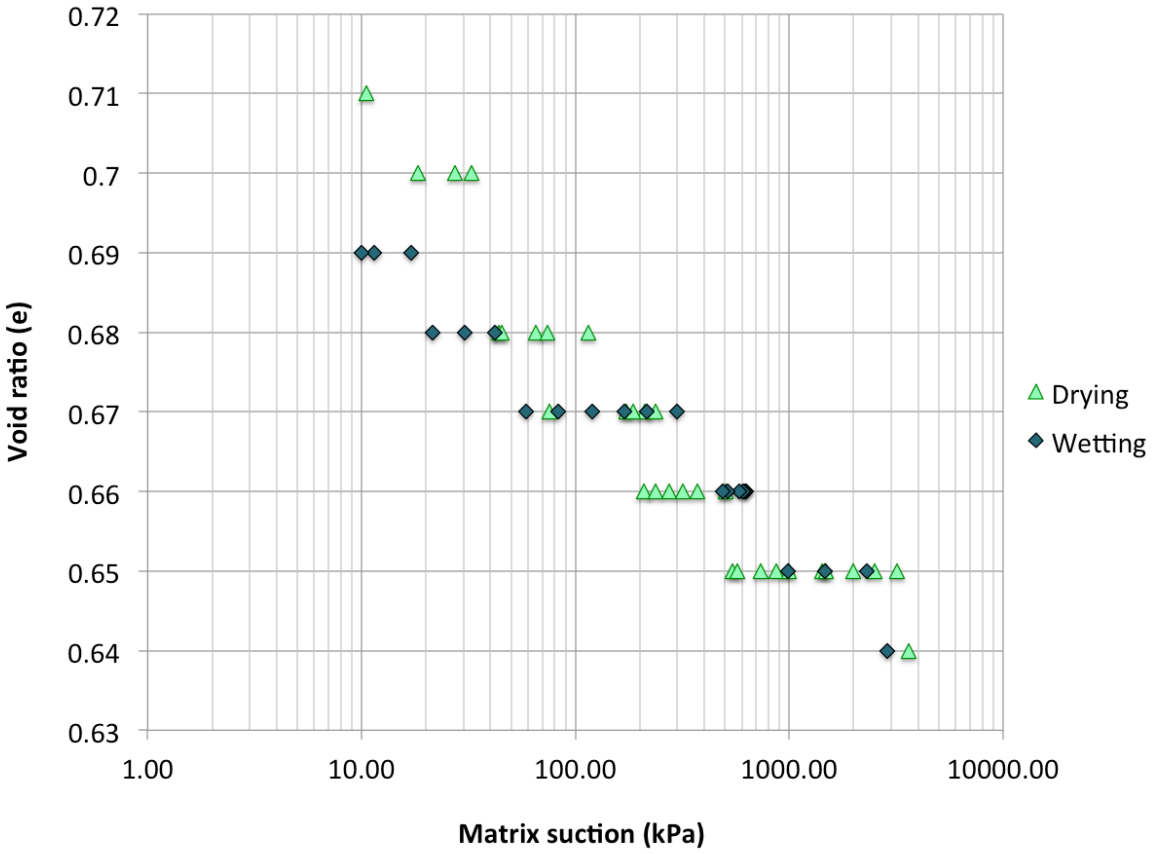


Figure 5.34 SWRCs suction vs. void ratio: sample 4207/4

Thanet Sand Formation

SWRCs were developed for four samples of silty fine sand from the Thanet Sand Formation. Sample 5015/72 is from the bottom, clay-rich, 2 m of the stratum, whilst the remaining three samples, 5015/70, 5013/45 and 5013/43 have been taken from progressively higher up in the sequence. Sample 5013/43 is from the top 2 m of the stratum, in which desaturation occurs without any significant increase in matrix suction (Figure 5.35) and is characteristic of sand material with very little clay or silt. The drying curves for 5013/45 and 5015/70 indicate desaturation of the samples without any significant increase in matrix suction. However, at about 30% saturation there is a notable increase in matrix suction with increasing desaturation, indicative of a progressive increase in clay content compared to sample 5013/43 and coarsening upward sequence within the stratum. Sample 5015/72 is interpreted as significantly more clayey than the other three samples, which were notably more friable in nature and needed more delicate handling during the laboratory testing. The drying curve (Figure 5.35) displays a relatively steep initial response, in which desaturation is accompanied by very little increase in matrix suction, thereafter demonstrating significantly greater increase in matrix suction with desaturation. It is very similar to the drying curves for 4001/6 and 4207/6 from the Upnor Formation, indicating similar material types and providing evidence for clay enrichment in the base of the Thanet Sand Formation. In addition,

the drying cycles for all of the Thanet Sand samples were able to achieve zero or near zero residual degree of saturation.

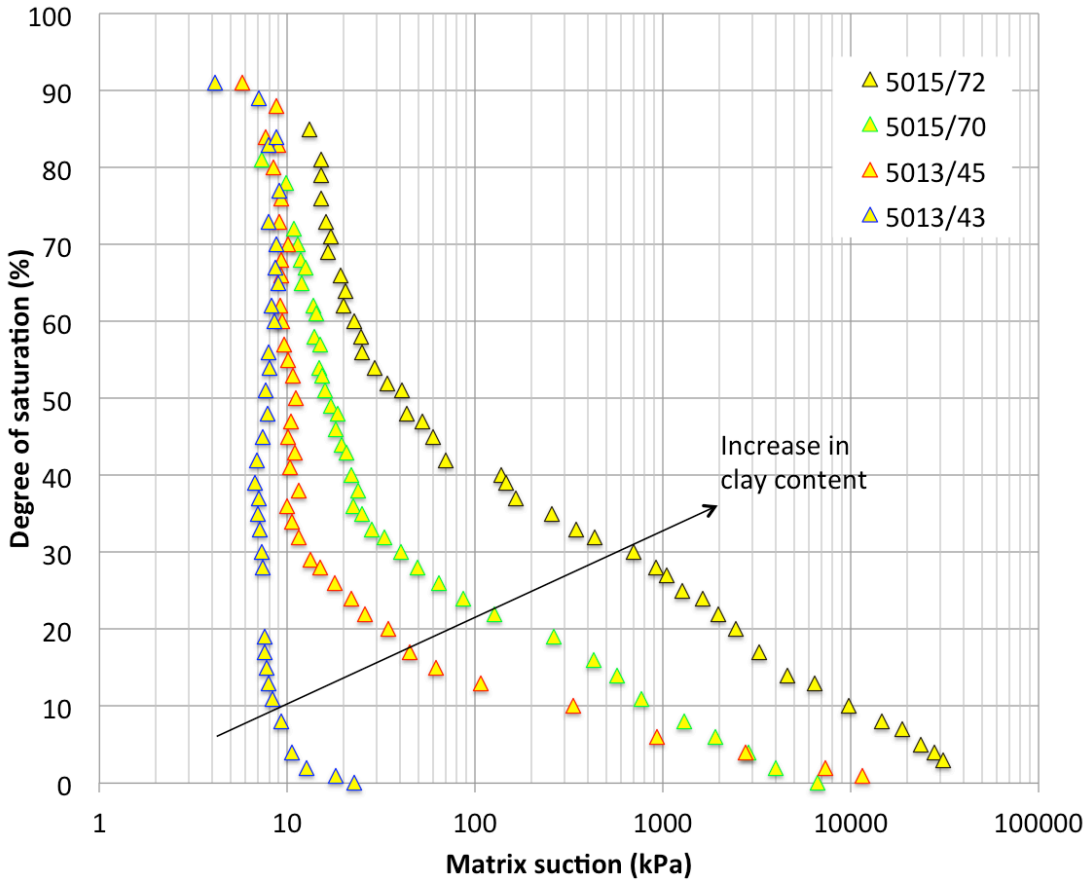


Figure 5.35 Drying curves for the Thanet Sand Formation

Very little hysteresis is evident between the drying and wetting curves for sample 5013/45 (Figure 5.36) as reflected by the volumetric water content during wetting, being only slightly lower than that during the drying cycle at the equivalent value of matrix suction (Figure 5.37). Very similar void ratios during the drying and wetting cycles (Figure 5.38) indicate that no significant shrinkage or swelling of the material has taken place throughout the experiment.

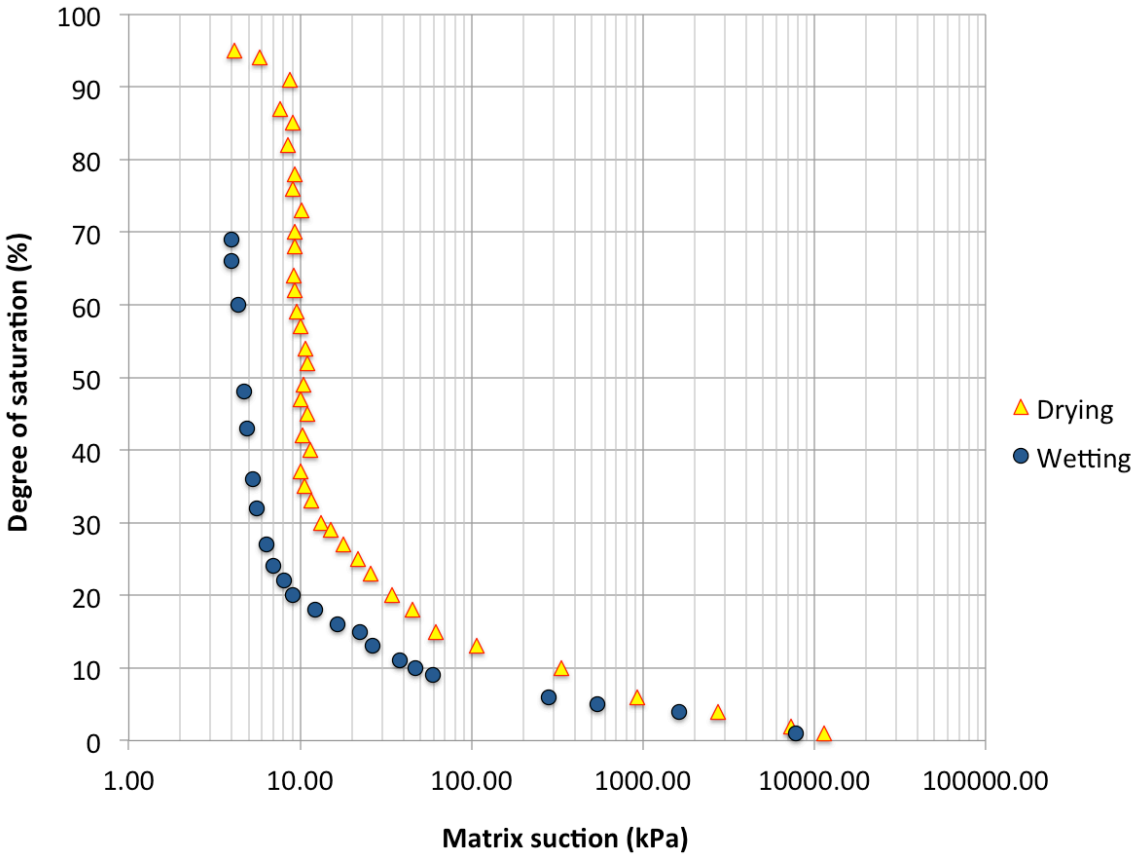


Figure 5.36 SWRCs suction vs. saturation: sample 5013/45

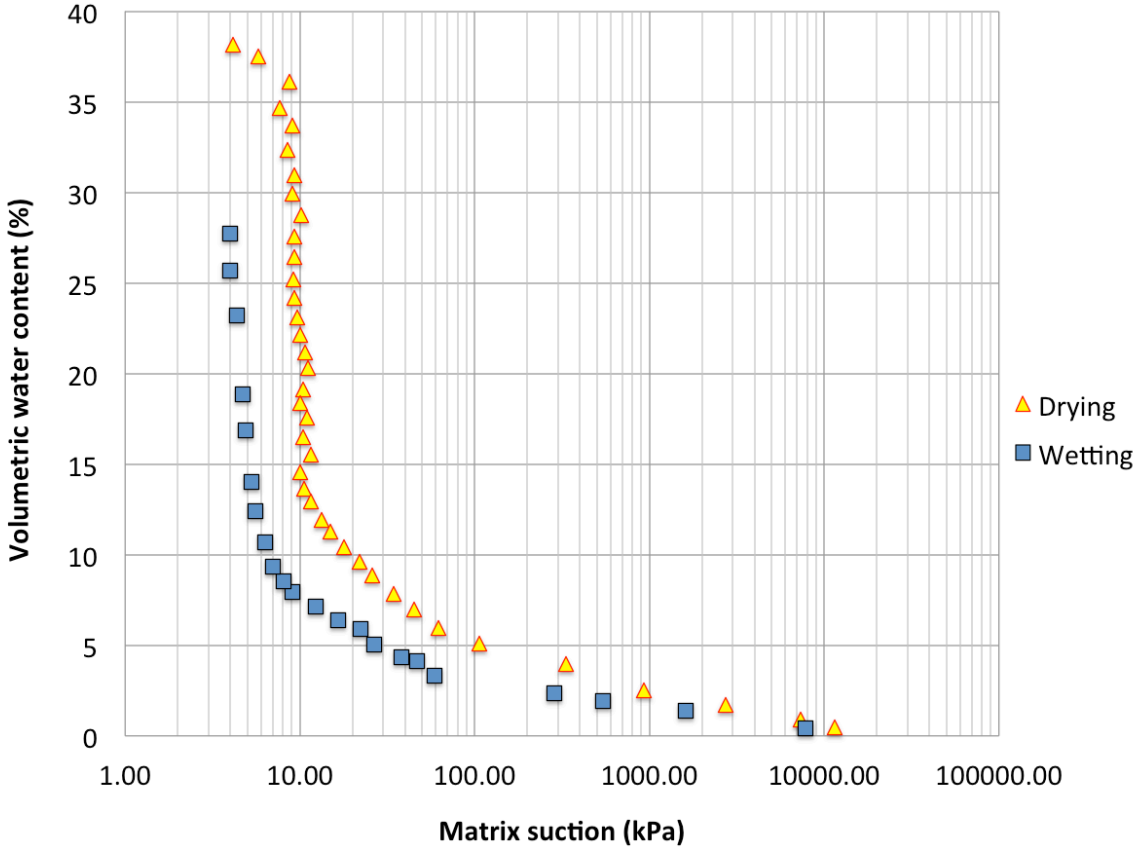


Figure 5.37 SWRCs suction vs. volume water content: sample 5013/45

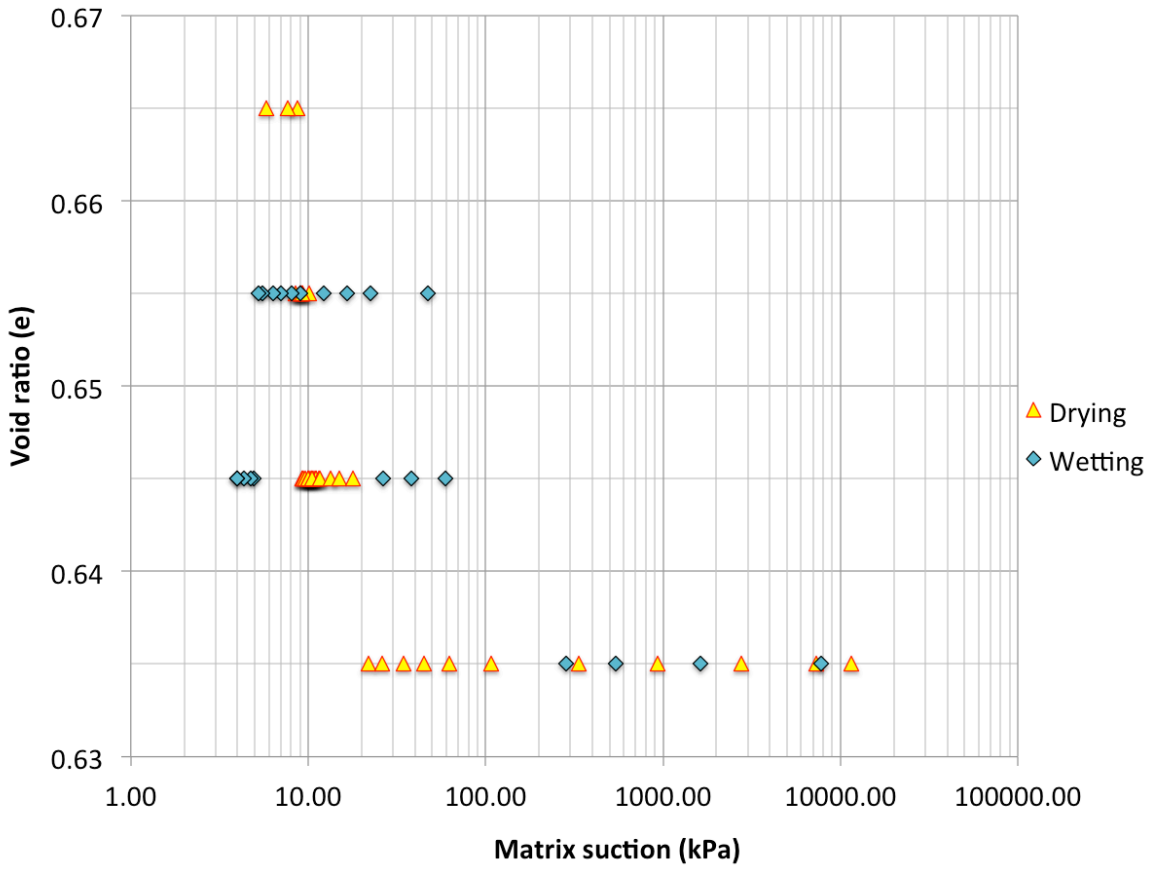


Figure 5.38 SWRCs (drying and wetting) suction vs. void ratio: sample 5013/45

Drying curves were continued for a number of samples (Table 5.5) until residual saturation or, in the case of 4006/2, the capacity of the filter paper was reached. Relatively lower values of matrix suction are confirmed for three of the (non-clayey) Thanet Sand samples whilst the sample from the clay-rich base of this stratum, 5015/72, possesses similar suction characteristics to the two Upnor formation samples, 4001/6 and 4207/6.

Table 5.5 Summary of matrix suction at residual saturation

Sample reference	Stratum	Matrix suction (kPa)	Residual degree of saturation (%)
4006/2	Lower Mottled Beds (sandy)	32863	17
4001/6	Upnor Formation	28968	0
4207/6	Upnor Formation	32162	4
5015/72	Thanet Sand Formation	31032	3
5015/70	Thanet Sand Formation	6647	0
5013/45	Thanet Sand Formation	11484	1
5013/43	Thanet Sand Formation	22	0

5.4 Field tests

5.4.1 Borehole gas monitoring

Gas monitoring standpipes were installed within the Upnor Formation in eight Tideway Tunnel investigation boreholes (Figure 4.27). Data were collected between April 2011 and July 2013, with additional data collected for Borehole SA1066D between August and September 2009 (Appendix H), prior to the project budget review (Section 4.4.1).

All boreholes were saturated, i.e., beneath the piezometric level of the lower aquifer water table. Atmospheric oxygen levels were present at all times within the monitoring installations with the exception of Borehole SA1066D, and there was no significant methane, carbon monoxide, or hydrogen sulphide. Barometric pressure has no influence on the readings.

Oxygen and carbon dioxide levels remained below 0.6% and 0.02% respectively (Figure 5.39) throughout the monitoring period in Borehole SA1066D. Changes in barometric pressure had no effect on these levels; gas vented constantly at an average of 20 litres/min throughout monitoring (Figure 5.40).

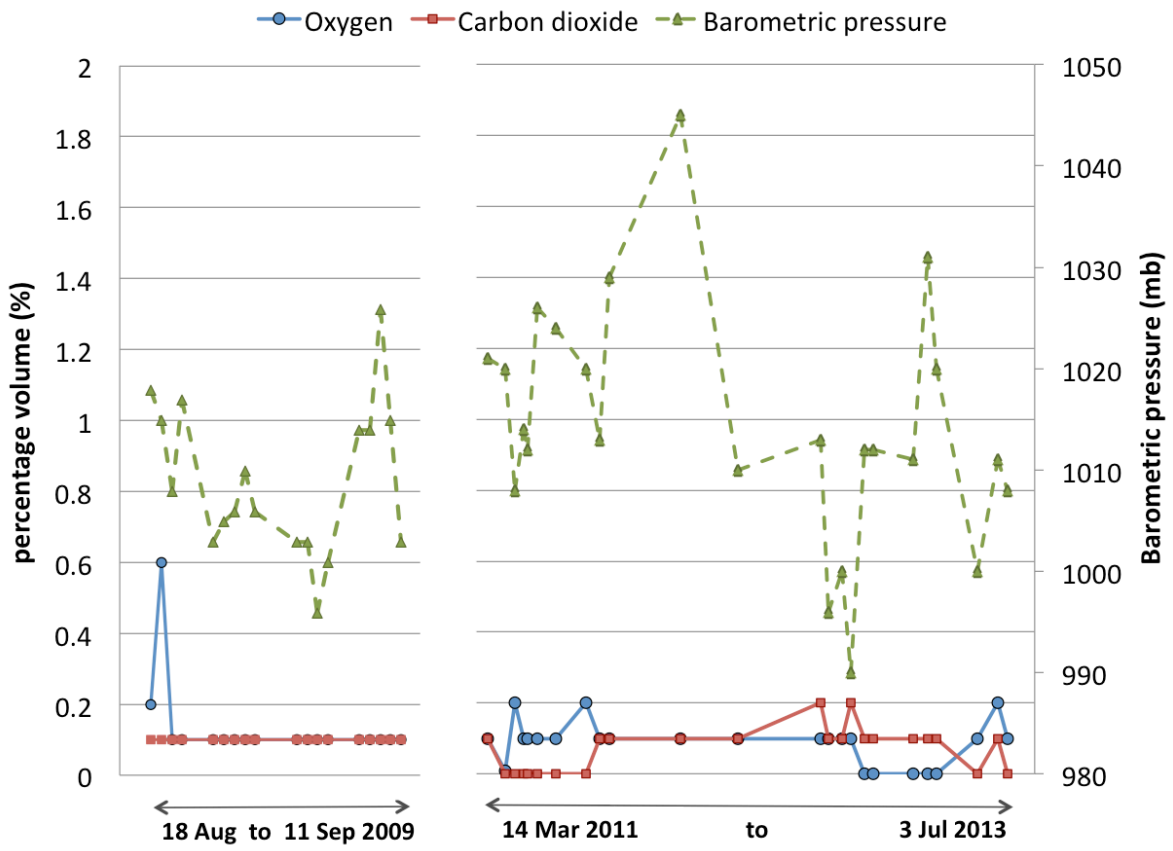


Figure 5.39 Gas monitoring at Borehole SA1066D

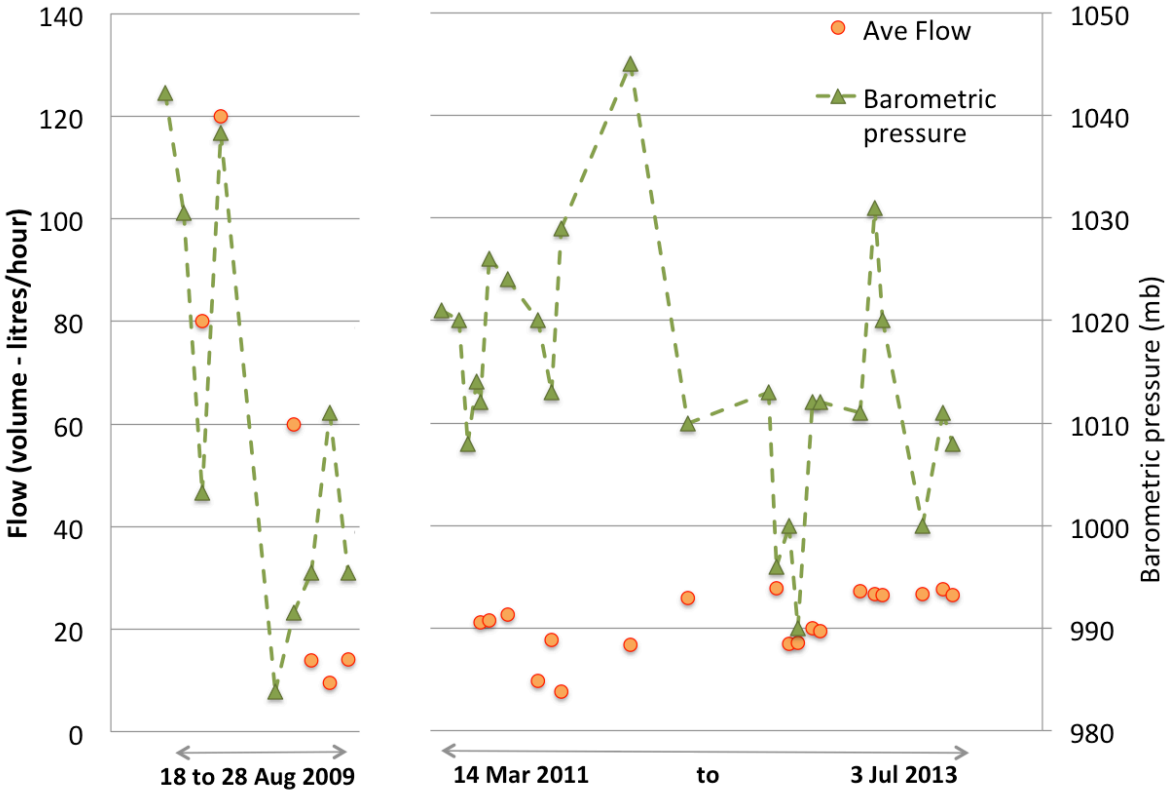


Figure 5.40 Gas flow at Borehole SA1066D

Three boreholes were selected for gas monitoring in upper Lambeth Group sediment (Figure 4.27) known to contain pyrite and carbonaceous material (Table 5.6). The boreholes were saturated to partially saturated during monitoring by confined (intermediate) aquifers found at this level of the London Basin stratigraphic sequence. Depleted oxygen levels and enrichment in carbon dioxide were observed in all three boreholes at various times.

Table 5.6 Summary of gas monitoring in the upper Lambeth Group

Borehole	Stratum	$\%O_2$ (range)	$\%CO_2$ (range)	Piezometric level above response zone (m in range)
SR1031	LtB	0 – 19.9	0.4 – 2.2	-1.1 – 1.8
PR1060	LtB	14.0 – 20.8	0.1 – 5.2	12.3 – 17.8
SR1092	USB	4.1 – 5.5	10.8 – 11.8	39.0 – 39.0

LtB = Laminated Beds; USB = Upper Shelly Beds

The piezometric data for Borehole SR1031 indicates that the groundwater level fell below the top of the borehole response zone, resulting in the introduction of oxidising conditions that caused oxygen levels to fall below 5% and CO_2 to rise to 2.2% (Figure 5.41). Barometric pressure arguably affects these levels since they both rise during high pressure and fall under low or falling pressure.

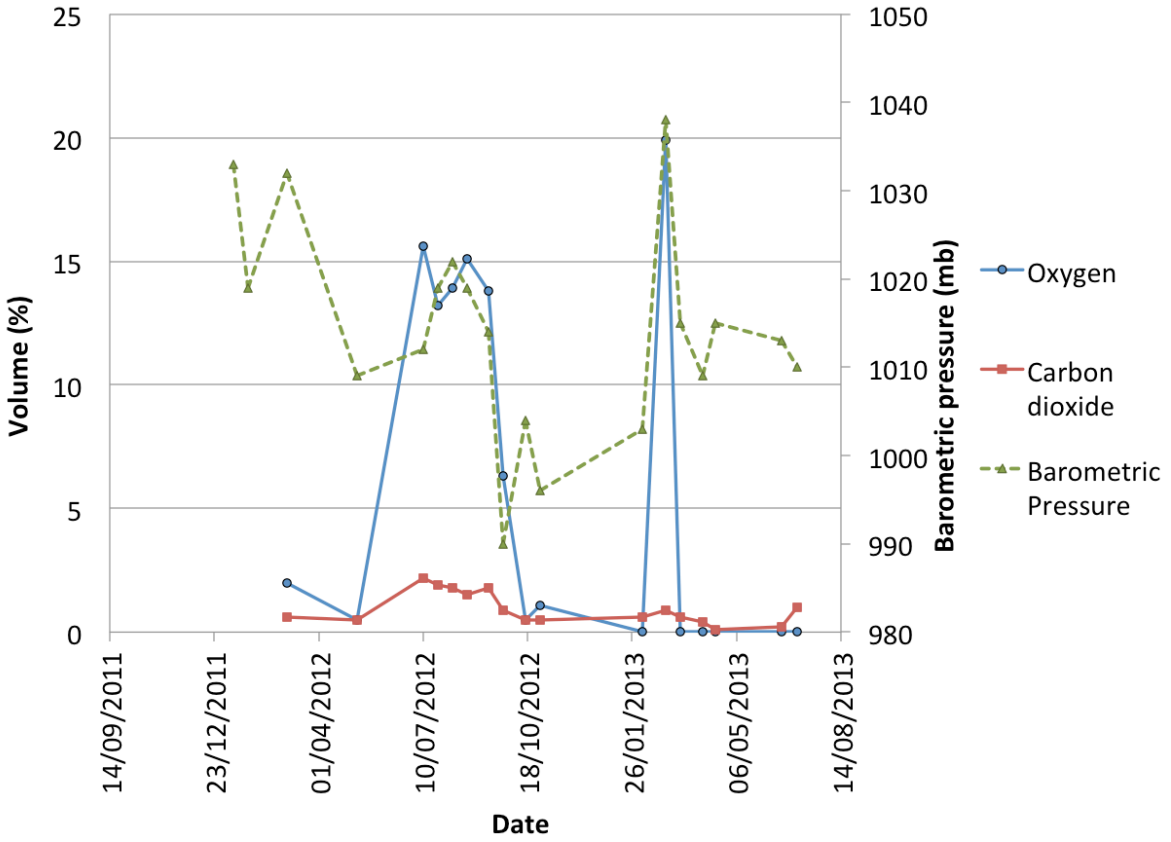


Figure 5.41 Gas monitoring at Borehole SR1031

Four boreholes from the NLFRS tunnel (Figure 4.27) were recommissioned for gas monitoring within the Upnor Formation (Table 5.7). Dry, oxidising conditions were recorded in all four boreholes, and each had depleted oxygen and elevated carbon dioxide. Rising barometric pressure is correlated with elevated oxygen in Borehole 278D/7 (Figure 5.42) and with decreased flow rates (Figure 5.43) in all four boreholes (Appendix H) supporting the inference of MacLean (1966) in that boreholes "blow" (bad air) during low barometric pressure and "suck" (atmospheric air) during increasing barometric pressure.

Table 5.7 Summary of gas monitoring in the NLFRS tunnel boreholes

Borehole	Visits (No.)	$\%O_2$ (range)	$\%CO_2$ (range)
278D/2	37	0.1 – 20.2	0.3 – 5.9
278D/6	25	0 – 20.9	0.0 – 3.2
278D/7	32	0 – 21.2	0.0 – 2.3
278D/9	22	0 – 12.0	1.4 – 4.2

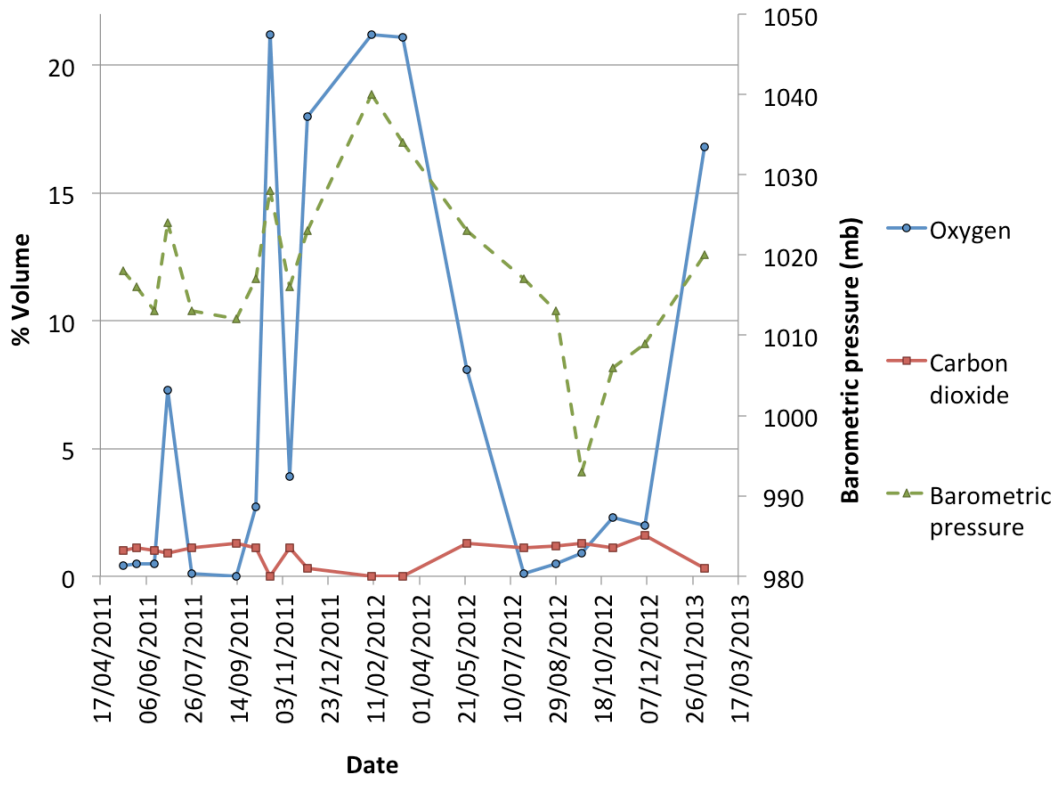


Figure 5.42 Gas monitoring at NLFRS tunnel Borehole 278D/7

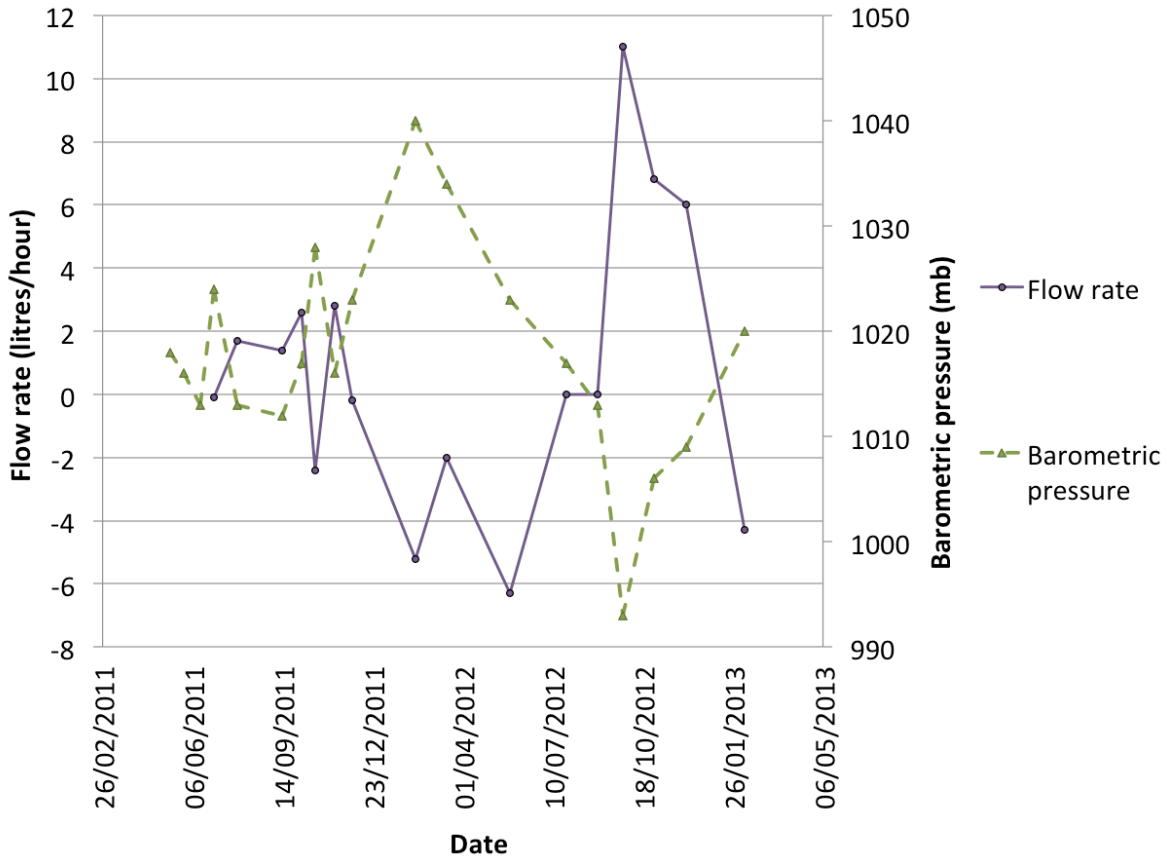


Figure 5.43 Gas flow at NLFRS tunnel Borehole 278D/7

Two boreholes from the TWRM southern extension were recommissioned for gas monitoring within the Upnor Formation (Figure 4.27). Saturated conditions were recorded in Borehole 773B/2 in which no significant depletion of oxygen or elevation in carbon dioxide has been detected. Dry, oxidising conditions were recorded in Borehole 773B/12, in which continually depleted levels of oxygen, typically less than 5%, have been recorded (Figure 5.44). Rising barometric pressure is correlated with elevated oxygen coinciding with periods of high atmospheric pressure, supporting the inference of MacLean (1966).

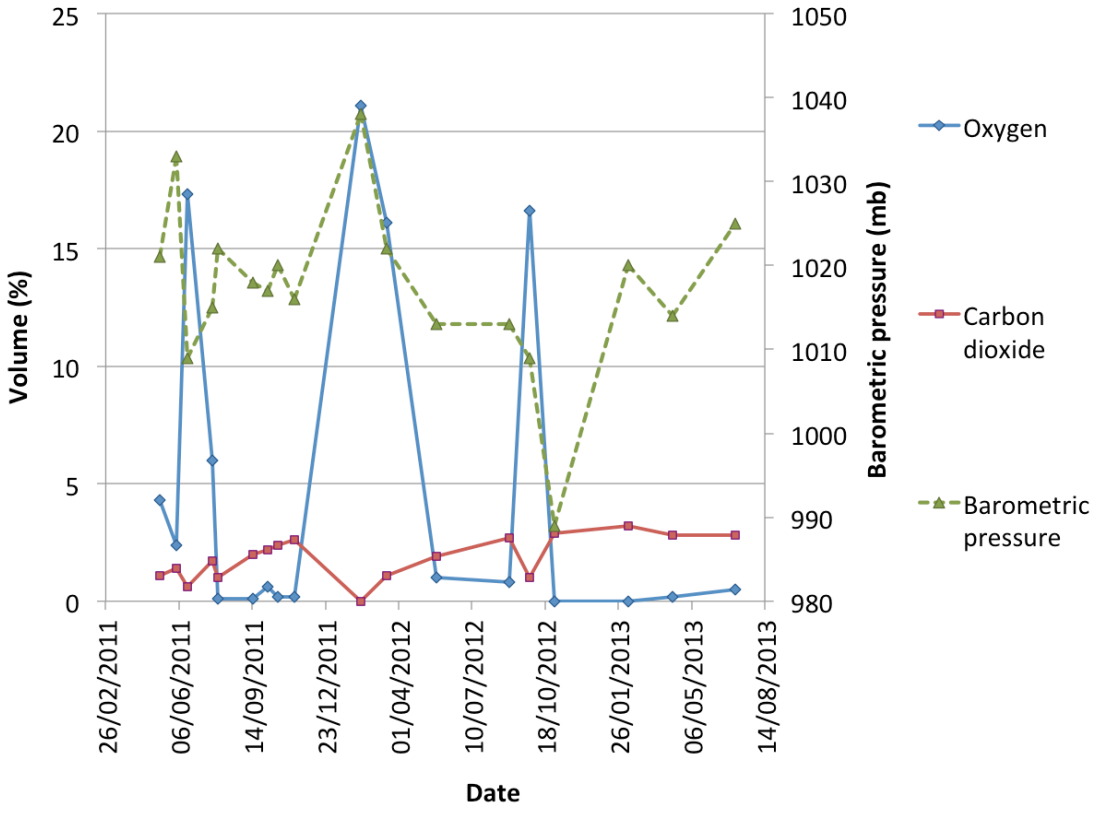


Figure 5.44 Gas monitoring at TWRM Ext Borehole 773B/12

5.4.2 Borehole gas sampling

Laboratory analysis of gas collected from Borehole 773B/12 indicates 2.3% O_2, 96% N_2 and 1.4% CO_2. Sampling at Borehole SA1066D has continued since it first intercepted pressurised, nitrogen-rich gas in 2009, as discussed in Section 2.3.3 (Figure 2.7a and Figure 2.7b). Less than 4.6% O_2, more than 95% N_2 and 0.06 to 0.1 % CO_2 have been recorded continuously up to three years after the event.

5.4.3 Borehole pump-out test

Nearly 14 m of water table drawdown was achieved in Borehole SR4003 during the first 15 hours of pumping operations, exposing the Upnor Formation to an oxidising atmosphere. In this time, the oxygen level decreased from 19.1 to 7.5 % and remained between 7.5 and 3.0% for the next 105 hours until the pump was switched off (Figure 5.45). Ensuing recovery of the

groundwater table resulted in an increase in oxygen levels from 5.3 to 20.2%, within 45 minutes.

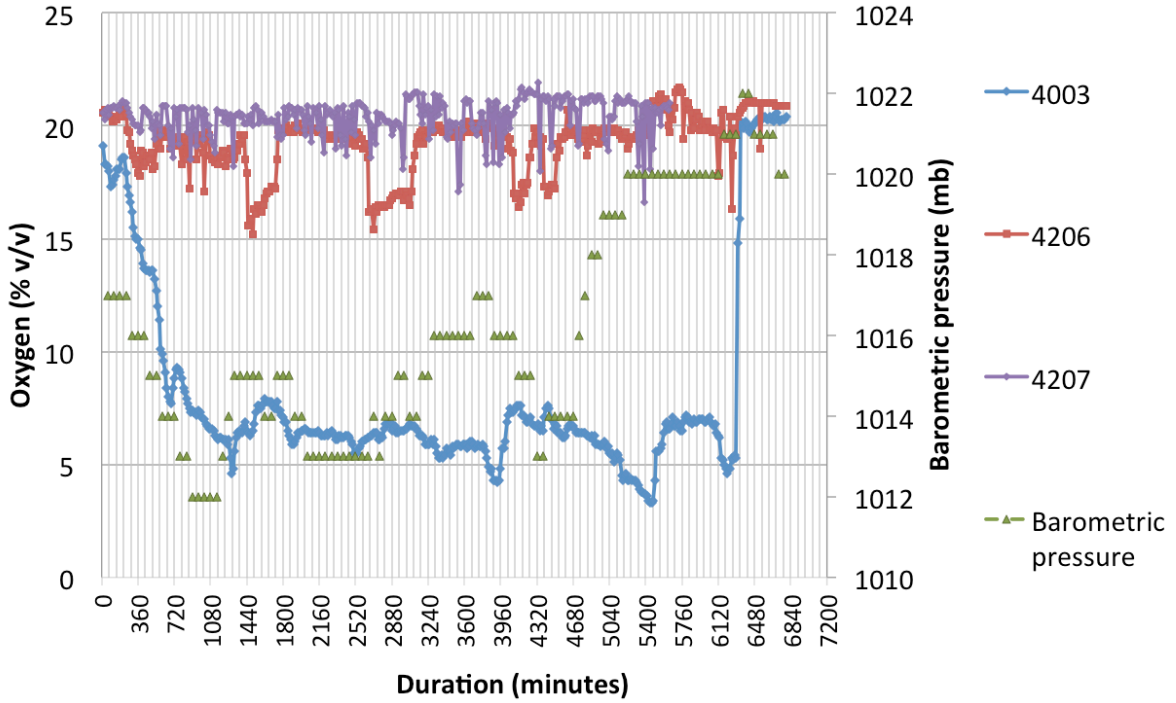


Figure 5.45 Oxygen depletion in pump-out test in Borehole SR4003

Pumping operations were unable to achieve drawdown of the water table in Borehole SR4207, which remained saturated, and as a result no oxygen depletion was recorded. Only partial drawdown was achieved in Borehole SR4206, resulting in very limited dewatering but even so, oxygen levels fell to as low as 15% during discrete periods of up to 7 hours in duration.

Ideally, a greater depth and longer duration of pumping at Borehole SR4003 might have produced the required drawdown, but neither was possible because of the time constraints placed upon the site operations. Nonetheless, the pump-out test demonstrates the rapid decrease in oxygen level within the Upnor Formation during dewatering and exposure to atmospheric conditions. The precise reasons for this remain uncertain; it may be due to a reaction of air with the ground in the exposed borehole walls or, just as plausibly, could be cavitation of dissolved air from the falling water table. In considering the latter, the dissolved oxygen content was recorded in groundwater samples from borehole SR4003 on three separate occasions immediately following the pump out test, and were found to range between 6.0 and 7.2 mg/l, equating to between 21.9 and 25.1% oxygen respectively in the air cavitated during the water table drawdown.

In reference to Figure 5.45 the dewatered ground is clearly able to reduce the oxygen in the cavitated air from approximately 21% per volume to between 3.0 and 7.5%, consuming as much as 17.0% in the process.

5.4.4 Borehole permeability tests

Variable head permeability tests (VHTs) were conducted within a number of boreholes during the Tideway Tunnel investigation (Table 5.8) to indicate the average (and maximum) values of permeability encountered in the lower Lambeth Group and Thanet Sand deposits. Values for the Seaford Chalk aquifer and the London Clay Formation, generally accepted as an impermeable barrier to pore water migration, are also given for comparison.

The permeability of the Upnor and Thanet Sand formations are broadly similar, implying hydraulic connectivity between the two strata. Only limited data are available for the Lower Mottled Beds but it appears to be similar to the London Clay Formation and likely acts as an impermeable barrier to pore water/gas flow. The average permeability in the pedogenic Upnor Formation is similar to that in the fresh Upnor and Thanet Sand formations, but minimum values are very low, indicating considerable variability at this level.

The VHT is subject to a number of imperfections, leading to inaccuracies in its results. The test may disturb the surrounding soil such as by the loosening of cohesive material and compaction or smearing of clay layers in granular material. In addition, the borehole test zone represents only a small proportion of an actual soil stratum and is often prone to clogging or silting, giving misrepresentative results. It is therefore recommended that the test be used with caution (Preene et al., 2001) and as such Table 5.8 is purely for indicative purposes.

Some of the higher values of permeability for the London Clay Formation and Lower Mottled Beds are clearly over-estimated when compared to those from published sources and represent VHTs undertaken in response to evidence (such as water seepage) of groundwater during borehole construction.

Table 5.8 Summary of VHT permeability values

Stratum	Tests (No.)	Permeability k (ms^{-1})			
		Min	Max	Ave	Published data
London Clay Formation	62	9.36×10^{-11}	5.00×10^{-6}	2.81×10^{-8}	10^{-9} to 10^{-10} *
Lower Mottled Beds	4	6.49×10^{-8}	5.58×10^{-7}	3.08×10^{-7}	10^{-8} to 10^{-9} **
Pedogenic Upnor	9	1.61×10^{-9}	8.00×10^{-6}	1.93×10^{-6}	
Upnor Formation	10	1.20×10^{-8}	3.00×10^{-6}	1.20×10^{-6}	
Thanet Sand Formation	23	4.80×10^{-8}	9.90×10^{-6}	3.27×10^{-6}	
Seaford Chalk Formation	140	6.19×10^{-10}	1.80×10^{-5}	2.47×10^{-6}	

*Data from Tideway Tunnel ground investigation. * Hight et al. (2003); **Hight et al. (2004).*

5.4.5 VHT in Borehole SR1031

A gas escape was witnessed from Borehole SR1031 during operation of a variable head permeability test. A 3 m test section was installed within the Laminated Beds of the Woolwich Formation that contained pyrite and carbonaceous material. The test employed the rising head technique where, initially, groundwater was purged from the test section that subsequently aerated. On its recovery, gas was heard bubbling through the rising column of groundwater as a result of oxidation of the pyrite and/or carbonaceous material during the purging stage.

5.5 Further laboratory experimentation

Further crude laboratory deoxygenation observations, in which samples of Upnor Formation and a gas monitor are placed within a sealed desiccator (Figure 5.46), were undertaken to demonstrate the extreme rapidity of deoxygenation and to confirm the observations made during the borehole pump-out test in section 5.4.3.

When plotted against the square root of time (Figure 5.47), a good linear relationship between percentage oxygen and root time appears to exist up to about 25 hours with the rate of oxygen depletion reducing after that towards an equilibrium or saturation value. The experiment demonstrates that during tunnel construction it is possible that oxygen in the underground atmosphere can be reduced to dangerous levels (even fatal) in as little as an hour, posing an

extreme hazard for underground working. Positive pressures used during tunnelling to reduce groundwater ingress will act in a similar way to barometric pressure, which explains why deoxygenation coincides with a cessation of positive pressure.

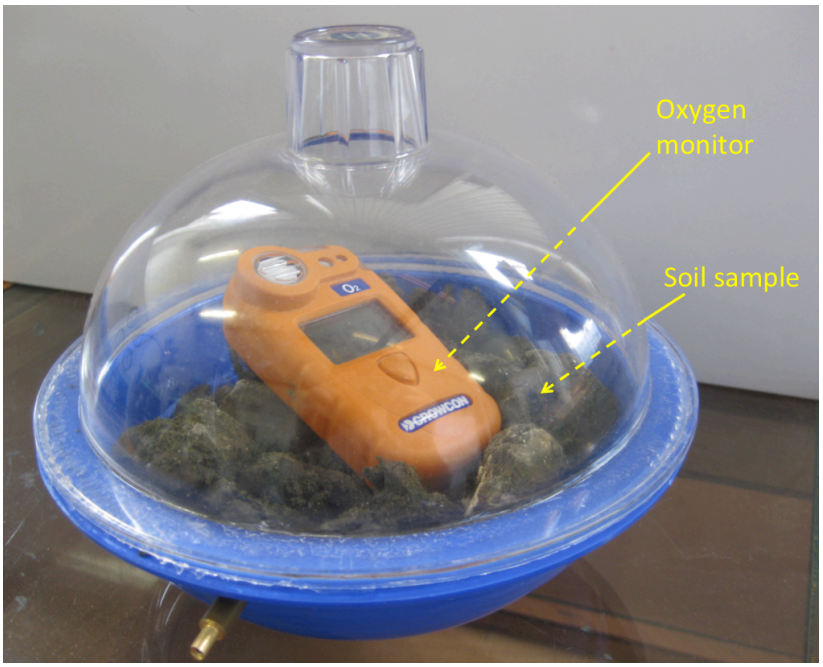


Figure 5.46 Observation of oxygen depletion in Upnor Formation (sample AM325)

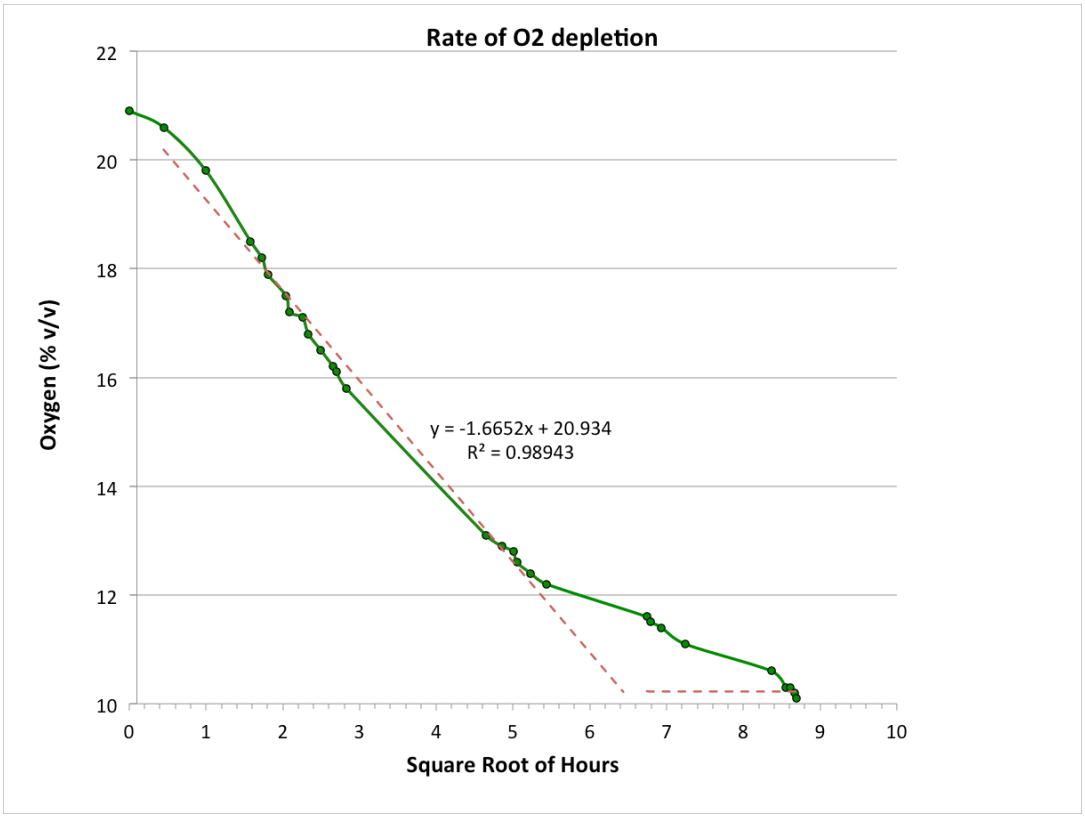


Figure 5.47 Measured rate of oxygen depletion in the Upnor Formation

6 CONCLUSIONS

6.1 Research summary

The research investigates the causes of confined space hypoxia within the lower Lambeth Group deposits and tests the existing assumption that the mineral glauconite oxidises rapidly upon exposure to atmospheric conditions.

There is strong evidence in the literature that the lower Lambeth Group deposits pose a significant ground hazard for confined space hypoxia during underground construction, in spite of limited data on the subject and concern that many cases of confined space hypoxia may not have been made public. Most occurrences were encountered within the Upnor Formation, especially after dewatering of the stratum or where already dry. The effect is apparently exacerbated during periods of low barometric pressure.

Borehole sampling confirms that the gas within the Upnor Formation constitutes 'normal air' with its oxygen removed, i.e., with no other by-products such as H_2S, CO_2, CH_4 or CO, and so leaving a predominantly nitrogen-rich gas. The gas is thus hypoxic (deficient in oxygen), comprising less than 5% oxygen and as much as 98% nitrogen and is confined and under pressure beneath stiff clay of the Lower Mottled Beds. These extend across London and based on the filter paper tests, act as an impermeable barrier to upward migration of the gas that remains trapped within the underlying Upnor Formation, even when the gas is further pressurised under a piston-like mechanism from the rising of the lower aquifer groundwater table.

Extensive borehole analyses provide a better understanding of the extent of pedogenesis at the top of the Upnor Formation. Unweathered glauconite is identified within the pedogenically altered Upnor Formation and Lower Mottled Beds in a number of hand specimens and proven in several laboratory tests including optical microscopy, SEM and FTIR, and it is indicated in XRD analyses. All these tests were conducted under atmospheric conditions, clearly demonstrating that glauconite does not rapidly oxidise. Furthermore, the mineral was likely exposed to oxidising conditions for long periods during the deposition of the lower Lambeth Group sediments. It is therefore unlikely that further oxidation/alteration occurred within the 100 to 200 year period of water table drawdown during formation of the 'cone of depression' in central London.

Goethite pseudomorphs of glauconite were detected in a small number of thin sections but only within the Lower Mottled Beds. These were found adjacent to relatively unweathered glauconite, indicating a mixture of highly evolved and nascent glauconite at the time of burial. It is likely that the nascent glauconite was weathered but only over a period of probably

thousands of years during pedogenesis and not at the time of formation of the modern 'cone of depression'.

In disproving glauconite as the cause of confined space hypoxia, the alternative mineral suspects pyrite and organic material were assessed. Both pyrite and organic material can be potent causes of hypoxia, but laboratory XRD, FTIR, SEM and optical thin section analyses demonstrate that both are either absent or in only minute quantities within the Upnor and Thanet Sand formations; too small to cause confined space hypoxia.

A rapid colour change was observed in a number of hand specimens, changing from blue-green to yellow-brown within a very short period of time. This colour change is indicative of green rust, which rapidly oxidises in air and is now suspected as being the primary cause of deoxygenation.

Goethite, an alteration product of green rust, has been detected in thin sections, SEM and XRD, but it may already be within the sample, or formed from the alteration of other minerals such as glauconite or pyrite. Nonetheless, its presence is consistent with green rust within unoxidised Upnor Formation.

One problem in proving the existence of green rust is that it oxidises too rapidly to be captured in laboratory analyses. The majority of the Tideway Tunnel core samples were exposed to too much oxygen prior to laboratory testing and it is likely that the mineral was lost at this stage or during transfer of the sample to the testing apparatus.

Because green rust is so rarely recovered from the natural environment, it is more commonly synthesised under laboratory conditions for experimental research. Its environment of formation is at the top of the water table which, in London, corresponds to the Upnor Formation. This was oxidised by air cavitated during drawdown of the lower aquifer water table in the development of the 'cone of depression' (Standing et al., 2013). Any green rust present would have oxidised to iron oxide-bearing minerals such as goethite, resulting in the formation of oxygen-depleted gas. A chemical reversal of the iron oxide back into green rust is possible during recovery of the water table and a return to saturated conditions, although only in the presence of the iron-reducing bacteria, *Shewanella putrefaciens*, the prevalence of which at the current depths of the Upnor Formation is not known.

Clearly, the Upnor Formation is potentially hazardous ground and should be given careful consideration in risk assessments for underground construction. The presence or absence of glauconite should not now be a concern, although pyrite and organic material are if present. Saturated Upnor Formation that retains its bright blue-green colour is likely to contain sufficient green rust to pose a significant ground hazard.

6.2 Conclusions

This research demonstrates that the lower Lambeth Group deposits, in particular dry or dewatered Upnor Formation, pose a very high risk of confined space hypoxia during underground construction or excavation.

Most of the case histories discussed come from Thames Water projects, because of the accessibility of (largely anecdotal) information for this research. It is not known whether similar information exists for tunnels completed by other utility companies or the Post Office, but Thames Water experience implies that the phenomenon must have been encountered by others and been poorly communicated throughout the industry.

For more than 25 years oxidation of the mineral glauconite was assumed to be the primary cause of oxygen depletion in shafts and tunnels within the Upnor Formation. However, this research eliminates glauconite as a possible cause, given its presence within heavily oxidised sediment, in hand specimen and in petrographic thin sections, SEM, FTIR and XRD analysis. Glauconite should no longer be considered a hazard in respect of oxygen depletion.

Pyrite and organic matter remain a serious hazard where present. Pyrite is known to cause confined space hypoxia but is considered to be more of a risk within dry or dewatered upper Lambeth Group deposits, specifically within the Laminated and Upper Shelly Beds. However, it is not present in the Upnor and Thanet Sand formations in sufficient quantities to be a primary factor in these layers. Although it cannot be eliminated entirely, because even small quantities will react with air, it is very unlikely to account for the rates and amounts of oxygen depletion that have been outlined in Chapters 2 and 5.

Instead, a relatively unknown mineral, green rust, is shown to be the most likely geochemical cause of oxygen depletion. It forms in saturated ground just below the lower aquifer water table and is particularly concentrated within the Upnor Formation. The detection of iron oxide and zinc in SEM analysis indicates that it may formerly have been present in Upnor Formation samples. It is identifiable by primary mineralogical evidence, i.e., colour and rate of colour change (Figure 6.1), although its immediate reactivity in air makes it both difficult to capture using conventional field sample techniques and extremely hazardous in the ground. Any observation of a bright blue-green mineral in the soil, however fleeting, should be treated with the utmost concern. Even when unobserved, dewatering of saturated Upnor Formation appears to always cause a reduction in oxygen and site risk assessments should recognise this. It is not present in significant quantities in the Thanet Sand Formation because it is too far below the top of the water table for green rust formation and Thanet Sand does not contain the required mineralogy to facilitate its growth.

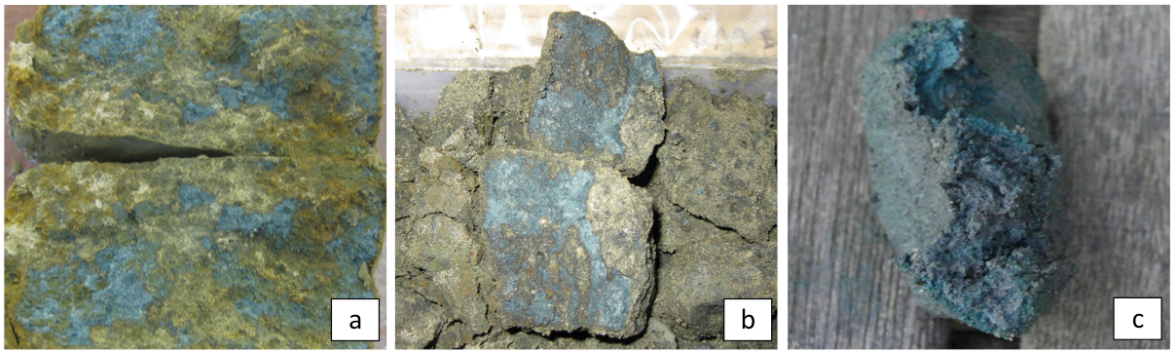


Figure 6.1 Evidence of green rust in Tideway Tunnel core samples

a from borehole SR4095; b from borehole SR1057 (courtesy of B. Patel); c from borehole SR5018 (courtesy of J. Huggett).

Confined space hypoxia does not occur in saturated sediments, requiring a physical mechanism, ground dewatering, for the hazard to occur, even when the ground contains the prerequisite geochemical mechanism (i.e., green rust in the Upnor Formation or pyrite in the Laminated Beds). The lower aquifer was drawn down to below the Upnor Formation across much of London within the last 200 years and it is during this period that air entered the stratum, most likely as a result of cavitation (Standing et al., 2013) and/or through 'windows' in the London Clay Formation, causing oxidation of the green rust and resulting in a nitrogen-rich hypoxic gas. Hysteresis in the soil water retention curves show that this gas is unable to redissolve during the subsequent recovery of the water table and consequently it became trapped beneath the impermeable Lower Mottled Beds, compressed and pressurised, and so causing the 'blow-outs' experienced at the tideway tunnel boreholes SA1066D and SR2071.

Results of the Teviot Street pump-out test and numerous borehole monitoring observations prove that the rate of deoxygenation within dewatered Upnor Formation is rapid and prolonged. Changes in barometric pressure can immediately affect oxygen levels within a number of boreholes and underground excavations.

It is not yet clear why pressurised hypoxic gas has been intercepted in already dry ground in some areas but not in others. It may be that localised faulting forms a geological structural trap, or that lithological variations in the sand:clay ratio within the Upnor Formation lead to localised accumulations of gas. The lack of homogeneity within the stratum suggests that deoxygenation will occur randomly within an excavation or tunnel and not necessarily near a gas detector. Pressurised hypoxic gas appears to be encountered irregularly across London, making it almost impossible to mitigate the risk at any one location. Therefore, the potential for confined space hypoxia *must* be assumed *anywhere* that dewatered Upnor Formation is encountered underground.

6.3 Recommendations for future research

In the future, improved preservation of site samples is essential to prevent oxidation of green rust in the time between sample recovery and laboratory analysis. Freezing samples immediately after recovery, using liquid nitrogen, was considered for this research but dismissed on health and safety grounds. However, it may be possible in the future.

The sample transit time from site to the laboratory can be eliminated by an on-site laboratory, containing a glove box and, if feasible, some of the specialist testing equipment. A significant factor in the loss of green rust is additional exposure of the sample to the atmosphere when loading it into various testing apparatus. Resolving this implies a number of impracticalities, such as finding a large enough glove box in which to house the apparatus. Nonetheless, several improvements can be made to the glove box, such as increasing its size to allow for more efficient sample grinding and preparation. Facilitating an inflow of hydrogen (to 5%) and incorporating palladium-scavenging devices would contribute to reducing oxygen levels to zero.

In the rare event of ground freezing during underground construction, as was done at Tooting Bec (Newman, 2009), core samples of frozen ground would allow for sub-sampling procedures to be unaffected by oxidation. However, this is an opportunistic rather than planned approach.

On a more practical basis, future ground investigations for proposed underground construction in the Lambeth Group should incorporate borehole monitoring installations within the Upnor Formation as a standard procedure.

Further to this research and in particular the pump-out test at Teviot Street, large-scale pumping tests are currently in operation, as part of continuing investigations for the Thames Tideway tunnel, to underdrain the Chalk at a number of locations. Gas monitoring installations have been placed within the Upnor Formation in a number of observation boreholes at each site to record changes in the level of oxygen commensurate with the introduction of oxidising conditions within the stratum. Site operations for these are in the early stages and results of monitoring unavailable at the time of writing.

Two rotary core boreholes, within 10 m of either side of Borehole SA1066D, are planned for excavation in early to mid-2014. It is intended to gain additional gas monitoring data from these to enable closer scrutiny of the ground, such as looking for gas-escape features, which was not practicable with the cable percussion methods used for SA1066D.

Current laboratory work is being continued on discrete samples from the lower Lambeth Group, to monitor the rate of oxygen depletion within a sealed desiccator, using gas-monitoring equipment. The results from the laboratory deoxygenation observations in Section

5.5 suggest that there is potential for determining a coefficient of oxygen depletion for a unit volume of soil in a manner analogous to the determination of c_v values from oedometer tests and also show promise for assessing the total volume of oxygen consumption per unit volume of soil.

References

Ahmed, I.A.M., Benning, L.G., Kakonyi, G., Sumoondur, A.D., Terrill, N.J. and Shaw, S., 2010. Formation of Green Rust Sulfate: A Combined in Situ Time-Resolved X-ray Scattering and Electrochemical Study. Langmuir, 26(9): 6593-6603.

Ahmed, I.A.M., Shaw, S. and Benning, L.G., 2008. Formation of hydroxysulphate and hydroxycarbonate green rusts in the presence of zinc using time-resolved in situ small and wide angle X-ray scattering. Mineralogical Magazine, 72(1): 159-162.

Aldiss, D., 2012. The stratigraphical framework for the Palaeogene successions of the London Basin, UK, British Geological Survey, Keyworth, Nottingham.

Ali, J.R. and Jolley, D.W., 1996. Chronostratigraphic framework for the Thanetian and lower Ypresian deposits of southern England. Geological Society, London, Special Publications, 101(1): 129-144.

Amorosi, A., 1995. Glaucony and sequence stratigraphy; a conceptual framework of distribution in siliciclastic sequences. Journal of Sedimentary Research, 65(4b): 419-425.

Aubry, M.-P., Hailwood, E.A. and Townsend, H.A., 1986. Magnetic and calcareous-nannofossil stratigraphy of the lower Palaeogene formations of the Hampshire and London basins. Journal of the Geological Society, 143(5): 729-735.

Ayala-Luis, K.B., Koch, C.B. and Hansen, H.C.B., 2008. The standard Gibbs Energy of formation of Fe(II)Fe(III) hydroxide sulfate green rust. Clays and Clay Minerals, 56(6): 633-644.

Banks, D., Younger, P.L. and Dumpleton, S., 1996. The Historical Use Of Mine-Drainage And Pyrite-Oxidation Waters In Central And Eastern England, United Kingdom. Hydrogeology Journal, 4(4): 55-68.

Barbour, S.L., 1998. Nineteenth Canadian Geotechnical Colloquium: The soil-water characteristic curve: a historical perspective. Canadian Geotechnical Journal, 35(5): 873-894.

Bearcock, J.M. and Perkins, W.T., 2007. The use of green rust to accelerate precipitation of ochre for mine water remediation. Mako Edizioni, Cagliari, Italy.

Bearcock, J.M., Perkins, W.T., Dinelli, E. and Wade, S.C., 2006. Fe(II)/Fe(III) 'green rust' developed within ochreous coal mine drainage sediment in South Wales, UK. Mineralogical Magazine, 70(6): 731-741.

Bell, A. and Whaite, H.M., 1957. Two deaths from anoxaemia during the construction of a sewerage system. Medical Journal of Australia, 44(22): 791-795.

Bender Koch, C. and Morup, S., 1991. Identification of green rust in an ochre sludge. Clay Minerals, 26(4): 577-582.

Bentor, Y.K. and Kastner, M., 1965. Notes on the mineralogy and origin of glauconite. Journal of Sedimentary Petrology, 35(1): 155-166.

Berner, R.A., 1981. A new geochemical classification of sedimentary environments. Journal of Sedimentary Research, 51(2): 359-365.

Bicalho, K.V., Gomes Correia, A., Ferreira, S., Fleureau, J.-M. and Marinho, F.A.M., 2007. Filter paper method of soil suction measurement, XIII Pan American Conference on Soil Mechanics and Geotechnical Engineering: proceedings. Isla Margarita, Venezuela, Venezuela.

Bierens de Haan, S., 1991. A review of the rate of pyrite oxidation in aqueous systems at low temperature. Earth-Science Reviews, 31(1): 1-10.

Bierens de Haan, S., Rae, J.E. and Parker, A., 1994. Pyrite oxidation in the Tertiary sands of the London Basin aquifer. Applied geochemistry, 9(2): 161.

Bird, M.J., Cook, J.M., Darling, W.G., Kinniburgh, D.G., McKittrick, R.P., Perkins, M.A. and Robins, N.S., 1989. An investigation into the occurrence of acidic groundwater beneath City Road, London. British Geological Survey, Keyworth, Nottingham.

Bracegirdle, A., Jefferis, S.A., Tedd, P., Crammond, N.J., Chudleigh, I. and Burgess, N., 1996. The investigation of acid generation within the Woolwich and Reading Beds at Old Street and its effect on tunnel linings. In: M. Taylor (Editor), Geotechnical Aspects of Underground Construction in Soft Ground. Balkema, Rotterdam, pp. 653-658.

Brown, A.D. and Jurinak, J.J., 1989. Mechanism of pyrite oxidation in aqueous mixtures. Journal Name: Journal of Environmental Quality; (United States); Journal Volume: 18:4: Medium: X; Size: Pages: 545-550.

BSI, 2011. Code of practice for health and safety in tunnelling in the construction industry. British Standards Institute, London.

Burst, J.F., 1958. "Glauconite" pellets: their mineral nature and applications to stratigraphic interpretations. Bulletin of the American Association of Petroleum Geologists, 42(2): 310-327.

Buurman, P., 1980. Palaeosols in the Reading Beds (Paleocene) of Alum Bay, Isle of Wight, U.K. Sedimentology, 27(5): 593-606.

Chan, K.L.A. and Kazarian, S.G., 2003. New Opportunities in Micro- and Macro-Attenuated Total Reflection Infrared Spectroscopic Imaging: Spatial Resolution and Sampling Versatility. Appl. Spectrosc., 57(4): 381-389.

Chandler, R.J., Crilly, M.S. and Montgomery-Smith, G., 1992. A low-cost method of assessing clay desiccation for low-rise buildings. Proceedings of the Institution of Civil Engineers, 92(2): 82-89.

Chandler, R.J. and Gutierrez, C.I., 1986. The filter-paper method of suction measurement. Geotechnique, 36(2): 265-268.

Chaves, L.H.G., 2005. The role of green rust in the environment: a review. Revista Brasileira de Engenharia Agrícola e Ambiental, 9: 284-288.

Christiansen, B.C., Balic-Zunic, T., Dideriksen, K. and Stipp, S.L.S., 2009. Identification of green rust in groundwater. Environmental science & technology, 43(10): 3436-3441.

Clark, K.A., 1970. Discussion, on: Follenfant et al. (1969). The Victoria Line. Proceedings of the Institution of Civil Engineers, Supplement: 328-329.

CNPlus, 1991. Thames Water and Davey Mining fined over lapse in safety standards at Thames Ring Main Project in London, Construction News.

Courbe, C., Velde, B. and Meunier, A., 1981. Weathering of glauconites:reversal of the glauconitization process in a soil profile in western France. Clay Minerals, 16(3): 231-243.

Critchfield, J.W., 1985. Tunneling in Gassy Ground, Rapid Excavation and Tunnelling Conference (RETC). Society for Mining Metallurgy, New York, pp. 441-461.

Cumbers, J.M., Nelson, J.D., Chao, K.C. and Overton, D.D., 2008. An evaluation of soil suction measurements using the filter paper method and their use in volume change prediction. Taylor & Francis Group, London.

Curry, D., 1992. Tertiary. In: P.M. Duff, D and A.J. Smith (Editors), Geology of England and Wales. The Geological Society Publishing House, Bath, pp. 651.

Davesne, E., Dideriksen, K., Christiansen, B.C., Sonne, M., Ayala-Luis, K.B., Koch, C.B., Hansen, H.C.B. and Stipp, S.L.S., 2010. Free energy of formation for green rust sodium sulphate ($NaFe^{2+}_6Fe^{3+}_3(OH)_{18}(SO_4)_2(s)$). Geochimica et Cosmochimica Acta, 74(22): 6451-6467.

Doyle, B.R., 2001. Hazardous Gases Underground: Applications to Tunnel Engineering. Marcel Dekker, Inc., New York, 375 pp.

Drissi, S.H., Refait, P., Abdelmoula, M. and Génin, J.M.R., 1995. The preparation and thermodynamic properties of Fe(II)Fe(III) hydroxide -carbonate (green rust 1); Pourbaix diagram of iron in carbonate-containing aqueous media. Corrosion Science, 37(12): 2025-2041.

Eder, V.G., Martin-Algarra, A., Sanchez-Navas, A., Zanin, Y.N., Zamirailova, A.G. and Lebedev, Y.N., 2007. Depositional controls on glaucony texture and composition, Upper Jurassic, West Siberian Basin. Sedimentology, 54(6): 1365-1387.

Elliot, T., Andrews, J.N. and Edmunds, W.M., 1999. Hydrochemical trends, palaeorecharge and groundwater ages in the fissured Chalk aquifer of the London and Berkshire Basins, UK. Applied Geochemistry, 14(3): 333-363.

Ellison, R.A., 1983. Facies distribution in the Woolwich and Reading Beds of the London Basin, England. Proceedings of the Geologists' Association, 94(4): 311-319.

Ellison, R.A., Ali, J.R., Hine, N.M. and Jolley, D.W., 1996. Recognition of Chron C25n in the upper Paleocene Upnor Formation of the London Basin, UK. Geological Society, London, Special Publications, 101(1): 185-193.

Ellison, R.A., Knox, R.W.O.B., Jolley, D.W. and King, C., 1994. A revision of the lithostratigraphical classification of the early Palaeogene strata of the London Basin and East Anglia. Proceedings of the Geologists' Association, 105(3): 187-197.

Ellison, R.A., Woods, M.A., Allen, D.J., Forster, A., Pharoah, T.C. and King, C., 2004. Geology of London. . British Geological Survey, Keyworth, 114 pp.

Entwisle, D.C., Hobbs, P.R.N., Northmore, K.J., Skipper, J.A., Raines, M.R., Self, S.J., Ellison, R.A. and Jones, L.D., 2013. Engineering geology of British rocks and soils: Lambeth Group. British Geological Survey, Nottingham, pp. 316.

Fanning, D.S., Rabenhorst, M.C., May, L. and Wagner, D.P., 1989. Oxidation state of iron in glauconite from oxidized and reduced zones of soil-geologic columns1. Clays and Clay Minerals, 37(1): 59-64.

Feder, F., Trolard, F., Klingelhöfer, G. and Bourrié, G., 2005. In situ Mössbauer spectroscopy: Evidence for green rust (fougerite) in a gleysol and its mineralogical transformations with time and depth. Geochimica et Cosmochimica Acta, 69(18): 4463-4483.

Flavin, R.J. and Joseph, J.B., 1983. The hydrogeology of the Lee Valley and some effects of artificial recharge. Quarterly Journal of Engineering Geology and Hydrogeology, 16(1): 65-82.

Fredlund, D.G. and Rahardjo, H., 1993. Soil Mechanics for Unsaturated Soils. John Wiley & Sons, U.S.A., 517 pp.

Fredlund, M.D., Wilson, G.W. and Fredlund, D.G., 2002. Representation and estimation of the shrinkage curve. In: Juca., d. Campos. and Marinho. (Editors), Third International Conference on Unsaturated Soils. Swets & Zeitlinger, Lisse., Recife, Brazil., pp. 145-149.

Génin, J.-M.R., Aïssa, R., Géhin, A., Abdelmoula, M., Benali, O., Ernstsen, V., Ona-Nguema, G., Upadhyay, C. and Ruby, C., 2005. Fougerite and FeII–III hydroxycarbonate green rust; ordering, deprotonation and/or cation substitution; structure of hydrotalcite-like compounds and mythic ferrosic hydroxide. Solid State Sciences, 7(5): 545-572.

Hansen, H.C.B., 1989. Composition, stabilization, and light absorption of Fe (II) Fe (III) hydroxycarbonate(green rust). Clay minerals, 24(4): 663.

Hansen, H.C.B. and Bender Koch, C., 1998. Reduction of nitrate to ammonium by sulphate green rust: activation energy and reaction mechanism. Clay minerals, 33(1): 87-101.

Harder, H., 1980. Synthesis of glauconite at surface temperatures. Clays and Clay Minerals, 28(3): 217-222.

Harrick, N.J., 1967. Internal Reflection Spectroscopy. John Wiley & Sons, New York, 327 pp.

Harrington, J.F. and Horseman, S.T., 1999. Gas transport properties of clays and mudrocks. Geological Society, London, Special Publications, 158(1): 107-124.

Hawkins, A.B., 2012. Sulphate heave: a model to explain the rapid rise of ground-bearing floor slabs. Bulletin of Engineering Geology and the Environment, 71(1): 113-117.

Hester, S.W., 1965. Stratigraphy and Palaeogeography of the Woolwich and Reading Beds. Bulletin of the Geological Survey of Great Britain, 23: 117-137.

Hight, D.W., Ellison, R.A. and Page, D.P., 2004. Engineering in the Lambeth Group. CIRIA, London.

Hight, D.W., McMillan, F., Powell, J.J.M., Jardine, R.J. and Allenou, C.P., 2003. Some characteristics of London Clay. In: T.S. Tan, K.K. Phoon, D.W. Hight and S. Leroueil (Editors), Characterisation and Engineering Properties of Natural Soils. Swets & Zeitlinger, Lisse, pp. 1531.

Hu, P., Yang, Q. and Li, P.-y., 2010. Direct and indirect measurement of soil suction in the laboratory. EJGE, 15.

Huggett, J.M., Adenteju, J., Wray, D. and Longstaffe, F., *in preparation*.

Huggett, J.M. and Gale, A.S., 1998. Petrography and diagenesis of the Thames Group at Whitecliff Bay, Isle of Wight, UK. Proceedings of the Geologists' Association, 109(2): 99-113.

Huggett, J.M. and Knox, R.W.O.B., 2006. Clay mineralogy of the Tertiary onshore and offshore strata of the British Isles. Clay Minerals Clay Minerals, 41(1): 5-46.

Hurst, C.W. and Wilkinson, W.B., 1986. Rising groundwater levels in cities. Geological Society, London, Engineering Geology Special Publications Geological Society, London, Engineering Geology Special Publications, 3(1): 75-80.

Ingram, G.M. and Urai, J.L., 1999. Top-seal leakage through faults and fractures: the role of mudrock properties. Geological Society, London, Special Publications, 158(1): 125-135.

Jewell, P. and O'Conner, M., 2012. The Lee Tunnel Shafts, Wastewater Treatment and Sewerage. UK Water Projects Ltd, Lancaster, pp. 33-37.

Jimenez Millan, J., Molina, J.M., Nieto, F., Nieto, L. and Ruiz-Ortiz, P.A., 1998. Glauconite and phosphate peloids in Mesozoic carbonate sediments (eastern Subbetic Zone, Betic Cordilleras, SE Spain). Clay minerals, 33(4): 547-559.

Jones, M.A., 2007. Rising groundwater in central London. Water and Sewerage Journal(4): 35-36.

Kaldi, J., Daniel, R., Tenthorey, E., Michael, K., Schacht, U., Nicol, A., Underschultz, J. and Backe, G., 2010. Caprock Systems for CO2 Geological Storage. RPT10-2774, CO2CRC Technologies.

Kinniburgh, D.G., Gale, I.N., Smedley, P.L., Darling, W.G., West, J.M., Aldous, P.J. and O'Shea, M.J., 1994. The effects of historic abstraction of groundwater from the London Basin aquifers on groundwater quality. Applied geochemistry, 9(2): 175-195.

Knox, R.W.O.B., 1996. Tectonic controls on sequence development in the Palaeocene and earliest Eocene of southeast England: implications for North Sea stratigraphy. Geological Society, London, Special Publications, 103(1): 209-230.

Kohyama, N. and Hayashi, H., 1972. Oxygen consumption of clay minerals in the quarry at Oya, Utsunomiya City, Tochigi Prefecture, Japan. Industrial Health, 10: 24-51.

Kwon, S.-K., Kimijima, K., Kanie, K., Suzuki, S., Muramatsu, A., Saito, M., Shinoda, K. and Waseda, Y., 2007. Influence of silicate ions on the formation of goethite from green rust in aqueous solution. Corrosion Science, 49(7): 2946-2961.

Lambe, T.W. and Whitman, R.V., 1979. Soil Mechanics, SI Version. John Wiley & Sons, New York, 553 pp.

Legrand, L., Mazerolles, L. and Chaussé, A., 2004. The oxidation of carbonate green rust into ferric phases:solid-state reaction or transformation via solution. Geochimica et Cosmochimica Acta, 68(17): 3497-3507.

Lewis, D.G., 1997. Factors Influencing the Stability and Properties of Green Rusts. Advances in GeoEcology, 30: 345-372.

Lewis, J.D. and Harris, J.R., 1998. The engineering implications of deoxygenated gases in the Lambeth Group of north east London: a case history. In: CIRIA (Editor), Engineering properties of the Mercia Mudstone and Lambeth Groups. CIRIA, Derby, pp. 1153-1178.

Lucas, H.C. and Robinson, V.K., 1995. Modelling of rising groundwater levels in the Chalk aquifer of the London Basin. Quarterly Journal of Engineering Geology and Hydrogeology, 28(S): S51-S62.

MacLean, R.D., 1966. "Foul Air" in wells and boreholes in the London area., Proceedings of the Society for Water Treatment and Examination, pp. 271-283.

Marsh, T.J. and Davies, P.A., 1983. The Decline and Partial Recovery of Groundwater Levels below London, ICE Proceedings. Ice Virtual Library, pp. 731-733.

Mazeina, L., Navrotsky, A. and Dyar, D., 2008. Enthalpy of formation of sulfate green rusts. Geochimica et Cosmochimica Acta, 72(4): 1143-1153.

McKibben, M.A. and Barnes, H.L., 1986. Oxidation of pyrite in low temperature acidic solutions: Rate laws and surface textures. Geochimica et Cosmochimica Acta, 50(7): 1509-1520.

Melgarejo Corredor, M.L., 2004. Laboratory and numerical investigations of soil water retention curves, Imperial College, London.

Michaelsen, G.S. and Park, W.E., 1954. Asphyxiation in Street Manholes. In: P.H. Reports (Editor). Minnesota Department of Health, pp. 29-36.

Misawa, T., Suetaka, W. and Shimodaira, S., 1969. Infrared absorption spectra and oxidation of iron (II) hydroxide and green rust 1. Bulletin of the Chemical Society of Japan, 42: 3339-3340.

Mitchell, J.K., 1993. Fundamentals of soil behaviour. John Wiley & Sons, New York.

Monroe, W.H., 1947. Rapid oxidation of glauconite in glauconitic sand. Bulletin of the American Association of Petroleum Geologists, 31(8).

Moore, D.M. and Reynolds, R.C., 1997. X-Ray Diffraction and the Identification and Analysis of Clay Minerals. Oxford University Press, 378 pp.

Morgan, H.D. and Bartlett, J.V., 1969. Tunnel Design, in: The Victoria Line. Proceedings of the Institution of Civil Engineers, Supplement Volume: 377-395.

Morrison, P.R.J., McNamara, A.M. and Roberts, T.O.L., 2004. Design and construction of a deep shaft for Crossrail, Proceedings of the ICE - Geotechnical Engineering, pp. 173-182.

Morton, A.C., 1982. The provenance and diagenesis of Palaeogene sandstones of southeast England as indicated by heavy mineral analysis. Proceedings of the Geologists' Association, 93(3): 263-274.

Nagata, F., Inoue, K., Shinoda, K. and Suzuki, S., 2009. Characterization of Formation and Oxidation of Green Rust (Cl-) Suspension. ISIJ International, 49(11): 1730-1735.

Namduri, H. and Nasrazadani, S., 2008. Quantitative analysis of iron oxides using Fourier transform infrared spectrophotometry. Corrosion Science, 50(9): 2493-2497.

Newman, T.G., 2009. The impact of adverse geological conditions on the design and construction of the Thames Water Ring Main in Greater London, UK. Quarterly Journal of Engineering Geology and Hydrogeology, 42(1): 5-20.

Newman, T.G., Ghail, R.C. and Skipper, J.A., 2013. Deoxygenated gas occurrences in the Lambeth Group of central London, UK. Quarterly Journal of Engineering Geology and Hydrogeology.

Newman, T.G. and Hadlow, N., 2011. Ground challenges for the Thames Tunnel. In: S. Redmond and V. Romero (Editors), Rapid Excavation and Tunnelling Conference (RETC). Society for Mining, Metallurgy and Exploration, San Francisco, pp. 204-218.

Newman, T.G. and Wong, H.-Y., 2011. Sinking a jacked caisson within the London Basin geological sequence for the Thames Water Ring Main extension. Quarterly Journal of Engineering Geology and Hydrogeology, 44(2): 221-232.

Newman, T.G., Yuan, L.F.V. and O'Keeffe, L.C., 2010. Using tunnel boring data to augment the geological model. Geotechnical Engineering, 163(GE3): 157-166.

Nordstrom, D.K., 1982. Aqueous pyrite oxidation and the consequent formation of secondary iron minerals. Soil Science Society of America.

O'Loughlin, E.J., Larese-Casanova, P., Scherer, M. and Cook, R., 2007. Green Rust Formation from the Bioreduction of γ–FeOOH (Lepidocrocite): Comparison of Several *Shewanella* Species. Geomicrobiology Journal, 24(3): 211-230.

Odin, G.S., 1988. Glaucony from the Gulf of Guinea. In: G.S. Odin (Editor), Green Marine Clays. Elsevier Science, Amsterdam, pp. 446.

Odin, G.S. and Fullagar, P.D., 1988. Geological significance of glaucony facies. In: G.S. Odin (Editor), Green Marine Clays. Elsevier Science, Amsterdam, pp. 446.

Odin, G.S. and Lamboy, M., 1988. Glaucony from the margin off northwest Spain. In: G.S. Odin (Editor), Green Marine Clays. Elsevier Science, Amsterdam, pp. 446.

Odin, G.S. and Matter, A., 1981. De glauconiarum origine. Sedimentology, 28(5): 611-641.

Olowe, A. and Genin, J., 1990. Kinetics of formation of green rust 2 in the steady acidic sulphated medium. Hyperfine Interactions, 57(1): 2029-2035.

Ona-Nguema, G., Abdelmoula, M., Jorand, F., Benali, O., Block, J.-C. and Génin, J.-M.R., 2001. Iron(II,III) Hydroxycarbonate Green Rust Formation and Stabilization from Lepidocrocite Bioreduction. Environmental science & technology, 36(1): 16-20.

Page, D.P. and Skipper, J.A., 2000. Lithological characteristics of the Lambeth Group. Ground Engineering(February): 38-43.

Pantke, C., Obst, M., Benzerara, K., Morin, G., Ona-Nguema, G., Dippon, U. and Kappler, A., 2011. Green Rust Formation during Fe(II) Oxidation by the Nitrate-Reducing Acidovorax sp. Strain BoFeN1. Environmental science & technology, 46(3): 1439-1446.

Parmar, N., Gorby, Y.A., Beveridge, T.J. and Ferris, F.G., 2001. Formation of Green Rust and Immobilization of Nickel in Response to Bacterial Reduction of Hydrous Ferric Oxide. Geomicrobiology Journal, 18(4): 375-385.

Pecharsky, V. and Zavalij, P., 2009. Fundamentals of Powder Diffraction and Structural Characterization of Materials. Springer, New York, 741 pp.

PerkinElmer, 2005. FT-IR Spectroscopy: Attenuated Total Reflectance (ATR). PerkinElmer Life and Analytical Sciences, pp. 5.

Péron, H., 2007. An improved volume measurement for determining soil water retention curves. Geotechnical testing journal, 30(1): 1.

Peulon, S., Legrand, L., Antony, H. and Chaussé, A., 2003. Electrochemical deposition of thin films of green rusts 1 and 2 on inert gold substrate. Electrochemistry Communications, 5(3): 208-213.

Phillips, D.H., Gu, B., Watson, D.B. and Roh, Y., 2003. Impact of Sample Preparation on Mineralogical Analysis of Zero-Valent Iron Reactive Barrier Materials. J. Environ. Qual., 32(4): 1299-1305.

Popov, V., Gorbunov, A. and Levina, E., 2010. Regularities of the formation of iron(III) nanocrystalline particles during the oxidation of iron(II) compounds in a neutral medium. Russian Journal of Inorganic Chemistry, 55(7): 995-1001.

Povarennykh, A.S., 1978. The use of infrared spectra for the determination of minerals. American Mineralogist, 63(9-10): 956-959.

Preene, M., Roberts, T.O.L., Powrie, W. and Dyer, M.R., 2001. Groundwater control: design and practice. CIRIA, London, 204 pp.

Rainey, T.P. and Rosenbaum, M.S., 1989. The adverse influence of geology and groundwater on the behaviour of London Underground railway tunnels near Old Street Station. Proceedings of the Geologists' Association, 100(1): 123.

Read, H.H., 1970. Rutley's Elements of Mineralogy. George Allen & Unwin Ltd, London, 560 pp.

Refait, P., Abdelmoula, M., Trolard, F., Génin, J.-M.R., Ehrhardt, J.J. and Bourrié, G., 2001. Mössbauer and XAS study of a green rust mineral; the partial substitution of Fe2+ by Mg2+. American Mineralogist, 86(5-6): 731-739.

Refait, P., Benali, O., Abdelmoula, M. and Génin, J.-M.R., 2003. Formation of 'ferric green rust' and/or ferrihydrite by fast oxidation of iron(II-III) hydroxychloride green rust. Corrosion Science, 45(11): 2435-2449.

Rimstidt, J.D. and Vaughan, D.J., 2003. Pyrite oxidation: a state-of-the-art assessment of the reaction mechanism. Geochimica et Cosmochimica Acta, 67(5): 873-880.

RSA Geotechnics Ltd, 2005. Ground Investigation Report. No. 9705/1.

Ruby, C., Upadhyay, C., Géhin, A., Ona-Nguema, G. and Génin, J.-M.R., 2006. In Situ Redox Flexibility of FeII-III Oxyhydroxycarbonate Green Rust and Fougerite. Environmental science & technology, 40(15): 4696-4702.

Sánchez-Navas, A., Martín-Algarra, A., Eder, V., Reddy, B.J., Nieto, F. and Zanin, Y.N., 2008. Color, mineralogy and composition of Upper Jurassic West Siberian glauconite: useful indicators of palaeoenvironment. The Canadian Mineralogist, 46(5): 1249-1268.

Schlömer, S. and Krooss, B.M., 1997. Experimental characterisation of the hydrocarbon sealing efficiency of cap rocks. Marine and Petroleum Geology, 14(5): 565-580.

Schowalter, T.T., 1979. Mechanics of Secondary Hydrocarbon Migration and Entrapment. AAPG Bulletin, 63: 723-760.

Schwertmann, U. and Fechter, H., 1994. The formation of green rust and its transformation to lepidocrocite. Clay Minerals Clay Minerals, 29(1): 87-92.

Shahriar, K., Rostami, J. and Khademi Hamidi, J., 2009. TBM tunneling and analysis of high gas emission accident in Zagros long tunnel., ITA-AITES World Tunnel Congress and 35th ITA General Assembly, Budapest, Hungary.

Simon, L., François, M., Refait, P., Renaudin, G., Lelaurain, M. and Génin, J.-M.R., 2003. Structure of the Fe(II-III) layered double hydroxysulphate green rust two from Rietveld analysis. Solid State Sciences, 5(2): 327-334.

Simpson, B., Blower, T., Craig, R.N. and Wilkinson, W.B., 1989. The engineering implications of rising groundwater levels in the deep aquifer beneath London. CIRIA, London, 116 pp.

Skipper, J.A., 1999. The Stratigraphy of the Lambeth Group (Palaeocene) of South East England., Imperial College, London University, London University.

Skipper, J.A., Newman, T.G. and Mortimore, R.N., 2008. The engineering geology of the Lee Tunnel, east London, UK., Euroengeo. Cities and their underground environment, Madrid, pp. 1-3.

Soil Mechanics Ltd, 1986. Site investigation for the Stoke Newington to Coppermills section of London Water Ring Main, London. 7209/7/B.

Standing, J., Ghail, R. and Coyne, D., 2013. Gas generation and accumulation by aquifer drawdown and recharge in the London Basin. Quarterly Journal of Engineering Geology and Hydrogeology, 46(3): 293-302.

Su, C. and Puls, R.W., 2004. Significance of Iron(II,III) Hydroxycarbonate Green Rust in Arsenic Remediation Using Zerovalent Iron in Laboratory Column Tests. Environmental science & technology, 38(19): 5224-5231.

Taylor, R.M., 1980. Formation and properties of Fe(II)Fe(III) hydroxy-carbonate and its possible significance in soil formation. Clay Minerals Clay Minerals, 15(4): 369-382.

Taylor, R.M. and McKenzie, R.M., 1980. The influence of aluminum on iron oxides; VI, The formation of Fe(II)-Al(III) hydroxy-chlorides, sulfates, and -carbonates as new members of the pyroaurite group and their significance in soils. Clays and Clay Minerals, 28(3): 179-187.

Tedrow, J.C.F., 2002. Greensand and greensand soils of New Jersey : a review. Rutgers Cooperative Extension, N.J. Agricultural Experiment Station, Rutgers, the State University of New Jersey, New Brunswick.

Thames Water, 1988. Ring main deaths mystery unsolved, Thames Water News, pp. 1.

Trolard, F. and Bourrié, G., 2006. Structure of fougerite and green rusts and a thermodynamic model for their stabilities. Journal of Geochemical Exploration, 88(1-3): 249-251.

Trolard, F., Bourrié, G., Abdelmoula, M., Refait, P. and Feder, F., 2007. Fougerite, a new mineral of the Pyroaurite-Iowaite group: description and crystal structure. Clays and Clay Minerals, 55(3): 323-334.

Trolard, F., Génin, J.M.R., Abdelmoula, M., Bourrié, G., Humbert, B. and Herbillon, A., 1997. Identification of a green rust mineral in a reductomorphic soil by Mossbauer and Raman spectroscopies. Geochimica et Cosmochimica Acta, 61(5): 1107-1111.

Van Genuchten, M.T., 1980. A closed-form equation for predicting the hydraulic conductivity of unsaturated soils. Soil Science Society of America, 44(5): 892-898.

Vanapalli, S.K., Fredlund, D.G. and Pufahl, D.E., 1999. The influence of soil structure and stress history on the soil-water characteristics of a compacted till. Geotechnique, 49(2): 143.

Watts, N.L., 1987. Theoretical aspects of cap-rock and fault seals for single- and two-phase hydrocarbon columns. Marine and Petroleum Geology, 4(4): 274-307.

Wilkinson, B., 1985. Rising Groundwater Levels in London and Possible Effects on Engineering Structures. Memoires of the 18th Congress of the International Association of Hydrogeologists, Hydrology in the Service of Man: 145-157.

Zegeye, A., Bonneville, S., Benning, L.G., Sturm, A., Fowle, D.A., Jones, C., Canfield, D.E., Ruby, C., MacLean, L.C., Nomosatryo, S., Crowe, S.A. and Poulton, S.W., 2012. Green rust formation controls nutrient availability in a ferruginous water column. Geology.

Zegeye, A., Ona-Nguema, G., Carteret, C., Huguet, L., Abdelmoula, M. and Jorand, F., 2005. Formation of Hydroxysulphate Green Rust 2 as a Single Iron(II-III) Mineral in Microbial Culture. Geomicrobiology Journal, 22(7-8): 389-399.

Zugibe, F.T., Costello, J.T., Breithaupt, M.K., Zappi, E. and Allyn, B., 1987. The Confined Space-Hypoxia Syndrome. Journal of Forensic Sciences, 32(2): 554-560.